

Washington University in St. Louis
Washington University Open Scholarship

Engineering and Applied Science Theses &
Dissertations


McKelvey School of Engineering

Spring 5-15-2018

Functional Electrical Stimulation of Peripheral Nerve Tissue Via Regenerative Sieve Microelectrodes

Matthew Reagan Macewan
Washington University in St. Louis

Follow this and additional works at: https://openscholarship.wustl.edu/eng_etds

 Part of the [Biomedical Engineering and Bioengineering Commons](#), [Electrical and Electronics Commons](#), and the [Neuroscience and Neurobiology Commons](#)

Recommended Citation

Macewan, Matthew Reagan, "Functional Electrical Stimulation of Peripheral Nerve Tissue Via Regenerative Sieve Microelectrodes" (2018). *Engineering and Applied Science Theses & Dissertations*. 328.
https://openscholarship.wustl.edu/eng_etds/328

This Dissertation is brought to you for free and open access by the McKelvey School of Engineering at Washington University Open Scholarship. It has been accepted for inclusion in Engineering and Applied Science Theses & Dissertations by an authorized administrator of Washington University Open Scholarship. For more information, please contact digital@wumail.wustl.edu.

WASHINGTON UNIVERSITY IN ST. LOUIS

School of Engineering & Applied Sciences

Dissertation Examination Committee:

Shelly Sakiyama-Elbert, Chair

Dennis Barbour

Jianmin Cui

Eric Leuthardt

Daniel Moran, Co-Chair

Functional Electrical Stimulation of Peripheral Nerve Tissue

Via Regenerative Sieve Microelectrodes

by

Matthew R. MacEwan

A dissertation presented to
The Graduate School
of Washington University in
partial fulfillment of the
requirements for the degree
of Doctor of Philosophy

May 2018

St. Louis, Missouri

© 2018, Matthew R. MacEwan

Table of Contents

List of Figures	v
List of Tables	ix
Acknowledgments.....	x
Abstract of the Dissertation.....	xi
Chapter 1: Introduction and Specific Aims	1
1-1: Introduction	1
1-2: Research Objectives and Specific Aims.....	4
1-3: Thesis Dissertation Overview and Organization.....	7
Chapter 2: Background Research.....	12
2-1: Functional Electrical Stimulation of the Peripheral Nerve	12
2-2: Peripheral Nerve Interfaces: Cuff Electrodes.....	13
2-3: Peripheral Nerve Interfaces: Intraneural Electrodes.....	16
2-4: Peripheral Nerve Interfaces: Regenerative Electrodes.....	19
2-5: Nerve Regeneration / Neurotrophic Support.....	23
Chapter 3: Micro-Sieve Electrode Fabrication and Testing	26
3-1: Introduction	26
3-2: Fabrication of Micro-Sieve Electrodes.....	26
3-3: Construction of Sieve Electrode Assemblies	29
3-4: Preparation of Fibrin-Based Delivery System	31
3-5: Surgical Implantation / Rodent Model	34
3-6: Regenerative Nerve Morphometry	39
3-7: Regenerative Nerve Histology	46
Chapter 4: Peripheral Nerve Interfacing Via Micro-Sieve Electrode.....	52
4-1: Introduction	52

4-2: Electrophysiology: Nerve Conduction	53
4-3: Electrophysiology: Evoked Muscle Force Measurement.....	58
4-4: Electrophysiology: Selective Nerve Interfacing.....	67
Chapter 5: Macro-Sieve Electrode Fabrication and Testing.....	76
5-1: Introduction	76
5-2: Fabrication of Macro-Sieve Electrodes	77
5-3: Construction of Sieve Electrode Assemblies	81
5-4: Preparation of Fibrin-Based Delivery System.....	84
5-5: Surgical Implantation / Rodent Model	86
5-6: Regenerative Nerve Morphometry	91
5-7: Regenerative Nerve Histology	96
Chapter 6: Peripheral Nerve Interfacing Via Macro-Sieve Electrode	103
6-1: Introduction	103
6-2: Electrophysiology: Nerve Conduction	104
6-3: Electrophysiology: Electromyography.....	110
6-4: Electrophysiology: Evoked Muscle Force Measurement.....	113
6-5: Functional Motor Recovery.....	121
6-6: Computational Modeling of Electrical Stimulation	125
6-7: Electrophysiology: Selective Nerve Interfacing - Monopolar Stimulation.....	132
6-8: Electrophysiology: Selective Nerve Interfacing - Multipolar Stimulation	141
Chapter 7: Clinical Enhancement of Macro-Sieve Electrodes	150
7-1: Introduction	150
7-2: Dual-Layer Macro-Sieve Electrodes.....	151
7-3: Selective Stimulation of Orthodromic Action Potentials.....	154
7-4: Wireless Stimulation	158

7-5: Therapeutic Electrical Stimulation.....	163
Chapter 8: Discussion	176
8-1: Conclusions	176
8-2: Future Research.....	181
References.....	184
Curriculum Vita	197
Appendix A: Regenerative Nerve Morphometry / Histology.....	201
Appendix B: Evoked Muscle Force Measurement	212
Appendix C: Computational Modeling of Macro-Sieve Electrodes.....	221

List of Figures

Figure 2.1	Silicone nerve cuff electrode.	14
Figure 2.2	Flat interface nerve electrode (FINE)	15
Figure 2.3	Utah slant electrode array (USEA)	17
Figure 2.4	Longitudinal intrafascicular electrode (LIFE)	18
Figure 2.5	Regenerative sieve electrode.....	19
Figure 2.6	Effect of NGF-loaded delivery system on axonal regeneration	24
Figure 3.1	SolidWorks model of custom regenerative micro-sieve electrode	27
Figure 3.2	Fabricated micro-sieve electrodes and sieve electrode assemblies.....	30
Figure 3.3	Surgical implantation of micro-sieve electrode assembly	36
Figure 3.4	High magnification view of implanted micro-sieve electrode.....	37
Figure 3.5	Trimetric views of 3-D reconstructions of explanted nerve segments	43
Figure 3.6	Regenerative nerve tissue explanted from micro-sieve electrode assembly containing fibrin-based delivery system loaded with NGF	45
Figure 3.7	Histomorphometric analysis of regenerative nerve tissue present in micro-sieve electrode assemblies and silicone nerve guidance conduits	50
Figure 4.1	CNAPs conducted through implanted micro-sieve electrode assemblies and silicone nerve guidance conduits.	56
Figure 4.2	Maximum amplitude of CNAPs conducted through implanted micro-sieve electrode assemblies and silicone nerve guidance conduits.	57
Figure 4.3	Maximum twitch response of reinnervated EDL muscles upon stimulation of the sciatic nerve using silver wire electrodes.....	61
Figure 4.4	Maximum isometric twitch force evoked by reinnervated EDL muscles upon stimulation of sciatic nerve using silver wire electrodes	62
Figure 4.5	Maximum isometric tetanic force evoked by reinnervated EDL muscles upon stimulation of sciatic nerve using silver wire electrodes	64

Figure 4.6	Comparison of nerve fiber recruitment via micro-sieve electrode assemblies.	69
Figure 4.7	Motor response to nerve activation via micro-sieve electrodes.....	71
Figure 5.1	Fabricated macro-sieve electrodes.....	78
Figure 5.2	Scanning electron micrographs of macro-sieve electrodes.....	79
Figure 5.3	Impedence measurements of electrode sites on macro-sieve electrodes ...	80
Figure 5.4	Fabricated macro-sieve electrodes and sieve electrode assemblies.....	82
Figure 5.5	High magnification view of implanted macro-sieve electrode.....	87
Figure 5.6	Explanted macro-sieve electrodes and regenerative nerve tissue.....	92
Figure 5.7	Explanted regenerative nerve tissue.....	93
Figure 5.8	Integration of macro-sieve electrodes into regenerative nerve tissue.....	94
Figure 5.9	Explanted regenerative nerve tissue.....	98
Figure 5.10	Epoxy nerve sections obtain at the macro-sieve/nerve interface.....	99
Figure 5.11	Histomorphometric analysis of regenerative nerve tissue present in macro-sieve electrode assemblies and silicone nerve guidance conduits.....	101
Figure 6.1	CNAPs conducted through implanted macro-sieve electrode assemblies and silicone nerve guidance conduits.....	107
Figure 6.2	Maximum amplitude of CNAPs conducted through implanted macro-sieve electrode assemblies and silicone nerve guidance conduits.....	108
Figure 6.3	EMGs recorded distal to implanted macro-sieve electrode assemblies and silicone nerve guidance conduits.....	110
Figure 6.4	Maximum amplitude of EMGs recorded distal to implanted macro-sieve electrode assemblies and silicone nerve guidance conduits.....	112
Figure 6.5	Maximum isometric force production in reinnervated EDL muscles.....	117
Figure 6.6	Calculation of sciatic function index via walking track analysis.....	122
Figure 6.7	Grid grip analysis.....	123
Figure 6.8	Measurement of maximal extension of ankle joint.....	124

Figure 6.9	Computational modeling of macro-sieve electrode assembly	127
Figure 6.10	Computational modeling of monopolar stimulation paradigms	129
Figure 6.11	Computational modeling of multipolar stimulation paradigms	130
Figure 6.12	Motor response to monopolar stimulation of peripheral nerve tissue via macro-sieve electrodes.....	134
Figure 6.13	Maximal selectivity of muscle activation achieved upon monopolar stimulation of peripheral nerve tissue via macro-sieve electrodes	135
Figure 6.14	Maximum isometric force production achieved upon electrical stimulation of peripheral nerve tissue via macro-sieve and micro-sieve electrodes.....	136
Figure 6.15	Motor response to multipolar stimulation of peripheral nerve tissue via macro-sieve electrodes.....	143
Figure 6.16	Maximal selectivity of muscle activation achieved upon multipolar stimulation of peripheral nerve tissue via macro-sieve electrodes	145
Figure 6.17	Comparative selectivity of monopolar / multipolar stimulation paradigms	146
Figure 6.18	Comparative performance of monopolar / multipolar stimulation paradigms	147
Figure 6.19	Comparative performance of novel macro-sieve electrodes and contemporary peripheral nerve interfaces.....	148
Figure 7.1	Assembly of dual-layer macro-sieve electrodes	151
Figure 7.2	Fabricated dual-layer macro-sieve electrodes.....	152
Figure 7.3	Maximum isometric tetanic force production via single-layer and dual-layer macro-sieve electrodes.....	153
Figure 7.4	Computational modeling of unidirectional action potential propagation ..	155
Figure 7.5	In vivo testing of unidirectional action potential initiation and propagation	156
Figure 7.6	Implantable wireless stimulator circuit.....	158
Figure 7.7	Stimulus output from implantable wireless stimulator circuit.....	159
Figure 7.8	In vivo implementation of wireless stimulation system	160

Figure 7.9	Functional electrical stimulation of peripheral nerve tissue via wireless macro-sieve electrodes.....	161
Figure 7.10	System of implantable wireless nerve stimulators for use in applying brief electrical stimulation.....	164
Figure 7.11	Output of wireless nerve stimulators upon chronic in vivo implantation..	166
Figure 7.12	Accelerated functional recovery after brief electrical stimulation.....	170

List of Tables

Table 3.1	Experimental Design: Study of regenerative micro-sieve electrode.....	38
Table 5.1	Experimental Design: Study of regenerative macro-sieve electrode.....	89
Table 7.1	Overview of functional recovery observed in the presence and absence of brief electrical stimulation.	173

Acknowledgments

It has been an honor and a privilege to complete my training in the Department of Biomedical Engineering at Washington University. I would like to thank my thesis advisor, Dr. Daniel Moran, who has provided me with invaluable support, guidance, and opportunities throughout my time in the department. I would like to thank my colleagues in the lab, including Erik Zellmer, Jesse Wheeler, Daku Siewe, Adam Rouse, Manu Stephen, Paul Gamble, and Zack Ray for all of their insight and assistance. Finally, I would like to thank my family, including my wife Sarah, my daughters Ava and Felicity, and my parents for their love and support.

Matthew R. MacEwan

Washington University in St. Louis

May 2018

ABSTRACT OF THE DISSERTATION

Functional Electrical Stimulation of Peripheral Nerve Tissue
Via Regenerative Sieve Microelectrodes

by

Matthew R. MacEwan

Doctor of Philosophy in Biomedical Engineering

Washington University in St. Louis, 2018

Professor Shelly Sakiyama-Elbert, Chair

Professor Daniel Moran, Co-Chair

Functional electrical stimulation (FES) of peripheral nervous tissue offers a promising method for restoring motor function in patients suffering from complex neurological injuries. However, existing microelectrodes designed to stimulate peripheral nerve are unable to provide the type of stable, selective interface required to achieve near-physiologic control of peripheral motor axons and distal musculature. Regenerative sieve electrodes offer a unique alternative to such devices, achieving a highly stable, selective electrical interface with independent groups of regenerated nerve fibers integrated into the electrode. Yet, the capability of sieve electrodes to functionally recruit regenerated motor axons for the purpose of muscle activation remains largely unexplored. The present dissertation aims to examine the potential role of regenerative electrodes in FES applications by testing the unifying hypothesis that sieve electrodes of various design and

geometry are capable of selectively stimulating regenerated motor axons for the purpose of controlling muscle activation. This hypothesis was systematically tested through a series of experiments examining the ability of both micro-sieve electrodes and macro-sieve electrodes to achieve a stable interface with peripheral nerve tissue, electrically activate small groups of regenerated motor axons, and selectively recruit motor units present in multiple distal muscles. Custom sieve electrodes were fabricated via sacrificial photolithography. In vivo testing in rat sciatic nerve validated the ability of chronically-implanted regenerative sieve electrodes to support motor axon regeneration and integrate into peripheral nerve tissue. Sieve electrode geometry was shown to strongly modulate axonal regeneration, muscle reinnervation, and device functionality, as high-transparency macro-sieve electrodes facilitated superior neural integration and functional recovery compared to low-transparency micro-sieve electrodes. Inclusion of neurotrophic factors into sieve electrode assemblies increased axonal regeneration through implanted electrodes and improved the quality of the sieve/nerve interface in low-transparency devices. In vivo testing in rat sciatic nerve further validated the ability of chronically-implanted regenerative sieve electrodes to facilitate FES of regenerated motor axons and selective recruitment of distal musculature. Selective stimulation of regenerated motor axons using implanted micro- and macro-sieve electrodes enabled effective, external control of muscle activation within anterior and posterior compartments of the lower leg (e.g. ankle plantarflexion / dorsiflexion). Selective activation of distal musculature was achieved through modulation of stimulus amplitude, channel activation, and field steering. In summary, the present body of work provides initial evidence of the utility of regenerative electrodes as a means of selectively interfacing peripheral nerve tissue for

the purpose of restoring muscle activation and motor control. These findings further highlight the clinical potential of implantable microelectrodes capable of intimately integrating into host neural tissue.

Chapter 1: Introduction and Specific Aims

1-1: Introduction

Spinal cord injury (SCI) is a devastating condition that represents a significant domestic and international public health problem (Ackery et al; 2004). The incidence of new SCIs is estimated at nearly 12,000 cases annually in the United States and nearly 130,000 cases annually world-wide (Alexander et al; 2007). Recovery from a complete SCI is exceedingly rare; thus most patients are left with permanent disability including paraplegia and tetraplegia. Provided the average age of affected individuals is less than 40 years, SCI commonly results in a significant impact on quality of life, longevity, and economic productivity (Alkadhi et al; 2005, Jackson et al; 2012). Unfortunately, the range of contemporary therapeutic and rehabilitative interventions for individuals with SCI is limited. To date, no medical intervention exists that is capable of facilitating functional restoration and use of a patient's paralyzed limbs; rated by individuals with SCI as one of the highest priorities in their continued care and recovery.

Numerous types of microelectrodes have been designed to electrically interface peripheral nerve tissue, yet few have achieved stable, high-specificity stimulation and recording of peripheral nerve fibers (Navarro et al; 2005). Nerve cuff electrodes represent the most common interface to the peripheral nervous system (Loeb et al; 1996). Cuff electrodes consist of an implantable elastomeric conduit that wraps around a target nerve and ensures a stable electrical interface between integrated metallic electrode sites

and underlying nerve tissue. Due to the extraneural location and low channel count, cuff electrodes require high stimulus amplitudes to activate nervous tissue and dramatically limit recruitment of axonal populations deep within nerve fascicles. Prior studies have suggested that cuff electrodes are poorly suited for selective, subfascicular nerve stimulation, and are unable to elicit fine motor control in distal musculature needed for advanced neuroprosthetic applications in SCI populations (Veraat et al; 1993). Multi-electrode arrays, such as the Utah slanted electrode array (USEA), represent an alternative class of electrode commonly used to interface peripheral nerves (Normann et al; 2007, Branner et al; 2004). USEAs consist of a 10-by-10 grid of silicon needle electrodes of varying length (0.5-1.5 mm) that is pneumatically inserted into target nerves in order to achieve close proximity between conducting metalized contacts and peripheral nerve fibers. Prior studies examining acute in vivo implementation of USEAs in human and animal models have demonstrated highly selective activation of peripheral axons at low current amplitudes ($< 20 \mu\text{A}$). Yet, paired studies demonstrated that USEAs are prone to failure in vivo and may damage proximal neural tissue. Mechanical mismatch between silicon needle electrodes and peripheral nerve tissue typically results in breakage of numerous tines, damage of local axons, and degradation of the neural interface following long-term implantation (Branner et al; 2004). Taken together, these results demonstrate the critical functional limitations of existing microelectrodes and conventional nerve interfacing strategies.

Regenerative sieve electrodes offer a novel approach to achieving a chronic, stable, high-specificity interface with peripheral nerve tissue. Unlike extraneural and intraneural devices, sieve electrodes are designed to fully integrate into the native

structure of the nerve and thereby achieve an intimate electrical interface with peripheral nerve fibers (Kovacs et al; 1992). To accomplish this goal, thin-film regenerative sieve electrodes are microsurgically implanted within a peripheral nerve (Zhao et al; 1997). Regenerating axons pass through via holes in the electrode, simultaneously integrating the electrode into the structure of the nerve and parsing axons into small, independent groups. Bi-directional electrical interfacing of integrated axons may then be achieved utilizing active electrode sites circumscribing select via holes. Prior studies support the novel utility of regenerative electrodes, and confirm the ability of devices to facilitate axonal regeneration and nerve integration (Navarro et al; 2005). Yet, the capability of regenerative sieve electrodes to functionally recruit motor axons, control distal musculature, and serve as a critical component of advanced FES systems is largely unknown. The work presented in this thesis will investigate the capability of regenerative sieve electrodes to serve as an advanced interface to peripheral motor axons and test the unifying hypothesis that sieve electrodes of various design and geometry are capable selectively controlling muscle activation for future rehabilitative applications.

1-2: Research Objectives and Specific Aims

Functional electrical stimulation (FES) of peripheral nervous tissue offers a promising method for restoring motor function in patients suffering from complex neurological injuries. However, existing microelectrodes designed to stimulate peripheral nerve are unable to provide the type of stable, selective interface required to achieve near-physiologic control of peripheral motor axons and distal musculature. Regenerative sieve electrodes offer a unique alternative to such devices, achieving a highly stable, selective interface with independent groups of regenerated nerve fibers integrated into the electrode. Yet, the capability of sieve electrodes to functionally recruit regenerated motor axons for the purpose of muscle activation remains largely unexplored. The present dissertation aims to examine the potential role of regenerative electrodes in FES applications by testing the unifying hypothesis that sieve electrodes of various design and geometry are capable of selectively stimulating regenerated motor axons for the purpose of controlling muscle activation. This hypothesis was systematically tested through a series of experiments examining the ability of both micro-sieve electrodes (Specific Aim 1) and macro-sieve electrodes (Specific Aim 2) to achieve a stable interface with peripheral nerve tissue, electrically activate small groups of regenerated motor axons, and selectively recruit motor units present in multiple distal muscles.

Specific Aim 1: To test the hypothesis that *micro-sieve* electrodes are capable of selectively stimulating regenerated motor axons for the purpose of functionally recruiting distal musculature.

Micro-sieve electrodes (sieve electrodes containing 100-600 via holes, 10-200um in diameter) achieve an intimate interface with peripheral nerve tissue by forcing regenerating axons to extend through numerous, small-diameter via holes in the body of the electrode. Small groups of regenerated axons present within individual via holes may then be independently interfaced through metallic ring electrodes circumscribing some holes. In this manner, select groups of axons throughout the regenerated nerve can be interfaced by activating specific ring electrodes within the porous region of the device. Previous studies have demonstrated that this method of interfacing is particularly useful in selectively recording neural activity from small groups of sensory fibers in vivo. Yet, few studies have investigated whether routing electrical impulses to specific metalized rings enables selective recruitment of small groups of regenerated motor axons, and, subsequently, innervated musculature. To assess this capability it is necessary to examine the degree to which micro-sieve electrodes facilitate the regeneration of motor axons through integrated via holes.

Part 1A will examine the ability of micro-sieve electrodes to support the regeneration of functional motor axons, and investigate methods for improving axonal regeneration through via holes in the electrode. To assess whether micro-sieve electrodes may be useful in FES applications, the ability of micro-sieve electrodes to electrically activate regenerated motor axons and associated motor units must be evaluated. **Part 1B will examine the ability of micro-sieve electrodes to stimulate independent groups of regenerated motor axons as a means of selectively recruiting distal musculature.**

Specific Aim 2: To test the hypothesis that *macro-sieve* electrodes are capable of selectively stimulating greater numbers of regenerated motor axons, and more effectively recruiting distal musculature than *micro-sieve* electrodes.

Micro-sieve electrodes possess many features that limit their ability to selectively stimulate large numbers of regenerated motor axons. The low transparency of the porous region dramatically reduces the number of nerve fibers regenerating through the electrode, while the small size and finite number of metalized rings limit the percentage of regenerated fibers interfaced. In an effort to develop a more effective regenerative electrode, a novel electrode geometry has been proposed. The “macro-sieve electrode” contains a small number of large via holes (9 via holes, 600um in diameter), maximizing nerve regeneration through the device, and larger metalized electrodes around the via holes, increasing the percentage of nerve fibers interfaced. Utilizing field steering techniques and stimulus amplitude modulation, macro-sieve electrodes possess the potential to selectively interface greater numbers of motor axons regenerating through the electrode. To assess whether macro-sieve electrodes provide a more effective means of interfacing peripheral nervous tissue, it is necessary to examine whether macro-sieve electrodes facilitate increased regeneration of motor axons through integrated via holes. **Part 2A will examine the ability of macro-sieve electrodes to support the regeneration of increased numbers of functional motor axons, and investigate methods for improving axonal regeneration through via holes in the electrode.** To assess whether macro-sieve

electrodes gain more effective control over distal motor groups, the ability of macro-sieve electrodes to selectively recruit larger numbers of regenerated motor axons and larger proportions of distal musculature must be evaluated. **Part 2B will examine the ability of macro-sieve electrodes to independently stimulate greater numbers of regenerated motor axons as a means of more selectively recruiting distal musculature.**

1-3: Thesis Dissertation, Overview, and Organization

In this dissertation, novel micro-sieve and macro-sieve electrodes will be fabricated, assembled, and implanted into rodent peripheral nerve. All animals will be recovered prior to terminal evaluation of the nerve / electrode interface. Histological, behavioral, and electrophysiological means will be utilized to evaluate the ability of implanted electrodes to support axonal regeneration in vivo, and to facilitate selective, functional recruitment of peripheral motor axons and distal musculature. In order to complete this objective, two key hurdles must be overcome: 1) development, fabrication, and assembly of micro-sieve and macro-sieve electrodes, and 2) cultivation of a mammalian animal model and related metrics best suited for chronic in vivo evaluation of axonal regeneration and functional nerve interfacing.

In total, this thesis is divided into six chapters. The first chapter introduces the dissertation and provides background on the project. The first chapter describes previous research in the areas of functional electrical stimulation, peripheral nerve interfacing, and nerve regeneration / neural engineering. The project background is provided to demonstrate the clinical need and technological feasibility of the present project, and

highlight alternative strategies for interfacing and recruiting peripheral nerve tissue for functional purposes.

The second chapter of this thesis describes the design, fabrication, and in vivo evaluation of novel regenerative micro-sieve electrodes. Fabrication of micro-sieve electrodes via sacrificial photolithography is outlined, along with methods for pre-operative testing and terminal construction of implantable sieve electrode assemblies. A description of the selected in vivo animal model, a rat sciatic nerve model, is also described. An evaluation of the microsurgical application of fabricated micro-sieve electrodes within the animal model is then provided. Following in vivo implementation, the ability of micro-sieve electrodes to support axonal regeneration and functional nerve integration is evaluated via terminal explantation, nerve morphometry, and nerve histology performed at the nerve / electrode interface. Verification of the ability of micro-sieve electrodes to support axonal regeneration and peripheral nerve integration will enable further testing and evaluation of the ability of micro-sieve electrodes to functionally interface and recruit regenerative nerve tissue.

The third chapter of this thesis examines the ability of chronically-implanted micro-sieve electrodes to functionally interface regenerative peripheral nerve tissue, specifically regenerated motor axons. Electrophysiological evaluation of functional nerve regeneration through implanted micro-sieve electrodes is presented. Conduction of CNAPs through implanted sieve electrode assemblies and activation of distal musculature are presented as measured of functional nerve regeneration. Verification of the functional status of regenerative nerve tissue present within implanted micro-sieve electrodes will enable detailed examination of peripheral nerve interfacing via

chronically-implanted micro-sieve electrodes. Induction of CNAPs and recruitment of distal musculature via implanted micro-sieve electrodes is then presented. Specifically, activation of distal musculature is examined as a measure of the ability of micro-sieve electrodes to selectively recruit regenerative motor axons and innervated motor targets. The performance of micro-sieve electrodes as a means of selectively interfacing peripheral nerve tissue is presented and utilized as a baseline for the design and evaluation of macro-sieve electrodes.

The fourth chapter describes the design, fabrication, and in vivo evaluation of novel regenerative macro-sieve electrodes. Macro-sieve electrodes are designed to maximize device transparency, and thereby support maximal axonal regeneration and preservation of distal motor target. Fabrication of macro-sieve electrodes via sacrificial photolithography is outlined, along with methods for construction of macro-sieve electrode assemblies. A description of the microsurgical implantation of fabricated macro-sieve electrodes is then provided. The ability of micro-sieve electrodes to support axonal regeneration and functional nerve integration is evaluated via terminal explantation, nerve histology, and retrograde labelling performed at the nerve / electrode interface. Comparative evaluation of nerve regeneration through macro-sieve electrodes and micro-sieve electrodes, both with and without neurotrophic support, is presented. Verification of the ability of macro-sieve electrodes to support axonal regeneration and peripheral nerve integration will enable evaluation of selective interfacing and recruitment of regenerative nerve tissue.

The fifth chapter examines the ability of chronically-implanted macro-sieve electrodes to functionally interface regenerative peripheral nerve tissue and distal

musculature. Electrophysiological evaluation of functional nerve regeneration through implanted macro-sieve electrodes is presented. Comparisons between functional nerve regeneration through macro-sieve and micro-sieve electrodes are made. Computational modeling is then presented as a means of examining the potential of macro-sieve electrodes to successfully facilitate selective axonal stimulation via current routing techniques. A detailed examination of peripheral nerve interfacing via chronically-implanted macro-sieve electrodes is then described. Selective recruitment of distal musculature via monopolar and multi-polar stimulation paradigms, applied via chronically-implanted macro-sieve electrodes, is outlined. Activation of distal musculature is examined as a measure of the ability of macro-sieve electrodes to selectively recruit regenerative motor axons and innervative motor targets. The performance of macro-sieve electrodes as a means of selectively interfacing peripheral nerve tissue is presented and compared to previous results obtained using micro-sieve electrodes.

The sixth and final chapter of this thesis will examine approaches to improve the clinical performance and translation of regenerative sieve electrodes. Clinical translation of implantable micro-electrode technologies is dependent on multiple factors, including the selectivity of the electrode, the quality of the interface, and the usability of the device. Approaches to improve the quality of the nerve/electrode interface and the usability of the device, such as the implementation of alternative nerve conduits and the implementation of wireless technologies are presented and evaluated. Demonstrations of further refinement of sieve electrode system are outlined as a means of validating future pathways for clinical translation.

The dissertation will conclude with a discussion of the results, implications for further development of peripheral nerve interface technologies, and future directions for research into regenerative electrodes.

Chapter 2: Background Research

2-1: Functional Electrical Stimulation of the Peripheral Nerve

Peripheral nerves represent a critical component of the human nervous system.

These cord-like structures are composed of multiple nerve fibers which transmit sensorimotor information between the central nervous system and the remainder of the body. While it has long been known that peripheral nerve tissue is excitable (Galvani et al.), an advanced understanding of the bioelectric mechanisms underlying peripheral nerve function was only established in the middle of the 20th century. Pioneering work conducted by Cole and Curtis and Katz and Hodgkin, provided key demonstrations that depolarization of the cell membrane and the imbalance of sodium ions was directly related to action potential initiation (Cole et al; 1939, Katz et al; 1949). Hodgkin and Huxley provided further insight in that current flow across the axonal membrane was directly related to sodium and potassium conductance and that the conductance varied according to the membrane voltage (Hodgkin et al; 1952). These advances resulted in the mathematical characterization of membrane dynamics and action potential propagation, which set the stage for contemporary discoveries of voltage-gated ion channels and the modern study of neurophysiology. Presently, it is well understood that peripheral nerves conduct information in the form of high-frequency trains of electrical impulses which propagate along the length of individual axons. Exogenous stimulation or recording of

the electrical signals carried within peripheral nerve tissue provides a unique and effective means of accessing and controlling various processes throughout the body.

The peripheral nervous system is a common biological target for neuroprosthetic devices (Navarro et al; 2005). Peripheral nerves are easily exposed, possess a consistent architecture, and allow simultaneous access to numerous motor, sensory, and autonomic pathways. Microelectrode devices implanted in or around peripheral nerves have the potential to simultaneously stimulate and record select motor and sensory fibers, effectively establishing a bi-directional neural interface. Functional electrical stimulation of motor axons via implanted microelectrodes provides a superior method for controlling distal musculature and restoring motor function. Specifically, electrical stimulation of nerve tissue requires low current amplitude, allows for simultaneous recruitment of motor units in multiple muscles, and elicits graded fatigue-resistant responses in distal musculature (Wei et al; 2009). While many microelectrode devices have been designed and tested toward this end, few studies have demonstrated chronic, high resolution motor control through functional electrical stimulation of peripheral nerves *in vivo*. The primary cause of this failure remains the inability of current microelectrode devices to achieve a stable, chronic, high specificity interface with peripheral nervous tissue.

2-2: Peripheral Nerve Interfaces: Cuff Electrodes

Numerous types of microelectrodes have been designed to electrically interface peripheral nerve tissue, yet few have elicited fine motor control in chronic *in vivo* applications (Naples et al; 1990). The cuff electrode is the most common device utilized to interface peripheral nerves. Based on an extraneural design, cuff electrodes

consist of two or more metal electrodes embedded in an insulated elastomeric sheath that wraps around a target nerve. Metal electrodes are maintained in epineurial positions around the circumference of the host nerve by the coiled elastomeric sheath, which simultaneously exerts a compressive force ensuring a stable electrical interface between the electrodes and the nerve tissue.

Prior studies demonstrating prolific *in vivo* use of cuff electrodes in both human and animal trials have fully described both the advantages and disadvantages of the device (Naples et al; 1990). Cuff electrodes are generally favored for their simplicity, resulting from their basic

construction, general resilience, minimal effect on nerve tissue, and ease of implantation. Yet, cuff electrodes generally possess inferior nerve interface capabilities. Due to the epineurial location and low

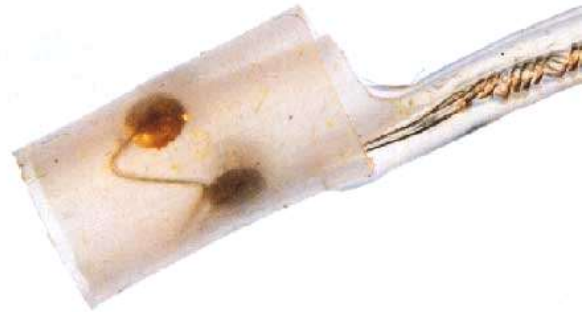


Figure 2-1. Silicone nerve cuff electrode.
(Adapted from Tarler et al.; 2004; Grill et al.; 2000)

numbers of metal electrodes, cuff electrodes require high stimulus amplitudes to activate nervous tissue and dramatically limit electrode access to axonal populations present in nerve fascicles.

Prior studies have suggested that cuff electrodes are poorly suited for selective, subfascicular nerve stimulation required to achieve fine motor control, and are instead better suited for stimulation of whole nerves (Loeb et al; 1996, Veraat et al; 1993). Even through the use of field steering, cuff electrodes are also generally incapable of

selectively stimulating individual axons or small groups of axons within an interfaced nerve, and are instead limited to electrical stimulation of small subfascicular regions.

Additional types of extraneural electrodes have been designed to address the limitations exhibited by standard cuff electrodes. Slowly penetrating interfascicular nerve electrodes (SPINEs) and flat-interface nerve electrodes (FINEs) were both designed to improve selective nerve stimulation by increasing metal electrode access to axonal populations (Tyler et al; 2002,

Tyler et al; 1994). Specifically, SPINE electrodes contain blunt elastomeric processes projecting radially from the inner surface of the electrode sheath

which support embedded metal electrodes. Once introduced to a host

nerve, compressive force exerted by the elastomeric sheath slowly forces the processes between individual nerve fascicles, effectively rearranging the epineurium and bringing metal electrodes in closer proximity to axonal populations. Prior studies examining the use of SPINE electrodes *in vivo* have demonstrated reduced stimulus thresholds and superior selectivity compared to cuff electrodes (Tyler et al; 1997). Additional studies suggest that the constant force applied to the host nerve by the penetrating processes may result in compressive axonopathy, limiting use in chronic applications (Tyler et al; 2003).

In contrast, FINE electrodes consist of multiple metal electrodes embedded in a flat elastomeric sheath. When introduced to a host nerve, compressive force applied by the sheath gently reshapes nerve tissue into an ovoid or rectangular geometry. Nerve

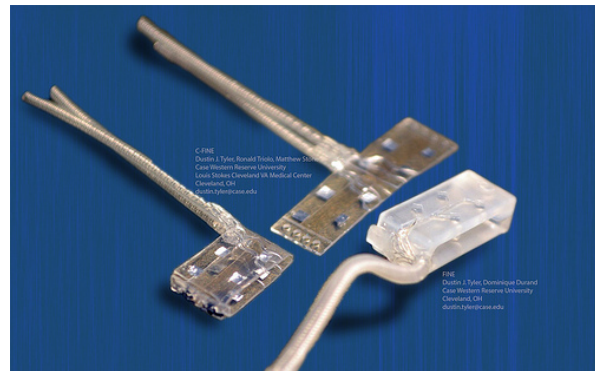


Figure 2-2. Flat interface nerve electrode (FINE).
(Adapted from Tyler et al.; 2014)

reshaping flattens and separates nerve fascicles typically located in the center of peripheral nerves, thereby reducing the distance between metal electrodes and axonal populations. Investigations of FINE electrode capabilities *in vivo* demonstrate similar reductions in stimulus thresholds and superior selectivity compared to cuff electrodes (Leventhal et al; 2004). Long-term studies also suggest that the application of compressive force required for nerve reshaping induces compressive axonopathy, damages large nerve fibers, and reduces nerve fiber myelination, possibly limiting chronic *in vivo* use of FINE electrodes (Tyler et al; 2003). Overall, extraneural microelectrodes may excel in ease of use but demonstrate inferior nerve stimulation capabilities resulting from the innate restriction of metal electrodes to epineurial positions. Extraneural microelectrodes are therefore unable to elicit fine motor control in distal musculature and are sub-optimal for advanced neuroprosthetic applications.

2-3: Peripheral Nerve Interfaces: Intraneural Electrodes

Intraneural microelectrode devices have demonstrated superior stimulation selectivity compared to extraneural devices upon implantation in peripheral nerve tissue. Multi-electrode arrays, such as the Utah electrode array (UEA) and Utah slanted electrode array (USEA), represent the most common type of intraneural electrode used to interface peripheral nerves (Normann et al; 2007). USEAs, in specific, consist of a 10-by-10 grid of silicon needle electrodes of varying length (0.5-1.5 mm) projecting out of a silicon-glass substrate. USEAs are pneumatically inserted into target nerves and anchored through the use of silicone conduits such that the tips of the various needle

electrodes are evenly spaced throughout the cross-sectional area of the nerve. Unlike extraneural electrodes, needle electrodes of USEAs penetrate both the epineurium and perineurium of interfaced nerves, allowing close proximity between conducting tips of the needle electrodes and axons present in nerve fascicles.

Prior studies examining acute *in vivo* implementation of USEAs in human and animal models have demonstrated nerve fiber activation at low current amplitudes (< 20 uA) and highly selective activation of small groups of axons in interfaced peripheral nerves (McDonnall et al; 2004, Branner et al; 2001). Yet, despite superior nerve

stimulation capabilities, USEAs are prone to failure *in vivo* and may damage neural tissue during implantation. While insertion of needle electrodes into nerve fascicles greatly improves electrode access to axonal populations, the mechanical mismatch between silicon needle electrodes and

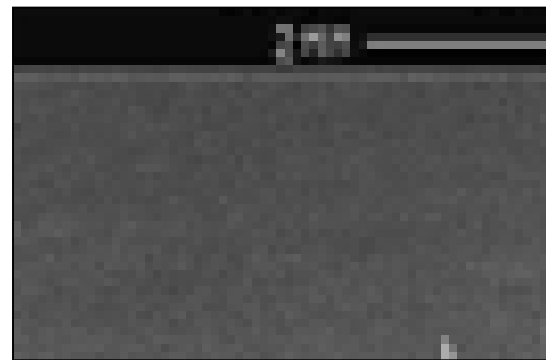


Figure 2-3. Utah slant electrode array (USEA).
(Adapted from Branner et al.; 2001)

peripheral nerve tissue places great stress on both the device and the interfaced tissue.

Micro-translation and micro-vibration of the implanted USEA *in vivo* typically results in breakage of numerous electrodes, damage of local axons, and induction of reactive tissue changes and fibrous capsule formation around the device. Together these effects slowly limit both USEA access to peripheral nerve tissue and the efficacy of the device at chronic time-points (Branner et al; 2004). Prior studies have also demonstrated that micro-translation exhibited by implanted USEAs also reduces the stability of single-unit

recordings, suggesting that USEAs may be limited in their ability to form a reliable bi-direction interface with peripheral nerve tissue.

Additional microelectrodes have also been designed using an intrafascicular approach to nerve interfacing. Longitudinally implanted intrafascicular electrodes (LIFEs) consist of thin, insulated filaments containing a conductive core and one or more exposed contact sites (Lawrence et al; 2003). Single LIFE electrodes are longitudinally inserted into individual nerve fascicles via microsurgical techniques such that the active contact site of the electrode is located inside the fascicle. Prior *in vivo* studies of implanted LIFE electrodes demonstrated fascicular activation at low stimulus amplitudes, yet little sub-fascicular stimulation selectivity (Yoshida et al; 1993). Implantation of LIFE electrodes was also noted to be very challenging, resulting in decreased regularity and consistency in electrode placement throughout target nerves. The one-to-one ratio of LIFE electrodes to nerve

fascicles also demands multiple devices, rather than one standard device, to interface multiple fascicles innervating various muscle



Figure 2-4. Longitudinal intrafascicular electrode (LIFE).
(Adapted from Micera et al.; 2011)

groups. Further evaluation of implanted LIFE electrodes revealed that, similar to USEAs, the rigidity of the conductive filaments made electrodes prone to micro-translation and micro-vibration, which lead to pronounced fibrous encapsulation of implanted electrodes and reduced interface capabilities over time. Overall, intraneural microelectrodes provide superior nerve interface capabilities and sub-fascicular selectivity, but do not possess the

stability, resilience, and biocompatibility necessary for chronic *in vivo* use. Current intraneural microelectrodes are therefore also unsuitable for advanced neuroprosthetic applications.

2-4: Peripheral Nerve Interfaces: Regenerative Electrodes

Regenerative sieve microelectrodes represent a novel approach to achieving a chronic, stable, high-specificity interface with peripheral nerve tissue for the purpose of fine motor control. Unlike extraneural and intraneural devices, sieve microelectrodes are designed to become fully integrated into the native structure of peripheral nerves, allowing devices to achieve an intimate electrical interface with surrounding nerve tissue

(Navarro et al; 2005). To accomplish this goal, sieve microelectrodes, consisting of a thin polymeric or silicon substrate containing numerous small via holes circumscribed by thin metal ring electrodes, are microsurgically implanted between the transected ends of a peripheral nerve

(Kovacs et al; 1992). Regenerating axons

originating in the proximal nerve stump pass through via holes in the electrode, simultaneously integrating the electrode into the structure of the nerve and parsing axons into small, independent groups. Bi-directional electrical interfacing of individual axons

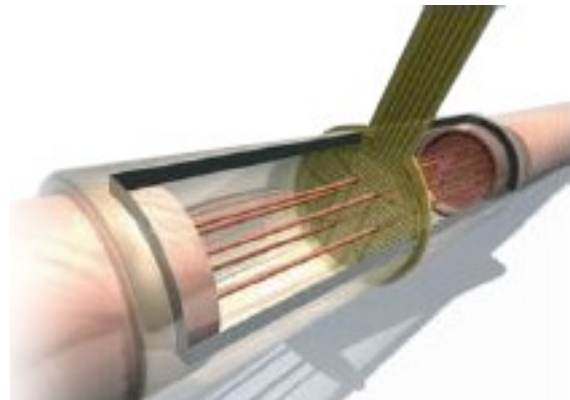


Figure 2-5. Regenerative sieve electrode.
(Adapted from Lago et al.; 2004)

or small groups of axons present within individual via holes is then facilitated through the metal ring electrode circumscribing select holes.

Utilizing this strategy, sieve microelectrodes have the potential to achieve an electrical interface with peripheral nerve tissue superior to that of conventional extraneural and intraneural electrodes. Specifically, sieve microelectrodes offer a more stable interface than conventional devices, and are capable of selectively stimulating and recording smaller independent groups of axons than conventional devices. The potential capabilities of sieve microelectrodes suggest they may be useful in interfacing individual motor axons to achieve fine motor control in distal musculature, and may therefore be highly useful in advanced neuroprosthetic systems.

To date, multiple studies have confirmed the superior nerve interface capabilities of sieve microelectrodes. Many studies have demonstrated successful implantation of sieve microelectrodes in peripheral nerves and successful axonal regeneration through implanted sieve electrodes of varying geometry and design (Zhao et al; 1997, Steiglitz et al; 1997, Akin et al; 1994, Wallman et al; 2001). In select cases of robust axonal regeneration through implanted sieve microelectrodes, upwards of 19,000 nerve fibers and 8,800 myelinated fibers were exhibited passing through substrates implanted in rat sciatic nerves (Lago et al; 2007). Additional histological studies determined that robust axonal regeneration through sieve electrodes resulted in 20 - 40 axons inside individual via holes (Klinge et al; 2001). Such findings confirm that peripheral nerves are able to fully integrate implanted porous arrays into the native structure of the nerve, as predicted. The ability of sieve microelectrodes to electrically interface regenerated nerve tissue was assessed in additional studies achieving successful

nerve regeneration through implanted electrodes. A majority of these studies focused on the use of implanted sieve microelectrodes to obtain single-unit recordings from peripheral nerve tissue *in vivo*. Prior studies demonstrated that sieve electrodes are capable of reliably recording spontaneous and evoked action potentials in individual axons and small groups of axons in various types of nerves, including rat sciatic nerve (Ramachandran et al; 2006), glossopharyngeal nerve (Della Santina et al; 1997, Mensinger et al; 2000), vagus nerve (Kawada et al; 2004), etc., for up to 11 months, post-operatively. These results demonstrate the ability of sieve microelectrodes to electrically interface small, independent groups of axons within the regenerated nerve, and confirm sieve electrodes form an electrical interface with nerve tissue that is superior to that achieved by conventional electrodes.

Despite these capabilities, relatively few studies have attempted to use sieve microelectrodes to selectively stimulate small, independent groups of motor axons. Prior studies have demonstrated that stimulation of ring electrodes on implanted sieve microelectrodes initiates propagating action potentials in regenerated axons of unknown modality (Lago et al; 2007). Additional studies have demonstrated anecdotal evidence that stimulation of similar groups of regenerated axons via individual ring electrodes results in an electrophysiological response in distal musculature (Lago et al; 2005). Yet, this qualitative observation was limited to one animal, and lacked further exploration of muscle recruitment or force production resulting from electrical activation of the implanted sieve electrode. To date, the capability and use of sieve microelectrodes to control motor output through selective stimulation of regenerated motor axons remains largely unexplored.

One cause for the lack of information concerning the use of sieve microelectrodes as means of stimulating small groups of regenerated motor axons is the variability of successful nerve regeneration through implanted electrodes. While select studies have demonstrated robust axonal regeneration through sieve electrode assemblies (Lago et al; 2007, Lago et al; 2005), a survey of all studies involving regenerative microelectrodes revealed that nerve regeneration through implanted devices is highly variable. Previous investigations corroborated results obtained by pilot studies conducted in our laboratory, which suggest that identical groups of un-modified sieve microelectrodes are capable of supporting both robust axonal regeneration and no axonal regeneration when implanted in similar nerves. Additional studies demonstrated that implanted sieve electrodes impede nerve regeneration, both quantitatively and temporally, compared to polymeric nerve guidance conduits (Navarro et al; 1996). Results of retrograde labeling studies also revealed that this impedance affects large, myelinated motor axons to a greater extent than smaller sensory and autonomic fibers (Negredo et al; 2004). Together, variability in the presence of nerve regeneration and impedance of regenerating nerve tissue results in delayed and frequently unsuccessful reinnervation of distal motor targets by regenerating motor axons. This paucity of functional reinnervation of distal musculature precludes assessment of functional electrical interfacing via sieve microelectrodes. As a result very few studies have been successful in functionally electrically stimulating regenerated motor axons using sieve microelectrodes. While limiting the study of electrode interface capabilities, significant variability in sieve electrode capabilities *in vivo* also dramatically hinders the investigation of more sophisticated clinical applications for sieve microelectrodes which require consistent functionality of implanted devices. Therefore,

advancement of both the basic study and clinical implementation of sieve microelectrodes as neural interfaces depends on the improved reliability and increased quantity of axonal regeneration through implanted device.

2-5: Nerve Regeneration and Neurotrophic Support

One approach to increasing peripheral nerve regeneration through implanted sieve microelectrodes relies on the use of modified sieve electrode assemblies containing neuroregenerative features. To date many nerve guidance conduits and neuroregenerative matrices have been investigated as a means of improving peripheral nerve regeneration *in vivo* (Fine et al; 2007). Such neuroregenerative systems rely on various polymeric conduits, neuroregenerative scaffolds and hydrogels, and the controlled delivery of growth factors, extracellular matrix proteins, and glial cells to induce axonal sprouting and regeneration across gaps in peripheral nerve tissue. One neuroregenerative system that has demonstrated considerable promise in enhancing peripheral nerve regeneration is a heparin-containing, fibrin-based delivery system capable of controlled release of various neurotrophic factors (Sakiyama-Elbert et al; 2001, Sakiyama-Elbert et al; 2000, Maxwell et al; 2005, Sakiyama-Elbert et al; 2000, Willerth et al; 2007, Taylor et al; 2004). In general, the delivery system consists of heparin-bound neurotrophic factors non-covalently immobilized within a fibrin matrix through the use of a bi-domain peptide containing a heparin-binding domain and transglutaminase substrate. Sequestration within the fibrin matrix allows slow, controlled diffusion of loaded neurotrophic factors from the scaffold until cellular infiltration occurs during axonal regeneration, effectively timing NGF release to occur upon the arrival of

extending neurites. Prior studies have demonstrated the system's neuroregenerative potential, as fibrin-based delivery system loaded with 100 ng/ml β -NGF enhanced neurite extension from cultured embryonic chick dorsal root ganglia *in vitro* (Wood et al; 2008).

Additional *in vivo* trials demonstrated that silicone nerve guidance conduits containing fibrin-based delivery

system loaded with 50 ng/ml β -NGF or 100 ng/ml GDNF enhanced nerve regeneration across 13 mm defects in rat sciatic nerve compared to empty silicone conduits (Lee et al; 2003, Wood et al; 2008; Wood et al; 2010). While previous studies have not investigated the ability of fibrin-based delivery system to enhance nerve regeneration through artificial substrates or microdevices, it is believed that the application of such a regenerative matrix to sieve electrode assemblies could increase axonal regeneration through implanted electrodes and functional reinnervation of distal motor targets, as well as improve chronic survival of regenerated axons and protect against compressive axonopathy.

The present dissertation aims to test the hypothesis that regenerative sieve electrodes enable selective functional electrical stimulation of peripheral nerve tissue and effective control of muscle activation. The effect of sieve electrode geometry and

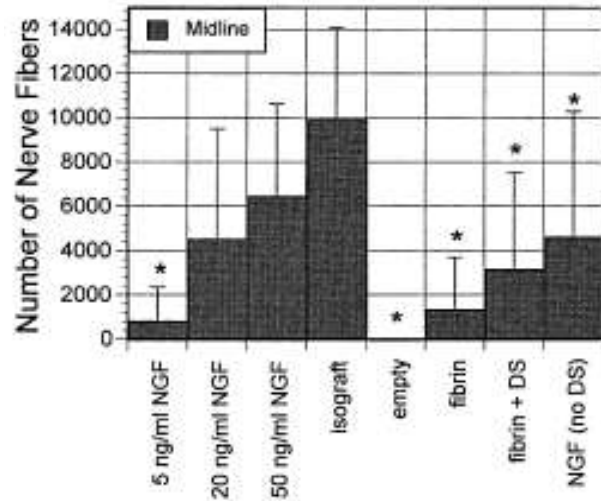


Figure 2-6. Effect of NGF-loaded delivery system on axonal regeneration. Fibrin-based delivery system containing heparin-immobilized B-NGF enhances axonal regeneration in a 13 mm rat sciatic nerve defect. (NGF = Nerve Growth Factor, DS = Delivery System) (Adapted from Lee et al.; 2003)

incorporated neuroregenerative cues on 1) functional nerve regeneration through regenerative electrodes and 2) peripheral nerve interfacing by implanted electrodes will also be examined. High-transparency electrode geometries and presence of fibrin-based delivery system loaded with β -NGF and GDNF are both hypothesized to enhance axonal regeneration through implanted sieve electrodes and improve the ability of implanted devices to interface peripheral motor axons. Custom-designed sieve electrode assemblies both with and without the NGF-loaded and GDNF-loaded fibrin-based delivery system were fabricated and implanted in rat sciatic nerve for periods of 3-9 months. Functional nerve regeneration through implanted sieve electrodes was electrophysiologically assessed in situ and compared to that observed through silicone nerve conduits both with and without the fibrin-based delivery system. The ability of implanted sieve electrodes to electrically interface regenerated nerve tissue was also evaluated electrophysiologically. The capability of various sieve electrodes to specifically interface regenerated motor axons and control motor output was assessed through evoked force production in distal musculature. Qualitative and quantitative examination of axonal regeneration through implanted sieve electrodes was conducted through morphological and histomorphometric assessment and compared to that observed in healthy uninjured sciatic nerve. Results of the present study are poised to present the first demonstration that regenerative sieve electrodes possess significant potential as a means of chronically interfacing peripheral motor axons for use advanced neuroprosthetic systems.

Chapter 3: Micro-Sieve Electrode Fabrication and Testing

3-1: Introduction

Evaluation of the ability of micro-sieve electrodes to support the regeneration of functional motor axons proceeded in six steps. The first step was to fabricate individual micro-sieve electrodes utilizing sacrificial photolithography. The second and third steps were to construct implantable sieve electrode assemblies and load the assemblies with fibrin matrices containing NGF. The fourth step was to microsurgically implant regenerative sieve electrode assemblies into rodent sciatic nerve for evaluation of nerve integration into the implanted construct. The fifth and sixth steps were to terminally evaluate regenerative nerve morphometry and histology at the micro-sieve / nerve interface. Construction, implantation, and histological / histomorphometric evaluation of micro-sieve electrodes will be described in this chapter, while measures of functional nerve regeneration and nerve interfacing will be detailed in the next chapter.

3-2: Fabrication of Micro-Sieve Electrodes

The first step in examining the capability of regenerative sieve electrodes to support functional axonal regeneration and facilitate selective nerve activation was to construct implantable micro-electrodes for use in vivo testing.

Custom regenerative sieve electrodes were designed for use in the present study. Micro-sieve electrodes were comprised of a central interface region, two ribbon cables,

and two peripheral connector tabs. The round central interface region (diameter = 3 mm) contained a porous area (diameter = 2 mm) comprised of 330 via holes, each 60 μm in diameter, arranged in a hexagonal array (pitch = 80 μm). Transparency of the porous region was approximately 30%, comparable to previously described sieve microelectrodes (Lago et al; 2005). The porous region contained 16 active ring electrodes (I.D = 70 μm , O.D. = 90 μm) positioned around via holes spaced evenly throughout the porous area. The central interface region also possessed two small tabs containing active reference electrodes (diameter = 300 μm). Ribbon cables (width = 2 mm, length = 12 mm) served to connect active ring electrodes in the central interface region to connector pads in the connector tabs via integrated metal traces (width = 10 μm , thickness = 260 nm). Each ribbon cable supported 9 metal traces facilitating this electrical connection. Connector tabs (width = 7 mm, length = 9 mm), located at the periphery of the electrode, each contained 10 contact pads which facilitated an electrical

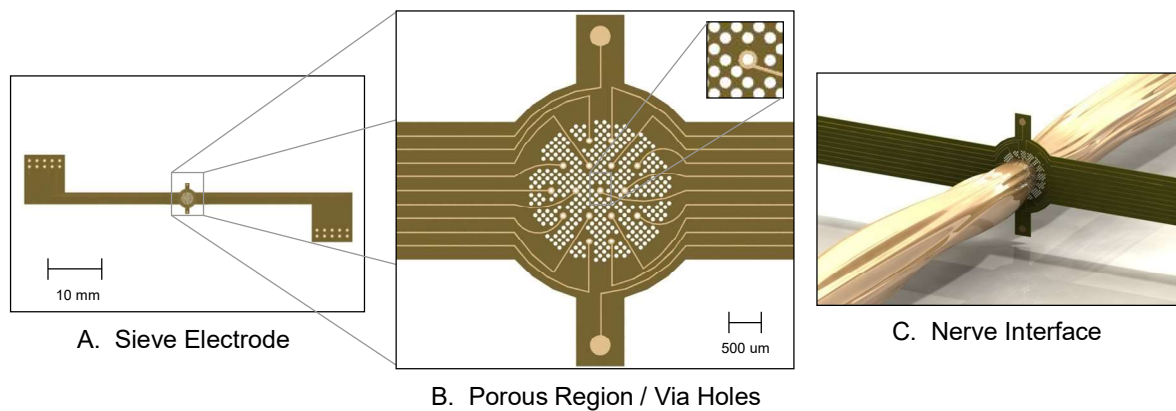


Figure 3-1. SolidWorks model of custom regenerative micro-sieve electrode. Low magnification view (A) demonstrates the central interface region (outlined), ribbon cables, and connector tabs of the sieve electrode. High magnification view (B) demonstrates the arrangement of ring electrodes and traces on the porous area of the sieve electrode, which are highlighted in higher magnification views (inset). Rendering (C) demonstrates expected regeneration of peripheral nerve tissue through the porous region of the electrode.

interface between integrated metal traces and a 10-pin connector.

Micro-sieve electrodes were fabricated according the proposed design in the laboratory of Dr. Justin Williams at the University of Wisconsin (Madison, WI). Regenerative electrodes were fabricated using polyimide resin (PI-2721, HD Microsystems, Parlin, NJ) as the substrate and insulation material with a single metallization layer (Metz et al; 2004). Briefly, wafers were prepared by evaporating chrome (10 nm) and aluminum (300 nm) onto 100 mm silicon substrates. Polyimide (5 μm) was then deposited onto the substrate, photo-patterned, and cured in a nitrogen atmosphere oven. A metallization layer (10 nm Cr / 250 nm Au) was deposited on the initial polyimide layer using e-beam evaporation, and ring electrodes, traces, and connector pads were patterned using a lift-off technique. A second insulating layer of polyimide (5 μm) was then applied to the construct and photo-defined, resulting in a total thickness of approximately 10 μm . Sieve electrodes were released from the wafer via anodic dissolution of the sacrificial aluminum layer. Specifically, wafers were submerged in a sodium chloride solution while a 0.8 V potential, provided by a constant voltage source (E3631A, Agilent Technologies Inc., Santa Clara, CA) was applied between the wafer and a Pt counter electrode placed in the solution. Following release from the wafer, platinum black was electrochemically deposited onto ring electrodes and connector pad sites in order to reduce interfacial impedance, as measured at 1 kHz using an impedance check module (FHC Inc., Bowdoin, ME).

Utilizing this approach micro sieve electrodes were successfully fabricated via sacrificial photolithography. Micro-sieve electrodes possessed a unique flexibility and compliance ideally suitable for in vivo use due to the polyimide construction. Fabricated

devices further demonstrated acceptable electrical performance for use in functional electrical stimulation applications. Specifically, individual ring electrodes located in the porous area of fabricated devices possessed impedances ranging from 23 k Ω – 41.8 M Ω at 1kHz, with $5.5 \pm 5.3\%$ of electrodes possessing an impedance < 100 k Ω . Following platinization, individual ring electrodes possessed impedances ranging from 8 k Ω – 23.6 M Ω , with $56.3\% \pm 19.3\%$ of electrodes possessing an impedance < 100 k Ω . Sieve electrodes with >75% of ring electrodes possessing impedances < 100k Ω were selected for use *in vivo*.

While yields of micro-sieve electrodes were low in initial production runs, fabricated devices demonstrate suitable mechanical and electrical performance for use in *in vivo* experimentation.

3-3: Construction of Sieve Electrode Assemblies

Fabricated micro-sieve electrodes were modified in order to optimize the devices for chronic *in vivo* application in mammalian peripheral nerve tissue. Modifications were employed to reinforce the micro-sieve electrodes and protect against mechanical stresses experience *in vivo*. Modifications were also made in order to properly orient and appose the fabricated electrodes to the target peripheral nerve. Finally, modifications were made in order to optimally prepare the device for electrical activation and functional nerve interfacing following chronic implantation. Construction of robust sieve electrode assemblies was completed in order to facilitate an un-obstructed evaluation of the chronic performance of fabricated electrodes.

Micro-sieve electrodes were post-modified in preparation for chronic implantation into peripheral nerve tissue. Segments of silicone nerve guidance conduit (length = 5 mm, I.D. = 2 mm, O.D. = 4 mm, A-M Systems Inc., Carlsborg, WA) were attached to both sides of each sieve electrode. Silicone conduit segments were centered around the porous area within the central interface region using a custom-designed jig and attached to the electrode using silastic medical adhesive (Type A, Dow Corning, Midland, MI). Adhered silicone conduits served as a means of securing peripheral nerve stumps within the sieve electrode assembly, guiding regenerating nerve fibers through the porous region of the electrode, and controlling the regenerative microenvironment at the nerve/electrode interface. Connector tabs of micro-sieve electrodes were subsequently protected using small Teflon envelopes (width = 12 mm, length = 12 mm). All sieve electrode assemblies were encapsulated in 1-2 mm of medical grade elastomer (MDX4-4210, Dow Corning, Midland, MI). Silicone encapsulation served to protect electrode integrity and provide mechanical support to the electrode *in vivo*. Silicone nerve

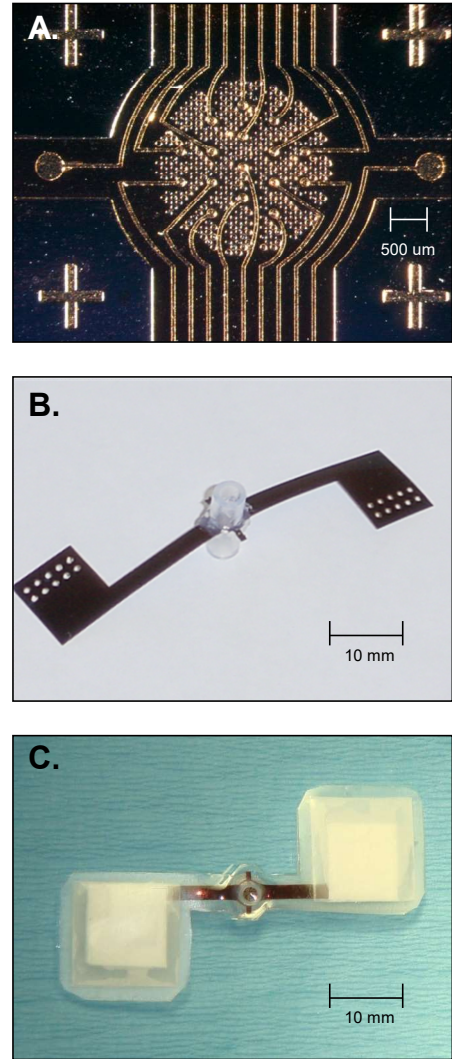


Figure 3-2. Fabricated micro-sieve electrodes and constructed micro-sieve electrode assemblies. Optical micrograph of the porous region of a sieve electrode fabricated via sacrificial photolithography (A). Sieve electrode with attached silicone nerve guidance conduit segments surrounding the porous area of the central interface region (B). Completed sieve electrode assembly encapsulated in silicone elastomer (C).

guidance conduits (length = 10 mm) lacking sieve electrodes were prepared from similar conduit material to serve as controls to implanted sieve electrode assemblies. Completed sieve electrode assemblies and control silicone conduits were gas sterilized with ethylene oxide and soaked in 70% ethanol prior to use.

Successful modification of micro-sieve electrodes and fabrication of sterile sieve electrode assemblies verified the translatable nature of the fabricated polyimide microelectrodes. Construction of a robust system of encapsulation and support further suggests the ability to successfully evaluate the chronic performance of custom micro-electrodes *in vivo*.

3-4: Preparation of Fibrin Matrices

Prior studies suggest that regenerative sieve electrodes containing small diameter via holes (<100um) permit axonal regeneration yet may impede robust regeneration of functional motor axons *in vivo*. Provided the importance of robust axonal regeneration (particularly that of motor axons) to the chronic performance of micro-sieve electrodes as a functional neural interface, strategies for modulating axonal regeneration through implanted constructs were examined. Incorporation of neuroregenerative features into micro-sieve electrode assemblies was identified as an ideal means of improving regeneration of motor axons through implanted assemblies in order to facilitate successful nerve interfacing and motor control by implanted micro-sieve electrodes.

One neuroregenerative system that has demonstrated considerable promise in enhancing peripheral nerve regeneration is a heparin-containing, fibrin-based delivery system capable of controlled release of various neurotrophic factors (Sakiyama-Elbert et

al; 2001, Sakiyama-Elbert et al; 2000, Maxwell et al; 2005, Sakiyama-Elbert et al; 2000, Willerth et al; 2007, Taylor et al; 2004). Designed in the laboratory of Dr. Shelly Sakiyama-Elbert at Washington University in St. Louis, the delivery system consists of heparin-bound neurotrophic factors non-covalently immobilized within a fibrin matrix through the use of a bi-domain peptide containing a heparin-binding domain and transglutaminase substrate. Sequestration within the fibrin matrix allows slow, controlled diffusion of loaded neurotrophic factors from the scaffold until cellular infiltration occurs during axonal regeneration, effectively timing NGF release to occur upon the arrival of extending neurites. Prior studies have demonstrated the system's neuroregenerative potential, as fibrin-based delivery system loaded with 100 ng/ml β -NGF enhanced neurite extension from cultured embryonic chick dorsal root ganglia *in vitro* (Lee et al; 2003). Additional *in vivo* trials demonstrated that silicone nerve guidance conduits containing fibrin-based delivery system loaded with 50 ng/ml β -NGF enhanced nerve regeneration across 13 mm defects in rat sciatic nerve compared to empty silicone conduits (Wood et al; 2010). While previous studies have not investigated the ability of fibrin-based delivery system to enhance nerve regeneration through artificial substrates or micro-devices, it is believed that the application of such a regenerative matrix to sieve electrode assemblies may increase axonal regeneration through implanted electrodes and functional reinnervation of distal motor targets, as well as improve chronic survival of regenerated axons and protect against compressive axonopathy.

Due to the positive neuroregenerative potential and the fibrin-based delivery system, and the flexibility of the delivery system with the design of the implantable micro-sieve electrode assembly, samples were prepared for use with final finished micro-

sieve devices. Specifically, fibrin matrices containing the affinity-based delivery system were prepared in the laboratory of Dr. Shelly Sakiyama-Elbert at Washington University (St. Louis, MO) (Lee et al; 2003). Fibrinogen solutions (8 mg/ml) were prepared by dissolving human plasminogen-free fibrinogen (Calbiotech Inc., Spring Valley, CA) in deionized water for 1 hour at 37° C then dialyzing the solution against 4 L of Tris-buffered saline (TBS) containing 33 mM Tris, 8 g/L NaCl, and 0.2 g/L KCl (Sigma-Aldrich, St. Louis, MO). The fibrinogen solution was sterile filtered using 5.0 um and 0.22 um syringe filters and the concentration of fibrinogen was confirmed by spectrophotometry. Just prior to surgical implantation of either silicone conduits or sieve electrode assemblies containing the delivery system, fibrinogen, TBS, 50mM CaCl₂ in TBS, 20 U/ml thrombin, 25 mg/ml a₂PI₁₋₇-ATIII₁₂₄₋₁₃₄ peptide, 45 mg/ml heparin, and 20 ug/ml recombinant human β-NGF (Peprotech, Rocky Hill, NJ) were mixed in an Eppendorf tube to a final concentration of 50 ng/ml β-NGF. Immediately after mixing, silicone conduits were injected with 30 ul of the resulting mixture while silicone conduit segments attached to the sieve electrode assemblies were each injected with 15 ul of the resulting solution. Applied fibrin matrices containing the heparin-binding delivery system were allowed to polymerize for 5 min prior to surgical implantation.

Successful application of prepared fibrin matrices to constructed sieve electrode assemblies verified the compatibility of the present approach with proposed in vivo animal testing. Demonstration of successful placement and retention of NGF-loaded fibrin-based hydrogels within attached nerve guidance conduits and around the porous region of integrated micro-sieve electrodes confirmed the ability of delivery system to provide neurotrophic support at the nerve/electrode interface. While the present study

did not validate the functional nature of neurotrophic factors loaded into fibrin-based delivery systems, prior work conducted in the Sakiyama-Elbert laboratory provide extensive support for the validity and functionality of the system (Lee et al; 2003, Wood et al; 2010, Wood et al; 2009).

3-5: Surgical Implantation / Rodent Model

Following successful construction of micro-sieve electrode assemblies, a suitable animal model was required for long-term evaluation of peripheral nerve regeneration and peripheral nerve interfacing. Animal models are highly leveraged to gain in-depth insight into the efficacy of various nerve interfacing strategies, nerve repair techniques, and the biomolecular processes underlying nerve regeneration. While a wide range of animal models have been utilized in past studies, the rat sciatic nerve model represents a gold-standard due to its low-cost, regenerative potential, and general ease of use (Varejo et al; 2004).

In order to evaluate the efficacy of implanted micro-sieve electrodes using the rat sciatic nerve model robust methods for assessing nerve regeneration and functional recovery are needed (Myckatyn et al; 2004). Existing analytical methods for evaluating functional nerve regeneration include histological, behavioral, and functional assessments (Wood et al; 2011). Histological analyses provides critical information regarding axonal regeneration and nerve repair, yet are limited to terminal time points and lacks direct correlation to behavioral outcomes (Yan et al; 2011). Behavioral studies, such as walking track / gait analysis and measurement of sciatic function index (SFI), present an unique view of end terminal function (Urbanek et al; 1999) Electrophysiological studies

provide direct information regarding peripheral nerve function and can provide quantifiable metric for assessment of recovery (Lee et al; 2013). Prior studies documenting robust characterization of peripheral nerve regeneration in the rat sciatic nerve provided an ideal model and baseline for the examination of novel micro-sieve electrodes assemblies with and with integrated neurotrophic factors.

Upon selection of a suitable animal model, specific attention was paid to the development of appropriate surgical methods for introducing micro-sieve electrodes to the rat sciatic nerve. Techniques were identified which would allow for: 1) appropriate placement of micro-sieve electrode assemblies within the proper tissue place, 2) optimal alignment of the porous region of the micro-sieve electrode orthogonal to the natural course of the sciatic nerve, 3) secure apposition of the proximal / distal nerve stumps to the attached nerve guidance conduits, and 4) optimal positioning of connector tabs / contact pads for terminal interfacing of chronically-implanted sieve electrodes.

Resulting surgical procedure were conducted in the following manner. Male, Lewis rats (275-300 g) were anesthetized using 4% Isoflurane / 96% oxygen (induction) and 2% Isoflurane / 98% oxygen (maintenance) administered IH. Following preparation and sterilization of the lateral aspect of the right leg, the right sciatic nerve was exposed through a dorsolateral gluteal muscle-splitting incision followed by blunt dissection. Utilizing an operating microscope, the sciatic nerve was transected proximal to the trifurcation and the proximal and distal nerve stumps were inserted into either: 1.) the ends of a prepared silicone nerve guidance conduit, or 2.) the ends of silicone nerve guidance conduit segments attached to a prepared sieve electrode assembly. Proximal and distal nerve stumps were secured inside respective silicone conduits with four

interrupted microepineurial 9-0 nylon sutures, such that an 8 mm gap existed between stumps in all implanted systems. Following implantation of micro-sieve electrode assemblies into transected sciatic nerves, encapsulated ribbon cables and connector pads were routed through anterior and posterior muscle groups in the leg such that the connector pads rested in subcutaneous pockets created rostral and caudal to the right hind leg. Incisions were closed in two layers using uninterrupted and interrupted 4-0 vicryl suture to close the muscle and skin, respectively. VetBond™ tissue adhesive (3M, St. Paul, MN) was also applied to the incision in order to ensure closure, and all animals were fitted with a poly-ethylene collar for one week in order to prevent autophagia and disturbance of the operative site. All operative and post-operative procedures described were conducted under sterile conditions using aseptic techniques.

Utilizing this technique micro-sieve electrode assemblies and nerve guidance conduits, containing either fibrin-based delivery system or saline, were implanted in the right sciatic nerve of Lewis rats. Surgical

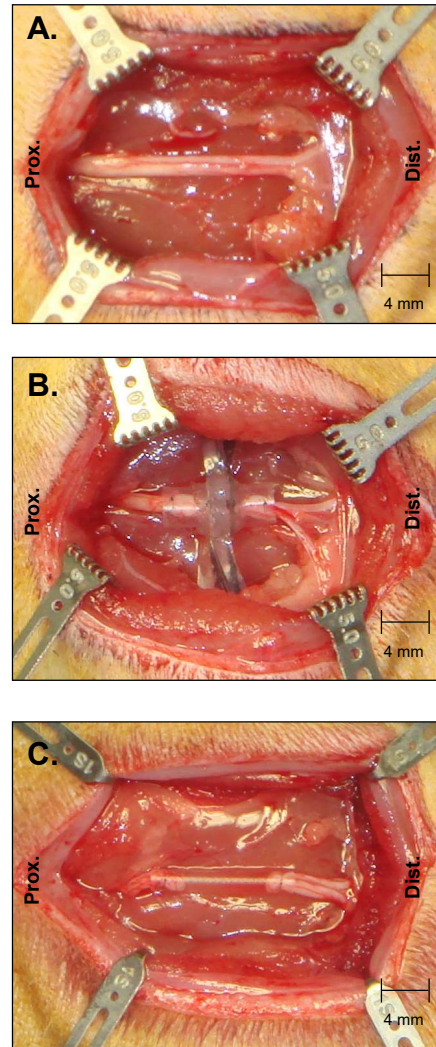


Figure 3-3. Surgical implantation of micro-sieve electrode assembly.

Intraoperative photograph of a microsurgically-isolated rat sciatic nerve exposed through a dorsolateral gluteal muscle-splitting incision (A). Sieve electrode assembly implanted between the transected ends of the sciatic nerve (B), secured inside the silicone conduit segments attached to the sieve electrode. Silicone nerve guidance conduit without a sieve electrode similarly implanted between the transected ends of the sciatic nerve (C).

implantation was successful and well tolerated by all animals, as tension-free coaptation of transected nerve stumps and silicone conduits was achieved in all cases. Few complications were noted post-operatively, and intermittent evaluation of motor function via calculation of sciatic function index demonstrated progressive motor recovery in operative limbs over the course of the study (data not shown). Demonstration of successful surgical introduction of micro-sieve electrode assemblies into the rat sciatic nerve validated the selected animal model and the chosen device configuration.

Confirmation of successful surgical deployment of the micro-sieve electrode assembly enabled expanded examination of implanted sieve electrode devices. An initial animal study was designed to examine axonal regeneration through micro-sieve electrode assemblies with and without

integrated neuroregenerative cues.

This study additionally served to evaluate the ability of micro-sieve electrodes to achieve a stable interface to peripheral nerve tissue and thereby provide a means of

facilitating therapeutic or rehabilitative electrical stimulation of interfaced nerve.

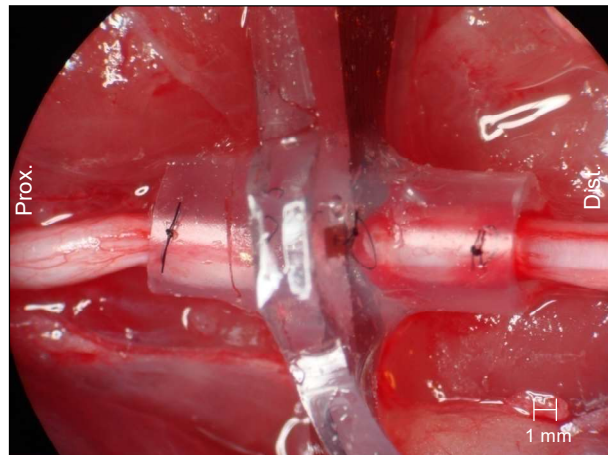



Figure 3-4. High magnification view of implanted micro-sieve electrode. Intraoperative photograph of a micro-sieve electrode assembly implanted between the transected ends of the sciatic nerve.

In this study thirty adult male Lewis rats were randomized into 5 experimental groups (I-V) of 6 animals each (n=6). Animals in Group I served as unoperative controls and did not undergo surgical exposure or transection/repair of the sciatic nerve. Animals

in Group II-V underwent surgical exposure and transection of the sciatic nerve, followed by microsurgical implantation of either a silicone nerve guidance conduit or a sieve electrode assembly. In Group II, a silicone conduit containing sterile saline was implanted between the transected ends of the sciatic nerve. In Group III, a silicone conduit containing the fibrin-based delivery system loaded with β -NGF was implanted between the transected ends of the sciatic nerve. In Group IV, a sieve electrode assembly containing sterile saline was implanted between the transected ends of the sciatic nerve. In Group V, a sieve electrode assembly containing the fibrin-based delivery system loaded with β -NGF was implanted between the transected ends of the sciatic nerve. Animals in all groups underwent *in situ* evaluation of sciatic nerve function upon termination of the study 9 months, post-operatively. A terminal time-point of 9 months was selected a suitable market for chronic *in vivo* use due to prior reports documenting stabilization of the nerve/electrode interface after 6 months post-operatively. Following *in situ* assessment, all sciatic nerves were explanted and fixed for morphological and histomorphometric analysis.

In total, 100% of animals implanted survived to the terminal time point. At the terminal



Group:	Sieve -GDNF	Sieve +GDNF	Conduit -GDNF	Conduit +GDNF	Control
Electrode:	Micro-sieve	Micro-sieve	None	None	None
Conduit:	Silicone Conduit	Silicone Conduit	Silicone Conduit	Silicone Conduit	None
Regen. System:	Saline	Fibrin DS +50ng/ml β -NGF	Saline	Fibrin DS +50ng/ml β -NGF	None
	n=6	n=6	n=6	n=6	n=6

Table 3-1. Experimental design: Study of regenerative micro-sieve electrodes. Experimental groups utilized in the investigation of micro-sieve electrodes with and without NGF-loaded delivery system. (DS, delivery system; NGF, nerve growth factor.)

time point all implanted devices and host sciatic nerves were surgically exposed. All implanted devices were covered by a similar, thin layer of fibrous tissue. Implanted silicone guidance conduits consistently maintained their position and orientation *in vivo*. Gross examination of implanted nerve guidance conduits revealed that 100% of nerve guidance conduits injected with fibrin-based delivery system, and 100% of nerve guidance conduits injected with saline, contained regenerative nerve cables bridging the imposed nerve defect. Implanted sieve electrode assemblies demonstrated variable degrees of rotation, yet minimal migration *in vivo*. *In vivo* rotation of sieve electrode assemblies did not appear to affect the presence of regenerative nerve tissue within sieve electrode assemblies.

Successful development and implementation of surgical methods for deploying micro-sieve electrode assemblies confirmed the translational capacity of micro-fabricated sieve electrode constructs. Demonstration of animal survival throughout the course of the initial study highlights the safety of implanted devices, as well as the chronic subsistence of implanted micro-sieve constructs. Furthermore, gross observation of regenerative nerve tissue present within implanted nerve guidance conduits and regenerative sieve electrode assemblies suggest positive axonal regeneration through the implanted device. These results provide preliminary evidence for successful integration of micro-sieve electrodes into rodent peripheral nerve tissue, which will be examined in greater detail in subsequent sections.

3-6: Regenerative Nerve Morphometry

Previous sections outlined the design and fabrication of an implantable micro-sieve electrode assembly, as well as successful surgical implantation of the device in a rodent peripheral nerve model. While initial observations document the presence of

regenerative nerve tissue within chronically-implanted nerve conduits and micro-sieve assemblies, dissection of regenerative nerve tissue for morphological and histological examination was conducted to further evaluate neural integration of implanted constructs. Specifically, morphological analysis of regenerative nerve tissue crossing implanted nerve guidance conduits and micro-sieve electrode assemblies was conducted in order to: 1) document the presence and degree of axonal regeneration within the implanted constructs, and 2) examine the influence of implanted constructs on local nerve tissue.

Unoperative (n=3) and regenerative nerve segments (n=3) from all experimental groups were explanted and fixed using 4% paraformaldehyde in 0.1 M phosphate buffer (pH = 7.2) for 24 hours. All regenerative nerve tissue was dissected from silicone nerve guidance conduits. Regenerative nerve segments contained in sieve electrode assemblies were removed without disturbing the integrated porous area of the implanted sieve electrode. All nerve tissue was cryopreserved in a 30% sucrose solution for 72 hours and subsequently divided at mid-conduit into two portions, proximal and distal, each 5 mm in length. Nerve segments containing integrated sieve electrodes were divided just distal to the implanted electrode, such that the porous area of the electrode remained embedded in the proximal portion. Proximal and distal portions of harvested nerve tissue were embedded in Tissue Tek OCT compound (PELCO International, Redding, CA) at -80° C and sectioned using a cryostat (Lauda 1720, Leitz, Rockleigh, NJ). Cross-sections 5 um and 10 um thick were cut every 200 um along the length of the nerve segment and mounted on SuperFrost Plus glass slides (Fisher Scientific Inc., Pittsburgh, PA). Sections were numbered and organized such that their exact position along the length of the nerve segment was known. Collected sections were stained with 1% toluidine blue for

examination under light microscopy. Stained sections were imaged at 4X magnification using an Olympus IX70 microscope (Olympus America, Melville, NY) and Magnafire camera (Optronics, Goleta, CA). Images were qualitatively analyzed for macroscopic nerve architecture and fascicular organization. Cross-sectional nerve area was quantitatively measured from stained sections using modified Image J software (NIH, Bethesda, MD).

Three-dimensional reconstructions of explanted nerve segments were then created to better visualize the macroscopic architecture and morphology of regenerated nerve tissue. Two-dimensional, digital images of stained, frozen nerve sections were imported into Rhinoceros modeling software (McNeel Inc., Seattle, WA), adjusted to scale, and aligned in the X,Y-plane. The epineurial/perineurial boarder was digitally outlined on each imported image and positioned along the Z-axis according to the relative position of the nerve section along the length of the subject nerve segment. Lofted epineurial/perineurial outlines were digitally extruded to form a three-dimensional model of the subject nerve segment, which was subsequently imported into SolidWorks 2008 software (SolidWorks Corp., Concord, MA). Models of regenerative nerve segments obtained from sieve electrode assemblies were combined with a scale model of a sieve electrode, created previously using SolidWorks software. Positioning of the electrode model within the regenerative nerve model was based on the actual positioning of the electrode within the explanted nerve segment, as determined by the presence of electrode shards and debris within frozen nerve sections. Digital reconstructions of healthy, unoperative sciatic nerve segments, regenerative nerve segments, and regenerative nerve segments combined with a sieve electrode model were rendered and compared.

Frozen sections of explanted nerve tissue demonstrated normal fascicular architecture proximal and distal to implanted devices and regenerative architectures within implanted devices. Sections acquired at the midpoint of silicone nerve guidance conduits exhibited numerous regenerated axons organized into a singular nerve cable. Sections acquired at a similar position in sieve electrode assemblies (immediately proximal to the sieve electrode) demonstrated numerous regenerated axons organized into multiple, distinct microfascicles. Sections acquired at the sieve/nerve interface confirmed the presence of microfascicles within individual via holes in the sieve electrode, suggesting regenerating nerve tissue successfully passed through the porous area of the

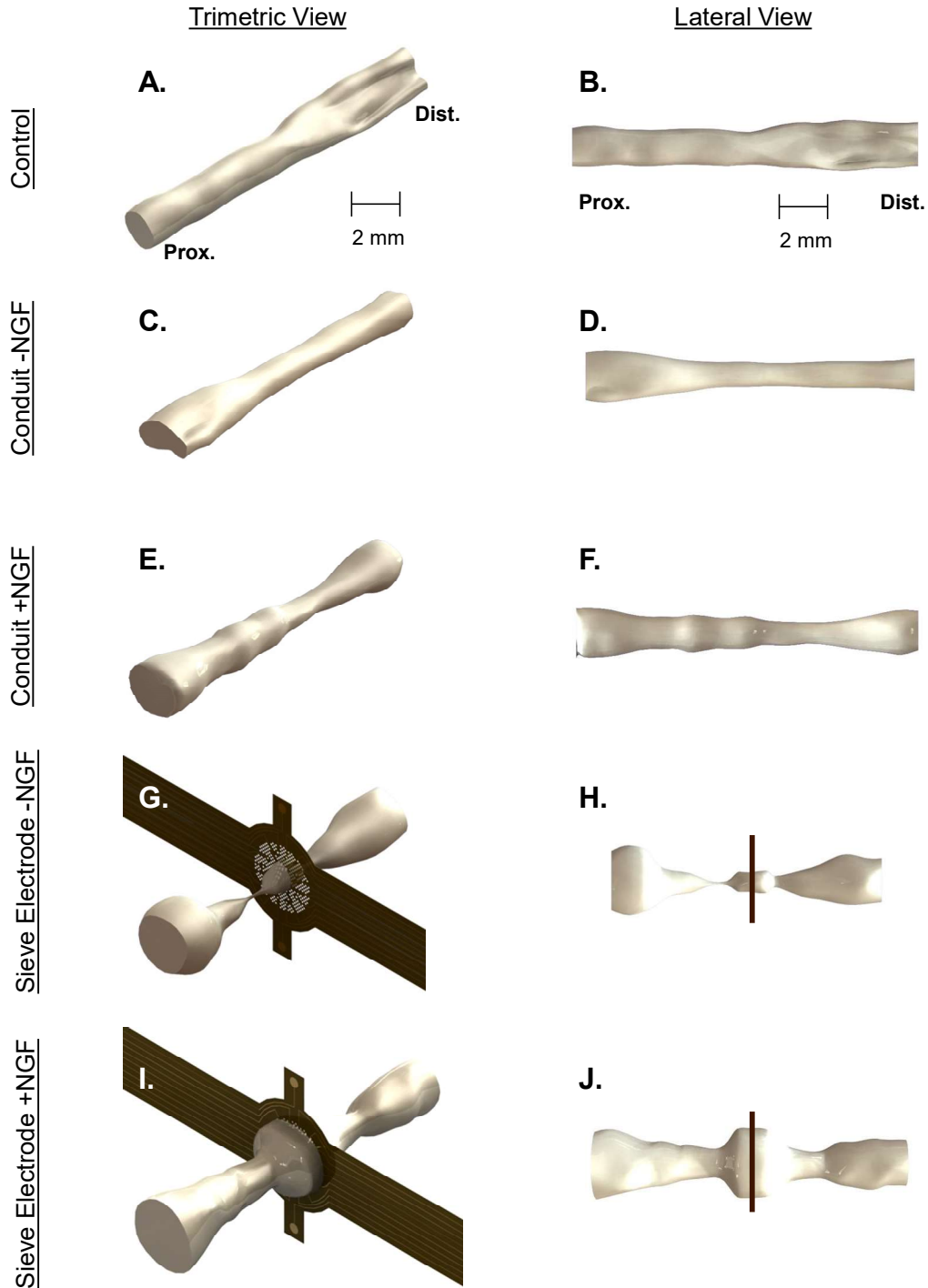


Figure 3-5. Trimetric and lateral views of three-dimensional reconstructions of explanted nerve segments. Reconstruction of unoperative sciatic nerve (A, B), regenerative nerve tissue contained in silicone nerve guidance conduits with (E,F) and without (C,D) the fibrin-based delivery system, and regenerative nerve tissue contained in micro-sieve electrode assemblies with (I,J) and without (G,H) the fibrin-based delivery system. Representative reconstructions from each experimental group are shown in similar scale.

implanted electrode. Single-cable and microfascicular architectures were consistently

observed in silicone conduits and sieve electrode assemblies in both the presence and absence of the delivery system.

Three-dimensional reconstruction of sciatic nerves containing sieve electrode assemblies demonstrated a unique “conic enlargement” in regenerative nerve tissue at the nerve/electrode interface unlike the “tapered” morphology observed in nerve tissue within silicone conduits. Examination of individual frozen sections confirmed the presence of numerous nerve “microfascicles” at the nerve/electrode interface, suggesting the “enlargement” is a result of regenerating axons extending radially from the center of the porous region to cross the limited number of via holes in the electrode. Sieve electrode assemblies with and without NGF-loaded delivery system demonstrated similar “enlargements” around the nerve/electrode interface, though a greater volume of nerve tissue was observed at the nerve/electrode interface in the presence of the delivery system.

Observation of regenerative nerve tissue within implanted micro-sieve electrode assemblies and integrated via holes confirms successful integration of implanted electrodes into host nerve tissue. Micro-sieve electrode assemblies therefore provide a suitable microenvironment to support axonal regeneration in vivo. Formation of numerous micro-fascicles at the nerve/electrode interface further demonstrate that micro-sieve electrodes are capable of parsing regenerating axons into small independent groups, ideal for selective electrical interfacing. Observation of “conic enlargements” in regenerative nerve tissue further demonstrate the unique interaction between implanted micro-sieve constructs and regenerating nerve tissue. Morphological differences

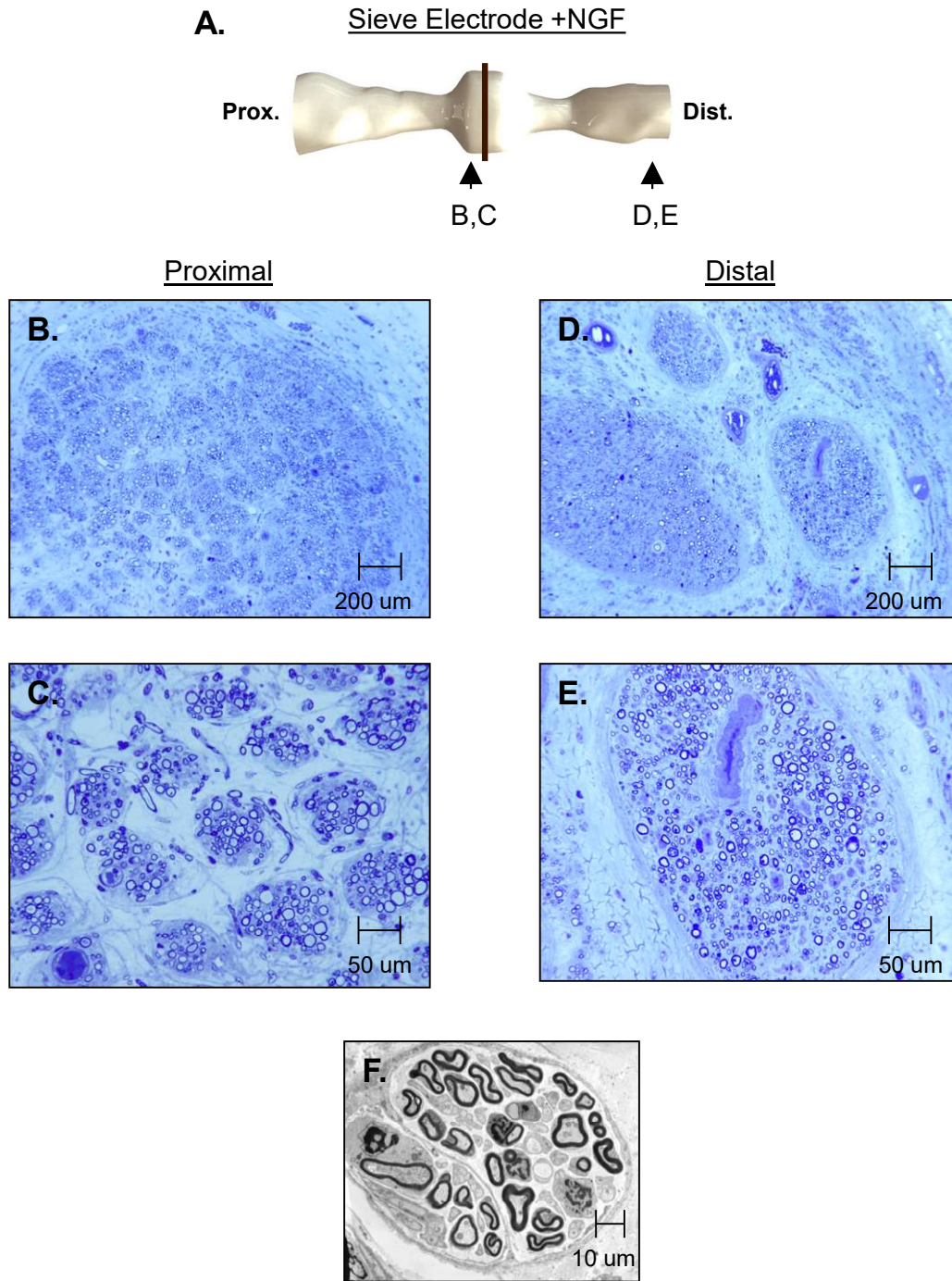


Figure 3-6. Regenerative nerve tissue explanted from micro-sieve electrode assembly containing fibrin-based delivery system loaded with NGF. Three-dimensional reconstruction of explanted nerve segment (A) demonstrates locations of displayed sections. Sections taken at the sieve electrode interface (B,C) demonstrate microfascicles containing multiple myelinated axons, while sections taken 5 mm distal to the electrode (D) demonstrate numerous myelinated axons reinnervating all three branches of the sciatic nerve, specifically the peroneal nerve (E).

observed in regenerative nerve tissue obtained from nerve guidance conduits and micro-sieve electrode assemblies suggest the presence of two distinct processes of nerve regeneration through the two constructs. While confirming an active link between sieve electrode geometry and nerve morphology, the observation of “conic enlargement” most likely signifies the physical impedance of regenerating nerve tissue by the low-transparency electrode. This observation may also suggest that micro-sieve electrodes functionally impact, and moderately impede, axonal regeneration in vivo. Incorporation of neuroregenerative features into micro-sieve electrode assemblies appears to present a promising method for overcoming this limitation and improving volume of regenerative nerve tissue at the nerve/electrode interface, though more detailed histological examination of regenerative nerve tissue is required.

More rigorous histological and histomorphometric examination of regenerative nerve tissue within chronically-implanted micro-sieve electrode assemblies is outlined in the following section.

3-7: Regenerative Nerve Histology

Histological and histomorphometric analysis was conducted in order to accurately assess regenerative nerve tissue integrated into chronically implanted micro-sieve electrodes. Unlike morphological analysis, histological analysis via epoxy sectioning provides a detailed view of regenerative nerve microstructure, including the number and density of peripheral nerve fibers, diameter of peripheral nerve fibers / axons, and presence of axonal injury, cellular debris, and foreign body response. Histological examination additionally offers an ability to examine nerve micro-structure at various

points along a segment of regenerative nerve. In the present study, ultra-thin sections of regenerative nerve tissue were obtained immediately proximal, immediately distal, and 5 mm distal to implanted electrodes. Evaluation of epoxy sections proximal and distal to the nerve/electrode interface was performed to examine penetration of regenerating axons through the porous region of the implanted device. Evaluation of epoxy sections distal to the nerve/electrode interface was performed to examine the success of axonal regeneration into the distal nerve stump following sieve electrode implantation. Epoxy sections stained with Toluidine Blue were evaluated to measure the quantity, density, and myelination of regenerated nerve fibers.

Sieve electrode assemblies (n=6) from each experimental group were explanted and fixed in cold 3% glutaraldehyde in 0.1 M phosphate buffer (pH = 7.2). Regenerative nerve tissue including the porous area of the sieve electrode was dissected from the silicone conduit segments, post-fixed with 1% osmium tetroxide, ethanol dehydrated, and embedded in Araldite 502 epoxy resin (Polysciences, Warrington, PA). Cross sections <1 μ m thick were cut 5 mm proximal, immediately proximal, immediately distal, and 5 mm distal to the integrated electrode with an LKB III Ultramicrotome (LKB-Produkter A.B., Bromma, Sweden) and stained with 1% toluidine blue. Slides were examined using light microscopy and were evaluated by an observer blinded to the experimental groups for overall nerve architecture, quantity of regenerated nerve fibers, degree of myelination, and Wallerian degeneration.

Quantitative analysis was performed on toluidine blue stained sections using a semi-automated digital image analysis system linked to a custom software package (LECO Instruments, St. Joseph, MI) adapted for nerve morphometry, as previously

described (Hunter et al; 2007). The system digitized microscope images and displayed them on a video monitor calibrated to 0.125 $\mu\text{m}/\text{pixel}$. Images of sectioned nerve tissue were divided into $5.5 \times 10^4 \mu\text{m}^2$ frames and evaluated using eight-bitplane digital pseudocoloring and thresholding-based algorithms to select for myelinated axons. At 1000X magnification six fields were selected at random per cross section, or a minimum of 500 myelinated fibers, were evaluated to calculate myelin width, axon width, and fiber diameter. The following morphometric indices were calculated using these primary measurements: number of nerve fibers, nerve fiber density (fiber number/ mm^2) percent nerve tissue ($100 \times \text{neural area} / \text{intrafascicular area}$), mean fiber width (μm), myelinated fiber area (μm^2), myelin area (μm^2), microfascicle diameter (μm), and number of nerve fibers per microfascicle.

Ultrathin sections (90 nm) were additionally cut using a LKB III Ultramicrotome for analysis via electron microscopy. Sections were stained with uranyl acetate and lead citrate and imaged with a Zeiss 902 electron microscope (Zeiss Instruments, Chicago, IL) at 4360X magnification, scanned at 400 dots/inch resolution, and evaluated with MicroBright Field Stereo Investigator (Version 7.0, MBF Bioscience Stereo Investigator, Williston, VT), as previously described (Hunter et al; 2007). Composition of microfascicles, quality of myelination, and the relative prevalence of unmyelinated fibers were qualitatively evaluated.

Regenerated nerve segments dissected from sieve electrode assemblies were embedded in epoxy resin for high resolution histological analysis. Thin sections were taken proximal to the sieve electrode, at the sieve electrode/nerve interface, and distal to the sieve electrode to examine regenerated nerve fibers and quantify various

morphometric indices. Toluidine blue-stained sections taken proximal to integrated sieve electrodes demonstrated pronounced microfascicular architecture, previously noted upon analysis of frozen sections. Detailed examination of proximal sections under high magnification demonstrated geometric organization of regenerated microfascicles into hexagonal patterns, identical to the patterning of via holes in the porous area of the sieve electrodes. Microfascicles possessed a consistent diameter (range: 51-73 μm), which was similar to the diameter of via holes in the porous area of the sieve electrodes. Further examination revealed the presence of numerous myelinated and unmyelinated axons within each microfascicle. Quantification via high magnification views of individual microfascicles revealed 27 ± 7 myelinated axons (range: 15-37) per microfascicle. Sections taken at the sieve electrode/nerve interface demonstrated minimal evidence of any foreign body reaction to the electrode or fibrous encapsulation of the porous region of the device (data not shown). Sections taken distal to the integrated sieve electrode demonstrated numerous regenerated nerve fibers reinnervating tibial, peroneal, and sural branches of the sciatic nerve. Presence of regenerated nerve fibers in distal branches of the sciatic nerve, as seen in high magnification views of the peroneal branch, suggest that nerve fibers present in proximal microfascicles successfully regenerated through via holes in the sieve electrode and reinnervated distal nerve stumps.

Comparison of representative sections taken at the sieve electrode/nerve interface in assemblies filled with either fibrin-based delivery system or saline revealed significant differences in the quantity and quality of regenerative nerve tissue. Sections taken from regenerative nerve tissue contained in assemblies filled with the delivery system revealed distinct microfascicular organization, large cross sectional nerve area, and high fiber density (14,901 fibers/mm²). Comparatively, sections taken from regenerative nerve tissue contained in assemblies filled with saline exhibited disorganized nerve architecture, minimal microfascicular organization, small cross-sectional nerve area, and lower fiber density (9,566 fibers/mm²). Lower cross sectional nerve area and lower fiber density in regenerative nerve tissue present at the sieve electrode/nerve interface in assemblies

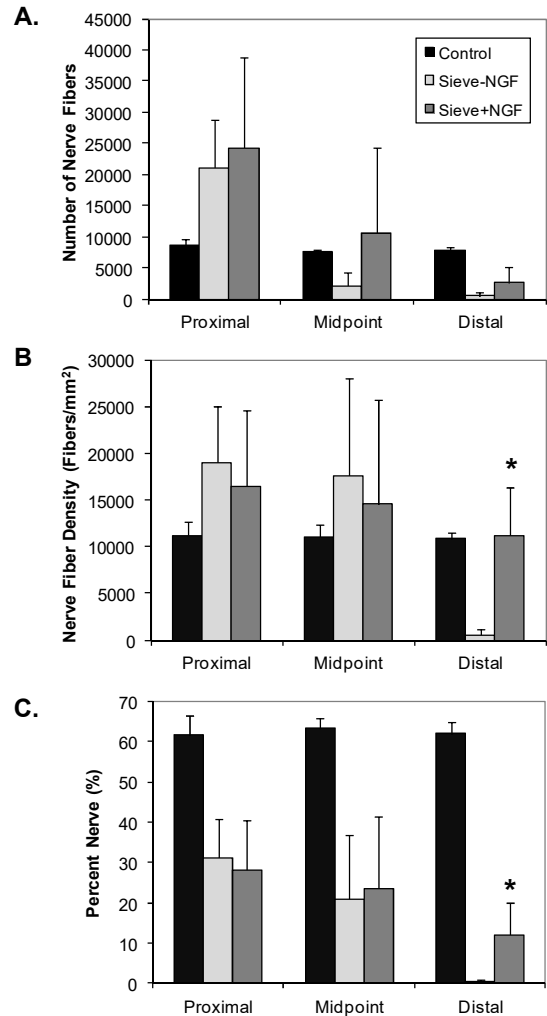


Figure 3-7. Histomorphometric analysis of regenerative nerve tissue present in micro-sieve electrode assemblies and silicone nerve guidance conduits. (A) Nerve fiber count, (B) nerve fiber density, and (C) percent nerve tissue was assessed proximal to implanted sieve electrodes/nerve conduits, at the sieve/nerve interface, and distal to implanted sieve electrodes/nerve conduits. Greater nerve fiber density and percent nerve tissue was noted in regenerative nerve tissue distal to sieve assemblies containing delivery system compared to sieve assemblies containing saline. Mean values and standard deviations are shown. * denotes $p < 0.05$ versus sieve electrode assembly without fibrin-based delivery system loaded with NGF.

containing saline resulted in significantly lower total fiber counts (239 fibers) compared to similar regenerative tissue in assemblies containing delivery system (12,381 fibers). Quantitative assessment demonstrated that individual regenerated fibers contained in sieve electrode assemblies filled with saline were smaller (mean fiber diameter: 3.4 μm vs. 4.3 μm), less often myelinated (axon/myelin ratio: 55% vs. 69%), and had thinner myelin sheaths (myelin width: 0.81 μm vs. 0.92 μm) than those contained in sieve electrode assemblies filled with the delivery system. Histological examination suggested that regenerative nerve tissue present inside sieve electrode assemblies containing saline was less organized and less mature than tissue present inside sieve electrode assemblies containing delivery system.

In summary, histological analysis of regenerative nerve tissue confirms successful axonal regeneration through chronically-implanted micro-sieve electrodes. Epoxy sections validate the capability of implanted micro-sieve electrodes to integrate into native nerve tissue and modulate regenerative nerve ultrastructure. Formation of numerous micro-fascicles at the nerve/electrode interface demonstrate that micro-sieve electrodes are capable of parsing regenerating axons into small independent groups. Simultaneously, histological analysis confirms that low-transparency sieve electrodes mildly impede axonal regeneration in vivo. Incorporation of neurotrophic cue into micro-sieve electrode assemblies presents assists in overcoming the physical barrier posed by low-transparency device. Observation of improved axonal regeneration through micro-sieve electrodes containing the NGF-loaded delivery system confirm that neuroregenerative therapies may enhance the ability of micro-sieve electrodes to achieve a robust, intimate interface with peripheral nerve tissue in vivo. In total, the present study

confirms that micro-sieve electrodes are capable of supporting regenerative axonal populations and an intimate interface with peripheral nerve tissue required for selective electrical stimulation of peripheral axons.

Chapter 4: Peripheral Nerve Interfacing **Via Micro-Sieve Electrode**

4-1: Introduction

In Chapter 3, novel regenerative micro-sieve electrodes were fabricated and evaluated in vivo using a rodent peripheral nerve model. Presented data confirmed the ability of the micro-sieve electrodes to support axonal regeneration through the porous region of the device and integrate into the structure of native peripheral nerve. Morphological and histological data demonstrate that implanted micro-sieve electrodes modulate the structure and organization of regenerative nerve tissue and are capable of chronically subsisting within peripheral nerve tissue. Histological analysis further revealed that low transparency micro-sieve electrodes presented a physical impediment to regenerating axons and limited axonal regeneration compared to nerve guidance conduits alone. Inclusion of neurotrophic cues within the micro-sieve device, as delivered by fibrin-based delivery system, effectively enhanced axonal regeneration through the electrodes thereby improving quality of the nerve/electrode interface and improving the potential for functional electrical stimulation of integrated nerve fibers.

In the present chapter, electrophysiological studies will be presented in order to: 1) elucidate the functional status of regenerative nerve tissue crossing implanted micro-sieve electrodes, and 2) evaluate the capability of implanted micro-sieve electrodes to functionally and selectively recruit regenerative motor axons and distal musculature.

Electrophysiological evaluation of regenerative nerve tissue and chronically-implanted micro-sieve electrodes proceeded in three steps. The first step was to evaluate CNAP conduction in regenerative peripheral nerve tissue and confirm the functional nature of nerve fibers crossing implanted micro-sieve electrodes. The second step was to conduct evoked muscle force measurement and confirm that regenerating axons crossing implanted sieve electrodes reinnervated distal musculature. The third and final step was to evaluate the ability of chronically-implanted micro-sieve electrodes to functionally recruit integrated peripheral nerve fibers and selectively recruit distal musculature.

4-2: Electrophysiology: Nerve Conduction

Morphological and histological studies confirm the presence of regenerative nerve tissue within chronically implanted micro-sieve assemblies, and successful regeneration of individual axons through integrated via holes. Despite evidence of numerous myelinated axons crossing the porous region of implanted electrodes, histological analysis was unable to determine the functional status of regenerative nerve tissue and the motor / sensory composition of regenerated nerve fibers. In order to determine whether regenerative nerve tissue crossing implanted micro-sieve electrodes was capable of conducting action potentials, and thereby receptive to exogenous electrical stimulation, an electrophysiological study of CNAP conduction through implanted constructs was performed.

Electrophysiological function of regenerative sciatic nerve segments was examined *in situ* at 9 months postoperatively. Electrophysiological function was assessed

via nerve conduction study. At the terminal time point all animals underwent a non-survival surgery to expose the sciatic nerve and distal musculature for electrophysiological analysis. Animals were anesthetized using 4% Isoflurane / 96% oxygen (induction) and 2% Isoflurane / 98% oxygen (maintenance) administered IH. Following preparation of the sterile field, the right sciatic nerve and its branches were isolated from the sciatic notch to below the point of trifurcation, distal to the popliteal artery.

Sciatic nerve function was first assessed *in situ* by examining compound neural action potential (CNAP) conduction through regenerated nerve segments present inside implanted silicone conduits and sieve electrode assemblies. Cathodic, monophasic electrical impulses (duration = 50 usec, frequency = single, amplitude = 0-5 mA) were generated by a single-channel isolated pulse stimulator (Model 2100, A-M Systems Inc., Carlsborg, WA) and delivered to the sciatic nerve proximal to the implanted device via bipolar silver wire electrodes (4 mil, California Fine Wire, Grover Beach, CA). Resulting CNAPs were then differentially recorded distal to the implanted device at the peroneal nerve using similar bipolar silver wire electrodes. Measured signals were band-pass filtered (LP = 1 Hz, HP = 5 kHz, notch = 60 Hz) and amplified (gain = 1000X) using a two-channel microelectrode AC amplifier (Model 1800, A-M Systems Inc., Carlsborg, WA) before being recorded on a desktop PC (Dell Computer Corp., Austin, TX) equipped with a data acquisition board (DT3003/PGL, Data Translations, Marlboro, MA) and custom Matlab software (The MathWorks Inc., Natick, MA). Stimulation and recording were synchronized through custom software such that electrical stimulation coincided with the initiation of a 20 msec recording period, wherein data was sampled at

40 kHz. CNAP recordings were repeated 25 times per stimulus amplitude and averaged to obtain a mean CNAP response. Stimulus amplitude was incrementally increased until peak-to-peak amplitude of the mean CNAP response stabilized, at which time maximal CNAP amplitude was determined. Recruitment curves were constructed to demonstrate the dependence of CNAP amplitude on stimulus current amplitude and estimate stimulus threshold current for CNAP initiation. Absence of CNAPs resulting from retrograde stimulation of spinal motor reflexes was confirmed by repeating CNAP recording at the optimal stimulus amplitude after crushing the sciatic nerve at the sciatic notch for 30 sec using No. 5 Jeweler's forceps. Healthy, unoperative sciatic and peroneal nerves were similarly tested.

Nerve conduction studies administered across implanted devices / regenerated nerve segments demonstrated restored neural activity in 100% of nerves containing silicone nerve guidance conduits with and without the fibrin-based delivery system. In comparison, 83% of nerves containing sieve electrode assemblies filled with fibrin-based delivery system, and 50% of sciatic nerves containing sieve electrode assemblies filled with saline demonstrated restored neural activity.

Representative recordings of CNAPs conducted via regenerated nerve segments are displayed. CNAPs appeared as balanced, biphasic waveforms, typical of differential recording techniques. Identification of CNAPs was confirmed by patterns of recruitment, reversal of positive and negative deflections upon reversal of recording electrode polarity, and retention of waveforms after crushing the proximal sciatic nerve (data not shown). Quantitative evaluation demonstrated that peak-to-peak amplitude of CNAPs conducted through all regenerated nerve segments were significantly reduced compared to CNAPs

conducted through healthy, unoperative nerve (8.87 ± 1.86 mV). CNAPs recorded distal to implanted silicone guidance conduits tended to be of greater amplitude than those recorded distal to comparative sieve electrode assemblies. CNAPs recorded across silicone guidance conduits containing fibrin-based delivery system (4.31 ± 1.33 mV) were found to be significantly greater in amplitude than CNAPs recorded across sieve electrode assemblies containing delivery system (1.54 ± 0.90 mV). CNAP latency was additionally assessed and no statistically significant differences were noted between experimental groups (data not shown).

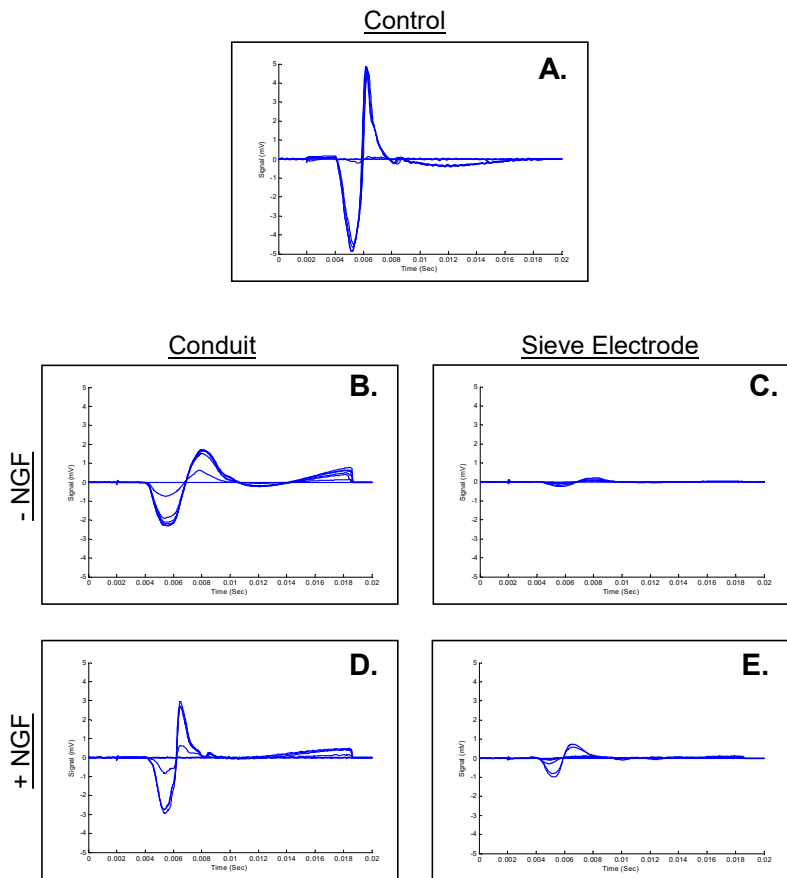


Figure 4-1. Compound neural action potentials (CNAPs) conducted through regenerative nerve tissue present in implanted micro-sieve electrode assemblies and silicone nerve guidance conduits. CNAPs were evoked using silver wire electrodes placed proximal to implanted devices and recorded distally in the peroneal nerve. CNAP recordings resulting from stimuli of varying amplitude were simultaneously plotted to demonstrate fiber recruitment. CNAPs were successfully conducted through unoperative sciatic nerves (A), silicone nerve guidance conduits with (D) and without (B) the fibrin-based delivery system, and sieve electrode assemblies with (E) and without (C) the fibrin-based delivery system. Representative CNAP recordings acquired from each experimental group are shown.

Electrophysiological recordings validate that regenerative nerve tissue crossing chronically-implanted micro-sieve electrodes is functional and capable of conducting propagating CNAPs. This observation confirms that functional axons are effectively penetrating individual via holes and successfully crossing the implanted sieve. Additionally, this data suggests that regenerating axons are successfully regenerating into the distal nerve stump and along the distal nerve towards functional end organs.

Confirmation of the functional status of regenerative nerve tissue further suggests that nerve tissue crossing implanted micro-sieve electrodes may be functionally recruited via electrical stimulation delivered by integrated ring electrodes proximal to regenerating axons.

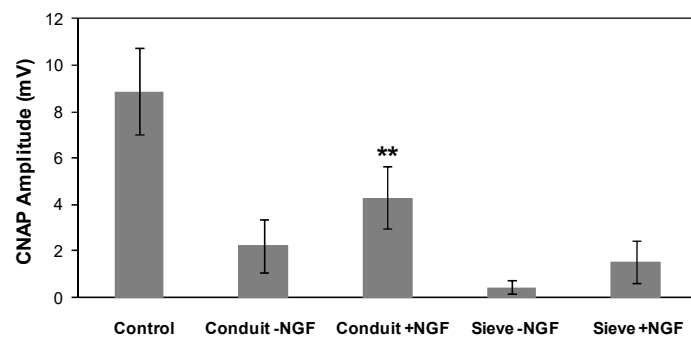


Figure 4-2. Maximum amplitude of compound neural action potentials (CNAPs) conducted through regenerative nerve tissue present in implanted micro-sieve electrode assemblies and silicone nerve guidance conduits. Mean values and standard deviations are shown. ** denotes $p < 0.05$ versus sieve electrode assembly with similar presence/absence of fibrin-based delivery system loaded with NGF.

Despite these promising results, electrophysiological analysis highlighted the limitations associated with low-transparency micro-sieve electrode assemblies. Specifically, micro-electrode assemblies without added neurotrophic support demonstrated functional nerve tissue in only 50% of implanted device. This observation validates prior assumptions suggesting that low-transparency sieve electrode limit functional nerve regeneration due to the presentation of a physical barrier to regenerating axons. Presence of NGF-loaded delivery system within sieve electrode assemblies was

demonstrated to improve the percentage of implanted devices supporting functional nerve tissue (83% vs. 50% of electrodes, respectively), suggesting that positive neurotrophic support improves axonal regeneration in the presence of an artificial physical barrier. Yet, even the presence of neurotrophic support was not able to encourage functional nerve regeneration through all the implanted low-transparency electrodes. This data suggests that while neurotrophic support may augment and encourage functional nerve regeneration through artificial constructs, the limitations of electrodes geometry play a more prominent role in setting regenerative nerve morphology and end functional recovery.

While examination of nerve conduction provided a clear demonstration of the functional status and continuity of regenerating axons passing through implanted electrodes, CNAP studies were unable to determine whether regenerating axons successfully innervated distal musculature. Evaluation of functional reinnervation and evoked muscle force measurement will be evaluated in the subsequent section.

4-3: Electrophysiology: Evoked Muscle Force Measurement

Nerve conduction studies confirm the successful regeneration of functional nerve fibers through implanted micro-sieve assemblies. Yet, evaluation of CNAP propagation through regenerative nerve tissue is unable to inform upon: 1) the presence of motor axons within regenerative nerve tissue crossing implanted electrodes, 2) the ability of regenerated axons crossing implanted sieve electrodes to functionally reinnervate distal musculature, and 3) the degree to which distal musculature is preserved following micro-

sieve implantation. Demonstration of successful integration of peripheral motor axons into implanted regenerative electrodes, and preservation of distal musculature is critical in evaluating micro-sieve electrodes as functional component of future motor neuroprosthetic systems. In order to determine whether regenerated motor axons crossed implanted micro-sieve electrodes and reinnervated distal musculature, an electrophysiological study of evoked muscle force measurement was performed.

Electrophysiological function of regenerative sciatic nerve segments was examined *in situ* at 9 months postoperatively. Electrophysiological function was assessed via evoked motor response in distal musculature. At the terminal time point all animals underwent a non-survival surgery to expose the sciatic nerve and distal musculature for electrophysiological analysis. Animals were anesthetized using 4% Isoflurane / 96% oxygen (induction) and 2% Isoflurane / 98% oxygen (maintenance) administered IH. Following preparation of the sterile field, the right sciatic nerve and its branches were isolated from the sciatic notch to below the point of trifurcation, distal to the popliteal artery. Additionally the extensor digitorum longus (EDL), tibealis anterior (TA), gastrocnemius, and soleus muscles were exposed through skin incisions extending along the anterior and posterior portion of the lower leg.

Sciatic nerve function was assessed by examining the motor response in reinnervated EDL muscle upon stimulation of the sciatic nerve. Following isolation, the distal portions of the extensor digitorum longus (EDL), tibealis anterior (TA), gastrocnemius, and soleus muscles were separated from the leg by severing the distal tendons. The distal tendons were fashioned into a loop and secured to stainless steel S-hooks at the musculotendinous junction using 5-0 nylon suture. Animals were

subsequently placed in a custom-designed force measurement jig where the leg was immobilized by anchoring the femoral condyles. The stainless steel S-hooks attached to the target muscles were connected to either 5 N or 20 N thin film load cells (S100, Strain Measurement Devices Inc., Meriden, CT) supported on an adjustable mount. Cathodic, monophasic electrical impulses (duration = 200 usec, frequency = single-200 Hz, amplitude = 0-3 V) were generated by a single-channel isolated pulse stimulator and delivered to the sciatic nerve proximal to the implanted device via bipolar silver wire electrodes. Resulting force output at muscle tendons was transduced via the load cells and the resulting signals were amplified (gain = 1000X) using instrumentation amplifiers (AD620, Analog Devices Inc., Norwood, MA) powered by a constant voltage source before being recorded on a desktop PC equipped with a data acquisition board and custom Matlab software. Stimulation and recording were synchronized through custom software such that electrical stimulation coincided with the initiation of a 500 msec recording period, wherein data was sampled at 4 kHz. Custom software calculated the passive force and active force for each recorded force trace.

Twitch contractions measured using the custom force recording system were utilized to determine the optimal stimulus amplitude (V_o) and optimal muscle length (L_o) for isometric force production in each muscle (Yoshimura et al; 1999). Stimulus amplitude was incrementally increased while individual muscle length was held constant. V_o was defined as the stimulus amplitude at which the largest active force was produced. Individual muscle length was then increased in 1 mm increments from a relaxed state while the stimulation amplitude was fixed at V_o . Upon determining the muscle length at which the largest active twitch force was produced, a single 300 msec burst of impulses

(frequency = 80 Hz) was delivered to the sciatic nerve, and muscle length was re-evaluated. L_o was directly measured as the length of target muscle from proximal to distal

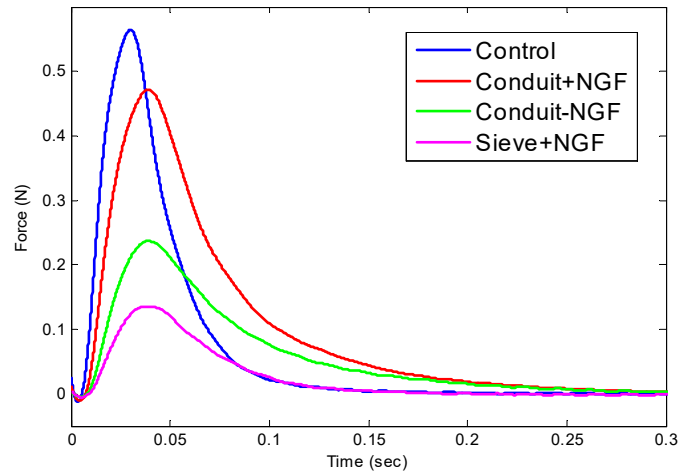


Figure 4-3. Maximum twitch response of reinnervated extensor digitorum longus (EDL) muscles upon stimulation of the sciatic nerve proximal to implanted devices using silver wire electrodes. Representative force recordings acquired from each experimental group are shown. No force recording is displayed for the experimental group employing sieve electrode assemblies without the fibrin-based delivery system as EDL muscles distal to the implanted device did not exhibit any functional recovery at the terminal time point.

musculotendinous junction. All subsequent isometric force measurements were made at V_o and L_o . Single twitch contractions were recorded, and

peak twitch force (F_t) was calculated. Tetanic contractions were recorded by delivering 300 usec bursts of increasing frequency (5-200 Hz) to the sciatic nerve, while allowing two minute periods between stimuli for muscle recovery. Maximum isometric tetanic force (F_o) was calculated from the active force plateau.

Physiological cross-sectional area (PCSA) of the EDL muscle was calculated according to the following:

$$PCSA = \frac{M \times \cos \theta}{(\rho)(L_o)(0.44)}$$

where PCSA = physiological muscle cross-sectional area (cm^2), M = EDL muscle mass (g), θ = angle of pinnation for EDL muscle (0°), ρ = density of mammalian skeletal muscle (1.06 g/cm^3), L_o = optimal muscle length (cm), $0.44 = L_t/L_o$ ratio for EDL muscle

determined previously (Mendez et al; 1960, Gans et al; 1982, Kalliainen et al; 2002, Urbanchek et al; 2001). Maximum specific isometric tetanic force (sF_o) was calculated as the maximum isometric tetanic force (F_o) normalized to muscle PCSA. Healthy, unoperative sciatic nerves and muscles were similarly evaluated.

Evoked motor response in reinnervated EDL muscle was measured upon electrical stimulation of regenerated sciatic nerve via epineurial hook electrode. Measurement of evoked force production demonstrated 100% of animals implanted with silicone nerve guidance conduits with and without fibrin-based delivery system exhibited functional reinnervation of distal motor targets in the EDL muscle. In comparison, 66% of animals implanted with sieve electrode assemblies containing fibrin-based delivery system, and 0% of animals implanted with sieve electrode assemblies containing saline exhibited functional reinnervation of similar motor targets.

Representative twitch and tetanic responses of reinnervated EDL muscles upon electrical stimulation of regenerated nerve are displayed. Quantitative examination of maximum isometric tetanic force

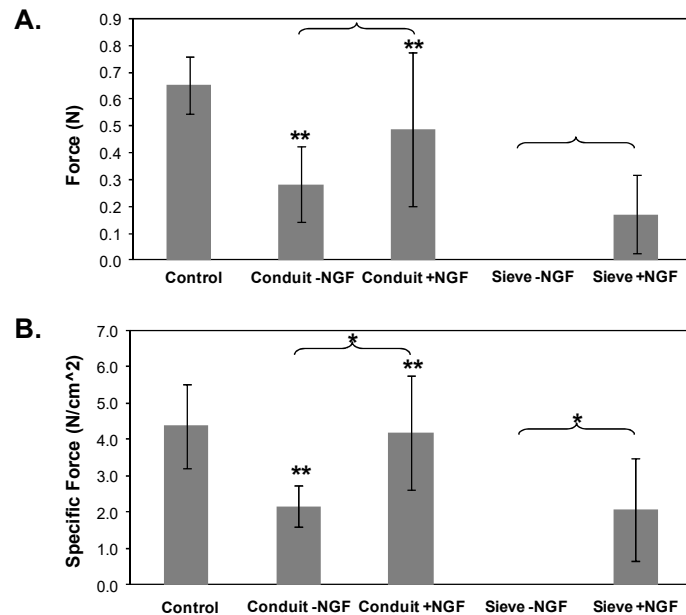


Figure 4-4. Maximum isometric twitch force (A) and maximum specific twitch force (B) evoked by reinnervated extensor digitorum longus (EDL) muscles upon stimulation of the sciatic nerve proximal to implanted devices using silver wire electrodes. Mean values and standard deviations are shown. * denotes $p < 0.05$ versus similar device with dissimilar presence/absence of fibrin-based delivery system loaded with NGF. ** denotes $p < 0.05$ versus sieve electrode assembly with similar presence/absence of fibrin-based delivery system loaded with NGF.

demonstrated that force production in all reinnervated muscles was significantly reduced compared to healthy, unoperative EDL muscle (3.09 ± 0.78 N). Tetanic force measurements demonstrated that silicone nerve guidance conduits tended to permit increased recovery of force production in EDL muscles versus comparable sieve electrode assemblies. EDL muscles reinnervated with silicone conduits containing fibrin-delivery system supported significantly greater tetanic force production (2.19 ± 0.60 N) compared to EDL muscles reinnervated with sieve electrode assemblies containing delivery system (0.71 ± 0.80 N). Examination of maximum isometric twitch force confirmed that silicone nerve guidance conduits with and without the delivery system permitted significantly greater recovery of force production (0.49 ± 0.29 N, 0.28 ± 0.14 N, respectively) than sieve electrode assemblies with and without the delivery system (0.17 ± 0.14 N, 0.0 ± 0.0 N, respectively). Maximum isometric tetanic force data additionally demonstrated that devices containing fibrin-based delivery system tended to promote greater recovery of force production than devices containing saline. Silicone nerve guidance conduits filled with NGF-loaded delivery system permitted significantly greater tetanic force production in reinnervated EDL muscle (2.19 ± 0.60 N) compared to silicone nerve guidance conduits filled with saline (0.83 ± 0.62 N). Maximum isometric twitch force measurements reflected a similar trend, though no statistically significant differences were noted.

Calculation of maximum specific tetanic force production provided a metric of functional recovery independent of length of denervation and degree of muscle atrophy (Aydin et al; 2004, Van der Meulen et al; 2003). Quantitative analysis of maximum specific tetanic force production confirmed trends observed in maximum isometric

tetanic force measurements. Specific force production in all experimental groups was significantly reduced compared to that of healthy, unoperated controls (20.96 ± 7.55 N/cm²), with the exception of silicone nerve guidance conduits containing delivery system (19.95 ± 0.94 N/cm²). Silicone nerve guidance conduits containing fibrin-based delivery system supported significantly increased specific tetanic force production in reinnervated EDL muscle (19.95 ± 0.94 N/cm²) compared to implanted sieve electrode assemblies containing delivery system (7.00 ± 3.22 N/cm²). Silicone conduits and sieve electrode assemblies containing fibrin-based delivery system supported significantly greater specific tetanic force

production in reinnervated EDL muscle (19.95 ± 0.94 N/cm², 7.00 ± 3.22 N/cm²) compared to similar implants filled with saline (6.20 ± 3.32 N/cm², 0.0 ± 0.0 N/cm²).

Electrophysiological evaluation of motor axon regeneration and muscle reinnervation provides critical validation of the underlying theory behind the design and implementation of regenerative electrodes. Specifically, functional

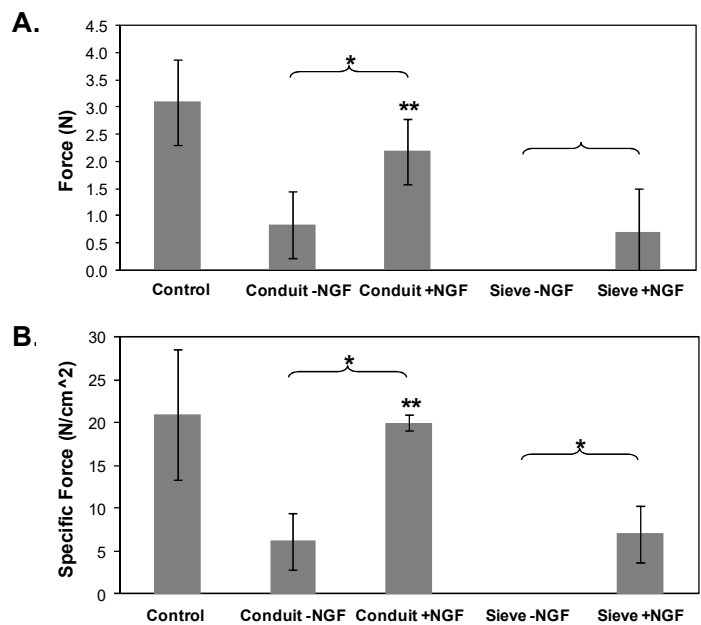


Figure 4-5. Maximum isometric tetanic force (A) and maximum specific tetanic force (B) evoked by reinnervated extensor digitorum longus (EDL) muscles upon stimulation of the sciatic nerve proximal to implanted devices using silver wire electrodes. Mean values and standard deviations are shown. * denotes $p < 0.05$ versus similar device with dissimilar presence/absence of fibrin-based delivery system loaded with NGF. ** denotes $p < 0.05$ versus sieve electrode assembly with similar presence/absence of fibrin-based delivery system loaded with NGF.

stimulation of peripheral nerve tissue proximal to implanted sieve electrodes and recruitment of distal musculature confirms the presence of intact motor axons within the micro-sieve array. Presence of motor axons within the integrated electrode confirm the ability of device to support regenerating motor axons, and more importantly validate the potential for the implanted electrode to functionally recruit integrated motor axons. Demonstration of evoked muscle force production further illustrates the ability of regenerative motor axons crossing the implanted electrodes to reinnervate distal musculature. Observation of muscle activation validates the functional capacity of motor axons present with the chronically-implanted sieve electrode and suggests that micro-sieve electrodes may be able to indirectly control or recruit distal musculature by interfacing local motor fibers. Finally, significant preservation of muscle function following chronic implantation of nerve guidance conduits and micro-sieve electrode assemblies demonstrates the ability of regenerative axons to maintain distal musculature long after device implantation. In total, the results of the present study provide direct evidence of successful regeneration of motor axons through implanted sieve electrodes and successful reinnervation and preservation of distal motor targets.

Similar to prior studies, though, evoked muscle force measurements further highlight the impact of low-transparency micro-sieve electrodes on functional nerve regeneration and post-operative recovery. In the absence of neurotrophic support, no micro-sieve electrode was observed to support regeneration of functional motor axons and reinnervation of distal musculature. In these cases preservation of distal musculature was significantly impacted, a fact generally overlooked in prior studies of regenerative microelectrode interfaces. Significant knock-down of motor reinnervation is most likely

attributed to the physical impediment provided by the small diameter via holes and limited porous region transparency, as noted previously. More pronounced inhibition of motor reinnervation and muscle preservation compared to restoration of nerve conductivity suggest either that motor fiber populations may be more susceptible to the effect of implanted electrode geometries. Specifically, motor fiber populations may be preferentially affected due to their limited population, significantly delayed in their reinnervation of distal musculature, or limited in their ability to regenerate greater distances to reach distal motor end organs. As a result, regenerative sieve electrodes designed to facilitate functional electrical stimulation of motor axons and distal musculature must possess a permissive porous region geometry suitable for robust regeneration of motor axons.

Presence of neurotrophic support in implanted micro-sieve electrode assemblies demonstrated a significant increase in motor reinnervation and functional recovery. In contrast to nerve conduction studies, the presence of neurotrophic support was observed to be critical in supporting regeneration of motor axons through implanted micro-sieve electrodes. Despite the lack of motor-specificity of NGF, focal delivery of neurotrophic factors improved muscle reinnervation and evoked muscle force measurements. Most importantly, validation of motor axon regeneration and reinnervation of distal musculature in the presence of neurotrophic support confirm the potential of micro-sieve electrodes to recruit local motor axons. In total, present testing highlights the critical nature of neurotrophic support in establishing motor axon regeneration and reinnervation through low-transparency artificial constructs.

Demonstration of successful regeneration of motor axon through implanted micro-sieve electrodes in the presence of neurotrophic support suggests that the implanted devices possess the capability to functionally recruit local motor axon populations and thereby control distal musculature. The subsequent section will evaluate the ability of chronically-implanted micro-sieve electrodes to facilitated functional electrical stimulation of integrated motor axons innervating distal muscle groups.

4-4: Electrophysiology: Selective Nerve Interfacing

The presence of functional motor axons within chronically-implanted micro-sieve electrodes suggests that implanted microelectrode possess the capability to functionally recruit local axons and thereby distal musculature. Prior demonstration of the functional connectivity of motor axons extending through the implanted sieve electrode with distal musculature suggest a direct correlation between axons proximal to the implanted interface and distal motor targets. Yet, the capability of micro-sieve electrodes to functionally recruit motor axons and activate distal musculature is largely unknown. Furthermore, the ability of micro-sieve electrodes to impart selective control of distal musculature to date has remained unexplored. Selective activation of various ring electrodes throughout the porous region of the micro-sieve electrodes is propose to offer recruitment of select cross sectional areas of integrated nerve tissue, yet the resulting selectivity of muscle activation is largely unknown. In order to investigate the interfacial capabilities of chronically-implanted micro-sieve electrodes an electrophysiological study of nerve and muscle activation in response to sieve electrode stimulation was performed.

Electrical impulses were delivered to regenerated nerve segments via implanted sieve electrodes in order to determine their ability to interface regenerative nerve tissue. Cathodic, monophasic electrical impulses were generated by a single-channel isolated pulse stimulator and routed in a monopolar configuration to either: 1.) individual ring electrodes, or 2.) all 16 ring electrodes simultaneously within the porous region of implanted micro-sieve electrodes. Electrical impulses will also be routed in various multi-polar configurations to multiple metalized electrodes simultaneously within the porous region of the implanted macro-sieve electrodes. Electrical impulses (duration = 50 usec, frequency = single, amplitude = 0-5 mA) were used to initiate CNAPs which were differentially recorded distal to the implanted device at the peroneal nerve, as previously discussed. Recruitment curves were recorded to demonstrate the dependence of CNAP amplitude on stimulus current amplitude and estimate stimulus threshold current for CNAP initiation. Resulting recruitment curves were compared to those generated using silver wire electrodes to stimulate identical regenerated nerve segments. Electrical impulses (duration = 200 usec, frequency = single, amplitude = 0-5 V) were delivered to regenerated sciatic nerves via implanted sieve electrodes to initiate distal motor responses which were recorded in the extensor digitorum longus (EDL), tibealis anterior (TA), gastrocnemius, and soleus muscles, as previously discussed. Selectivity of motor unit activation was assessed by comparing the motor response in the various muscles and calculating a selectivity index (SI) of each stimulation paradigm. Recorded force traces and peak twitch force (F_t) measurements resulting from stimulation of sciatic nerve via implanted sieve electrodes were compared to those acquired upon stimulation sciatic nerve via silver wire electrodes.

The ability of sieve electrodes to functionally recruit regenerative nerve tissue was assessed via simultaneous electrical activation of implanted electrodes and recording of evoked CNAPs and muscle force production. Testing demonstrated that 50% of implanted sieve electrode assemblies containing fibrin-based delivery system and 16% of assemblies containing

saline effectively

initiated propagating

CNAPs. In comparison,

33% of implanted sieve

electrode assemblies

containing fibrin-based

delivery system and 0% of

assemblies containing

saline were capable of

initiating motor responses in distal musculature.

Regenerative nerve segments within implanted sieve electrode assemblies were stimulated using either epineurial hook electrodes or integrated sieve electrodes.

Representative recruitment curves constructed from CNAP recordings are displayed.

CNAPs were initiated at lower current amplitudes upon electrical activation of embedded

sieve electrodes than upon electrical activation of epineurial hook electrodes. Sieve electrodes elicited neural activation in regenerative nerve segments contained within

sieve electrode assemblies filled with fibrin-based delivery system and with saline at 30 uA and 80 uA, respectively. Identical regenerated nerve segments were similarly

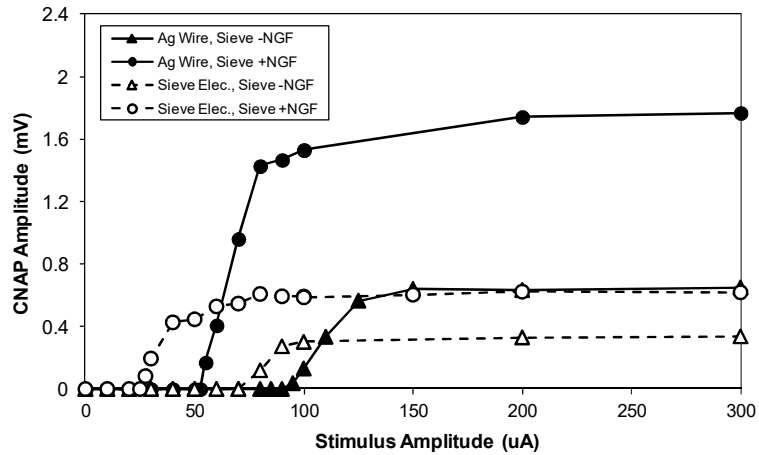


Figure 4-6. Comparison of nerve fiber recruitment via micro-sieve electrode assemblies. Comparison of nerve fiber recruitment via micro-sieve electrode assemblies with and without fibrin-based delivery system using either epineurial silver wire electrodes or implanted regenerative sieve electrodes. Representative recruitment curves acquired from each experimental group are shown.

recruited by epineurial hook electrodes at amplitudes of 55 μ A and 95 μ A, respectively. Current amplitudes required to produce half-maximal response in regenerated nerve segments contained in sieve electrode assemblies with and without delivery system were also lower upon use of sieve electrodes (35.0 μ A, 83.3 μ A, respectively) than upon use of epineurial electrodes (68.5 μ A, 109.5 μ A, respectively). Regenerative nerve segments contained within sieve electrode assemblies filled with fibrin-based delivery system demonstrated lower thresholds of activation (55 μ A) compared to nerve segments contained in sieve electrode assemblies filled with saline (95 μ A). Yet, regenerated nerve segments present inside sieve electrodes assemblies filled with delivery system exhibited CNAP responses of greater amplitude upon stimulation via epineurial hook electrodes (1.77 mV) than upon stimulation via implanted sieve electrodes (0.62 mV). CNAPs initiated in regenerated nerve segments present inside sieve electrodes assemblies filled with saline exhibited a similar trend (0.65 mV, 0.34 mV, respectively). Furthermore, recruitment curves formed upon electrical activation of embedded sieve electrodes were broader than those formed upon activation of epineurial hook electrodes.

Muscle activation resulting from electrical stimulation of regenerated nerve segments was measured to assess the ability of implanted sieve electrodes to functionally recruit regenerated motor axons. Evoked twitch responses in EDL and gastrocnemius

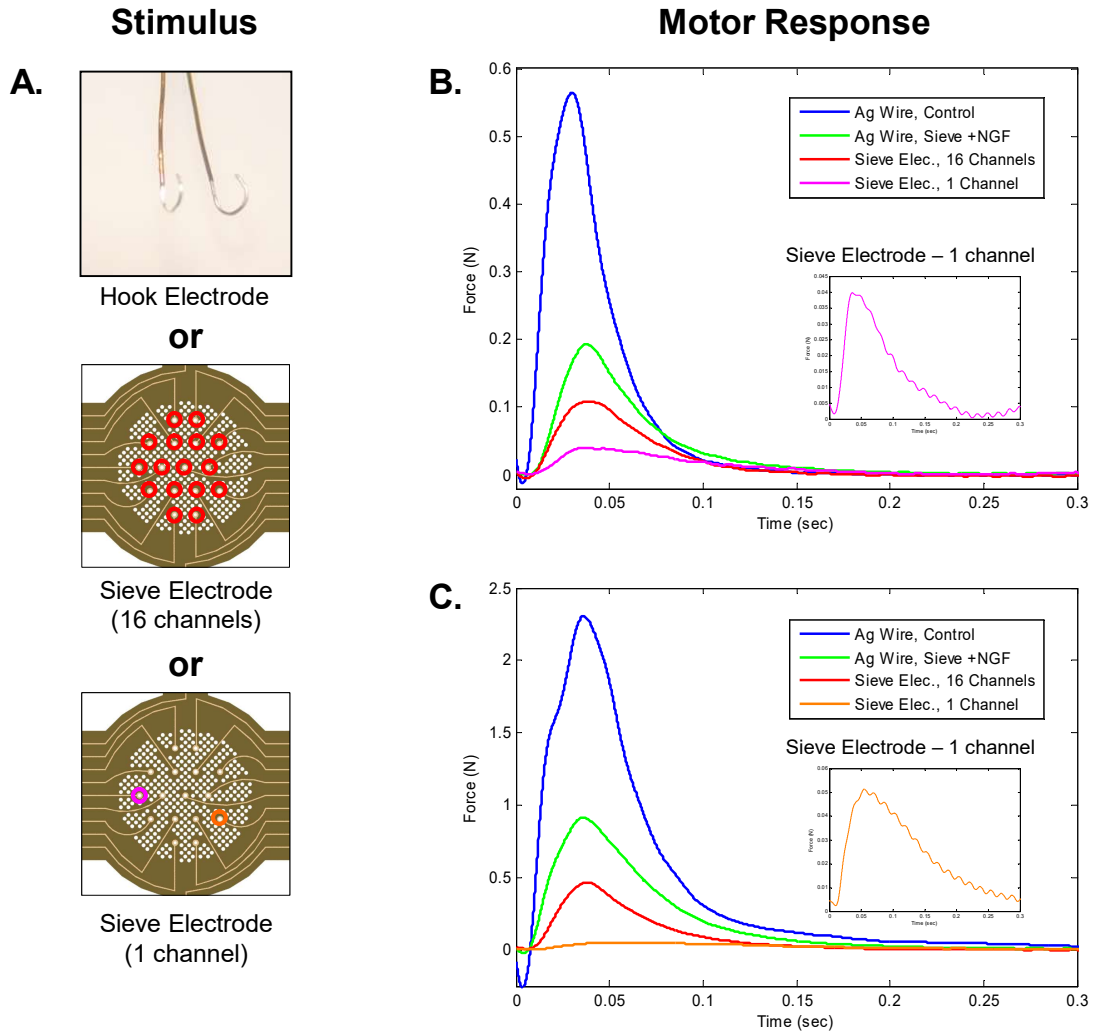


Figure 4-7. Motor response to nerve activation using micro-sieve interfaces. Recruitment of uninjured and regenerative sciatic nerve segments using epineurial silver wire electrodes and implanted sieve electrodes (A) resulted in variable maximum twitch response in uninjured or reinnervated extensor digitorum longus (EDL) muscles (B) and gastrocnemius muscles (C). No force recording is displayed for the experimental group employing sieve electrode assemblies without the fibrin-based delivery system as muscles distal to the implanted device did not exhibit any functional recovery at the terminal time point.

muscles resulting from electrical stimulation are displayed. Electrical activation of epineurial hook electrodes and implanted sieve electrodes both resulted in evoked contractions of varied amplitude in the EDL and gastrocnemius muscles. Examination of motor responses in the EDL muscle demonstrated greater maximum isometric twitch force production upon stimulation of regenerated nerve tissue using epineurial wire

electrodes (0.19 N) than upon simultaneous stimulation of all ring electrodes in the porous area of implanted sieve electrodes (0.11 N). Stimulation of individual ring electrodes in the porous area of implanted sieve electrodes resulted in minute twitch responses selectively in the EDL (0.04 N). Muscle activation resulting from activation of single ring electrodes on implanted sieve electrodes was significantly smaller than activation resulting from simultaneous stimulation of all ring electrodes on the sieve electrode. Neither stimulation of regenerated nerve tissue via epineurial or sieve electrode was able to achieve levels of force production in the healthy, unoperative EDL muscle (0.56 N). Electrical activation of reinnervated gastrocnemius muscle was also assessed. Traces recorded from gastrocnemius muscle demonstrated that stimulation of regenerated nerve tissue via epineurial hook electrodes generated greater force production (0.91 N) than simultaneous electrical activation of all ring electrodes on implanted sieve electrodes (0.46 N). Stimulation of individual ring electrodes on implanted sieves again generated smaller amplitude twitch responses (0.05 N) than simultaneous stimulation of all ring electrodes on identical devices. Stimulation of select individual ring electrodes on implanted sieves produced small, selective twitch responses in either the EDL or the gastrocnemius muscle alone. Muscle specificity exhibited by individual ring electrodes was eliminated upon stimulation of regenerated nerve tissue via epineurial wire electrodes or simultaneous stimulation of all ring electrodes on implanted sieve electrodes. In both cases, electrical activation resulted in simultaneous co-activation of EDL and gastrocnemius muscles. Stimulation of regenerated nerve tissue via epineurial hook electrode and sieve electrode were similarly unable to elicit levels of force production equivalent to healthy, unoperated gastrocnemius muscle and sciatic nerve

(2.307 N). Comparative analysis of the temporal characteristics of EDL and gastrocnemius force traces did not reveal any significant differences between epineurial stimulation and sieve electrode stimulation (data not shown).

To date the capability of micro-sieve electrodes to functionally recruit motor axons and control distal musculature has remained largely unexplored. Prior studies have demonstrated that micro-sieve electrodes achieve a stable, selective interface with peripheral nerve tissue and permit regeneration of functional motor axons. Micro-sieve electrodes have also been shown to electrically interface regenerated nerves, as independent ring electrodes on micro-sieve assemblies have been widely utilized to selectively record small groups of sensory nerve fibers. Existing data suggests that micro-sieve electrodes should be capable of recruiting regenerated axons by stimulating similar ring electrodes within the porous region of the device. Theoretically, micro-sieve electrodes should also possess the ability to selectively recruit regenerated motor axons, and innervated muscles, through activation of specific ring electrodes. The present study was designed to assess the ability of micro-sieve electrode assemblies with and without neuroregenerative features to support functional electrical stimulation by examining both recruitment of peripheral nerve tissue and distal musculature.

Results of the present study validate that micro-sieve electrode assemblies are capable of functionally recruiting regenerative nerve tissue *in vivo*. Observation of CNAP initiation upon electrical activation of ring electrodes on implanted devices confirm that micro-sieve electrodes enable stimulation of functional nerve fibers regenerating through integrated via holes. Micro-sieve electrodes also facilitate a unique and intimate electrical interface with regenerated nerve fibers, evidenced by initiation of

CNAPs at lower stimulus amplitudes compared to epineurial electrodes. The present study additionally demonstrated that micro-sieve electrodes facilitate selective, functional electrical stimulation of regenerated motor axons. Measurement of evoked force production confirm that activation of select ring electrodes on implanted micro-sieve devices recruit specific motor units in multiple muscles innervated by various branches of the interfaced sciatic nerve. Selective activation of ring electrodes on implanted devices additionally provided a successful method of controlling graded force output in antagonistic muscle groups, suggesting that micro-sieve electrode may provide an effective means of controlling motor function in neuroprosthetic applications.

The present study also confirms that the interfacial capabilities offered by implantable micro-sieve electrodes were limited to a certain extent. As predicted, micro-sieve electrodes facilitated a highly selective electrical interface at the great expense of robust axonal recruitment. Specifically, micro-sieve electrodes were capable of independently recruiting small numbers of regenerated motor units, yet were unable to recruit the majority of motor axons regenerating through the electrode. Both of these limitations may be attributed to the specific geometry of micro-sieve electrodes and the implementation of a limited number of small ring electrodes designed to preferentially facilitate focal stimulation. Incorporation of neuroregenerative features into micro-sieve electrode assemblies was found to be essential in establishing a selective interface between implanted electrodes and functional motor axons. Observation of successful recruitment of distal musculature solely by micro-sieve electrode assemblies containing the NGF-loaded delivery system largely confirms that integration of neuroregenerative features may be required to enable proper function of regenerative electrode in vivo.

In total, the present study confirms that micro-sieve electrodes offer a promising and effective means of chronically interfacing peripheral motor axons for the purpose of controlling motor activity. Additionally, this study concludes that incorporation of neuroregenerative features and/or modification of existing electrode geometries may be required to optimize the ability of regenerative electrodes to support functional electrical stimulation of peripheral nerve tissue.

Chapter 5: Macro-Sieve Electrode Fabrication and Testing

5-1: Introduction

Prior chapters describe how micro-sieve electrodes possess many features that limit their ability to selectively recruit regenerated motor axons and control distal musculature. Specifically, the low transparency of the porous region dramatically limits the size of the motor unit pool interfaced by implanted devices. In an effort to design a regenerative electrode better suited to facilitate functional electrical stimulation of peripheral nerve tissue, a novel electrode geometry is proposed. “Macro-sieve” electrodes contain a high-transparency porous region, comprised of a small number of large via holes, designed to maximize nerve regeneration through the implanted device. Theoretically, macro-sieve electrodes should support increased axonal regeneration through integrated via holes, thereby improving the number of functional nerve fibers available for interfacing and decreasing device dependence on neuroregenerative adjuncts. Macro-sieve electrodes should also support regeneration of greater numbers of motor axons through integrated via holes, thereby improving both the size of the accessible motor unit pool and the preservation of distal musculature. In Chapter 5 data will be presented to comparatively evaluate the ability of macro-sieve electrodes to support the regeneration of functional motor axons in vivo.

Evaluation of macro-sieve electrodes proceeded in six steps. The first step was to fabricate individual macro-sieve electrodes utilizing sacrificial photolithography. The

second and third steps were to construct implantable macro-sieve electrode assemblies and load the assemblies with fibrin matrices containing GDNF. The fourth step was to microsurgically implant regenerative sieve electrode assemblies into rodent sciatic nerve for evaluation of nerve integration into the implanted construct. The fifth and sixth steps were to terminally evaluate regenerative nerve morphometry and histology at the micro-sieve / nerve interface. Evaluation of functional nerve regeneration and nerve interfacing via macro-sieve electrodes will be detailed in Chapter 6.

5-2: Fabrication of Macro-Sieve Electrodes

The first step in examining the comparative ability of novel macro-sieve electrodes to support functional axonal regeneration and facilitate selective nerve activation was to construct implantable devices for use in vivo testing. Macro-sieve electrodes were designed utilizing an independent geometry and layout in order to alleviate critical limitations observed in prior micro-sieve electrodes. Specifically, macro-sieve electrodes were designed in order to meet the following key specifications: 1) optimize transparency of the porous region, 2) minimize the amount of wafer material present inside the porous region, 3) ensure adequate spacing of metallized electrode sites throughout the porous region, and 4) implement a design that facilitates electrical interfacing of regenerative nerve tissue across both acute and chronic periods of implantation. Based on these constraints, a novel sieve electrode geometry was composed involving a concentric pattern of radiating spokes and fabricated for in vivo testing.

Macro-sieve electrodes were comprised of a central interface region containing eight peripheral connector pads. The round central interface region (diameter = 5.2 mm) contained a porous area (diameter = 2 mm) comprised of 9 via holes, each ~600 μ m in diameter, arranged in a circular pattern. Transparency of the porous region was approximately 90%. The porous region contained 8 active metalized electrodes (600 μ m x 80 μ m) positioned around the central via hole and on spokes positioned radially within the porous area. Metalized electrodes were connected to eight peripheral connector pads by metalized traces. Peripheral connector pads facilitated ultrasonic bonding of polyimide macro-sieve electrodes to a circular, micro-printed circuit board (I.D. = 3.2 mm, O.D. = 5.2 mm). Micro-printed circuit boards connected traces on the polyimide electrode to metalized via holes utilized to join microwire leads. Eight microwire leads (3/4 inch, 36 AWG, Siliflex, Cooner Wire, Chatsworth, CA) were micro-soldered onto

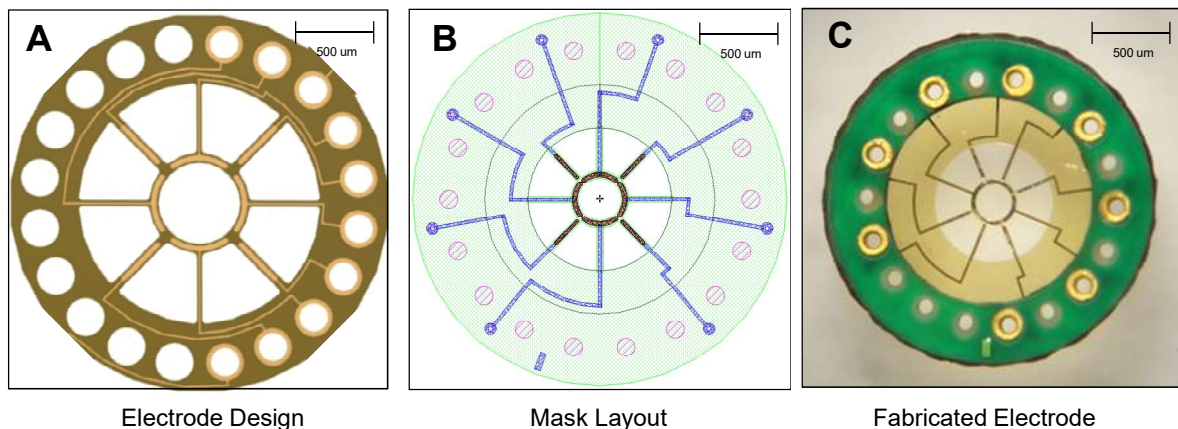


Figure 5-1. Fabricated macro-sieve electrodes. Layout of macro-sieve electrode porous region design (A). Macro-sieve schematic showing polyimide (green), gold traces (blue), and platinized contact pads (red) (B). Optical micrograph of macro-sieve electrode with ultrasonically-bonded micro PCB connector (C).

micro-printed circuit boards to facilitate an electrical interface between metal electrode sites on the polyimide electrode with external instrumentation.

Macro-sieve electrodes were fabricated according the proposed design by NeuroNexus Technologies (Ann Arbor, MI). Regenerative electrodes were fabricated using a similar technique to that

described previously. Similar polyimide resins were utilized as the substrate of the electrode and for the insulation material, while gold was utilized as the metalized layer. Exposed metalized electrode sites within the porous region of the device were functionalized with

platinum/iridium following fabrication. Select macro-sieve electrodes were additionally sent to

Biotechix (Ann Arbor, MI) for further functionalization of exposed metalized site with BTDOT and/or PEDOT coatings. All exposed electrode sites were assessed using cyclic voltammetry and impedance spectroscopy prior to use and/or implantation. Scanning electron microscopy was further utilized to validate electrode features.

Utilizing this approach macro-sieve electrodes were successfully fabricated via sacrificial photolithography. Un-bonded macro-sieve electrodes possessed a unique flexibility and compliance similar to prior micro-sieve electrodes. Bonding of polyimide

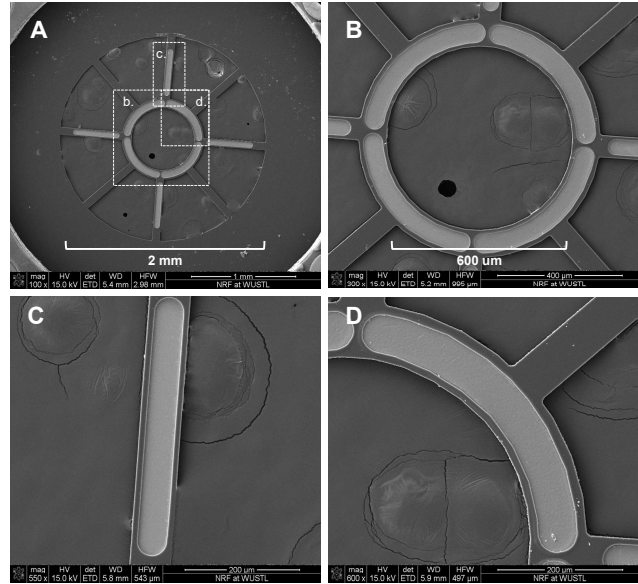


Figure 5-2. Scanning electron micrographs of macro-sieve electrodes. Scanning electron micrographs demonstrate the features of the porous region of novel macro-sieve electrodes (A) including central (B,D) and peripheral (C) metallized electrode sites.

macro-sieve wafer to micro-PCB board significantly increased the rigidity of the implantable construct. Bonding of polyimide macro-sieve wafer to micro-PCB further reinforced electrical connections to the polyimide wafer, as well as simplifying external connections to microwire leads.

Fabricated devices demonstrated acceptable electrical performance for use in functional electrical stimulation applications. Specifically, individual platinized electrode sites located in the porous area of fabricated devices possessed impedances ranging from 18 k Ω – 15.6 M Ω at 1kHz, with $48 \pm 16\%$ of electrodes possessing an impedance < 100 k Ω . Following coating with BTDOT, individual ring electrodes possessed impedances ranging from 9 k Ω – 11.6 M Ω , with $81\% \pm 9\%$ of electrodes possessing an impedance < 100 k Ω . Macro-sieve electrodes with >75% of electrode sites possessing impedances < 100k Ω were selected for use *in vivo*.

High transparency macro-sieve electrodes were successfully fabricated using advanced electrode geometries. Yields of macro-sieve electrodes were significantly improved compared to initial production runs of micro-sieve electrodes. Improvements in yield were most likely the direct result of the use of commercial-grade processes and

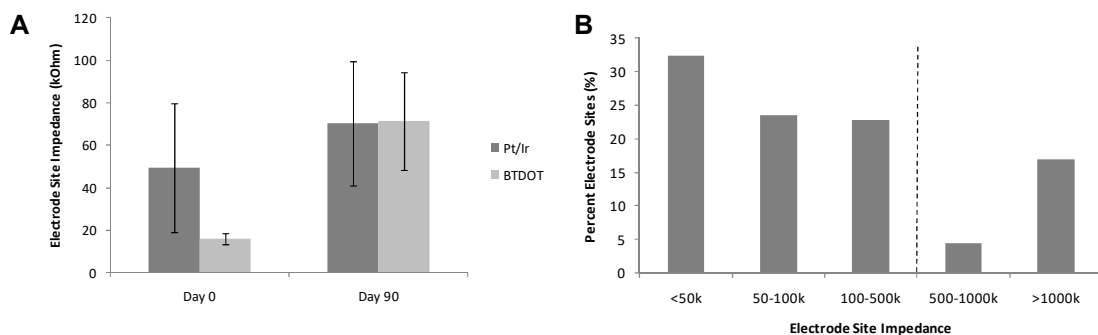


Figure 5-3. Impedance measurements of electrode sites on macro-sieve electrodes. Comparative impedance measurements obtained from macro-sieve electrode sites with and without BTDOT coatings both pre-operatively and post-operatively (90 days) (A). Distribution of impedance measurements across batch of macro-sieve devices (B).

masks by NeuroNexus. Additionally, application of BTDOT demonstrated effective reduction of electrode impedance. While minimal electrode impedance was not reduced by the coating, the general improvement of impedance measurements taken across the entire population of electrode sites was noted. Importantly, many electrodes still retained one or two non-functional electrode sites despite the use of commercial-grade processes. This observation speaks to the inherent limitation of fabrication techniques utilized to product micro-scale flexible electronics, but more importantly suggests that future production runs should be increase in order to allow for adequate selection of pristine device for use in vivo.

5-3: Construction of Sieve Electrode Assemblies

Fabricated macro-sieve electrodes were modified in order to optimize the devices for chronic in vivo application in mammalian peripheral nerve tissue. Modifications were employed to reinforce the macro-sieve electrode / PCB constructs and protect against mechanical stresses experience in vivo. Modifications were also made in order to properly orient and position the fabricated electrodes to the target peripheral nerve. Finally, modifications were made in order to optimally prepare the device for electrical activation and functional nerve interfacing following chronic implantation. Construction of robust sieve electrode assemblies was completed in order to facilitate an un-obstructed evaluation of the chronic performance of fabricated electrodes.

Macro-sieve electrodes were post-modified in preparation for chronic implantation into peripheral nerve tissue. Segments of silicone nerve guidance conduit (length = 5 mm, I.D. = 2 mm, O.D. = 4 mm, A-M Systems Inc., Carlsborg, WA) were

attached to both sides of each sieve electrode. Silicone conduit segments were centered around the porous area within the central interface region using a custom-designed jig and attached to the electrode using silastic medical adhesive (Type A, Dow Corning, Midland, MI). Adhered silicone conduits served as a means of securing peripheral nerve stumps within the sieve electrode assembly, guiding regenerating nerve fibers through the porous region of the electrode, and controlling the regenerative microenvironment at the nerve/electrode interface.

Pt/Ir microwire leads (MedWire, Inc.) were soldered onto gold connector pads present on the micro-PCB in order to functionally interface metallized contact sites on bonded polyimide

electrodes. Pt/Ir microwire leads were subsequently soldered to

a female Omnetics 20-pin connector which was potted for subcutaneous implantation.

Macro-sieve electrodes were then potted in medical grade epoxy (EpoTek 730, Epoxy Technologies Inc., Billerica, MA) in order to protect and insulate bonds adhering the polyimide electrode to the micro-circuit board and micro-solder connections on the micro-printed circuit board. All sieve electrode assemblies were encapsulated in 1-2 mm

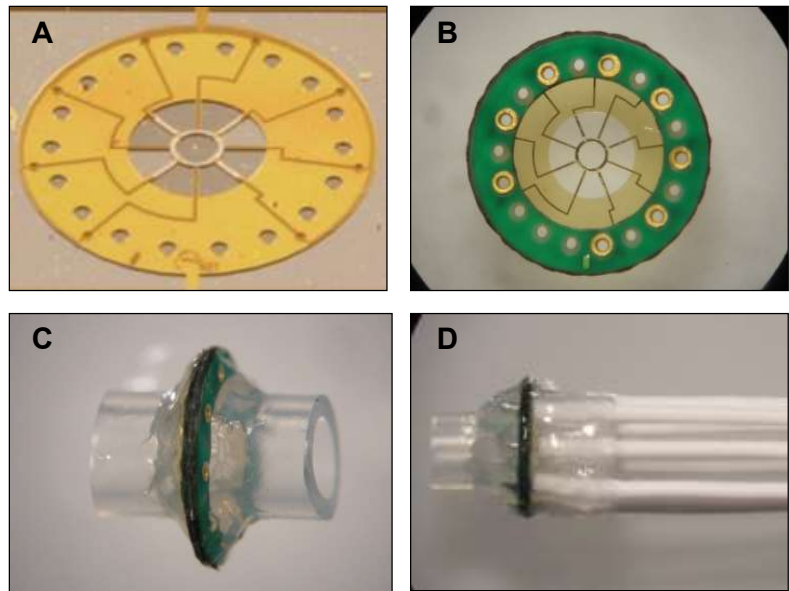


Figure 5-4. Fabricated macro-sieve electrodes and constructed sieve electrode assemblies. Optical micrograph of the porous region of a macro-sieve electrode fabricated via sacrificial photolithography (A). Sieve electrode with attached PCB (B), attached silicone nerve guidance (C), and completed sieve electrode assembly with microwire leads encapsulated in silicone elastomer (D).

of medical grade elastomer (MDX4-4210, Dow Corning, Midland, MI). Silicone encapsulation served to protect electrode integrity and provide mechanical support to the electrode *in vivo*. Silicone nerve guidance conduits (length = 10 mm) lacking sieve electrodes were prepared from similar conduit material to serve as controls to implanted macro-sieve electrode assemblies. Completed sieve electrode assemblies and control silicone conduits were gas sterilized with ethylene oxide and soaked in 70% ethanol prior to use.

Macro-sieve assemblies were designed to maximize mechanical stability of polyimide wafers and insure the fidelity of internal electrical connections. Compared to prior micro-sieve electrodes, macro-sieve electrode assemblies incorporated a number of design changes. Macro-sieve electrode assemblies successfully employed ultrasonically-bonded microPCB as both a mechanical backing and break-out board for metallized leads on the polyimide wafer. Macro-sieve assemblies were constructed utilizing multi-strand Pt/It microwire leads, rather than fragile polyimide ribbon cables. Finally, macro-sieve assemblies utilized implantable Omnetics 20-pin connectors, rather than compression-fit 10 pin connectors. In total, implementation of these design features resulted in a mechanically robust implant well able to withstand the forces and pressures of *in vivo* use. Successful post-modification of macro-sieve electrodes verified the translatable nature of the commercial-grade electrodes and ensured optimal performance of implanted devices during chronic *in vivo* use.

5-4: Preparation of Fibrin Matrices

Prior investigation of chronically-implanted micro-sieve electrodes demonstrated that low-transparency regenerative constructs impede axonal regeneration *in vivo*. Electrophysiological testing further validated that the reduction in axonal regeneration translated to reduced preservation of distal muscle function and increased muscle atrophy. Due to the critical nature of motor axon regeneration through sieve electrode constructs and successful reinnervation of distal musculature, strategies for improving nerve regeneration were investigated. Incorporation of fibrin-based delivery system loaded with B-NGF into micro-sieve electrode assemblies significantly improved axonal regeneration through implanted devices and improved the quality of the sieve/nerve interface. Furthermore, inclusion of neurotrophic factors into micro-sieve constructs enabled functional electrical stimulation of regenerated motor axons penetrating the chronically-implanted micro-arrays. Prior studies therefore demonstrate the necessity of neurotrophic support for successful performance of implanted regenerative electrodes.

Due to the importance of neurotrophic support in prior studies, macro-sieve electrode assemblies were examined with and without the inclusion of the fibrin-based delivery system. Unlike prior studies utilizing a neurotrophic factor selective for sensory axons (B-NGF), *in vivo* studies of macro-sieve electrodes were designed to examine the efficacy of fibrin-based delivery systems loaded with a neurotrophic factor selective for motor axons (Glial-Derived Neurotrophic Factor, GDNF) (Wood et al; 2009, Wood et al; 2011). Prior studies conducted in the laboratory of Dr. Shelly Sakiyama-Elbert at Washington University in St. Louis demonstrate the ability of identical fibrin-based delivery systems to controllable release loaded GDNF *in vivo* (Lee et al; 2003,

Sakiyama-Elbert et al; 2001, Sakiyama-Elbert et al; 2000). Controlled release of GDNF was demonstrated to improve functional nerve regeneration and motor recovery upon inclusion in empty nerve conduits utilized to repair critical 13mm sciatic nerve defects. Fibrin-based delivery systems incorporating GDNF therefore represent a logical selection for use in macro-sieve electrodes design for use in rodent sciatic nerve.

In the present study, fibrin-based delivery system containing GDNF was prepared for use with final finished micro-sieve devices. Specifically, fibrin matrices containing the affinity-based delivery system were prepared in the laboratory of Dr. Shelly Sakiyama-Elbert at Washington University (St. Louis, MO) (Lee et al; 2003). Fibrinogen solutions (8 mg/ml) were prepared by dissolving human plasminogen-free fibrinogen (Calbiotech Inc., Spring Valley, CA) in deionized water for 1 hour at 37° C then dialyzing the solution against 4 L of Tris-buffered saline (TBS) containing 33 mM Tris, 8 g/L NaCl, and 0.2 g/L KCl (Sigma-Aldrich, St. Louis, MO). The fibrinogen solution was sterile filtered using 5.0 um and 0.22 um syringe filters and the concentration of fibrinogen was confirmed by spectrophotometry. Just prior to surgical implantation of either silicone conduits or sieve electrode assemblies containing the delivery system, fibrinogen, TBS, 50mM CaCl₂ in TBS, 20 U/ml thrombin, 25 mg/ml a₂PI₁₋₇-ATIII₁₂₄₋₁₃₄ peptide, 45 mg/ml heparin, and 20 ug/ml recombinant human β-NGF (Peprotech, Rocky Hill, NJ) were mixed in an Eppendorf tube to a final concentration of 100 ng/ml GDNF. Immediately after mixing, silicone conduits were injected with 30 ul of the resulting mixture while silicone conduit segments attached to the sieve electrode assemblies were each injected with 15 ul of the resulting solution. Applied fibrin matrices containing the

heparin-binding delivery system were allowed to polymerize for 5 min prior to surgical implantation.

Prepared fibrin matrices were successfully applied to macro-sieve electrode assemblies and were compatible with surgical deployment and in vivo testing in rodent sciatic nerve models. Demonstration of successful placement and retention of GDNF-loaded fibrin-based hydrogels within attached nerve guidance conduits and around the porous region of integrated macro-sieve electrodes confirmed the ability of delivery system to provide neurotrophic support at the nerve/electrode interface. Deployment of GDNF-loaded delivery system in the present study provided a direct comparison of the efficacy of various neurotrophic factors in accelerating axonal regeneration through micro-fabricated constructs.

5-5: Surgical Implantation / Rodent Model

Following successful construction, macro-sieve electrode assemblies were tested in a rat sciatic nerve model identical to that utilized to evaluate micro-sieve electrode implants (Varejo et al; 2004). Prior to initiation of in vivo testing, surgical methods were optimized to implant macro-sieve electrodes in the rat sciatic nerve. Techniques were identified which would allow for: 1) appropriate placement of macro-sieve electrode assemblies, 2) optimal alignment of macro-sieve electrodes orthogonal to the sciatic nerve, 3) secure apposition of the proximal / distal nerve stumps to the attached nerve guidance conduits, and 4) optimal routing of Pt/It leads and subcutaneous placement of Omnetics connectors for terminal interfacing of chronically-implanted sieve electrodes.

Resulting surgical procedure were conducted in the following manner. Male, Lewis rats (275-300 g) were anesthetized using 4% Isoflurane / 96% oxygen (induction)

and 2% Isoflurane / 98% oxygen (maintenance) administered IH. Following preparation and sterilization of the lateral aspect of the right leg, the right sciatic nerve was exposed through a dorsolateral gluteal muscle-splitting incision followed by blunt dissection. Utilizing an

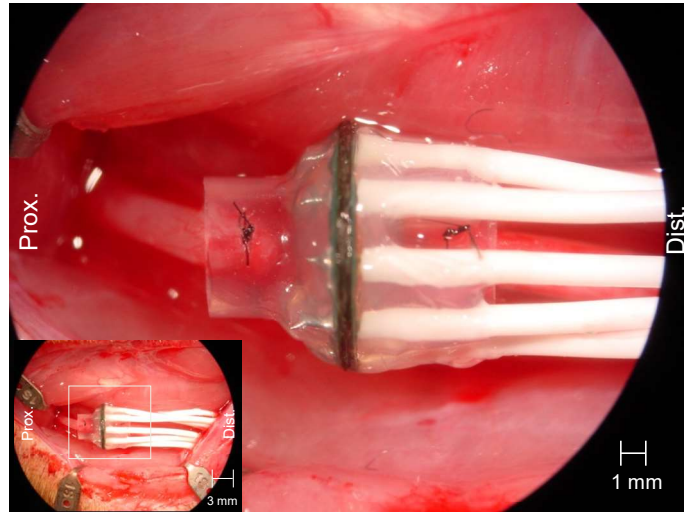


Figure 5-5. High magnification view of implanted macro-sieve electrode. Intraoperative photograph of a macro-sieve electrode assembly implanted between the transected ends of the rat sciatic nerve.

operating microscope, the sciatic nerve was transected proximal to the trifurcation and the proximal and distal nerve stumps were inserted into either: 1.) the ends of a prepared silicone nerve guidance conduit, or 2.) the ends of silicone nerve guidance conduit segments attached to a prepared sieve electrode assembly. Proximal and distal nerve stumps were secured inside respective silicone conduits with four interrupted epineurial 9-0 nylon sutures, such that an 4 mm gap existed between stumps in all implanted systems. Following implantation of macro-sieve electrode assemblies into transected sciatic nerves, Pt/Ir microwire leads were routed medially through later musculature into a subcutaneous pocket located on the back of the animal mid-way between the hind legs. Omnetics connectors were subcutaneously implanted for re-exposure and terminal nerve interfacing. Incisions were closed in two layers using uninterrupted and interrupted 4-0 vicryl suture to close the muscle and skin, respectively. VetBond™ tissue adhesive (3M, St. Paul, MN) was also applied to the incision in order to ensure closure, and all

animals were fitted with a poly-ethylene collar for one week in order to prevent autophagia and disturbance of the operative site. All operative and post-operative procedures described were conducted under sterile conditions using aseptic techniques.

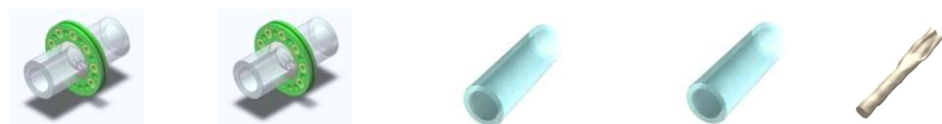
Utilizing this technique macro-sieve electrode assemblies and nerve guidance conduits, containing either fibrin-based delivery system or saline were successfully implanted in the right sciatic nerve of Lewis rats. Surgical implantation was well tolerated, as tension-free coaptation of transected nerve stumps and silicone conduits was achieved in all cases. Few complications were noted post-operatively, and intermittent evaluation of motor function via calculation of sciatic function index demonstrated progressive motor recovery in operative limbs over the course of the study. Generally, macro-sieve electrode assemblies more easily tolerated by laboratory animals and presented a lower profile during post-operative recovery and chronic implantation.

Successful deployment of macro-sieve electrodes enabled expanded testing and examination of axonal regeneration through macro-sieve electrode assemblies with and without integrated neurotrophic support. In vivo testing served to evaluate the ability of macro-sieve electrodes to achieve a stable interface to peripheral nerve tissue and thereby provide a means of facilitating therapeutic or rehabilitative electrical stimulation of interfaced nerve. In vivo testing further examined the comparative effect of high-transparency sieve electrode geometries on nerve regeneration and muscle reinnervation. Finally, in vivo testing facilitated examination of the ability of macro-sieve electrodes to facilitate FES of regenerated motor axons and innervated musculature.

Forty adult male Lewis rats were randomized into 5 experimental groups (I-IV) of 8 animals each (n=8). Animals in Group I served as unoperative controls and did not

undergo surgical exposure or transection/repair of the sciatic nerve. Animals in Group II-V underwent surgical exposure and transection of the sciatic nerve, followed by microsurgical implantation of either a silicone nerve guidance conduit or a macro-sieve electrode assembly. In Group II, a silicone conduit containing sterile saline was implanted between the transected ends of the sciatic nerve. In Group III, a silicone conduit containing the fibrin-based delivery system loaded with GDNF was implanted between the transected ends of the sciatic nerve. In Group IV, a macro-sieve electrode assembly containing sterile saline was implanted between the transected ends of the sciatic nerve. In Group V, a macro-sieve electrode assembly containing the fibrin-based delivery system loaded with GDNF was implanted between the transected ends of the sciatic nerve. Animals in all groups underwent *in situ* evaluation of sciatic nerve function upon termination of the study 3 months, post-operatively. Following *in situ* assessment, all sciatic nerves were explanted and fixed for morphological and histomorphometric analysis.

Macro-sieve electrodes were successfully implanted and well tolerated throughout the duration of the study. 100% of animals implanted survived to the terminal time point. At the terminal time point all implanted devices and host sciatic nerves were surgically



Group:	Sieve -GDNF	Sieve +GDNF	Conduit -GDNF	Conduit +GDNF	Control
Electrode:	Macro-sieve	Macro-sieve	None	None	None
Conduit:	Silicone Conduit	Silicone Conduit	Silicone Conduit	Silicone Conduit	None
Regen. System:	Saline	Fibrin DS +100ng/ml GDNF	Saline	Fibrin DS +100ng/ml GDNF	None
	n=8	n=8	n=8	n=8	n=8

Table 5-1. Experimental design: Study of regenerative micro-sieve electrodes. Experimental groups utilized in the investigation of micro-sieve electrodes with and without NGF-loaded delivery system. (DS, delivery system; NGF, nerve growth factor.)

exposed. Similar to prior macro-sieve electrodes, all implanted macro-sieve devices were covered by a similar, thin layer of fibrous tissue. Macro-sieve electrodes demonstrated improved ability to maintain proper orientation and placement in vivo with the majority of implanted devices oriented parallel to the course of the sciatic nerve upon explantation. Absence of polyimide ribbon cable and connector pads additionally allowed macro-sieve electrode assemblies to present a lower profile in vivo. No device damage was observed in macro-sieve assemblies, unlike ribbon cable shearing observed upon prior testing of micro-sieve electrodes.

Similar to prior studies, gross examination of implanted nerve guidance conduits revealed that 100% of nerve guidance conduits injected with fibrin-based delivery system, and 100% of nerve guidance conduits injected with saline contained regenerative nerve cables bridging the imposed nerve defect. Nerve regeneration through silicone nerve guidance conduits was consistent with prior studies. Gross examination of implanted macro-sieve electrodes revealed that 100% of macro-sieve assemblies loaded with fibrin-based delivery system, and 100% of macro-sieve assemblies loaded with saline contained robust regenerative nerve cables. Gross observations revealed significantly greater amounts of regenerative nerve tissue crossing implanted macro-sieve electrodes compared to implanted micro-sieve electrodes. Implanted macro-sieve electrode assemblies demonstrated minimal rotation and migration in vivo compared to prior micro-sieve electrodes.

Successful development and surgical implementation of macro-sieve electrodes confirmed the translational capability of novel high-transparency implants. Macro-sieve electrodes demonstrated noted stability and longevity in vivo. Specifically, selective

implementation of multi-strand Pt/It microwire leads and removal of polyimide ribbon cable significantly improved ease of surgical implantation and reduced post-operative breakage and shearing of the polyimide construct. Integration of circular micro-PCB board further reduced the profile of the implanted device and oriented microwire leads along the axis of the interface sciatic nerve. Gross observation of macro-sieve devices following implantation confirmed the chronic stability of the device, as well as the ability of the device to successfully integrate into native peripheral nerve tissue. Dissection and explantation of macro-sieve device revealed robust nerve regeneration through assemblies containing both fibrin-based delivery system and saline. The presence of regenerative tissue within macro-sieve electrode assemblies was notably increased compared to prior observations taken of micro-sieve constructs implant for longer durations. These preliminary results provide initial evidence for successful design of novel macro-sieve electrodes, as well as for robust integration of macro-sieve electrodes into rodent peripheral nerve tissue.

5-6: Regenerative Nerve Morphology

Previous sections outlined the design and implantation of novel macro-sieve electrode assemblies in a rodent peripheral nerve model. Gross observations document the presence of regenerative nerve tissue within chronically-implanted nerve conduits and micro-sieve assemblies, dissection of regenerative nerve tissue for morphological and histological examination was conducted to further evaluate neural integration of implanted constructs. Specifically, morphological analysis of regenerative nerve tissue crossing implanted nerve guidance conduits and macro-sieve electrode assemblies was

conducted in order to: 1) document the presence and degree of axonal regeneration within the implanted constructs, and 2) examine the influence of implanted constructs on local nerve tissue.

Unoperative (n=8) and regenerative nerve segments (n=8) from all experimental groups were explanted and fixed using 4% paraformaldehyde in 0.1 M phosphate buffer (pH = 7.2) for 24 hours. All regenerative nerve tissue was dissected from silicone nerve guidance conduits. Regenerative nerve segments contained in sieve electrode assemblies were removed without disturbing the integrated porous area of the implanted sieve electrode. Explanted regenerative nerve tissue was then examined under low magnification using a stereo microscope (Olympus).

Examination of regenerative nerve tissue obtained from silicone conduits and macro-sieve sieve electrode assemblies demonstrated similar single-cable morphologies both in the presence and absence of the delivery system. Closer examination of regenerative nerve tissue present at the nerve/electrode interface

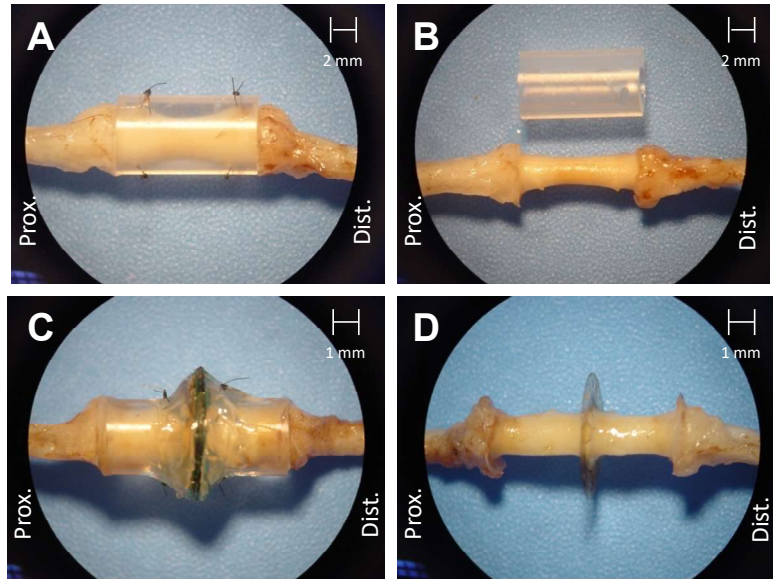


Figure 5-6. Explanted macro-sieve electrodes and regenerative nerve tissue. Optical micrographs of silicone nerve guidance conduits without delivery systems (A) and macro-sieve electrodes without delivery system (C) at 3 months post-operatively. Optimal micrographs of regenerative nerve tissue present within identical nerve guidance conduits without delivery systems (B) and macro-sieve electrodes without delivery system (D).

demonstrated multi-fascicular architectures mirroring the porous region geometry present in implanted macro-sieve electrodes. Similar to prior studies, regenerative nerve cable present inside of silicon nerve guidance conduits alone presented a “tapered” morphology wherein the diameter of the cable was smaller in the middle of the conduit and larger near the ends of the conduit. Observed tapered morphologies were consistent with prior studies and most likely the result of poor adhesion of regenerating axons and extracellular matrix to the inner lumen of the PDMS conduit.

Unlike prior studies examining micro-sieve implants, explanted macro-sieve electrode assemblies did not exhibit the “conic enlargement” in regenerative nerve tissue noted previously. Nerve cables crossing implanted macro-sieve electrodes appeared similar to those observed in silicone conduits both in the presence and absence of the

delivery system. The majority of implanted macro-sieve electrodes contained a robust regenerative nerve cable comprising the majority of the volume of attached silicone nerve guidance conduits. Examination of sections taken at the nerve/electrode interface

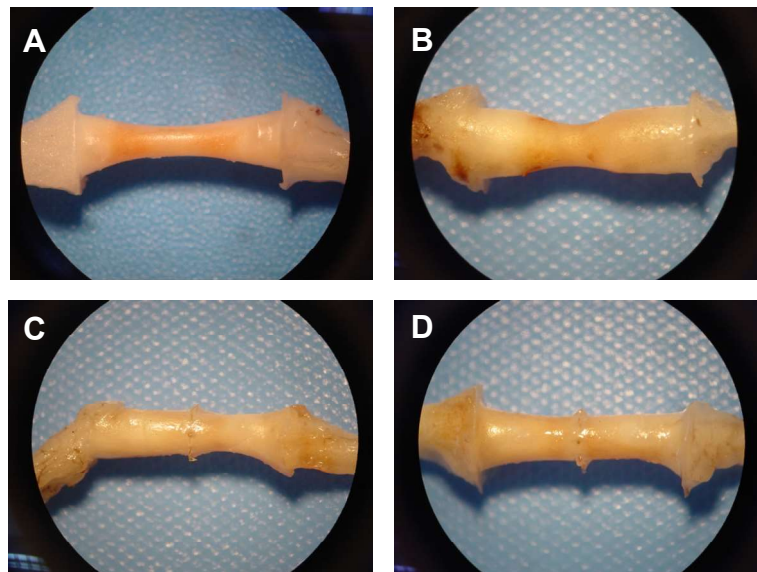


Figure 5-7. Explanted regenerative nerve tissue. Optimal micrographs of regenerative nerve tissue present within identical nerve guidance conduits with (B) and without (A) delivery systems and macro-sieve electrodes with (D) and without delivery system (C).

did not demonstrate the presence of numerous nerve “microfascicles” as seen in micro-

sieve electrodes. Instead regenerative nerve tissue demonstrated a small number of large diameter fascicles mirroring the organization of the implanted macro-sieve electrode. Macro-sieve electrode assemblies with and without the GDNF-loaded delivery system demonstrated similar a morphology. The observed volume of nerve tissue present at the nerve/electrode interface was similar both in the presence and absence of the delivery system.

Observation of regenerative nerve tissue and fascicles within implanted macro-sieve electrode assemblies validate the successful integration of implanted electrodes into host nerve tissue. Similar to prior micro-sieve electrodes, macro-sieve electrode assemblies are capable of supporting axonal regeneration in vivo. Formation of numerous fascicles at the

nerve/electrode demonstrate that macro-sieve electrodes similarly modulate regenerative nerve morphology. Yet, the morphological differences observed in regenerative nerve tissue obtained from micro- and macro-sieve electrode assemblies suggest that axonal regeneration occurs under independent processes in the presence of each

electrode. Specifically, the lack of a “conic enlargement” in regenerative nerve tissue

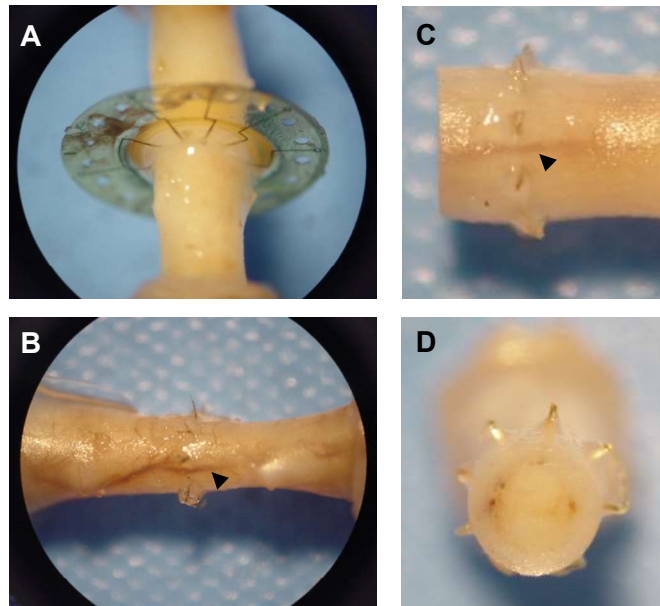


Figure 5-8. Integration of macro-sieve electrodes into regenerative nerve tissue. Optimal micrographs of regenerative nerve tissue crossing macro-sieve electrodes (A). Micro-vasculature crossing implanted macro-sieve electrode (B, C, D).

suggests that macro-sieve electrodes do not impart the same physical impedance of regenerating nerve tissue as low-transparency regenerative electrode. This observation may also suggest that macro-sieve electrodes are more permissive of axonal regeneration in vivo, and thereby better suited to promote rapid reinnervation and preservation of distal musculature.

Observations of regenerative nerve tissue also provide initial demonstration that the presence of neurotrophic factors has a distinctly different impact on macro-sieve electrode assemblies as compared to micro-sieve electrode assemblies. Specifically, the quality and morphology of regenerative nerve tissue crossing implanted macro-sieve electrodes was comparable in both the presence and absence of GDNF-loaded delivery system. Preliminary results therefore suggest that the presence of neuroregenerative factors is less critical in axonal regeneration through high-transparency implanted artificial constructs. More detailed histological examination of regenerative nerve tissue is required to draw firm conclusions on the effect of GDNF on nerve regeneration through implanted macro-sieve electrodes.

More rigorous histological and histomorphometric examination of regenerative nerve tissue within chronically-implanted macro-sieve electrode assemblies is outlined in the following section.

5-7: Regenerative Nerve Histology

Histological and histomorphometric analysis was conducted in order to accurately assess regenerative nerve tissue integrated into chronically implanted macro-sieve

electrodes. Histological analysis via epoxy sectioning provided a detailed view of regenerative nerve microstructure, including the number and density of peripheral nerve fibers, diameter of peripheral nerve fibers / axons, and presence of axonal injury, cellular debris, and foreign body response. Evaluation of epoxy sections immediately proximal and distal to the nerve/electrode interface was performed to examine successful penetration of regenerating axons through the porous region of the implanted device. Results were compared to retrograde labelling studies conducted on nerve tissue distal to implanted macro-sieve electrodes. Evaluation of epoxy sections 5mm distal to the nerve/electrode interface was additionally performed to examine axonal regeneration into the distal nerve stump following sieve electrode implantation. Epoxy sections stained with Toluidine Blue were evaluated to measure the quantity, density, and myelination of regenerated nerve fibers.

Macro-sieve electrode assemblies (n=8) from each experimental group were explanted and fixed in cold 3% glutaraldehyde in 0.1 M phosphate buffer (pH = 7.2). Regenerative nerve tissue including the porous area of the sieve electrode was dissected from the silicone conduit segments, post-fixed with 1% osmium tetroxide, ethanol dehydrated, and embedded in Araldite 502 epoxy resin (Polysciences, Warrington, PA). Cross sections <1 um thick were cut 5 mm proximal, immediately proximal, immediately distal, and 5 mm distal to the integrated electrode with an LKB III Ultramicrotome (LKB-Produkter A.B., Bromma, Sweden) and stained with 1% toluidine blue. Slides were examined using light microscopy and were evaluated by an observer blinded to the experimental groups for overall nerve architecture, quantity of regenerated nerve fibers, degree of myelination, and Wallerian degeneration.

Quantitative analysis was performed on toluidine blue stained sections using a semi-automated digital image analysis system linked to a custom software package (LECO Instruments, St. Joseph, MI) adapted for nerve morphometry, as previously described (Hunter et al; 2007). The system digitized microscope images and displayed them on a video monitor calibrated to 0.125 $\mu\text{m}/\text{pixel}$. Images of sectioned nerve tissue were divided into $5.5 \times 10^4 \mu\text{m}^2$ frames and evaluated using eight-bitplane digital pseudocoloring and thresholding-based algorithms to select for myelinated axons. At 1000X magnification six fields were selected at random per cross section, or a minimum of 500 myelinated fibers, were evaluated to calculate myelin width, axon width, and fiber diameter. The following morphometric indices were calculated using these primary measurements: number of nerve fibers, nerve fiber density (fiber number/ mm^2) percent nerve tissue ($100 \times \text{neural area} / \text{intrafascicular area}$), mean fiber width (μm), myelinated fiber area (μm^2), myelin area (μm^2), microfascicle diameter (μm), and number of nerve fibers per microfascicle.

Ultrathin sections (90 nm) were additionally cut using a LKB III Ultramicrotome for analysis via electron microscopy. Sections were stained with uranyl acetate and lead citrate and imaged with a Zeiss 902 electron microscope (Zeiss Instruments, Chicago, IL) at 4360X magnification, scanned at 400 dots/inch resolution, and evaluated with MicroBright Field Stereo Investigator (Version 7.0, MBF Bioscience Stereo Investigator, Williston, VT), as previously described (Hunter et al; 2007). Composition of fascicles, quality of myelination, and the relative prevalence of unmyelinated fibers were qualitatively evaluated.

Epoxy sections taken proximal to the macro-sieve electrode, at the sieve/nerve interface, and distal to the macro-sieve electrode were utilized to examine regenerated nerve fibers and quantify various morphometric indices. Toluidine blue-stained sections taken proximal to integrated macro-sieve electrodes demonstrated a large population of well-myelinated peripheral

nerve fibers. Sections obtained ~300um proximal to the sieve/nerve interface demonstrated a pronounced fascicular architecture mirroring the geometry and organization of the porous region of the macro-sieve electrode. Specifically, nine fascicles of varying size (dia:

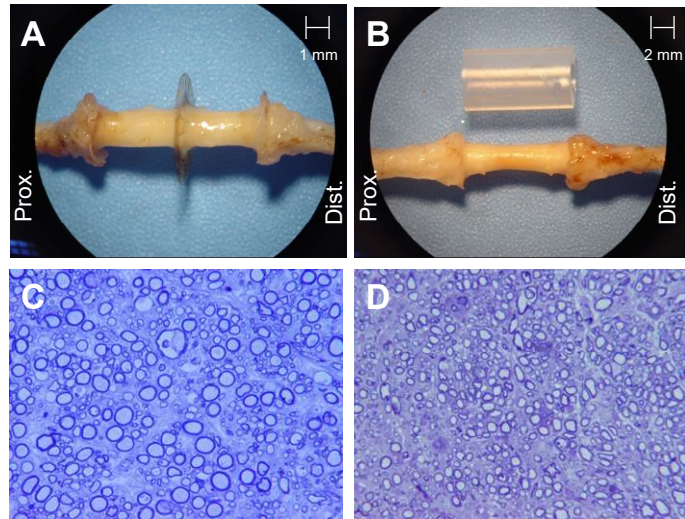


Figure 5-9. Explanted regenerative nerve tissue. Optimal micrographs of regenerative nerve tissue present within macro-sieve electrodes (A) and silicone guidance conduits (B) without delivery system and representative toluidine blue stained sections of regenerative nerve tissue (C, D).

300 – 550 μ m) and shape were observed. Examination of sections nearer the sieve/nerve interface demonstrate the progressive development and separation of fascicles. Unlike prior micro-sieve studies, the formation of micro-fascicles arranged in hexagonal pattern was not observed.

Further examination revealed the presence of numerous myelinated and unmyelinated axons within the regenerative nerve tissues and within each fascicle. Sections taken at the sieve electrode/nerve interface demonstrated minimal evidence of foreign body reaction to the electrode or fibrous encapsulation of the porous region of the

device. A thin layer of fibroblasts was noted lining the inner lumen of each large via hole within the porous region of the macro-sieve electrode, yet no

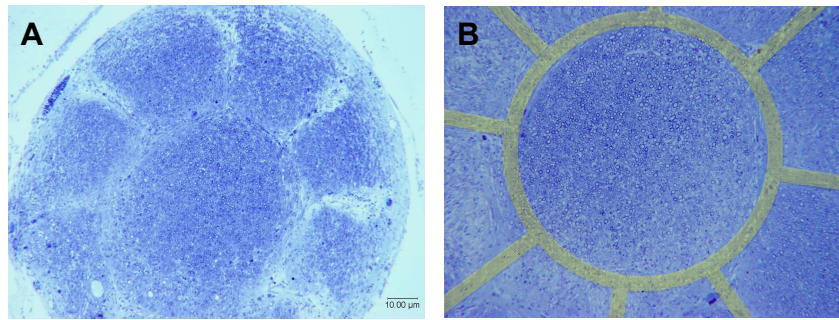


Figure 5-10. Epoxy nerve sections obtain at the macro-sieve/nerve interface. Optimal micrographs of epoxy nerve sections stained with toluidine blue under low magnification (A) and high magnification (B). Sections were acquired at the nerve/electrode interface.

evidence of fibrosis or chronic inflammation was observed. Sections taken distal to the macro-sieve electrode similarly demonstrated numerous regenerated nerve fibers reinnervating tibial, peroneal, and sural branches of the sciatic nerve. Presence of regenerated nerve fibers in distal branches of the sciatic nerve, as seen in high magnification views of the peroneal branch, suggest that nerve fibers successfully regenerated from the proximal nerve stump, through via holes in the macro-sieve electrode, and into the distal nerve stumps. Comparable appearance of regenerative axon proximal and distal to the implanted sieve electrode further suggests that the implanted micro array did not affect axonal health or function. Results of retrograde labelling studies and examination of nerve regeneration in GFP rats further confirm successful regeneration of peripheral axons through implanted macro-sieve electrodes.

Quantitative analysis of epoxy sections taken proximal and distal to implanted construct confirmed robust axonal regeneration through implanted macro-sieve electrodes comparable to empty silicone nerve guidance conduits. Representative sections taken at the sieve/nerve interface in macro-sieve assemblies filled with either fibrin-based

delivery system or saline revealed little difference in the quantity and quality of regenerative nerve tissue. Sections taken from regenerative nerve tissue contained in assemblies filled with the GDNF-loaded delivery system revealed distinct fascicular organization, large cross sectional nerve area, and high fiber density. Sections taken from regenerative nerve tissue contained in macro-sieve assemblies filled with saline similar fascicular organization, large cross sectional nerve area, and high fiber density. Observations therefore suggest that the presence of neurotrophic support in the case of implanted macro-sieve electrodes did not significantly affect axonal regeneration through the implanted construct. Regenerative nerve tissue present at the sieve electrode/nerve interface in macro-sieve electrodes assemblies containing saline demonstrated similar total fiber counts ($17,254 \pm 1,834$ fibers) compared to macro-sieve electrodes assemblies containing delivery system ($19,115 \pm 2,155$ fibers). Quantitative assessment further demonstrated that individual regenerated fibers contained in macro-sieve electrode assemblies with and without the delivery system were similar in diameter and in axon/myelin ratio. Unlike histological examination regenerative nerve tissue present inside micro-sieve electrode assemblies, the present study demonstrates significantly greater regenerative nerve tissue within macro-sieve electrodes assemblies. These results further demonstrate the limited impact of neurotrophic factors on the quality of regenerative nerve tissue within implanted macro-sieve constructs.

In total, histological analysis of regenerative nerve tissue validates successful and robust axonal regeneration through chronically-implanted macro-sieve electrodes. Epoxy sections validate the capability of implanted macro-sieve electrodes to integrate into native nerve tissue and modulate regenerative nerve ultrastructure. Formation of

numerous fascicles at
 the nerve/electrode
 interface confirm the
 ability of implanted
 regenerative electrodes
 to modulate nerve
 morphology.
 Specifically, high-
 transparency macro-
 sieve electrodes

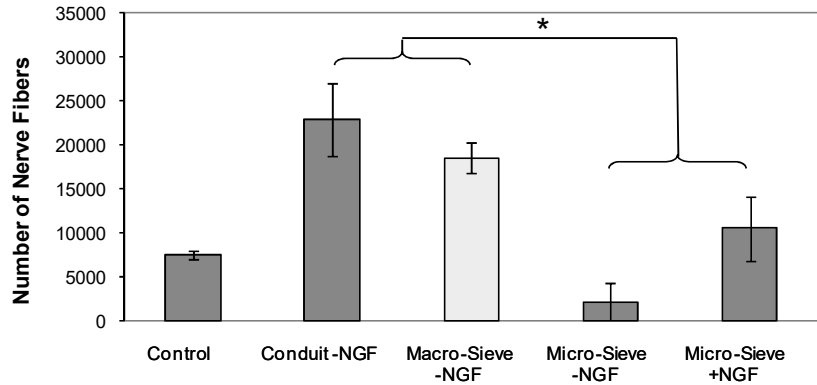


Figure 5-11. Histomorphometric analysis of regenerative nerve tissue present in macro-sieve electrode assemblies and silicone nerve guidance conduits. Nerve fiber count was assessed distal to implanted sieve electrodes/nerve conduits, at the sieve/nerve interface, and distal to implanted sieve electrodes/nerve conduits. Greater numbers of nerve fibers were noted in regenerative nerve tissue distal to macro-sieve assemblies compared to micro-sieve assemblies containing saline. Mean values and standard deviations are shown. * denotes $p < 0.05$.

enabled the formation of fewer, larger fascicles containing greater numbers of regenerative nerve fibers compared to micro-sieve electrodes. Histological analysis further confirms that high-transparency macro-sieve electrodes do not appear to impede axonal regeneration in vivo. Comparable numbers of regenerative nerve fibers crossing both implanted nerve guidance conduits and macro-sieve electrodes suggest a minimal impact of macro-sieve electrodes on axonal regeneration post-operatively.

Incorporation of neurotrophic support into macro-sieve electrode assemblies was also noted to have a different effect compared to that observed in micro-sieve electrodes. Inclusion of GDNF-loaded fibrin-based delivery systems did not have a profound impact on axonal regeneration through implanted macro-sieve electrodes and was not required to establish a sufficient interface between nerve/electrode. While these observations do not negate the importance of neurotrophic support in axonal /nerve regeneration, specifically in more challenging nerve defects, they suggest that optimal design of regenerative nerve

interfaces may reduce the need for additional inclusion of pro-regenerative cues. In total, the present study confirms that macro-sieve electrodes are capable of supporting robust populations of regenerated axons and achieve an intimate interface with peripheral nerve tissue ideal for electrical stimulation of peripheral axons even in the absence of added neurotrophic support.

Chapter 6: Peripheral Nerve Interfacing **Via Macro-Sieve Electrode**

6-1: Introduction

In Chapter 5, novel high-transparency macro-sieve electrodes were fabricated and evaluated in a rodent peripheral nerve model. Presented data confirmed the ability of macro-sieve electrodes to support superior axonal regeneration compared to micro-sieve electrodes and more successfully and reliably integrate into the structure of native peripheral nerve. Morphological and histological analysis revealed that high-transparency macro-sieve electrodes did not present a significant physical impediment to regenerating axons and supported levels of axonal regeneration similar to silicone nerve conduits even in the absence of neurotrophic cues. Despite successful demonstration of the regenerative capacity of macro-sieve electrodes, prior studies provide little evidence as to the functional status of regenerative nerve tissue crossing macro-sieve electrodes. Furthermore, provide little evidence as to whether novel macro-sieve electrodes are capable of facilitating selective nerve stimulation in the absence of numerous independent micro-fascicles.

In the present chapter, electrophysiological studies will be presented in order to: 1) elucidate the functional status of regenerative nerve tissue crossing implanted macro-sieve electrodes, and 2) evaluate the capability of implanted macro-sieve electrodes to functionally and selectively recruit regenerative motor axons and distal musculature. Electrophysiological evaluation of regenerative nerve tissue and chronically-implanted

macro-sieve electrodes proceeded in five steps. The first step was to evaluate CNAP conduction in regenerative peripheral nerve tissue and confirm the functional nature of nerve fibers crossing implanted micro-sieve electrodes. The second step was to conduct electromyography (EMG) studies and evoked muscle force measurement studies to confirm that regenerating axons crossing implanted sieve electrodes reinnervated distal musculature. The third step was to examine the impact of macro-sieve implantation on functional motor recovery and behavioral function post-operatively. The fourth step was to evaluate the ability of chronically-implanted macro-sieve electrodes to facilitate selective electrical stimulation of integrated nerve fibers via channel selection, amplitude modulation, and field steering. The fifth and final step was to evaluate the ability of chronically-implanted macro-sieve electrodes to facilitate functional recruitment of integrated peripheral nerve fibers and selective activation of distal musculature in vivo.

6-2: Electrophysiology: Nerve Conduction

Histological data confirmed the presence of regenerative nerve tissue within chronically implanted macro-sieve assemblies and crossing integrated via holes. Despite evidence of numerous myelinated axons crossing implanted electrodes, prior studies were unable to determine the functional status of the regenerative nerve tissue. In order to determine whether regenerative nerve tissue crossing implanted micro-sieve electrodes was capable of conducting action potentials, and thereby receptive to exogenous electrical stimulation, an electrophysiological study of CNAP conduction through implanted constructs was performed.

Electrophysiological function of regenerative sciatic nerve segments was examined *in situ* at 3 months postoperatively. Electrophysiological function was assessed via nerve conduction study. At the terminal time point all animals underwent a non-survival surgery to expose the sciatic nerve and distal musculature for electrophysiological analysis. Animals were anesthetized using 4% Isoflurane / 96% oxygen (induction) and 2% Isoflurane / 98% oxygen (maintenance) administered IH. Following preparation of the sterile field, the right sciatic nerve and its branches were isolated from the sciatic notch to below the point of trifurcation, distal to the popliteal artery.

Sciatic nerve function was first assessed *in situ* by examining compound neural action potential (CNAP) conduction through regenerated nerve segments present inside implanted silicone conduits and macro-sieve electrode assemblies. Cathodic, monophasic electrical impulses (duration = 50 usec, frequency = single, amplitude = 0-5 mA) were generated by a single-channel isolated pulse stimulator (Model 2100, A-M Systems Inc., Carlsborg, WA) and delivered to the sciatic nerve proximal to the implanted device via bipolar silver wire electrodes (4 mil, California Fine Wire, Grover Beach, CA). Resulting CNAPs were then differentially recorded distal to the implanted device at the peroneal nerve using similar bipolar silver wire electrodes. Measured signals were band-pass filtered (LP = 1 Hz, HP = 5 kHz, notch = 60 Hz) and amplified (gain = 1,000-10,000X) using a two-channel microelectrode AC amplifier (Model 1800, A-M Systems Inc., Carlsborg, WA) before being recorded on a desktop PC (Dell Computer Corp., Austin, TX) equipped with a data acquisition board (DT3003/PGL, Data Translations, Marlboro, MA) and custom Matlab software (The MathWorks Inc.,

Natick, MA). Stimulation and recording were synchronized through custom software such that electrical stimulation coincided with the initiation of a 20 msec recording period, wherein data was sampled at 40 kHz. CNAP recordings were repeated 25 times per stimulus amplitude and averaged to obtain a mean CNAP response. Stimulus amplitude was incrementally increased until peak-to-peak amplitude of the mean CNAP response stabilized, at which time maximal CNAP amplitude was determined. Recruitment curves were constructed to demonstrate the dependence of CNAP amplitude on stimulus current amplitude and estimate stimulus threshold current for CNAP initiation. Absence of CNAPs resulting from retrograde stimulation of spinal motor reflexes was confirmed by repeating CNAP recording at the optimal stimulus amplitude after crushing the sciatic nerve at the sciatic notch for 30 sec using No. 5 Jeweler's forceps. Healthy, unoperative sciatic and peroneal nerves were similarly tested.

Nerve conduction studies demonstrated restored neural activity across 100% of implanted macro-sieve electrodes and 100% of silicon nerve conduits both with and without the fibrin-based delivery system. In contrast with prior micro-sieve electrodes, macro-sieve electrode assemblies facilitated more successful and reliable restoration of neural activity across the implanted construct (100% vs. 83%, 50%). Macro-sieve electrodes further demonstrated successful restoration of neural activity in 100% of implanted constructs even in the absence of neurotrophic support. Results confirm histological data confirming more successful and reliable axonal regeneration through implanted macro-sieve electrodes.

Representative recordings of CNAPs conducted via regenerated nerve segments are displayed. CNAPs appeared as balanced, biphasic waveforms, as observed

previously in regenerative nerve tissue. Similar to prior studies, peak-to-peak amplitude of CNAPs conducted through regenerated nerve segments were significantly reduced compared to CNAPs conducted through healthy, unoperated nerve (8.44 ± 1.43 mV). Results were consistent with prior electrophysiological studies of regenerative / repaired rodent nerve tissue. In contrast with prior testing, CNAPs recorded distal to implanted macro-sieve electrodes demonstrated comparable amplitudes to those recorded distal to implanted silicone guidance conduits. CNAPs recorded across macro-sieve electrode assemblies with (4.37 ± 1.80 mV) and without (2.78 ± 1.38 mV) delivery system were comparable to those recorded distal to implanted silicone guidance conduits with (2.97 ± 1.85 mV) and without (1.74 ± 1.04 mV) delivery system. Presence of GDNF-loaded delivery system significantly increased conducted CNAP amplitude across implanted macro-sieve electrodes (4.37 ± 1.80 mV, 2.78 ± 1.38 mV). Presence of GDNF-loaded delivery system also increased conducted CNAP amplitude across implanted nerve

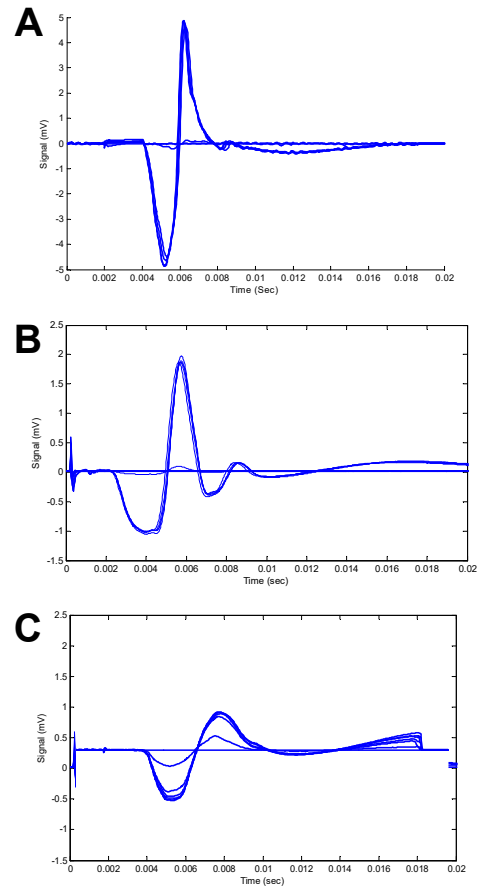


Figure 6-1. Compound neural action potentials (CNAPs) conducted through regenerative nerve tissue present in implanted macro-sieve electrode assemblies. CNAPs were evoked using silver wire electrodes placed proximal to implanted devices and recorded distally in the peroneal nerve. CNAP recordings resulting from stimuli of varying amplitude were simultaneously plotted to demonstrate fiber recruitment. CNAPs were successfully conducted through unoperative sciatic nerves (A) and macro-sieve electrode assemblies with (B) and without (C) the fibrin-based delivery system. Representative CNAP recordings acquired from each experimental group are shown.

guidance conduits, though results were not statistically significant ($2.97 \pm 1.85\text{mV}$, $1.74 \pm 1.04\text{ mV}$). CNAPs recorded distal to implanted macro-sieve electrodes ($4.37 \pm 1.80\text{ mV}$) were also shown to have significantly greater amplitudes than those recorded distal to implanted micro-sieve electrodes both with and without delivery system ($1.54 \pm 0.90\text{ mV}$). CNAP latency was additionally assessed and no statistically significant differences were noted between experimental groups (data not shown).

Electrophysiological recordings confirm successful regeneration of functional nerve tissue across chronically-implanted macro-sieve. This observation validates histological studies demonstrating robust axonal penetration of individual via holes and successfully regeneration into distal nerve tracts. Confirmation of the functional status of regenerative nerve tissue further suggests that nerve tissue crossing implanted macro-sieve electrodes is capable of supporting functional electrical stimulation.

Electrophysiological analysis further highlights the differing in vivo responses to high-transparency macro-sieve electrodes and low-transparency micro-sieve electrode.

Specifically, macro-sieve electrodes demonstrated more robust axonal regeneration and more reliable integration of functional nerve tissue. This observation validates the

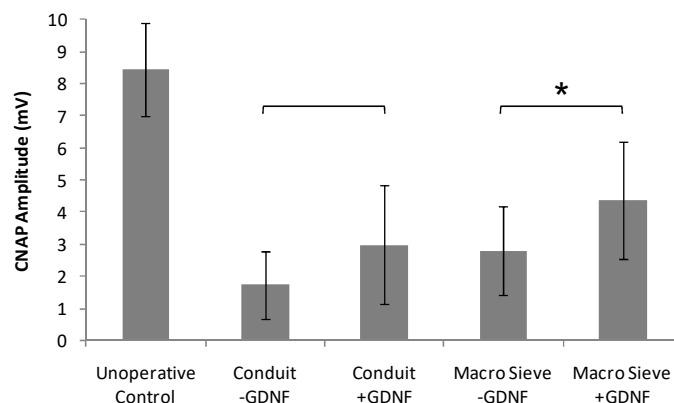


Figure 6-2. Maximum amplitude of compound neural action potentials (CNAPs) conducted through regenerative nerve tissue present in implanted macro-sieve electrode assemblies and silicone nerve guidance conduits. Mean values and standard deviations are shown. ** denotes $p < 0.05$ versus sieve electrode assembly with similar presence/absence of fibrin-based delivery system loaded with GDNF.

hypothesis that sieve electrode geometry dictates end regenerative potential, and confirms that increase electrode transparency precludes physical impedance of regenerating axons. Interestingly, robust axonal regeneration through macro-sieve electrodes was observed both in the presence and absence of neurotrophic support. Unlike prior micro-sieve electrodes, inclusion of neurotrophic factors into macro-sieve electrodes was not required for robust neural integration. These results may be explained by difference in the employed neurotrophic factors, NGF vs. GDNF, as the two factors work via separate biological mechanisms and pathways. Yet, evidence of robust axonal regeneration even in the absence of neurotrophic support suggest that the effect is more likely related to differences in sieve design and geometry.

Similar to prior studies, the presence of the delivery system within macro-sieve electrode assemblies was demonstrated to improve conducted CNAP amplitudes. This result confirms the positive effect of neurotrophic cues on axonal regeneration through artificial constructs. Together, these results further validate the conclusion that while neurotrophic support may augment and encourage functional nerve regeneration through artificial constructs, the inherent design of implantable electrodes play a more prominent role in setting regenerative nerve morphology and end functional recovery.

While examination of nerve conduction provided a clear demonstration of the functional capacity of nerve tissue passing through implanted macro-sieve electrodes, CNAP studies were unable to determine whether regenerating axons successfully innervated distal musculature. Evaluation of functional reinnervation, electromyography, and evoked muscle force measurement were subsequently evaluated to provide an additional comparison to prior micro-sieve electrodes.

6-3: Electrophysiology: Electromyography

Nerve conduction studies confirm robust regeneration of functional nerve fibers through implanted macro-sieve assemblies. Yet, evaluation of CNAP propagation through regenerative nerve tissue was unable to inform upon: 1) the presence of motor axons within regenerative nerve tissue crossing implanted electrodes, 2) the ability of regenerated axons crossing implanted sieve electrodes to functionally reinnervate distal musculature. Electrophysiological evaluation of evoked EMG response in distal musculature was therefore conducted as a measure of functional motor reinnervation.

At the terminal time point all animals underwent a non-survival surgery to expose the sciatic nerve and distal musculature for electrophysiological analysis. Animals were anesthetized using 4% Isoflurane / 96% oxygen (induction) and 2% Isoflurane / 98% oxygen (maintenance) administered IH. Following

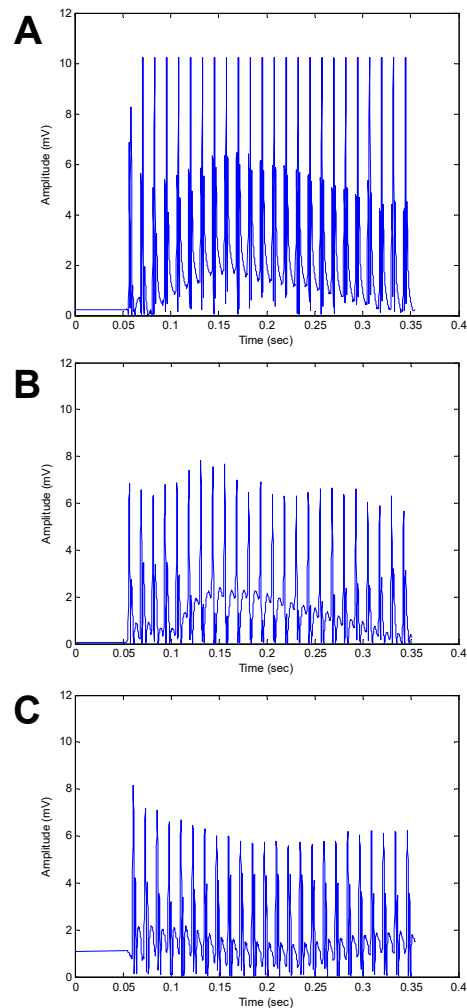


Figure 6-3. Electromyograms (EMGs) recorded distal to implanted macro-sieve electrode assemblies. EMGs were evoked using silver wire electrodes placed proximal to implanted devices and recorded distally in the EDL muscle. EMGs were successfully measured distal to unoperative nerve (A), macro-sieve electrode assemblies with delivery system (B), and nerve conduits with delivery system (C). Representative EMG recordings acquired from each experimental group are shown.

preparation of the sterile field, the right sciatic nerve and its branches were isolated from the sciatic notch to below the point of trifurcation, distal to the popliteal artery.

Cathodic, monophasic electrical impulses (duration = 50 usec, frequency = single, amplitude = 0-5 mA) were generated by a single-channel isolated pulse stimulator (Model 2100, A-M Systems Inc., Carlsborg, WA) and delivered to the sciatic nerve proximal to the implanted device via bipolar silver wire electrodes (4 mil, California Fine Wire, Grover Beach, CA). Resulting EMGs were then differentially recorded in the Tibialis Anterior (TA), Gastrocnemius (G), and Extensor Digitorum Longus (EDL) muscles using intramuscular microwire electrodes. Measured signals were band-pass filtered (LP = 1 Hz, HP = 5 kHz, notch = 60 Hz) and amplified (gain = 1,000X) using a two-channel microelectrode AC amplifier (Model 1800, A-M Systems Inc., Carlsborg, WA) before being recorded on a desktop PC (Dell Computer Corp., Austin, TX) equipped with a data acquisition board (DT3003/PGL, Data Translations, Marlboro, MA) and custom Matlab software (The MathWorks Inc., Natick, MA).

Stimulation and recording were synchronized through custom software such that electrical stimulation coincided with the initiation of a 500 msec recording period, wherein data was sampled at 10 kHz. Stimulus amplitude and frequency were mapped to construct recruitment curves and determine maximal peak-to-peak amplitude of evoked EMG responses. Healthy, unoperative sciatic nerves and distal musculature were similarly tested.

Evoked EMG responses in reinnervated musculature were measured upon electrical stimulation of regenerated sciatic nerve via epineurial hook electrode. EMG measurements demonstrated effective muscle activation in 100% of implanted macro-

sieve electrodes and 100% of silicon nerve conduits both with and without the fibrin-based delivery system. Evidence of successful activation of distal musculature confirms the presence of functional, regenerated motor axons within implanted macro-sieve electrode assemblies. Results further confirm histological data and CNAP measurements demonstrating successful and reliable axonal regeneration through implanted macro-sieve electrodes.

Representative EMG recordings from EDL muscles are displayed. EMGs appeared as balanced, biphasic waveforms upon initial recording, yet were rectified for quantitative offline analysis. Maximal amplitude of EMGs recorded from reinnervated EDL muscles was significantly reduced compared to healthy EDL muscle (9.38 ± 1.78 mV). EMG recording obtained distal to implanted macro-sieve electrodes demonstrated comparable amplitudes to those recorded distal to implanted silicone guidance conduits. EMG amplitude recorded distal to macro-sieve electrode assemblies with (5.06 ± 1.35 mV) and without ($4.10 \pm$

1.80 mV) delivery system was comparable to that recorded distal to implanted silicone guidance conduits with (3.02 ± 1.29 mV) and without (3.79 ± 1.72 mV)

delivery system. Presence of GDNF-loaded delivery system did not significantly

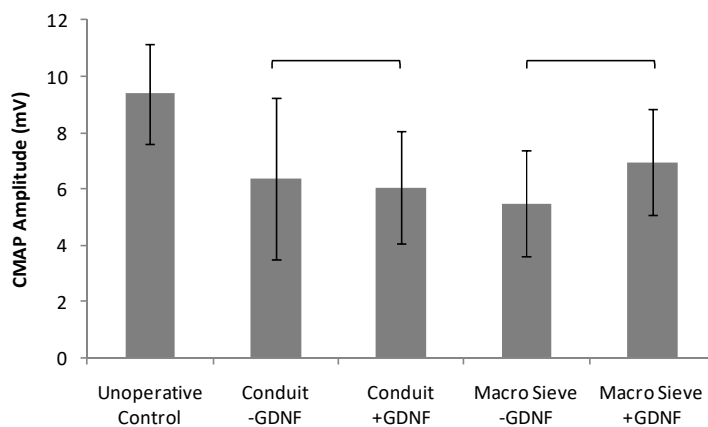


Figure 6-4. Maximum amplitude of electromyograms (EMGs) evoked distal to implanted macro-sieve electrode assemblies and silicone nerve guidance conduits. Mean values and standard deviations are shown. ** denotes $p < 0.05$ versus sieve electrode assembly with similar presence/absence of fibrin-based delivery system loaded with GDNF.

affect measured EMG amplitudes in the setting of implanted macro-sieve electrodes or implanted nerve guidance conduits.

Unlike prior CNAP studies, measurement of evoked EMG activity in distal musculature confirmed the presence of regenerative motor axons within implanted macro-sieve electrodes. Furthermore, EMG measurements provided validation that motor axons regenerating through implanted macro-sieve electrodes successfully reinnervated distal musculature. While electrophysiological analysis of evoked EMG activity was unable to discern significant differences between construct with and with the GDNF-loaded delivery system, results demonstrated comparable levels of nerve regeneration in macro-sieve electrode assemblies and silicone nerve conduits. Results provide additional evidence that the presence of macro-sieve electrodes do not impede motor axon regeneration and muscle reinnervation in vivo.

6-4: Electrophysiology: Evoked Muscle Force Measurement

Evaluation of CNAP propagation and evoked EMG activity in prior sections confirmed regeneration of functional motor axons through implanted macro-sieve electrodes. Yet, the degree to which distal muscle function is preserved following macro-sieve implantation was not evaluated. Preservation of distal musculature is critical to terminal function of macro-sieve electrodes as peripheral nerve interface within advanced motor neuroprosthetic systems. In order to determine whether regenerated motor axons crossed implanted micro-sieve electrodes, successfully reinnervated distal musculature,

and preserved distal muscle function a study of evoked muscle force measurement was performed.

Electrophysiological assessment of evoked motor response in distal musculature was examined *in situ* at 3 months postoperatively. At the terminal time point all animals underwent a non-survival surgery to expose the sciatic nerve and distal musculature for electrophysiological analysis. Animals were anesthetized using 4% Isoflurane / 96% oxygen (induction) and 2% Isoflurane / 98% oxygen (maintenance) administered IH. Following preparation of the sterile field, the right sciatic nerve and its branches were isolated from the sciatic notch to below the point of trifurcation, distal to the popliteal artery. Additionally the extensor digitorum longus (EDL), tibialis anterior (TA), and gastrocnemius (G) were exposed through skin incisions extending along the anterior and posterior portion of the lower leg.

Sciatic nerve and distal muscle function was assessed by examining the motor response in reinnervated EDL, TA, and G muscles upon stimulation of the sciatic nerve. Following isolation, the distal portions of the EDL, TA, and G muscles were separated from the leg by severing the distal tendons. The distal tendons were fashioned into a loop and secured to stainless steel S-hooks at the musculotendinous junction using 5-0 nylon suture. Animals were subsequently placed in a custom-designed force measurement jig where the leg was immobilized by anchoring the femoral condyles. The stainless steel S-hooks attached to the target muscles were connected to either 5 N or 20 N thin film load cells (S100, Strain Measurement Devices Inc., Meriden, CT) supported on an adjustable mount. Cathodic, monophasic electrical impulses (duration = 200 usec, frequency = single-200 Hz, amplitude = 0-3 V) were generated by a single-channel isolated pulse

stimulator and delivered to the sciatic nerve proximal to the implanted device via bipolar silver wire electrodes. Resulting force output at muscle tendons was transduced via the load cells and the resulting signals were amplified (gain = 1000X) using instrumentation amplifiers (AD620, Analog Devices Inc., Norwood, MA) powered by a constant voltage source before being recorded on a desktop PC equipped with a data acquisition board and custom Matlab software. Stimulation and recording were synchronized through custom software such that electrical stimulation coincided with the initiation of a 500 msec recording period, wherein data was sampled at 4 kHz. Custom software calculated the passive force and active force for each recorded force trace.

Twitch contractions measured using the custom force recording system were utilized to determine the optimal stimulus amplitude (V_o) and optimal muscle length (L_o) for isometric force production in each muscle (Yoshimura et al; 1999). Stimulus amplitude was incrementally increased while individual muscle length was held constant. V_o was defined as the stimulus amplitude at which the largest active force was produced. Individual muscle length was then increased in 1 mm increments from a relaxed state while the stimulation amplitude was fixed at V_o . Upon determining the muscle length at which the largest active twitch force was produced, a single 300 msec burst of impulses (frequency = 80 Hz) was delivered to the sciatic nerve, and muscle length was re-evaluated. L_o was directly measured as the length of target muscle from proximal to distal musculotendinous junction. All subsequent isometric force measurements were made at V_o and L_o . Single twitch contractions were recorded, and peak twitch force (F_t) was calculated. Tetanic contractions were recorded by delivering 300 msec bursts of increasing frequency (5-200 Hz) to the sciatic nerve, while allowing two minute periods

between stimuli for muscle recovery. Maximum isometric tetanic force (F_o) was calculated from the active force plateau.

Physiological cross-sectional area (PCSA) of the EDL muscle was calculated according to the following:

$$PCSA = \frac{M \times \cos \theta}{(\rho)(L_o)(0.44)}$$

where PCSA = physiological muscle cross-sectional area (cm^2), M = EDL muscle mass (g), θ = angle of pinnation for EDL muscle (0°), ρ = density of mammalian skeletal muscle (1.06 g/cm^3), L_o = optimal muscle length (cm), $0.44 = L_f/L_o$ ratio for EDL muscle determined previously (Mendez et al; 1960, Gans et al; 1982, Kalliainen et al; 2002, Urabnchek et al; 2001). Maximum specific isometric tetanic force (sF_o) was calculated as the maximum isometric tetanic force (F_o) normalized to muscle PCSA. Healthy, unoperative sciatic nerves and muscles were similarly evaluated.

Evoked motor response in reinnervated EDL, TA, and G muscles was measured upon electrical stimulation of regenerated sciatic nerve via epineurial hook electrode. Measurement of evoked force production demonstrated that 100% of animals implanted with macro-sieve electrode assemblies and 100% of animals implanted with silicone nerve guidance conduits exhibited functional reinnervation of distal motor. The percentage of animal demonstrating evoked force production following implantation of macro-sieve electrode or nerve guidance conduits was comparable in the presence and absence of GDNF-loaded delivery system. Animals implanted with macro-sieve electrode assemblies demonstrated a higher likelihood of functional motor reinnervation in the presence (100%) and absence (100%) of neurotrophic support compared to animals

implanted with micro-sieve electrode assemblies with (66%) and without (0%) neurotrophic support.

Quantitative examination of maximum isometric tetanic force demonstrated that force production in all reinnervated muscles was significantly reduced compared to

healthy, unoperative muscles. Tetanic

force measurements demonstrated that

macro-sieve electrode assemblies

supported comparable recovery of force

production in EDL, TA, and G muscles

compared to silicon nerve guidance

conduits. For example, EDL muscles

reinnervated following implantation of

macro-sieve electrodes containing fibrin-

delivery system supported similar tetanic

force production (1.83 ± 0.28 N)

compared to EDL muscles reinnervated

following implantation of silicone conduit

containing delivery system (1.66 ± 0.42

N). Similar trends were observed in TA and

G muscles. Implants containing GDNF-

loaded fibrin-based delivery system were also

observed to promote greater recovery of force

production compared to devices containing

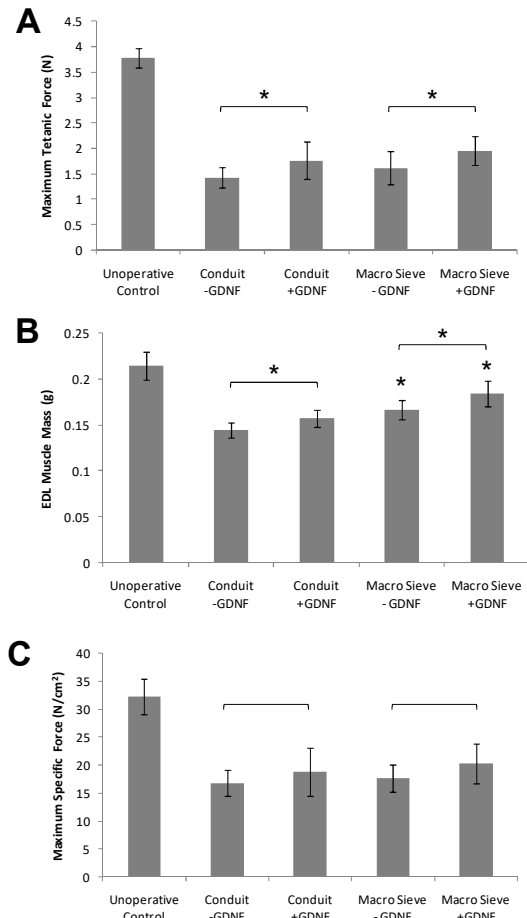


Figure 6-5. Maximum isometric force production in reinnervated extensor digitorum longus (EDL) muscles. Maximum tetanic force evoked in EDL muscle (A), EDL wet muscle mass (B), and maximum specific tetanic force in EDL muscle (C). Mean values and standard deviations are shown. * denotes $p < 0.05$ versus similar device with dissimilar presence/absence of fibrin-based delivery system loaded with GDNF. ** denotes $p < 0.05$ versus sieve electrode assembly with similar presence/absence of fibrin-based delivery system loaded with GDNF.

saline. For instance, macro-sieve electrodes containing GDNF-loaded delivery system permitted significantly greater tetanic force production in reinnervated EDL muscle (1.83 ± 0.28 N) compared to electrodes filled with saline (1.69 ± 0.30 N). Similar trends were observed in TA and G muscles, though statistical significance was not observed in some comparisons. Finally, examination of maximum isometric tetanic force confirmed that macro-sieve electrodes with and without the delivery system permitted significantly greater recovery of force production (1.83 ± 0.28 N, 1.69 ± 0.30 N, respectively) than micro-sieve electrode assemblies with and without the delivery system (0.17 ± 0.14 N, 0.0 ± 0.0 N, respectively). Maximum isometric twitch force measurements reflected a similar trend, though no statistically significant differences were noted.

Calculation of maximum specific tetanic force production provided a metric of functional recovery independent of length of denervation and degree of muscle atrophy (Aydin et al; 2004, Van der Meulen et al; 2003). Quantitative analysis of maximum specific tetanic force production confirmed trends observed in maximum isometric tetanic force measurements. Yet, differences observed in specific force production between experimental groups were not found to be statistically significant. These results suggest that differences observed in maximal isometric tetanic force production are primarily attributable to differences in the degree of muscle atrophy experienced post-operatively. Therefore, improvement of evoked muscle force production evidenced by inclusion of neurotrophic factors and by utilization of macro-sieve electrodes may directly result from improvement in the rate or degree of nerve regeneration and thereby muscle reinnervation.

In total, functional recruitment of distal musculature upon stimulation of peripheral nerve tissue proximal to implanted electrodes and confirms regeneration of intact motor axons through implanted macro-sieve arrays. Presence of motor axons within the integrated electrode again confirms the ability of macro-sieve electrodes to support regenerating motor axons. Demonstration of evoked muscle force production further illustrates the ability of regenerative motor axons crossing the implanted electrodes to reinnervate distal musculature and preserve terminal muscle function. Observation of muscle activation further suggests that macro-sieve electrodes may be able to indirectly control or recruit distal musculature by interfacing integrated motor fibers.

Interestingly, macro-sieve electrodes demonstrate superior preservation of muscle function following chronic implantation compared to micro-sieve electrodes.

The critical nature of maintaining distal musculature long after device implantation suggests that macro-sieve electrodes possess increasing clinical viability compared to micro-sieve devices reported previously. Evoked muscle force measurements further highlight the role of regenerative electrode geometry on terminal motor function.

In the absence of neurotrophic support, high-transparency macro-sieve electrodes enabled functional motor activation in 100% of implanted animals while low-transparency micro-sieve electrode enabled functional motor activation in 0% of implanted animals. The significant impact of sieve electrodes geometry on motor recovery should be duly noted, as prior studies of regenerative sieve electrode for sensory applications generally overlook the functional effect of device implantation. These results further confirm the finding that macro-sieve electrodes effectively preclude any

physical impediment of regenerating axonal, and thereby functional nerve regeneration. While present studies have not examined the long term (>12mo) chronic effect of macro-sieve electrodes implantation, observations of equivalent motor function following macro-sieve electrode and silicone nerve conduit implantation suggest that the presence of the high-transparency polyimide wafer has a negligible effect on regenerating axonal populations. These finding further confirm the preliminary conclusion that regenerative sieve electrodes designed to facilitate functional electrical stimulation of motor axons and distal musculature must possess a permissive geometry and high-transparency porous region in order to support the large population of motor axons needed for FES of distal muscle targets.

The role of neurotrophic support in implanted macro-sieve electrode assemblies also differs from that observed in micro-sieve electrode assemblies. Inclusion of neurotrophic support in macro-sieve electrode assemblies was shown to moderately improve CNAP amplitude and evoked muscle force measurement post-operatively, yet was not observed to be critical to establishing successful motor axon regeneration through implanted electrodes. In contrast, the effect of neurotrophic support in micro-sieve electrodes was shown to be much more prominent, whereas inclusion of NGF-loaded fibrin-based delivery system was shown to be necessary for functional regeneration and recovery. While these results may suggest that the neuroregenerative potential of NGF is greater than that of GDNF provided the selected doses utilized in the present study, these observations more likely demonstrate the comparative effective of physical barriers versus biological cues in axonal regeneration. Particularly, these studies confirm that the design and geometry of implanted synthetic constructs impact total

axonal regeneration to a much greater degree than local neurotrophic factors. While neurotrophic support is shown to improve and accelerate axonal regeneration through the implanted devices, implanted sieve geometry must be optimized to enable and support sufficient axonal regeneration and motor recovery for proper clinical function.

Demonstration of successful regeneration of motor axon through implanted macro-sieve electrodes further suggests that the implanted device possesses the capability to functionally recruit local motor axon populations and thereby control distal musculature. The subsequent sections will evaluate the ability of chronically-implanted micro-sieve electrodes to facilitate functional electrical stimulation of integrated motor axons innervating distal muscle groups.

6-5: Functional Motor Recovery

An evaluation of terminal motor function was performed in order to determine the functional impact of macro-sieve electrode implantation and neurotrophic support on end behavioral outcomes. Prior sections provide electrophysiological evidence of successful axonal regeneration and muscle reinnervation following implantation of macro-sieve electrodes with and without delivery system. Yet, the terminal impact of changing nerve and muscle function on behavioral metrics remains unknown. In order to examine the effect of macro-sieve electrodes and neurotrophic support on end motor function walking track analysis, grid grip analysis, and joint angle analysis was performed.

Walking track analysis was performed at 1, 2, and 3 months postoperatively. Walking tracks were conducted as previously described (Bain et al; 1989, Brown et al; 1989). The walking track consisted of an 8×40 cm track lined with exposed paper. The

hind feet of each animal were marked with red (right) and blue (left) ink prior to the rat walking down the length of the track. Hind footprints from the right and left leg were therefore made on the underlying paper strip. Marked paper strips were then scanned and digitized prior to being loaded into a custom-MATLAB program. Measurements of the footprints made during normal ambulation were made using a custom graphic user interface and subsequently utilized to calculate sciatic function index (SFI) as previously described (Bain et al; 1989, de Medinaceli et al; 1982).

Results of walking track analysis, along with representative prints from unoperative and operative hind limbs, are presented. Resulting SFI data demonstrates progressive functional recovery over the course of the 3 month study (-90 to -70), consistent with prior studies.

Functional recovery and reduced SFI scores were associated with progressive increase in toe spread and progressive decrease in print length.

Both outcomes have been previously correlated to successful reinnervation of distal musculature following nerve injury. Results further demonstrated that functional recovery was

comparable in animals implanted with macro-sieve electrodes and

silicone nerve conduits both with and without GDNF-loaded delivery system. Implants

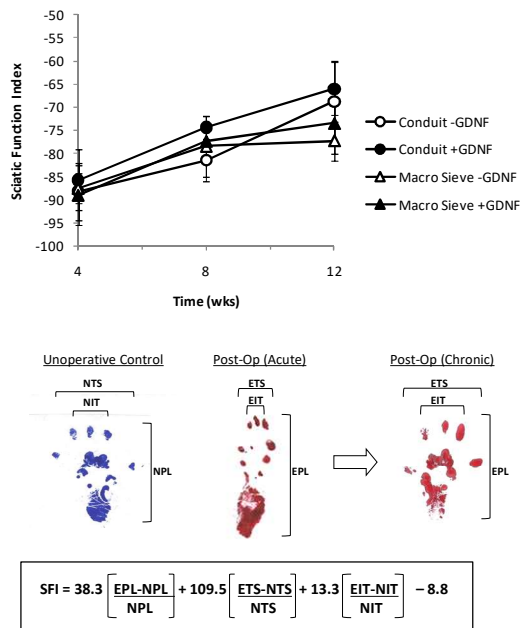


Figure 6-6. Calculation of sciatic function index (SFI) via walking track analysis. SFI measurements over 3 months of implantation (top). Representative hind limb prints at both acute and chronic time points (bottom).

loaded with delivery system demonstrated slight increases in SFI scores at 12 weeks post-operatively, yet no statistically significant differences were observed.

Grid-grip analysis was performed at 3 months post-operatively to measure functional recovery in the hindlimb (Wood et al; 2009, Johnson et al., 2010; Metz et al., 2000). Blinded participants observed each animal walking on a fixed grid of bars containing 1.5" x 1.5" gaps for a period of 3 min. Participants scored individual animals according to the number of successful grips of the grid, defined as two or more toes of the injured foot gripping the bar and facilitating movement to another bar without slipping, and the total number of unsuccessful grips with the injured foot. Data was then calculated as the percent of successful grips made by the injured foot. In all experiments, animals were required to make at least 20 steps in order to account for variability in the activity level and motility of individual animals.

Grid grip analysis demonstrated terminal sensorimotor deficits consistent with nerve transection / repair in a rodent sciatic nerve model. All animal tested demonstrated 7.6-11.5% successful grips, highlighting the residual motor deficit experienced following nerve injury. Comparison of grid grip performance amongst experimental groups demonstrated comparable levels of successful grips in animals implanted with macro-sieve electrodes and silicone nerve guidance conduits. Specifically, animals implanted

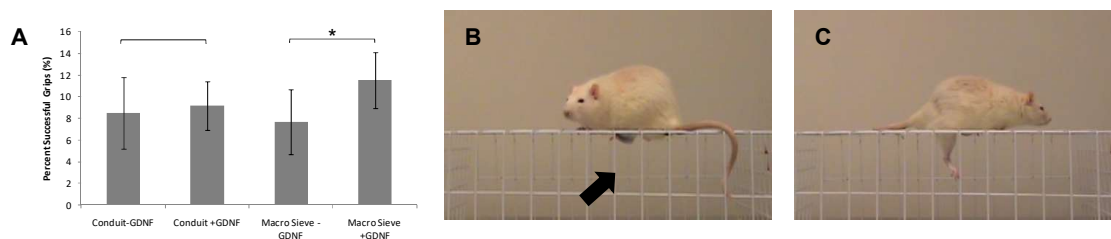


Figure 6-7. Grid grip analysis. Measurement of percent successful grips (A). Representative images of successful (B) and unsuccessful grips (C). * denotes $p < 0.05$ versus similar device with dissimilar presence/absence of fibrin-based delivery system loaded with GDNF

with macro-sieve electrodes assemblies with and without delivery system ($7.6 \pm 3.0\%$, $11.5 \pm 2.6\%$) demonstrated similar rates of successful grid grips compared to animals implanted with nerve guidance conduits with and without delivery system ($8.5 \pm 3.3\%$, $9.1 \pm 2.2\%$). The presence of GDNF-loaded delivery system in macro-sieve assemblies resulted in a moderate increase in the rate of successful grid grips ($11.5 \pm 2.6\%$ vs $7.6 \pm 3.0\%$). The presence of the delivery system did not affect rates of successful grid grips in animals implanted with nerve guidance conduits. Results demonstrate similar functional recovery in animals implanted with macro-sieve electrode and with empty silicone nerve guidance conduits, highlighting the negligible effect of macro-sieve electrodes on terminal motor function. These findings further suggest a positive effect of neurotrophic support on end sensorimotor function, though results were not consistently demonstrated across all groups.

Finally, quantification of the maximum angle of ankle extension in the operative limb was measured at 3 months post operatively. Joint angles were measured as a means

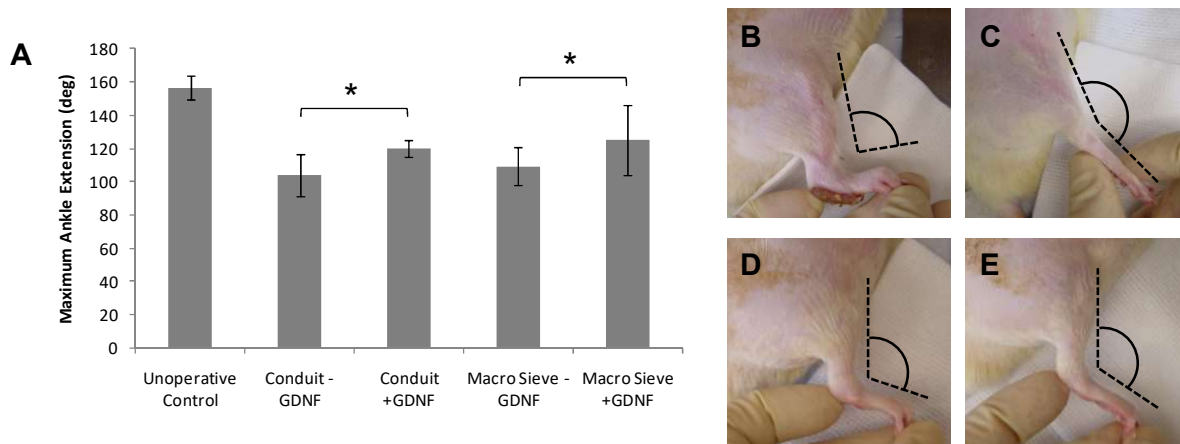


Figure 6-8. Measurement of maximal extension of ankle joint. Measurement of the maximal angle of extension in the ankle joint (A). Representative images of ankle extension in the case of contracture (A), unoperative limb (B), (C) macro-sieve electrode without the delivery system, and (D) macro-sieve with the delivery system. * denotes $p < 0.05$ versus similar device with dissimilar presence/absence of fibrin-based delivery system loaded with GDNF.

of evaluating maximum range of motion and the presence of contraction following surgical implantation of macro-sieve electrodes and silicone nerve guidance conduits. All animals were placed in a prone position and the ankle joint on the right leg was maximally extended. The maximal angle from the tibia to the metatarsus was then measured.

Representative images of maximal extension in the ankle joint in operative animals are displayed. All operative animals demonstrated reduced degrees of joint motion compared to healthy unoperative animals. Maximal ankle extension observed in animals implanted with macro-sieve electrodes with and without delivery system ($125 \pm 21\%$, $109 \pm 11\%$) was comparable to that observed in animals implanted with nerve guidance conduits with and without delivery system ($120 \pm 5\%$, $103 \pm 13\%$). The presence of GDNF-loaded delivery system in both macro-sieve assemblies ($125 \pm 21\%$ vs. $109 \pm 11\%$) and nerve guidance conduits resulted in a moderate but significant increase in maximal ankle extension ($120 \pm 5\%$ vs. $103 \pm 13\%$). Results further confirm observations that the presence of macro-sieve electrodes has a negligible effect of terminal motor function compared to silicone nerve guidance conduits. These findings validate prior demonstrations that macro-sieve electrodes do not impede nerve regeneration or functional recovery following implantation.

6-6: Computational Modeling of Electrical Stimulation via Regenerative Macro-Sieve Electrode

Demonstration of functional motor axons within chronically-implanted micro-sieve electrodes suggests the implanted electrodes possess the capability to functionally

recruit local axons and thereby distal musculature. Yet, the novel geometry of the porous region and unique layout of active sites on the macro-sieve electrode pose specific questions as to the ability of the device to facilitate selective electrical stimulation of integrated peripheral nerve fibers. Specifically, the absence of micro-scale via holes (a common feature in previous regenerative devices) and resulting microfascicles suggest that macro-sieve electrodes may not be capable of independently interfacing small groups of regenerated axons. In order to examine the ability of novel macro-sieve electrodes to selectively recruit integrated peripheral nerve fibers a hybrid finite element model and electrophysiologic model was constructed and implemented.

A hybrid finite element model / electrophysiological model of a macro-sieve electrode integrated into a peripheral nerve was constructed by Erik Zellmer in the laboratory of Dr. Daniel Moran in the Department of Biomedical Engineering at Washington University in St. Louis. Briefly, the hybrid model consisted of two parts: 1) a FEM of a macro-sieve electrode, and 2) an electrophysiologic model of an array of mammalian axons.

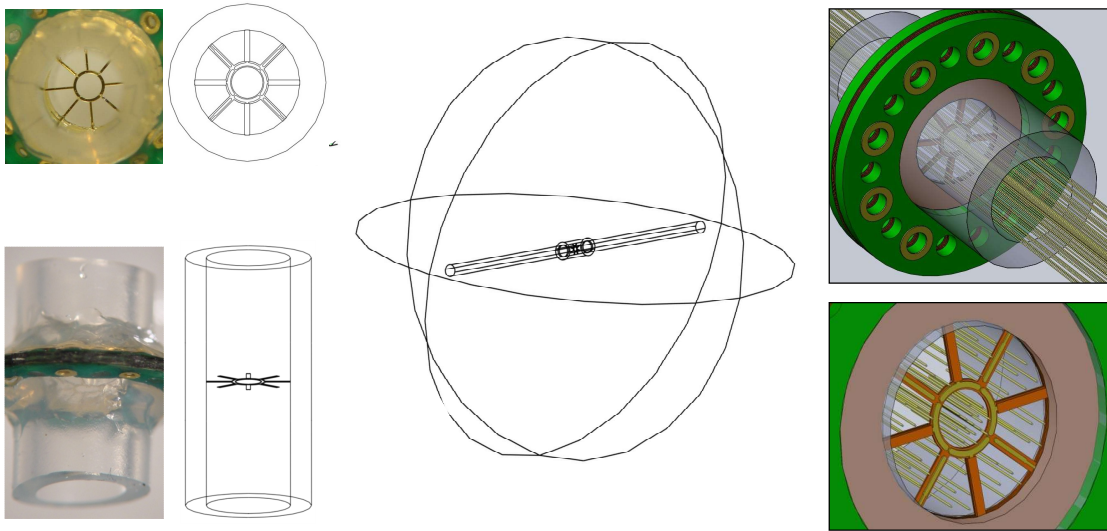


Figure 6-9. Computational modeling of macro-sieve electrode assembly. Hybrid computational models consist of a FEM model of macro-sieve electrodes and conduits (left) located within a conductive volume presenting an infinite ground (middle), and containing a virtual array of mammalian axons (right).

The FEM model consisted of a single-side polyimide macro-sieve electrode containing 8 metallized electrode sites which was contained in a 6mm long silicone nerve guidance conduit and surrounded by conductive media. The macro-sieve electrode was based on the geometric layout of actual electrodes fabricated for in vivo use. The FEM model was utilized to calculate the three-dimension potential distribution resulting from current injection through one or more of the metallized planar electrode sites in the porous region of the electrode. The volume present within the macro-sieve electrode and nerve guidance conduit was assumed to have the properties of axonal tissue, the stimulation pads were all assumed to operate independently, and model was assumed to have an infinite ground. Appropriate material properties and conductivities were applied to each structure and materials within the FEM. Polyimide and silicone structures were assumed to be perfectly insulating.

The electrophysiological model provided a computational approximation of the behavior of a virtual array of mammalian axons located within the macro-sieve electrode and attached nerve guidance conduit. Model axons were implemented in NEURON utilizing four different electrophysiologic models of the mammalian axonal membrane. Specifically, the CRRSS model described by Chiu et al. (Chiu et al; 1979) and the A, B, and C models described by Richardson et al. (Richardson et al; 2000) were utilized. The circuit diagram for each of the various models is displayed. Features of model axons were varied based on the specific trial. In the present study model axons were assigned properties associated with a homogenous caliber regenerated population of peripheral mammalian axons.

Upon each trial a single stimulation paradigm was selected. A stimulation paradigm consisted of a chosen: stimulus amplitude, stimulus duration, stimulus waveform, stimulus polarity, number of active electrode site, location of activated electrode site, etc. During each trial the selected stimulation paradigm was implemented in the FEM model and resulting currents were injected at selected active electrode sites. The FEM model then calculated the potential distribution associated with the prescribed current injection and calculate the potential along individual virtual axons crossing the macro-sieve electrode with respect to time. The time dependent array of induced potentials was then applied to the virtual axon array modeled in NEURON in order to infer the physiologic response to the induced potential gradients. The NEURON model was then utilized to determine which axons in the virtual axon array would depolarize and initiate a propagating axon potential. The number and location of activated axons was then noted and displayed graphically over the cross sectional area of the macro-sieve

model. Resulting plots therefore allowed for an in silico approximation of the spatial selectivity of various stimulation paradigms and conditions as applied to the novel macro-sieve electrode.

Resulting data validates both the capability of macro-sieve electrodes to selectively activate discrete cross-sectional areas within integrated peripheral nerve tissue and the mechanism by selective stimulation is achieved. Specifically, results of computational modeling studies demonstrate that selective activation of peripheral axons is successfully achieved by direct modulation of three parameters: stimulus amplitude, stimulus polarity, and location of active electrode sites.

Implementation of a monopolar stimulation paradigm (i.e. one or more active electrode sites serving solely as current sources) results in progressive recruitment of larger cross sectional areas of nerve tissue within the macro-sieve electrode with increasing current amplitude. Resulting data suggests that initial thresholds of recruitment upon monopolar stimulation via macro-sieve electrodes may range from 10-50 uA.

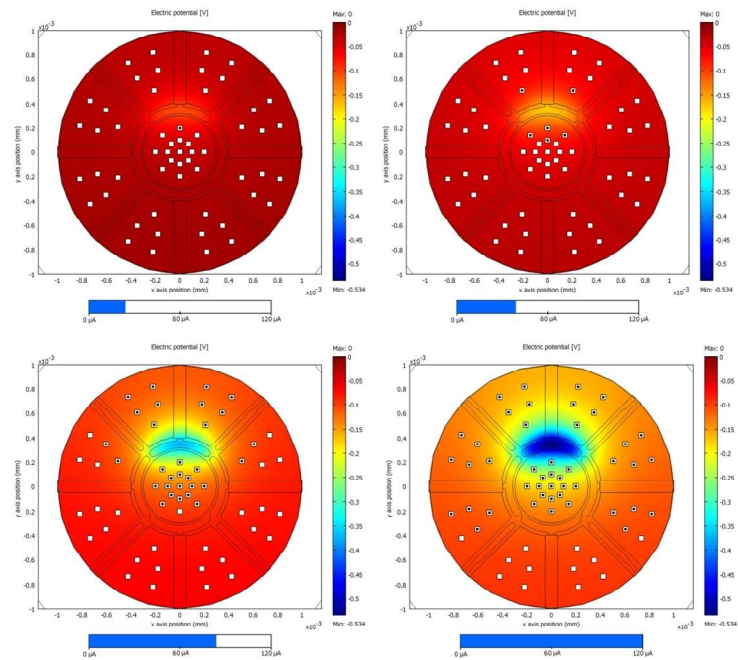


Figure 6-10. Computational modeling of monopolar stimulation paradigms. Hybrid computational models demonstrate progressive depolarization (blue) and recruitment of larger number of axons (filled boxes) at greater distance from the active electrode site upon increasing stimulus amplitude.

Increasing stimulus amplitude thereby results in a shift from selective recruitment of axons proximal to the active electrode site(s) to bulk recruitment of the entire regenerated nerve by 100-200 μA . Selective spatial activation of proximal axons under monopolar conditions was further demonstrated to be transferable depending on the specific number and location of active electrode sites. As a result activation of independent electrode sites across the porous region of the design was shown to activate distinct groups of virtual axons. Additive effects of multiple active electrode sites were further shown. In total, selective activation of virtual axons within the computational macro-sieve model was successfully achieved through modulation of stimulus amplitude and location of active electrode sites under monopolar conditions.

Further testing demonstrated the unique utility of multipolar stimulation paradigms in improving spatial selectivity of axonal activation via model macro-sieve electrodes. Multipolar stimulation (i.e. one or more active electrode sites serving independently as current sources or sinks), also known as “field steering”, enabled superior spatial control of potential gradients evoked by active electrode sites.

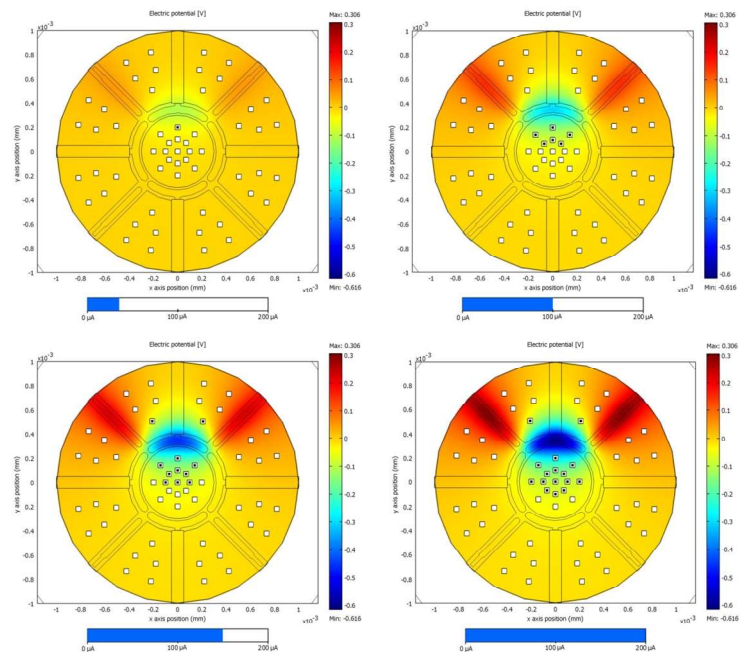


Figure 6-11. Computational modeling of multipolar stimulation paradigms. Hybrid computational models demonstrate highly focused depolarization (blue) and recruitment of larger number of axons (filled boxes) in only a select region around the active electrode site upon increasing stimulus amplitude.

Specifically, depolarization of proximal nerve tissue evoked by a single active electrode site (source) was shown to be modulated by simultaneous hyperpolarization evoked by multiple adjacent electrode sites (sinks). Resulting recruitment curve demonstrate increased spatial selectivity along with a broader recruitment curve. Specifically, resulting data suggests that initial thresholds of recruitment upon multipolar stimulation via macro-sieve electrodes may range from 10-50 uA with complete bulk recruitment of the entire regenerated nerve by 300-500 uA. Similar to monopolar stimulation paradigms, selective spatial activation of proximal axons under multipolar conditions was demonstrated to be transferable across a variety of active electrode sites. Provided the immense number of possible combinations, multipolar stimulation enables a multitude of stimulation paradigms well beyond that offered by direct monopolar stimulation of high-channel count electrodes.

In total, computational modeling studies provided a unique insight into the capability of novel macro-sieve electrodes to successfully facilitate selective stimulation of regenerated nerve fibers. Results of computational trials provide initial demonstration of the ability of macro-sieve electrode to facilitate monopolar stimulation of local axonal population, and further control the region of axonal activation via manipulation of stimulus amplitude and the location of active electrode sites. Computational modeling further confirm the ability of macro-sieve electrodes to facilitate multipolar stimulation or “field steering” as an effective means of improving spatial selectivity of axonal recruitment. This study provides the first report of field steering via an implantable regenerative electrode, and further demonstrates the potential capability of low-channel count electrodes to achieve level of selectivity typically achieved only by advanced, high-

channel count devices. Computational modeling further demonstrate the value and efficiency of in silico testing in the development of novel microelectrode interfaces. Hybrid modeling of microelectrode interfaces and virtual axon arrays provides a low-cost, high-throughput means of testing future electrode designs and optimizing regenerative sieve electrode geometries.

Together, results of computational modeling provide initial validation of the capability of macro-sieve electrodes to successfully achieve selective electrical stimulation of regenerated nerve fibers in vivo.

6-7: Electrophysiology: Selective Nerve Interfacing / Monopolar Stimulation

Electrophysiological and computational studies provide preliminary data suggesting that implanted macro-sieve electrodes are capable of functionally recruiting regenerated motor axons and controlling distal musculature. Demonstration of successful reinnervation of distal musculature by motor axons extending through the implanted macro-sieve electrode highlights the direct correlation between integrated motor axons and distal motor targets. Yet, ability of macro-sieve electrodes to impart selective control of distal musculature to date has remained unexplored. Monopolar activation of individual electrode sites throughout the porous region of the macro-sieve electrode is proposed to facilitate selective activation of integrated nerve tissue, yet the resulting selectivity of muscle activation is largely unknown. An electrophysiological study of nerve and muscle activation in response to monopolar stimulation of select active sites

was performed in order to investigate the interfacial capabilities of chronically-implanted macro-sieve electrodes.

Electrical impulses were delivered to regenerated nerve segments via chronically-implant macro-sieve electrodes ($t = 3$ mo) in order to determine their ability to interface regenerative nerve tissue. Cathodic, monophasic electrical impulses were generated by a single-channel isolated pulse stimulator and routed in a monopolar configuration to either: 1.) individual metallized electrode sites, or 2.) all 8 metallized electrode sites simultaneously within the porous region of implanted macro-sieve electrodes. Electrical impulses (duration = 50-200 usec, frequency = single, amplitude = 0-1 mA) were used to initiate evoked muscle force production in extensor digitorum longus (EDL), tibialis anterior (TA), and gastrocnemius (G) muscles. Resulting force output at muscle tendons was transduced via the load cells and the resulting signals were amplified (gain = 1000X) using instrumentation amplifiers (AD620, Analog Devices Inc., Norwood, MA) powered by a constant voltage source before being recorded on a desktop PC equipped with a data acquisition board and custom Matlab software. Stimulation and recording were synchronized through custom software such that electrical stimulation coincided with the initiation of a 500 msec recording period, wherein data was sampled at 4 kHz. Custom software calculated the passive force and active force for each recorded force trace.

Recruitment curves were constructed to demonstrate the dependence of evoked muscle force production on stimulus amplitude and active electrode site. Resulting recruitment curves were compared to those generated using silver wire electrodes to stimulate identical regenerated nerve segments. Electrical impulses (duration = 50-200 usec, frequency = single, amplitude = 0-1 mA) were delivered to regenerated sciatic

nerves via implanted macro-sieve electrode or nerve hook electrode to initiate distal motor responses which were recorded in the EDL, TA, and G muscles, as previously discussed. Selectivity of motor unit activation was assessed by comparing the motor response in the various muscles and calculating a selectivity index (SI) of each stimulation paradigm. Recorded force traces and peak twitch force (F_t) measurements resulting from stimulation of sciatic nerve via implanted macro-sieve electrodes were compared to those acquired upon direct stimulation of sciatic nerve via nerve hook electrodes.

The ability of macro-sieve electrodes to functionally recruit regenerative nerve

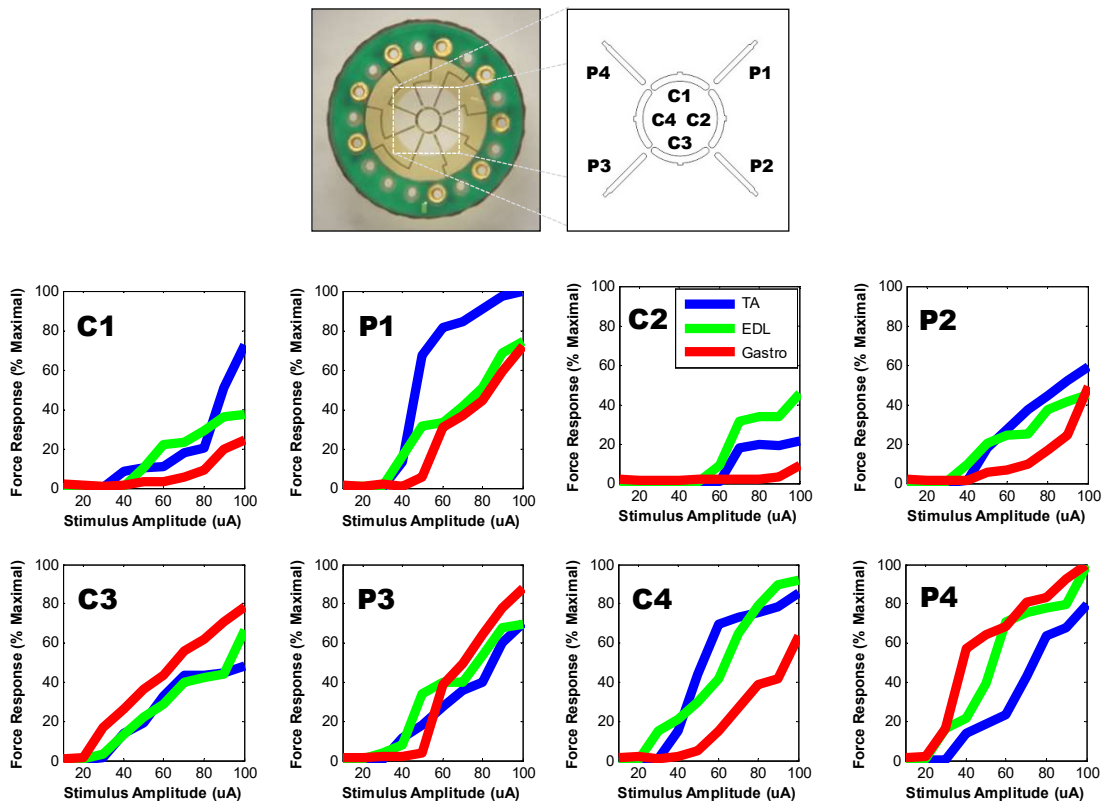


Figure 6-12. Motor response to monopolar stimulation of peripheral nerve tissue via macro-sieve electrodes. Recruitment curves generated upon monopolar stimulation of various electrode site on implanted macro-sieve electrodes and simultaneous recording of evoke force production in EDL, TA, and G muscles.

tissue was assessed via simultaneous electrical activation of implanted electrodes and recording of evoked muscle force production. Testing demonstrated that 75% of implanted sieve electrode assemblies with and without fibrin-based delivery system effectively recruited distal musculature upon peripheral nerve stimulation. In contrast, only 33% of implanted micro-sieve electrode assemblies containing fibrin-based delivery system capable of initiating motor responses in distal musculature. No micro-sieve electrode assembly (0%) containing saline was observed to recruit distal musculature.

Regenerative nerve segments integrated into macro-sieve electrode assemblies were stimulated using multiple electrode sites on integrated sieve electrodes. Representative recruitment curves constructed from evoked muscle force recordings are displayed. Recruitment of distal musculature was initiated at lower current amplitudes upon electrical activation of embedded macro-sieve electrodes compared to epineurial

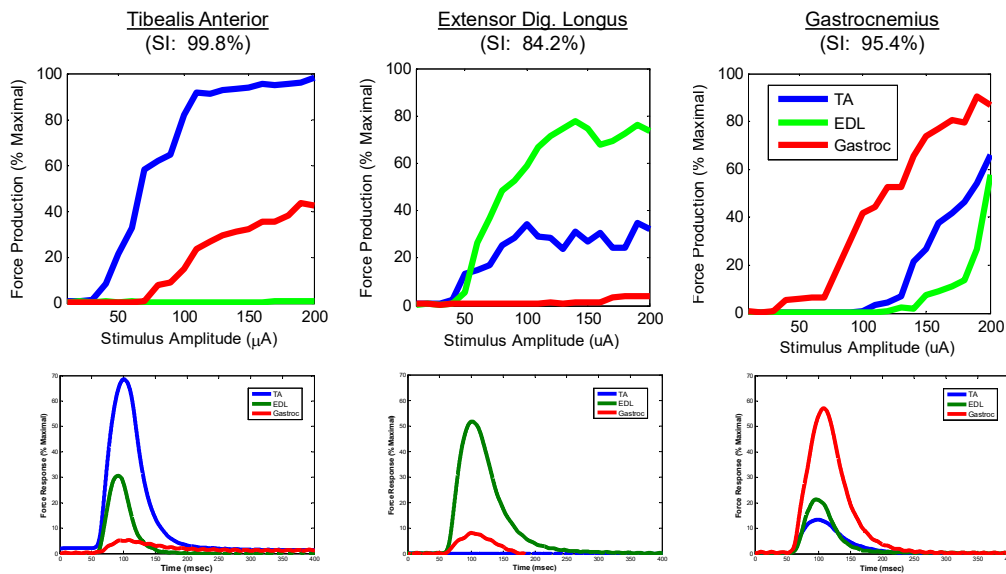


Figure 6-13. Maximal selectivity of muscle activation achieved upon monopolar stimulation of peripheral nerve tissue via macro-sieve electrodes. Recruitment curves highlight maximal selectivity of peripheral nerve interfacing achieved upon monopolar stimulation of various electrode site on implanted macro-sieve electrodes and simultaneous recording of evoke force production in EDL, TA, and G muscles.

hook electrodes. Monopolar stimulation via macro-sieve electrodes with and without delivery system exhibited a mean threshold of nerve activation of 48 ± 32 uA and 56 ± 28 uA, respectively. Identical regenerated nerve segments were similarly recruited by epineurial hook electrodes at amplitudes of 173 ± 61 uA, respectively. Current amplitudes required to produce half-maximal response in regenerated nerve segments contained in sieve electrode assemblies with and without delivery system were also lower upon use of macro-sieve electrodes than upon use of epineurial electrodes. The presence of fibrin-based delivery system within implanted macro-sieve electrode assemblies did not affect the threshold of activation, unlike prior micro-sieve studies. Evoked force production evoked via stimulation of regenerated nerve segments by implanted macro-sieve electrodes assemblies was comparable to that achieved in identical nerves using epineurial hook electrodes. Furthermore, recruitment curves formed upon electrical activation of embedded macro-sieve electrodes were broader than those formed upon activation of epineurial hook electrodes.

Muscle activation resulting from monopolar stimulation of regenerated nerve segments was measured to assess functional recruitment distal motor units by chronically-implanted macro-sieve electrodes. Evoked twitch

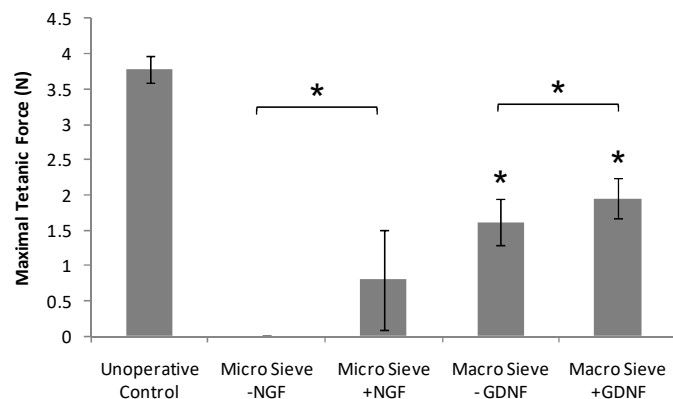


Figure 6-14. Maximum isometric force production via macro-sieve and micro-sieve electrodes. Maximum tetanic force in EDL muscle upon stimulation via macro- or micro-sieve electrodes. Mean values and standard deviations are shown. * denotes $p < 0.05$ versus similar device with dissimilar presence/absence of fibrin-based delivery system loaded with GDNF. **denotes $p < 0.05$ versus sieve electrode assembly with similar presence/absence of fibrin-based delivery system loaded with GDNF.

responses and recruitment curves from EDL, TA, and G muscles upon electrical activation of chronically-implanted macro-sieve electrodes are displayed. Monopolar stimulation of varying electrode sites located on the same macro-sieve electrode demonstrated selective recruitment of independent muscles in the lower leg. Specifically, monopolar stimulation via electrode site P1 demonstrates greater specificity for TA muscle, while stimulation via electrode site C2 demonstrated greater specificity for EDL muscle. Resulting data therefore confirm the ability of various electrodes sites to interface independent axonal populations and recruit separate end organs. Recruitment curves further demonstrate a high incidence of concurrent activation of multiple muscle groups upon monopolar stimulation of various electrodes sites (e.g. electrode site C3, and P3). Monopolar stimulation therefore results in lower selective indices (23-99%).

Examination of motor responses in the distal musculature demonstrated comparable maximum isometric twitch force production upon stimulation of regenerated nerve tissue using epineurial wire electrodes and simultaneous stimulation of all ring electrodes in the porous area of the macro-sieve electrodes. Stimulation of individual electrode sites on implanted macro-sieve electrodes resulted in minute twitch responses in selective muscle groups at low stimulus amplitudes. Muscle specificity exhibited by individual electrode sites was eliminated upon increasing stimulus amplitude, simultaneous stimulation via multiple electrode site, or stimulation of regenerated nerve tissue via epineurial wire electrodes. Neither stimulation of regenerated nerve tissue via epineurial or sieve electrode was able to achieve levels of force production in the healthy, unoperative muscle. Comparative analysis of the temporal characteristics of evoked force

traces did not reveal any significant differences between epineurial stimulation and sieve electrode stimulation.

To date the capability of macro-sieve electrodes to functionally recruit motor axons and control distal musculature has remained largely unexplored. Prior studies have demonstrated that micro-sieve electrodes achieve a stable, selective interface with peripheral nerve tissue and permit electrical stimulation and recording of regenerated nerves. Specifically, prior micro-sieve electrode have relied on the use of micro-scale via holes and ring electrodes to parse and interface small independent groups of nerve fibers. Existing data suggests that macro-sieve electrodes should be capable of recruiting regenerated axons by activation electrodes within the porous region of the device. Computational studies confirm the ability of macro-sieve electrodes to induce potential gradients sufficient for recruitment of regenerated motor axons, and evoke selective depolarization of small cross section areas of integrated nerve tissue. The present study was therefore designed to validate the ability of macro-sieve electrode assemblies with and without neuroregenerative features to support functional electrical stimulation of peripheral motor axons and distal musculature *in vivo*.

Results of the present study validate that macro-sieve electrode assemblies are capable of functionally recruiting regenerative nerve tissue *in vivo* using monopolar stimulation paradigms. Observation of muscle contraction in response to electrical activation of implanted macro-sieve electrodes confirm that macro-sieve electrodes enable stimulation of functional nerve fibers regenerating through integrated via holes. Macro-sieve electrodes further facilitate an intimate electrical interface with regenerated nerve fibers, evidenced by initiation of muscle activation at lower stimulus amplitudes

compared to epineurial electrodes. The present study additionally demonstrates that macro-sieve electrodes facilitate selective, functional electrical stimulation of regenerated motor axons and distal musculature. Measurement of evoked force production confirm that monopolar activation of individual electrode sites on implanted macro-sieve devices recruit specific motor units in independent muscles innervated by various branches of the interfaced sciatic nerve. Selective activation of electrode sites on implanted devices additionally provided a successful method of controlling graded force output in antagonistic muscle groups, suggesting that macro-sieve electrode may provide an effective means of controlling motor function in neuroprosthetic applications. Simultaneously, monopolar stimulation of individual electrodes site did not evidence consistent selectivity of motor recruitment (>90%). Future studies may therefore focus on the development and alternative stimulation paradigms capable of improving selective nerve interfacing and in vivo performance of chronically implanted macro-sieve electrodes.

The present study also confirms that the interfacial capabilities offered by novel macro-sieve electrodes greatly surpass that of prior micro-sieve electrodes. The present study validates the hypothesis that macro-sieve electrodes facilitate both robust axonal integration and selective electrical interfacing of distal musculature. Prior micro-sieve electrodes tested here and in prior studies relied on the use of micro-scale via holes to parse regenerating axons into small independent microfascicles. The formation of regenerative micro-fascicles was believe to be critical to selective interfacing, yet simultaneously resulted in a low-transparency electrode prohibitive of functional nerve regeneration and robust axonal integration. Results of the present study suggest that the

presence of micro-scale via holes may not be required and instead may be prohibitive to optimal function of regenerative electrodes as an effective neural interface. Specifically, the present study provide the first report of functional electrical stimulation of distal muscle tissue via an chronically-implanted regenerative electrode, as well as the first demonstration that application of field steering via regenerative electrodes enable selective nerve interfacing as well as more permissive electrode geometries.

Furthermore, the present study confirms that the use of neurotrophic factors is less critical in instances where the implanted electrode geometry inherently optimize axonal regeneration. Prior studies show that incorporation of neuroregenerative features into micro-sieve electrode assemblies is essential in establishing a selective interface between implanted electrodes and functional motor axons. Yet, the present study demonstrates equivalent recruitment of distal musculature by macro-sieve electrode assemblies both in the presence and absence of GDNF-loaded delivery system. These results suggest that while neurotrophic factors are effective in increasing axonal regeneration through synthetic constructs, they do not provide added value in cases where robust axonal regeneration is already supported. Interestingly, this observation may be skewed by the choice of animal model in the present study. Rat sciatic nerve has been previously shown to experience exceptional neuroregenerative capacity even in the presence of critical nerve injuries and defects. As a result, the use of neurotrophic factors in regenerative sieve electrodes designed for human use may provide added benefit above and beyond that outlined in the present study.

In total, the present study confirms that macro-sieve electrodes offer a promising and effective means of chronically interfacing peripheral motor axons for the purpose of

controlling motor activity. Additionally, this study concludes that the novel design of high-transparency macro-sieve electrodes is capable of facilitating both robust axonal regeneration and selective functional electrical stimulation of peripheral nerve tissue.

6-8: Electrophysiology: Selective Nerve Interfacing / Multipolar Stimulation

Prior sections confirm the ability of implanted macro-sieve electrodes to functionally recruit regenerated motor axons and distal musculature via monopolar activation of independent electrode sites. Presented data demonstrated that while monopolar stimulation was effective at recruiting independent musculature in the lower limb, mean selectivity of muscle activation was limited. Prior computation modeling suggests that macro-sieve electrodes are capable of delivering complex multi-polar stimulation paradigms capable of improving spatial selectivity of electrical activation in regenerated nerve tissue. To date no study has investigated applications of field steering via implantable regenerative electrodes and resulting selectivity of muscle activation is largely unknown. An electrophysiological study of nerve and muscle activation was therefore performed in order to investigate the ability of chronically-implanted macro-sieve electrodes to facilitate selective multipolar stimulation of integrated nerve tissue.

Electrical impulses were delivered to regenerated nerve segments via chronically-implanted macro-sieve electrodes ($t = 3$ mo) in order to determine their ability to interface regenerative nerve tissue. Cathodic, monophasic electrical impulses were generated by a multi-channel isolated pulse stimulator and routed in a multipolar configuration to one or more metallized electrode sites simultaneously within the porous

region of implanted macro-sieve electrodes. Specifically, testing was completed by defining one electrode site as the depolarizing source, and setting all remaining electrode sites as the hyperpolarizing sink. Electrical impulses (duration = 50-200 usec, frequency = single, amplitude = 0-1 mA) were used to initiate evoked muscle force production in extensor digitorum longus (EDL), tibealis anterior (TA), and gastrocnemius (G) muscles. Resulting force output at muscle tendons was transduced via the load cells and the resulting signals were amplified (gain = 1000X) using instrumentation amplifiers (AD620, Analog Devices Inc., Norwood, MA) powered by a constant voltage source before being recorded on a desktop PC equipped with a data acquisition board and custom Matlab software. Stimulation and recording were synchronized through custom software such that electrical stimulation coincided with the initiation of a 500 msec recording period, wherein data was sampled at 4 kHz. Custom software calculated the passive force and active force for each recorded force trace.

Recruitment curves were constructed to demonstrate the dependence of evoked muscle force production on stimulus amplitude and active electrode site. Resulting recruitment curves were compared to those generated via monopolar stimulation of identical regenerated nerve segments via macro-sieve electrodes. Electrical impulses (duration = 50-200 usec, frequency = single, amplitude = +/-0-1 mA) were delivered to regenerated sciatic nerves via implanted macro-sieve electrode to initiate distal motor responses which were recorded in the EDL, TA, and G muscles, as previously discussed. Selectivity of motor unit activation was assessed by comparing the motor response in the various muscles and calculating a selectivity index (SI) of each stimulation paradigm. Recorded force traces and peak twitch force (F_t) measurements resulting from stimulation

of sciatic nerve via implanted macro-sieve electrodes were compared to those acquired upon monopolar stimulation of sciatic nerve.

Regenerative nerve segments integrated into macro-sieve electrode assemblies were activated upon multipolar stimulation of electrode sites on integrated sieve electrodes. Representative recruitment curves constructed from evoked muscle force recordings are displayed. Recruitment of distal musculature was initiated at higher current amplitudes upon multipolar stimulation of implanted macro-sieve electrodes as compared to monopolar stimulation of implanted macro-sieve electrodes. Multipolar stimulation via macro-sieve electrodes with and without delivery system exhibited a

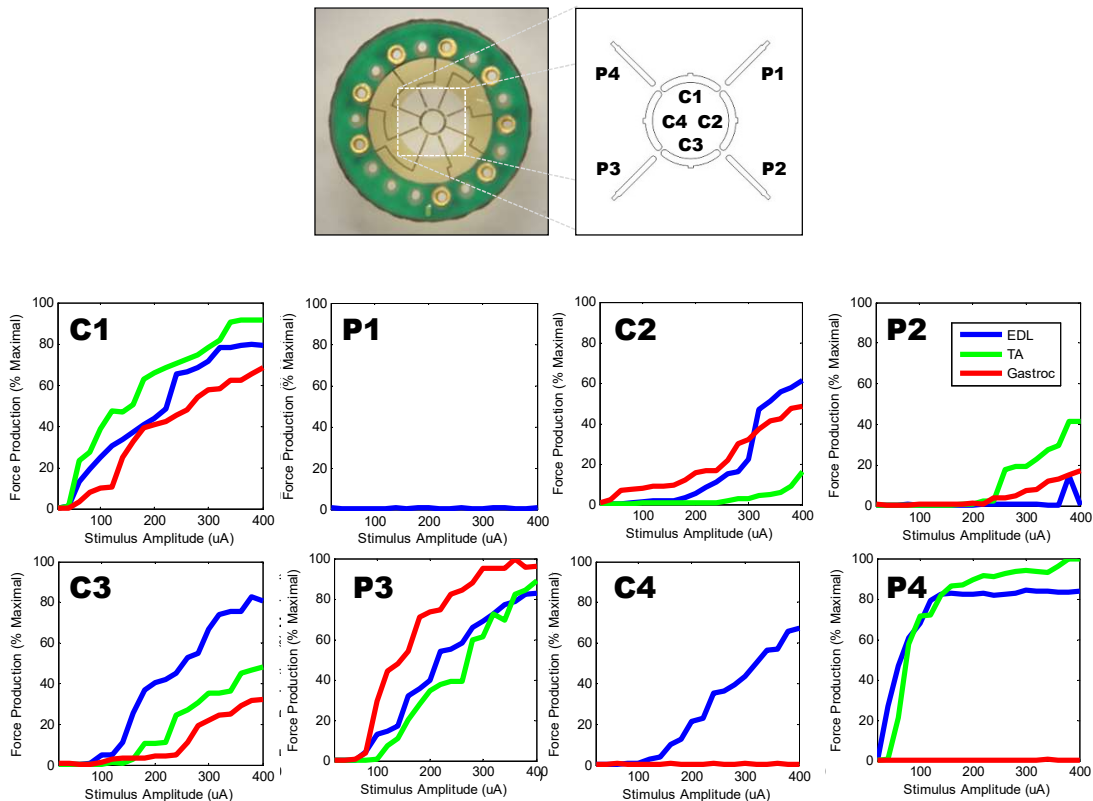


Figure 6-15. Motor response to multipolar stimulation of peripheral nerve tissue via macro-sieve electrodes. Recruitment curves generated upon multipolar stimulation of various electrode site on implanted macro-sieve electrodes and simultaneous recording of evoke force production in EDL, TA, and G muscles. Multipolar stimulation was defined as one depolarizing electrode site and 7 hyperpolarizing electrode sites.

mean threshold of nerve activation of 117 ± 65 uA and 91 ± 62 uA, respectively. Identical regenerated nerve segments were similarly recruited by monopolar stimulation at amplitudes of 48 ± 32 uA and 56 ± 27 uA, respectively. Recruitment curves formed upon multipolar electrical stimulation via macro-sieve electrodes were broader and shifted toward high current amplitudes compared to those generated upon monopolar stimulation. The presence of fibrin-based delivery system within implanted macro-sieve electrode assemblies did not affect the threshold of multipolar activation. Maximal evoked force production evoked via multipolar stimulation of regenerated nerve segments by implanted macro-sieve electrodes was comparable to that achieved via monopolar stimulation.

Evoked twitch responses and recruitment curves from EDL, TA, and G muscles upon multipolar stimulation via chronically-implanted macro-sieve electrodes are displayed. Multipolar stimulation of varying electrode sites located on the same macro-sieve electrode demonstrated highly selective recruitment of independent muscles in the lower leg. Specifically, multipolar stimulation via electrode site C4 demonstrates near complete specificity for EDL muscle, while stimulation via electrode site P2 demonstrated superior specificity for TA muscle. Measurements of maximal selectivity of recruitment demonstrated that multipolar stimulation was capable of achieving up to 99% selectivity for independent muscles in the lower leg. Representative recruitment curves are displayed. Highly selective recruitment of each independent muscle studied was observed across multiple electrodes throughout the course of the study. Recruitment curves further demonstrate a significantly lower incidence of concurrent activation of multiple muscle groups, as observed upon monopolar stimulation. Multipolar stimulation

resulted in higher selectivity indices ranging from 59-99%. These observations were further confirmed by examining the motor response to monopolar and multipolar

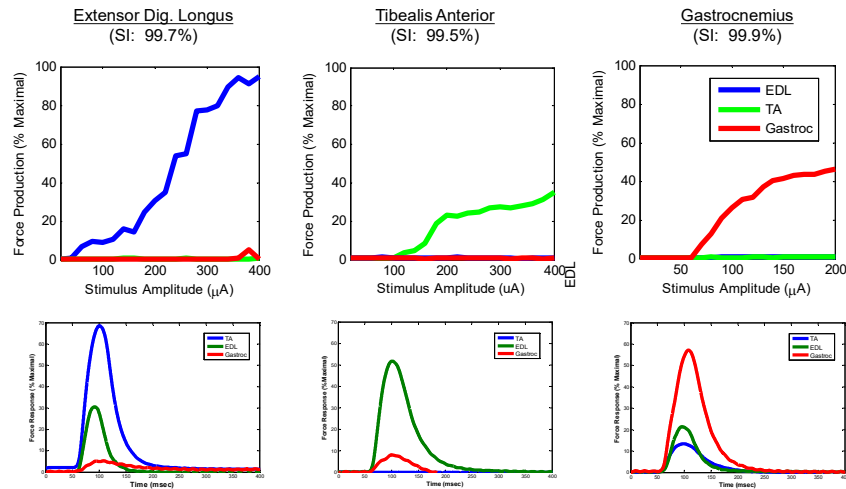


Figure 6-16. Maximal selectivity of muscle activation achieved upon multipolar stimulation of peripheral nerve tissue via macro-sieve electrodes. Recruitment curves highlight maximal selectivity of peripheral nerve interfacing achieved upon multipolar stimulation of various electrode site on implanted macro-sieve electrodes and simultaneous recording of evoke force production in EDL, TA, and G muscles.

activation of identical electrode sites in identical sieve electrodes. Direct comparison of recruitment curves generated upon monopolar and multipolar stimulation demonstrated improved selectivity for a single target muscle upon implementation of multipolar stimulation paradigm. Representative recruitment curves are displayed. Resulting data therefore validates prior computational modeling studies and confirms the ability of macro-sieve electrodes to facilitate field steering in order to improve selective recruitment of independent axonal populations and end organs.

Examination of motor responses in the distal musculature further demonstrated comparable maximum isometric twitch force production upon stimulation of regenerated nerve tissue using multipolar and monopolar stimulation paradigms. Multipolar stimulation of individual electrode sites on implanted macro-sieve electrodes resulted in minute twitch responses in selective muscle groups at low stimulus amplitudes. Interestingly, muscle specificity exhibited by individual electrode sites was not

significantly reduced upon increasing stimulus amplitude in many cases. Selectivity of muscle activation was lost upon switching to a monopolar stimulation paradigm applied via the same macro-sieve electrode and electrode site. Comparative analysis of the temporal characteristics of evoked force traces did not reveal any significant differences between monopolar and multipolar stimulation.

Results of the present study validate that regenerative sieve electrodes are capable of applying multipolar stimulation paradigms and field steering techniques as a means of improving selective electrical stimulation of regenerative nerve tissue in vivo.

Observation of muscle

contraction in response to multipolar stimulation of implanted macro-sieve electrodes confirm prior computational models and confirm that macro-sieve electrodes are capable of facilitating a highly-selective electrical interface with regenerated nerve fibers. The present study further

demonstrates that multipolar stimulation via macro-sieve electrodes facilitates increasingly selective, functional electrical stimulation of regenerated motor axons and distal musculature. Measurement of evoked force production confirm that multipolar

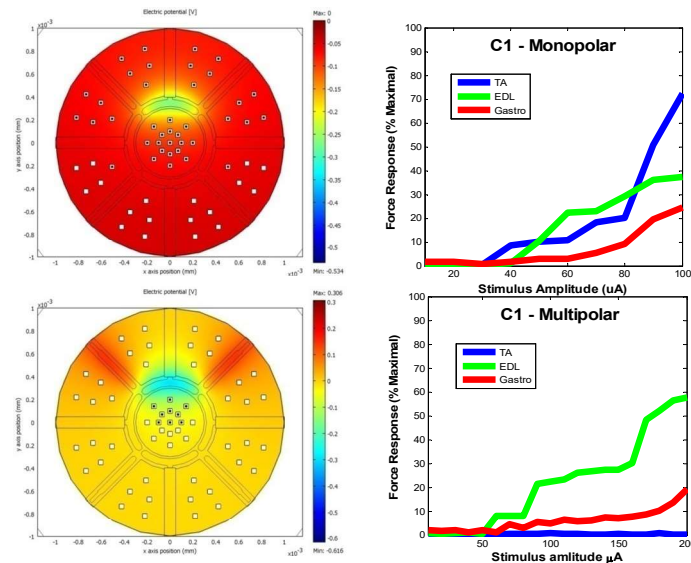


Figure 6-17. Comparative selectivity of monopolar and multipolar stimulation paradigms. Potential distribution and recruitment curve associated with monopolar stimulation of electrode site C1 (top). Comparative potential distribution and recruitment curve associated with multipolar stimulation of electrode site C1 (bottom).

activation of individual electrode sites on implanted macro-sieve devices recruits specific motor units in independent muscles. Direct comparison of recruitment curves obtained upon multipolar and monopolar stimulation of identical electrode site in the same sieve electrode further confirm that the effect is independent of the electrode site selected. Multipolar stimulation additionally demonstrates superior ability to activate independent musculature and evoke graded force output in antagonistic muscle groups compared to monopolar stimulation. Multipolar stimulation of individual electrodes evidenced more consistent selectivity of motor recruitment and higher mean selectivity indices across a larger number of electrode sites. Future studies may therefore focus on the use of multipolar stimulation paradigms in future in vivo testing of chronically implanted macro-sieve electrodes.

The present study also confirms that the interfacial capabilities offered by novel macro-sieve under multipolar stimulation paradigm surpass those of existing peripheral nerve interface presently in clinical use. The present study provides initial evidence that macro-sieve electrodes employing multipolar stimulation paradigm enable: chronic in

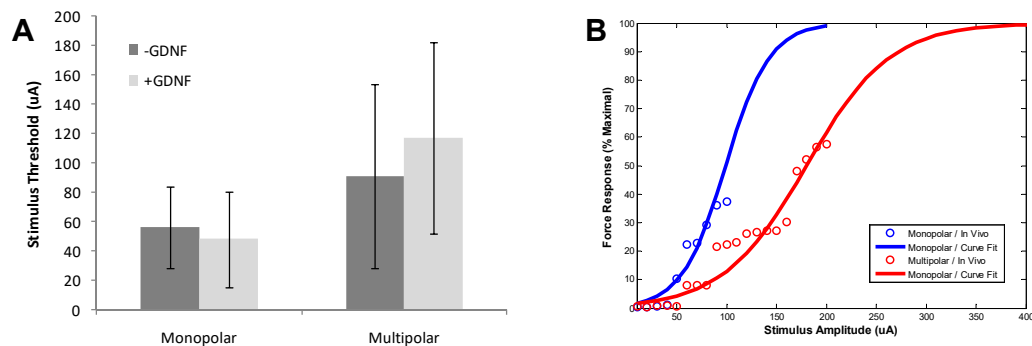


Figure 6-18. Comparative performance of monopolar and multipolar stimulation paradigms. Mean stimulus threshold observed upon monopolar and multipolar stimulation of regenerative nerve tissue in macro-sieve electrodes with and without delivery system (A). Comparative recruitment curves of monopolar and multipolar stimulation paradigms (B).

vivo performance, stable operating post-operatively, low threshold of activation, a high degree of selectivity, and broad recruitment curve ideal for graded control of distal musculature. Together these properties position the regenerative macro-sieve electrode as a unique alternative to existing neural interface technologies such as the USEA and the FINE electrode. The present study also suggests that future research into advanced field steering techniques may be a more attractive means of improving selective stimulation in implanted neural interface devices than the development of high-channel count electrodes. Specifically, the combinatorial nature of multipolar stimulation paradigms suggest that numerous

stimulation paradigms may be achieved through the use of only a small number of metallized electrode sites. Thereby advanced application of field steering techniques may provide a more rapid advance in electrode performance ahead of and in addition to further development in micro-scale fabrication techniques.

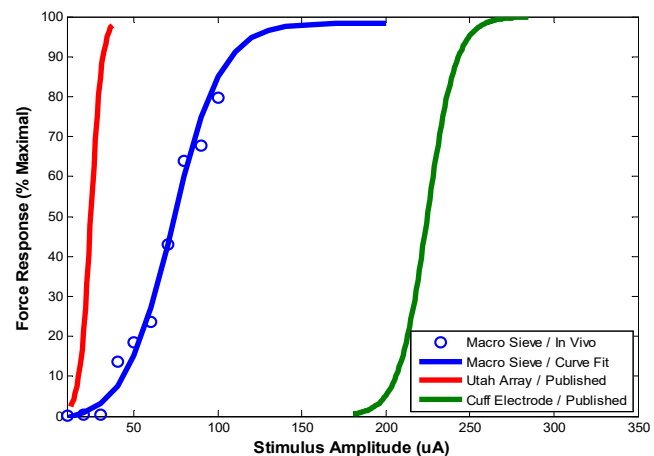


Figure 6-19. Comparative performance of macro-sieve electrodes versus clinical nerve interfaces. Comparative recruitment curves generated via Utah slant electrode arrays (USEA) (red), macro-sieve electrode (blue), and cuff electrode (green).

In total, the present study provide the first report of selective electrical stimulation of distal muscle tissue via multipolar stimulation of chronically-implanted regenerative electrode. The present study also demonstrated the first successful application of field steering via regenerative electrodes. Data presented confirms that macro-sieve

electrodes offer a unique means of chronically interfacing peripheral motor axons for the purpose of controlling motor activity in future neuroprosthetic systems. Additionally, this study concludes that the future implementation of field-steering technique with regenerative sieve electrodes is capable of facilitating a superior electrical interface with peripheral nerve tissue.

Chapter 7: Clinical Enhancement of Macro-Sieve Electrodes

7-1: Introduction

In the final chapter supplementary studies designed to enhance the performance and clinical potential of macro-sieve electrode assemblies will be presented. Prior chapters demonstrate the unique ability of macro-sieve electrodes to facilitate highly-selective stimulation of peripheral nerve tissue following chronic implantation. These studies confirm the unique capabilities of macro-sieve electrodes compared to existing neural interface technologies utilized in clinical practice. Despite this successful demonstration of macro-sieve electrode performance, multiple factors associated with the design and use of the macro-sieve electrode pose limitations to future clinical translation.

In the present chapter, a variety of studies will be presented in order to: 1) identify new avenues for improving sieve electrode performance, 2) enable unidirectional (orthodromic) action potential propagation, 3) employ novel power delivery strategies, and 4) improve the quality of the nerve/electrode interface. The first step was to evaluate methods of fabricating and evaluating dual-layer macro-sieve electrodes. The second step was to conduct an evaluation of the ability of dual layer macro-sieve electrodes to induce orthodromic action potential initiation. The third step was to investigate means of applying wireless power delivery strategic to the macro-sieve electrode assembly. The

fourth step was to examine the potential of utilizing electrical stimulation to enhance axonal regeneration through future macro-sieve implants.

7-2: Dual Layer Macro-Sieve Electrodes

One of the primary limitations associated with presented macro-sieve electrodes is the low channel count on the implantable device. In order to examine unique approaches to increasing the channel count on macro-sieve electrodes and enable unique functional capabilities a dual-layer sieve electrode was designed and tested *in vivo*.

Integrating a unique modular design, macro-sieve electrodes were placed back-to-back to form a single, 16-channel, high-porosity regenerative electrode capable of

initiating multi-polar stimuli along the length of regenerated axons. Chronic implantation in rat sciatic nerve facilitated assessment of the ability of dual-sided macro-sieve electrodes to functionally interface regenerative

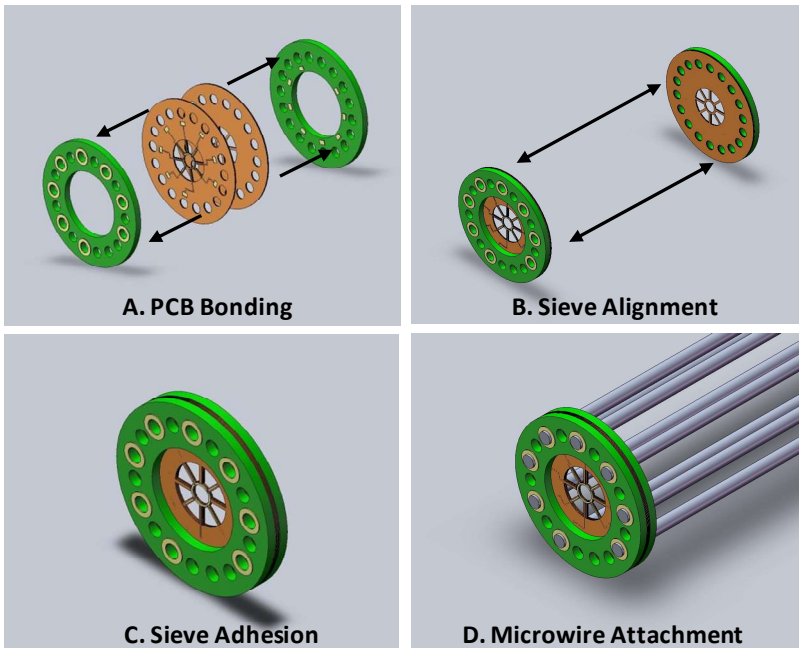


Figure 7-1. Assembly of dual-layer macro-sieve electrodes. Outline of steps required for the assembly of dual-layer macro-sieve electrodes containing 2 macro-sieve electrodes and 16 active sites (A-D).

nerve tissue and selectively recruit peripheral motor axons for graded control of distal musculature.

Modular macro-sieve electrodes fabricated via sacrificial photolithography were bonded to form 16-channel, dual-sided regenerative electrodes. Macro-sieve electrodes were micro-surgically implanted in the sciatic nerves of 300 g Lewis rats for a minimum of 3 months prior to functional assessment. Functional nerve regeneration through

implanted electrodes was assessed via nerve conduction studies and evoked muscle force measurement. Interfacial capabilities of implanted dual-sided macro-sieve electrodes were examined by routing monophasic stimuli (duration =10-200 μ s, amplitude=0-1000 μ A) to

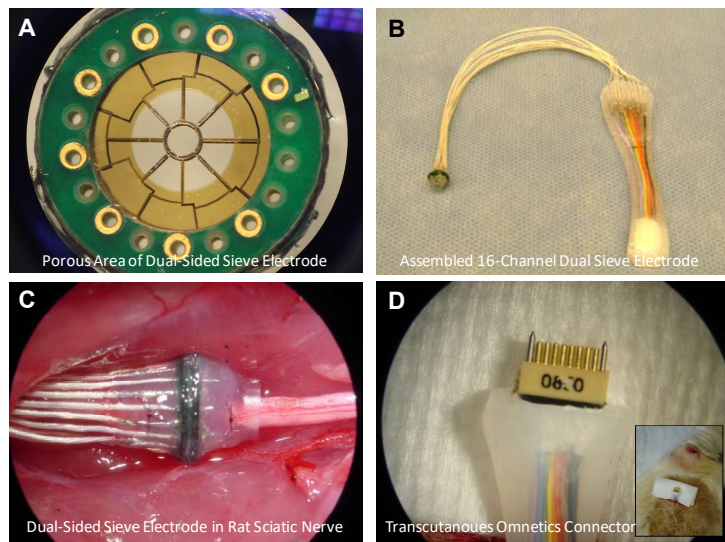


Figure 7-2. Fabricated dual-layer macro-sieve electrodes. Dual-layer macro-sieve electrodes demonstrate a comparable profile to single-layer macro sieve electrodes (A). Sixteen channel micro-wire connectors on dual-layer implant (B). Dual-layer sieve electrode implanted in rat sciatic nerve (C). Subcutaneous omnetics connector (D).

active electrode sites on both layers while simultaneously recording evoked force production in EDL, TA, and G muscles. Various electrode configurations (monopolar, bipolar, multipolar) were also evaluated to identify stimulation paradigms ideally suited to enable selective recruitment of regenerated motor axons.

Results demonstrate that dual-layer macro-sieve electrodes supported robust nerve regeneration and functional recovery *in vivo*. Dual-sided macro-sieve electrodes were

demonstrated to recruit regenerative nerve tissue at stimulus amplitudes as low as 10-40 μ A and enable graded activation of distal musculature comparable to single-layer macro-sieve electrodes. Multi-polar stimulation paradigms enacted across metalized sites on

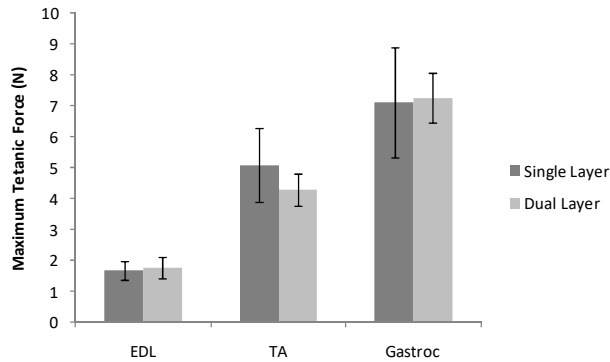


Figure 7-3. Maximum isometric tetanic force production via single-layer and dual-layer macro-sieve electrodes. Maximum tetanic force in EDL muscle upon stimulation via single layer and dual layer macro-sieve electrodes. Mean values and standard deviations are shown. * denotes $p < 0.05$ versus comparable device.

both sides of the device further demonstrated superior selectivity of muscle activation comparable to prior studies. Measurement of evoked force production in distal musculature further demonstrated the successful regeneration of motor axons through implanted dual-layer sieve electrodes, as well as successful reinnervation of

distal motor targets. Functional recovery of muscle activation was comparable between single-layer and dual-layer macro-sieve electrodes confirming that the presence of the second macro-sieve wafer did not impact axonal regeneration or functional recovery post-operatively.

The present study highlights the design and evaluation of a novel configuration of macro-sieve electrodes capable of facilitating increased channel counts as well as selective and graded recruitment of distal musculature following chronic implantation. Together, the distinct interfacial capability of dual-sided macro-sieve electrodes suggests a unique application for application of advanced stimulation paradigms and improved control of motor and sensory stimulation. In total, the success of dual-sided macro-sieve

electrodes in a chronic *in vivo* setting demonstrates a unique improvement to the novel regenerative electrode assembly.

7-3: Selective Stimulation of Uni-directional / Orthodromic Action Potentials

Electrical stimulation of peripheral axons by existing microelectrodes results in simultaneous initiation of action potentials propagating both in retrograde and anterograde directions. Simultaneous initiation of orthodromic and antidromic stimuli poses a significant barrier to the selective interfacing of motor versus sensory axons and the high-resolution graded activation of innervated musculature. The development of novel microelectrode devices capable of selectively inducing orthodromic stimulation of peripheral axons therefore serves as a critical step in the clinical translation of rehabilitative neuroprosthetic systems. The present study was designed in order to examine the ability of dual-layer regenerative sieve electrodes to selectively support orthodromic stimulation, without antidromic stimulation, of peripheral nerve fibers by simultaneously delivering depolarizing / hyperpolarizing stimuli at various points along the length of interfaced axons.

Hybrid computational models were implemented as previously described to examine the ability of dual layer macro-sieve constructs to initiate selective orthodromic activation of virtual axons placed throughout the macro-sieve electrode assembly. Simultaneous application of 600 usec cathodic and anodic stimuli to matching electrode sites on both layers of the dual-layer macro-sieve electrodes enabled initiation of

unidirectional
action
potentials
across a
variety of
stimulation
amplitudes.

Testing
demonstrated that
initiation of

unidirectional action potentials was dependent both on the stimulus amplitude, stimulus duration, as well as the distance between individual macro-sieve electrodes in the dual-layer assembly. Specifically, unidirectional action potential initiation was best observed upon implementation of stimulus durations >300 usec, and above stimulus amplitudes >500 uA. Results of computational model studies suggest that dual layer sieve electrode assemblies are capable of supporting selective initiation of orthodromic action potentials, and thereby may be capable of selectively inducing action potential progressing only medially or laterally from the point of the sieve/nerve interface.

In order to examine the ability of dual-layer macro-sieve electrodes to selectively induce orthodromic activation of peripheral axons, dual-layer macro-sieve electrodes were micro-surgically implanted in the sciatic nerves of 300 g Lewis rats for a minimum of 3 months prior to functional assessment. Functional nerve regeneration through implanted electrodes was assessed via nerve conduction studies and evoked muscle force

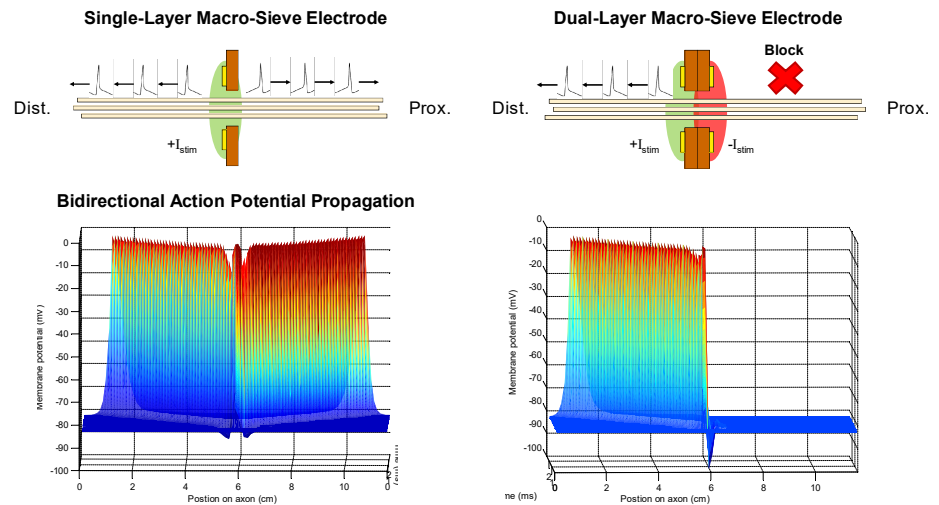


Figure 7-4. Computational modeling of unidirectional action potential propagation. Diagrammatic representation of the function of dual-layer macro-sieve electrodes (top). Computational results demonstrating successful initiation of unidirectional action potentials.

measurement. The capability of implanted dual-sided macro-sieve electrodes to induce orthodromic activation of peripheral axons was examined by routing simultaneous monophasic cathodic and anodic stimuli (duration =10-200 μ s, amplitude=0-1000 μ A) to matched active electrode

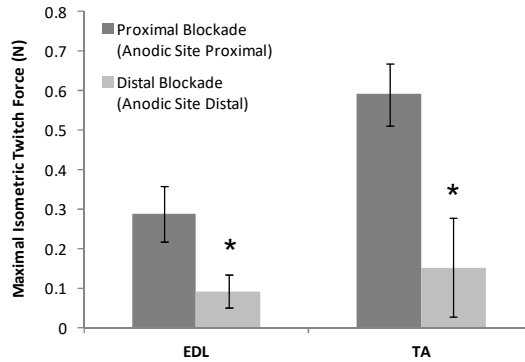


Figure 7-5. In vivo testing of unidirectional action potential initiation / propagation. Evoked isometric twitch force recorded upon stimulation either with the anodic site distal or the cathodic site distal.

sites on both layers of the dual-layer construct while simultaneously recording evoked force production in EDL, TA, and G muscles. Specifically, muscle force production was recorded under two conditions: 1) where the cathodic stimuli was delivered to the active electrode site located distally along the nerve, and to the anodic stimuli was delivered to the active electrode site located proximally along the nerve, and 2) where the anodic stimuli was delivered to the active electrode site located distally along the nerve, and to the cathodic stimuli was delivered to the active electrode site located proximally along the nerve. Comparison of muscle activation in these two scenarios, wherein action potentials would be routed in an anterograde fashion towards distal musculature and in a retrograde fashion away from distal musculature, was utilized to determine the efficacy of selectively induction of orthodromic activation.

Results of in vivo testing demonstrate a significant knockdown of distal muscle activation upon selective induction of action potentials propagating in a retrograde fashion away from the nerve/electrode interface as compared to selective induction of action potentials propagating in an anterograde fashion toward distal end organs.

Specifically, stimulation paradigms wherein anodic electrode sites were located distal to cathodic electrode sites induced significantly lower force production in EDL and TA muscles compared to stimulation paradigms wherein cathodic electrode sites were located distal to anodic electrode sites. These results suggest that simultaneous delivery of hyperpolarizing stimuli directly proximal / distal to the location of depolarization effectively reduces retrograde propagation of action potential induced upon electrical stimulation via macro-sieve electrodes. While the knock-down was not complete, the present results provide initial evidence to support prior computational modeling. This incomplete effect may be due to the imperfect nature of recruitment as provided by the sieve electrode or the heterogeneity of the interfaced axonal population. In total, these results provide preliminary evidence of the ability of dual-layer sieve electrodes to induce selective induction of orthodromic activation of peripheral nerve fibers, and potentially eliminate non-specific propagation of exogenously induce action potentials.

Paired computational modeling and in vivo testing demonstrate preliminary evidence of the ability of dual-layer sieve electrodes to simultaneously deliver depolarizing and hyperpolarizing stimuli along the length of interfaced axons and thereby selectively inducing orthodromic and inhibit antidromic activation. Future studies will focus on further elucidating the capabilities of dual-layer macro-sieve electrodes and improving the ability of sieve electrodes to reliably induce uni-directional action potential across a range of axonal populations and stimulation paradigms.

7-4: Wireless Electrical Stimulation

Prior studies conducted utilizing macro-sieve electrodes required the use of external power supplies and direct electrical connection to the implanted device through the use of subcutaneous or transcutaneous port. The present method of powering and interfacing advanced macro-sieve electrodes thereby provides significant hurdles to future clinical translation and use. The present study was conducted in order to examine the feasibility of integrating a novel system of wireless communication and power delivery with existing macro-sieve electrodes. The present study was further utilized to examine the ability of the wireless macro-sieve electrode to facilitate functional recruitment of

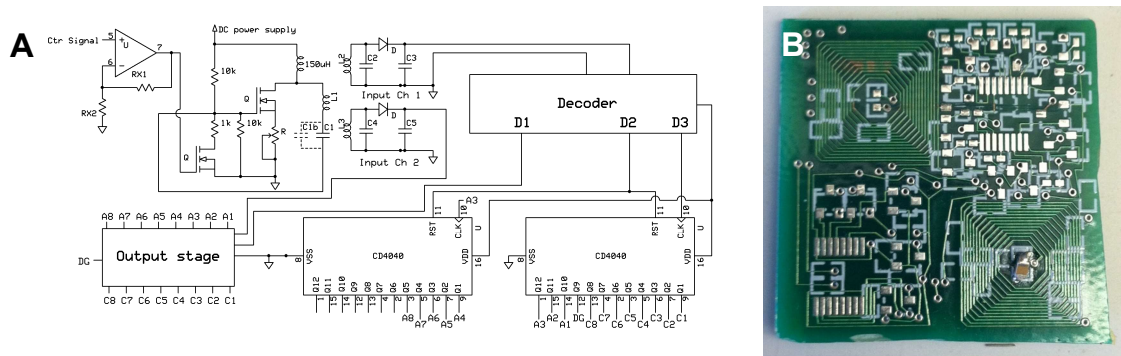


Figure 7-6. Implantable wireless stimulator circuit. Schematic (A) and fabricated PCB (B) related to the implantable wireless communication and power module connected to the macro-sieve electrode. peripheral nerve tissue and distal musculature in vivo.

Briefly, a system of wirelessly delivering power and logical control of implanted macro-sieve electrodes was designed by Erik Zellmer in the laboratory of Dr. Daniel Moran in the Department of Biomedical Engineering at Washington University in St. Louis. The system consisted of an external wireless transmitter circuit and an implantable set of wireless receivers / decoder circuit.

Implantable wireless receivers were fabricated using standard printed circuit board technology. Integrated receivers tuned to 5.0 MHz and 1.8 MHz supplied power and trigger/logical controls to onboard circuitry, respectively. Channel setup was executed by two cascaded 12 bit binary counters with clock signals delivered over the 1.8 MHz carrier frequency (5 Kbit/s). Power delivered over the 5.0 MHz carrier frequency is

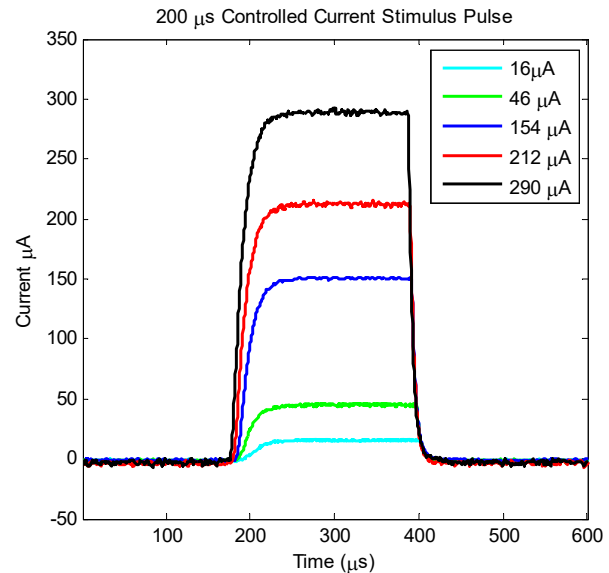


Figure 7-7. Stimulus output from implantable wireless stimulator circuit. Controllable stimulus output originating from implantable wireless nerve stimulator circuit. Wireless stimulator demonstrated the capability to control the stimulus output, duration, and channel count.

stored on an onboard stimulus capacitor used to drive initiated stimulus pulses triggered over the 1.8 MHz carrier frequency. Custom GUIs were designed to modulate external wireless transmitters and facilitate real-time control over channel selection as well as the duration, amplitude, frequency, and polarity of evoked electrical stimuli.

A decoder circuit was designed to allow input Ch 1 to be used for output channel setup, stimulus pulse triggering, and system reset. The state of node D1 was used to control the trigger circuit in the output stage. For any duration that D1 is pulled low, charge stored in the stimulus capacitor is injected into the tissue. Binary inputs to D3 are used to provide the clock signal to change the state of onboard binary counters. D2 is connected to the reset pin of the binary counter ICs. Signal decoding was achieved by

timing circuits used to divide each stimulus event into a cycle with a number of discrete phases.

The output stage consisted of a Greinacher voltage doubler, a stimulus pulse trigger allowing inputs from D1 to trigger the output of the system, and nine segments controlling the stimulation settings of eight electrode sites and one reference electrode.

The Greinacher voltage doubler is used to allow voltages in the excess of 200V to be generated and stored

over the stimulus

capacitor. Resistors

R11-R18 are used

increase the output

impedance of the system

which allows the system

to be roughly

approximated as a

controlled current

stimulator. Depending on

the input from the binary

counters, each electrode site could be set independently to either source or sink current

during stimulation.

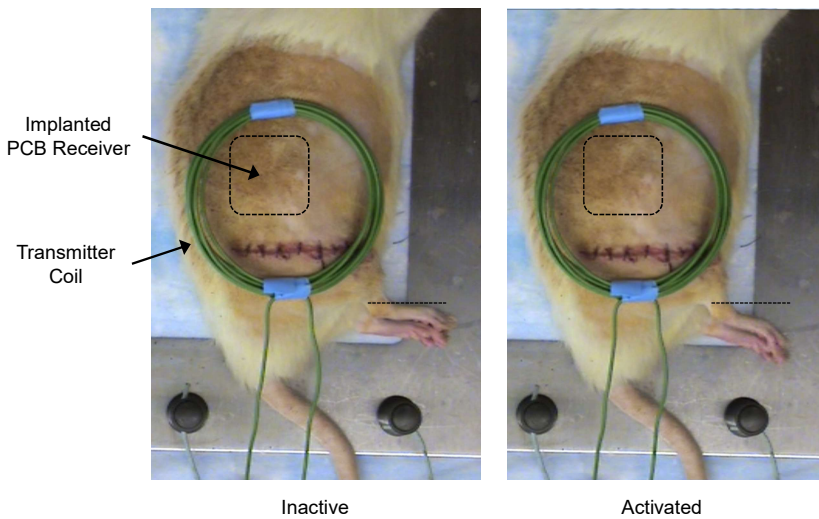


Figure 7-8. In vivo implementation of wireless stimulation system.

Implantable wireless receivers containing micro-scale controllers, regulators, and power capacitors were connected to implanted macro-sieve electrodes and implanted subcutaneously in male Lewis rats. Upon interfacing, a transmitter coil was placed over the implant in order to communicate and power the device via inductive coupling.

In order to examine the ability of the wireless system to facilitate functional electrical stimulation via implanted nerve interface, macro-sieve electrodes were micro-surgically implanted in the sciatic nerves of 300 g Lewis rats for a minimum of 3 months prior to functional assessment. The capability of implanted macro-sieve electrodes to wireless activate peripheral nerve tissue was examined by connecting implanted macro sieve electrodes to the implantable wireless receiver circuit. Monophasic cathodic stimuli (duration =10-200 μ s, amplitude=0-1000 μ A) were then routed to individual electrode sites on the implanted sieve electrode via the wireless receiver as powered by the remote transmitted circuit and coil. Upon electrical stimulation via macro-sieve electrodes simultaneously recording evoked force production was performed in EDL, TA, and G muscles.

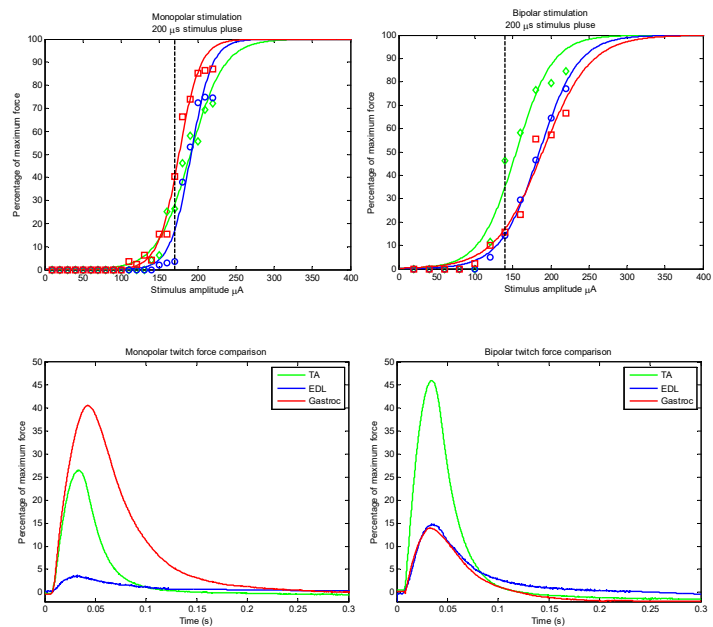


Figure 7-9. Functional electrical stimulation via wireless macro-sieve electrodes. Recruitment curves (top) and evoked muscle force traces (bottom) generated upon electrical activation of peripheral nerve tissue via monopolar stimulation (left) and multipolar stimulation (right).

Evoked muscle force measurement demonstrated successful recruitment of peripheral motor axons and distal musculature upon electrical stimulation of wirelessly powered macro-sieve electrodes. Results demonstrate the ability of the wireless system to deliver both a range of stimulation amplitude and stimulation paradigms, as well as enable remote channel selective on implanted macro-sieve electrodes. Wirelessly-

powered sieve electrodes demonstrated effective recruitment of all three muscles in the lower limb, comparable to prior devices. Recruitment curves demonstrated graded activation of distal musculature upon both monopolar and multipolar stimulation paradigms facilitated by the implanted macro-sieve electrode and implantable controller. Monopolar stimulation performed via wirelessly-powered macro-sieve electrodes was observed to have a lower stimulation threshold and lower threshold of half-maximal stimulation as compared to multipolar stimulation of identical muscles. These results were consistent with prior studies of hard-wired macro-sieve electrodes completed in prior chapters. Together, these results suggest successful implementation of a wireless communication and powering strategy with existing macro-sieve electrode assemblies.

Implantable wireless receivers were designed and fabricated to provide a stable, low-profile, non-invasive means of facilitating chronic nerve stimulation via macro-sieve electrodes. Results of the present study suggest that the present wireless implantable nerve stimulator system offers multiple advantages over existing approaches and solutions. Compared to transcutaneous or percutaneous systems methods of interfacing, the present wireless offers a completely implantable solution devoid of connecting wires and at lower risk of chronic infection in ambulatory animals. Absence of a solid-state power supply further reduces the profile of the device making it suitable for use in both small animal models in a laboratory setting and well as in future clinical applications. The passive nature of the implantable stimulator further suggests improved safety and biocompatibility of the device. The present system may therefore be ideally suited for eventual clinical translation and use in a variety of nerve interfacing scenarios. In total, the present study presents data suggesting that macro-sieve electrodes may be effectively

integrated with novel wireless communication technologies and strategies for future use in both basic science and clinical settings.

7-5: Therapeutic Electrical Stimulation

Prior chapters demonstrate the ability of implantable macro-sieve electrodes to support robust axonal regeneration in vivo. This capability has been demonstrated to primarily result from the high transparency of the novel porous region geometry of the macro-sieve electrode. Alternatively, these results may be influenced by the use of the rat sciatic nerve model in the present study. Prior reports suggest that rodent nerve possesses a significant greater regenerative potential compared to that of human peripheral nerve, and as a result may display more robust regeneration under comparable conditions or injury models. Therefore, future clinical translation of macro-sieve electrode technologies into human subjects may require further examination of adjunct capable of improving axonal regeneration through implanted nerve interface. While the present study demonstrates the positive role of neurotrophic support in promoting axonal regeneration through implanted electrode additional approach should be evaluated.

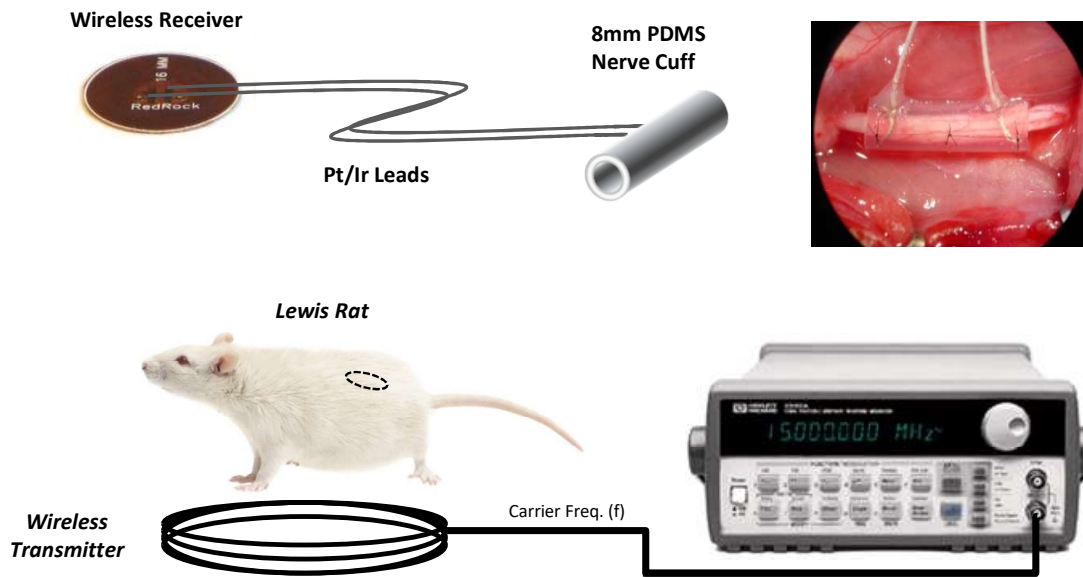


Figure 7-10. System of wireless nerve stimulators for use in applying brief electrical stimulation. Assembly of wireless receivers for in vivo implantation (top left). Flexible thin-film receivers are bonded to Pt/Ir leads that are integrated into a silicone nerve cuff electrodes sized for rat sciatic nerve. Implantable wireless nerve stimulators are implanted subcutaneously in laboratory rats and connected to the sciatic nerve (top right). Upon activation by an external transmitter coil, implanted receivers generate electrical impulses which provide brief electrical stimulation proximal to the site of sciatic injury.

Brief electrical stimulation of peripheral nerve tissue represents a promising method for enhancing axonal outgrowth and augmenting peripheral nerve function in vivo. Prior studies have demonstrated that brief, low-frequency electrical stimulation of injured peripheral nerve tissue enhances the rate of axonal regeneration and functional recovery in vivo in a number of animal models. One hour of low frequency electrical stimulation applied to rat nerve was observed to accelerate axonal outgrowth to promote regeneration of all motor axons within 3 rather than 8– 10 weeks post-operatively (Al-Majed et al; 2000, Brushart et al; 2002, Brushart et al; 2005, Geremia et al; 2007). Electrical stimulation has also been observed to accelerate axonal regeneration in mice (Ahlborn et al; 2007, English et al; 2007). Similar results have also been observed upon application of brief electrical stimulation to injured human peripheral nerve tissue (Gordon et al; 2010). Brief electrical stimulation of human median nerve during routine

carpal tunnel release surgery was observed to improve functional recovery post-operatively, suggesting that the therapeutic value of electrical stimulation is equally applicable across both animal and human models.

Unfortunately existing methods for clinically applying therapeutic electrical stimulation to peripheral nerves are limited. In the majority of published studies electrical stimulation of peripheral nerve tissue was delivered using nerve hook or wire electrodes applied directly to the target nerve during open surgical repair (Al-Majed et al; 2000, Brushart et al; 2002, Ahlborn et al; 2007). In this setting application of electrical stimulation is limited to a brief intraoperative period during which the patient is fully anesthetized and the target nerve is surgically exposed. Application of electrical stimulation is further limited by the need to physically connect the terminal nerve hook electrodes to an external power source.

The present study was designed to examine whether electrical stimulation of nerve tissue via wireless implantable nerve stimulators was capable of accelerating axonal regeneration functional recovery post-operatively, and whether such stimuli could be delivered via macro-sieve electrodes as a non-biologic means of accelerating neural integration.

Twenty five adult male Lewis rats were randomized into five groups (I-IV) of five animals each (n=5). Group I served as the positive control as all animals underwent sham surgical exposure of the sciatic nerve (no nerve injury) followed by surgical implantation of a wireless nerve stimulator. Groups II and III served as experimental groups as all animals underwent surgical exposure and crush injury of the right sciatic nerve followed by surgical implantation of a wireless nerve stimulator. Groups IV and V served as

experimental groups as all animals underwent surgical transection and repair of the right sciatic nerve followed by surgical implantation of a wireless nerve stimulator. Post-operatively, all animals in Groups III and V received one hour of therapeutic electrical stimulation delivered via implanted wireless nerve stimulator. All animals in Groups II and IV did not receive therapeutic stimulation. All animals underwent weekly assessment of functional recovery as measured via wireless stimulation of the sciatic nerve and measurement of resulting EMG signals in distal musculature.

Implantable wireless nerve stimulators were designed and fabricated to provide a stable, low-profile, non-invasive means of facilitating chronic nerve stimulation (Gamble et al; In press). Wireless implants consisted of three components: 1) receiver coil and demodulating circuit, 2) micro-wire leads, and 3) silicone nerve

cuff. Receiver coils comprising a spiral antenna and demodulating circuitry were fabricated on flexible polyimide substrates (dia. = 12 mm, thickness = 0.2 mm). 0603 surface mount components were soldered to the flexible PCB to tune receivers to a 5MHz carrier frequency and demodulate incoming signals. Two multiconductor PTFE-insulated Pt/Ir microwire leads (Medwire, Sigmund Cohn, Mt. Vernon, NY) were soldered on to the contact pads of the flexible polyimide PCB in order to provide an electrical conduit

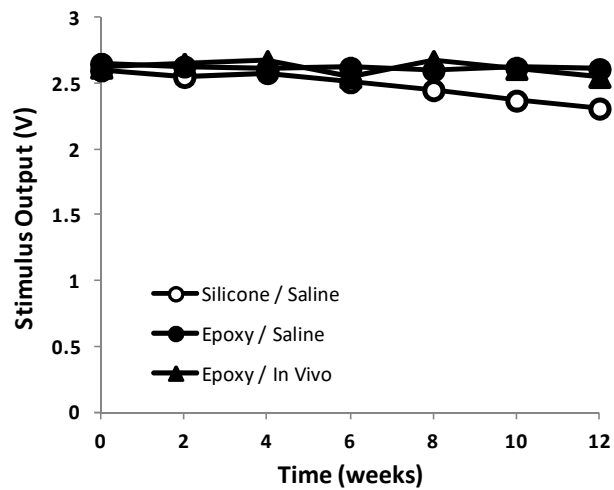


Figure 7-11. Output of wireless nerve stimulators over chronic in vivo implantation. Output voltage of wireless nerve stimulators measured upon variable tuning of integrated spiral receiver antenna.

between the receiver coil and interfaced peripheral nerves. Bared ends of the Pt/Ir microwire leads were then integrated into silicone nerve cuffs optimized for rodent sciatic nerve (ID = 2 mm, OD = 4mm, length = 8 mm). Silicone nerve cuffs were constructed of silicone nerve guidance conduit and designed to maintain close approximation of active Pt/It leads to interfaced peripheral nerve tissue. Following construction, flexible receiver coils were potted in medical grade silicone elastomer (Type A, Dow Corning, Midland, MI). Completed wireless implants were gas sterilized with ethylene oxide prior to use *in vivo*. Upon ex vivo / in vivo testing, modified class E oscillator circuits tuned to a 5 MHz carrier frequency were utilized to power and activate constructed wireless nerve stimulators (Zellmer et al; In press). Oscillator circuits were connected to circular transmitting coils / antenna placed near the wireless nerve stimulators. Inductive coupling between transmitter and receiver coils thereby facilitated wireless power delivery and activation of implantable wireless devices suitable for peripheral nerve stimulation.

Animals were anesthetized using 4% Isoflurane / 96% oxygen (induction) and 2% Isoflurane / 98% oxygen (maintenance) administered by inhalation. Following preparation and sterilization of the lateral aspect of the right leg, the right sciatic nerve was exposed through a dorsolateral gluteal muscle-splitting incision followed by blunt dissection. Utilizing an operating microscope, animals in Groups II and III underwent surgical induction of a crush injury 5 mm proximal to the trifurcation of the sciatic nerve. Crush injury was administered via two subsequent 30 sec crushes applied using Jeweler's forceps. Animals in Groups IV and V underwent surgical transection and repair of the sciatic nerve 5 mm proximal to the trifurcation. Nerves transected using fine iris scissors

were microsurgically repaired in a direct fashion using 10-0 nylon suture (Sharpoint™, Surgical Specialties Corp., Reading, PA). Animals in Group I did not undergo sciatic nerve injury.

Following surgical induction of sciatic nerve injuries, wireless nerve stimulators were implanted in each animal. Blunt dissection was utilized to create a subcutaneous pocket extending 5cm proximally from the lateral aspect of the right leg, along the right flank, to the back of the animal. A thin film receiver was then implanted into the subcutaneous pocket and Pt/Ir leads were routed to the exposed sciatic nerve. Silicone nerve cuffs integrating active Pt/Ir leads were then microsurgically fitted to the sciatic nerve 5mm proximal to the site of nerve crush / nerve transection and secured via 10-0 nylon. Following implantation, the incision was irrigated and the muscle fascia and skin were closed in two layers using 6-0 polyglactin (Vicryl™, Ethicon, Somerville, NJ) and 4-0 nylon suture (Ethilon™, Ethicon, Somerville, NJ), respectively.

Beginning one week after surgery, serial assessment of sciatic nerve function was conducted *in situ*. Implanted wireless nerve stimulators were utilized to electrically activate sciatic nerve tissue while resulting electromyograms (EMGs) were recorded in distal musculature. Animals were anesthetized using 4% Isoflurane / 96% oxygen (induction) and 2% Isoflurane / 98% oxygen (maintenance) administered by inhalation. A wireless transmitter coil was then placed over each animal and centered over the implanted wireless receiver. A 5 MHz carrier frequency was then utilized to wirelessly power the implanted nerve stimulator. Modulation of the carrier frequency generated cathodic, monophasic electrical impulses in implanted wireless receivers (duration = 200 usec, frequency = 0-100Hz, amplitude = 0-10 V) capable of recruiting interfaced

peripheral nerve tissue. Resulting EMGs were differentially recorded proximal and distal to the implanted device in the Gluteus Maximus (GM), Tibialis Anterior (TA), Gastrocnemius (G), Extensor Digitorum Longus (EDL) muscles using needle electrodes. Measured signals were band-pass filtered (LP = 1 Hz, HP = 5 kHz, notch = 60 Hz) and amplified (gain = 1000X) using a two-channel microelectrode AC amplifier (Model 1800, A-M Systems Inc., Carlsborg, WA) before being recorded on a desktop PC equipped with custom data acquisition software (Red Rock Laboratories, St. Louis, MO). Stimulus amplitude and frequency were mapped to construct recruitment curves and determine maximal peak-to-peak amplitude of evoked EMG responses. Serial measurement of sciatic nerve function was repeated weekly for 13 weeks after surgery.

Results demonstrate that wireless nerve stimulators were successfully fabricated and tested in vivo. Benchtop testing was performed by approximating wireless transmitter coils and fabricated wireless nerve stimulators while measuring evoked stimulus output. Benchtop testing demonstrated successful tuning and performance of implantable wireless receivers. Wireless receivers demonstrated stable output voltages ranging from 2.0 V – 2.8 V at a 5.0 MHz carrier frequency using a 10 Vpp carrier signal.

Serial activation of peripheral nerve tissue and innervated musculature via implanted wireless stimulators was performed in order to track functional recovery following peripheral nerve injury with and without therapeutic electrical stimulation. Wireless activation of implanted nerve stimulators elicited consistent activation of musculature both proximal (gluteal muscle) and distal (tibealis anterior, extensor digitorum longus, gastrocnemius, and plantaris) to the site of nerve injury as evidenced by recorded EMG activity. Serial EMG measurements demonstrated varied time courses

and degrees of functional motor recovery over 13 weeks following induced nerve injury and brief electrical stimulation.

Evoked EMGs recorded in animals undergoing sham surgery (no nerve injury) demonstrated consistent amplitudes throughout the duration of the study (GM: 9.60 ± 0.24 mV, TA: 10.31 ± 0.47 mV, GS: 10.15 ± 0.45 mV, PL: 7.59 ± 0.38 mV). Consistent activation of musculature by implanted wireless devices demonstrated both the repeatable nature of wireless nerve interfacing, as well as the preservation of interfaced peripheral nerve tissue and innervated musculature during chronic interfacing.

Directly after nerve crush and nerve transection injury evoked EMG responses demonstrated

effective knock-down of activation in musculature distal to the site of nerve injury (TA/Crush:

1.52 ± 0.69 mV, TA/Cut: 0.87 ± 0.56 mV, GS/Crush: 2.38 ± 0.65 mV, GS/Cut: 0.73 ± 0.49

mV, PL/Crush: 1.25 ± 0.62 mV, PL/Cut: 0.87 ± 0.47 mV). Evoked

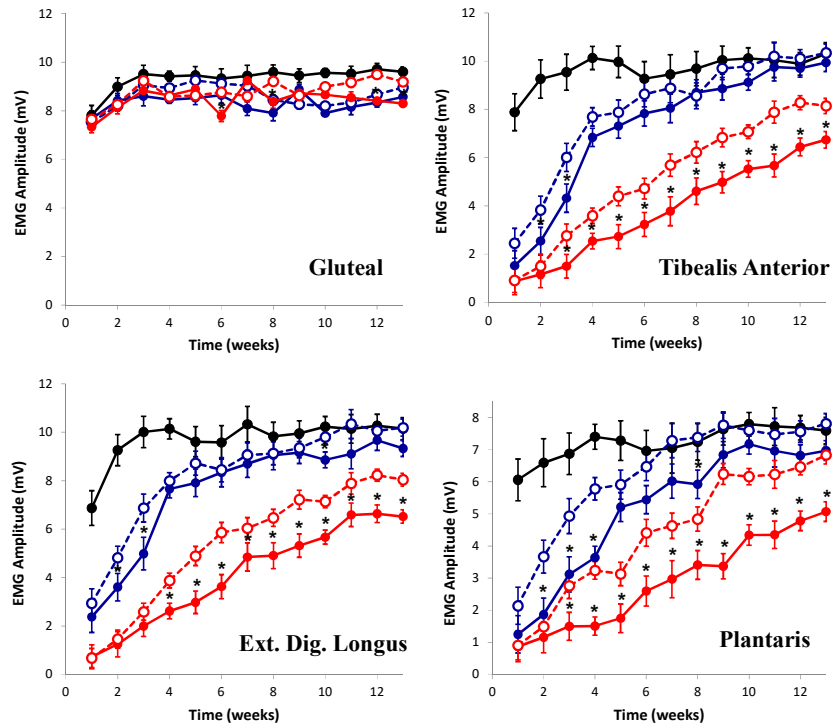


Figure 7-12. Accelerated functional recovery resulting from brief electrical stimulation. Maximum amplitude of electromyograms (EMGs) evoked in gluteal (G), extensor digitorum longus (EDL), tibialis anterior (TA), and gastrocnemius muscles (GS) upon electrical activation of uninjured, crushed, and transected sciatic nerve both in the presence and absence of brief electrical stimulation via implanted wireless nerve stimulator. Mean values and standard deviations are shown. * denotes $p < 0.05$ versus time-matched injury model without brief electrical stimulation.

EMG responses in musculature proximal to the site of nerve injury were minimally affected (GM/Crush: 7.67 ± 0.33 mV, GM/Cut: 7.34 ± 0.25 mV). Evoked EMG responses in musculature following sham surgery similarly demonstrated a transient, sub-acute reduction in EMG amplitude immediately following surgery (GM/Sham: 7.81 ± 0.41 mV, TA/Sham: 7.88 ± 0.76 mV, GS/Sham: 6.87 ± 0.71 mV, PL/Sham: 6.06 ± 0.65 mV). Reduction in EMG amplitude following sham surgery was observed to resolve within 2 weeks of surgery.

Serial activation of peripheral nerve tissue further elucidated varying time courses of functional motor recovery following nerve injury with and without therapeutic electrical stimulation. EMG responses in musculature proximal to the site of nerve injury demonstrated consistent EMG amplitude similar to those observed following sham surgery (GM/Sham: 9.33 ± 0.49 mV, GM/Crush: 8.32 ± 0.35 mV, GM/Crush+Stim: 8.62 ± 0.50 mV, GM/Cut: 8.45 ± 0.49 mV, GM/Cut+Stim: 8.80 ± 0.49 mV). EMG recordings in GM muscle demonstrated preservation of 82.5% - 98.2% of native function throughout the study irrespective of nerve injury or therapeutic modality. EMG recordings in proximal musculature demonstrate a negligible effect of brief electrical stimulation on healthy muscle tissue unaffected by nerve injury. EMG recording in proximal musculature further confirms the ability of implanted wireless stimulators to maximally recruit innervated musculature throughout the duration of the study.

Serial EMG measurement in musculature distal to the site of nerve crush injury demonstrated progressive recovery of function over 6 week post-operatively in the absence of brief electrical stimulation. EMG recordings in TA and GS muscles demonstrated recovery of 67.5% and 75.5% of native function at 4 weeks post-

operatively, while PL muscles demonstrated recovery of only 49.2% of native function at 4 weeks post-operatively. Serial EMG measurement facilitated by implanted wireless stimulators demonstrated a reduced rate of functional recovery in the distal PL muscle compared to the more proximal TA and GS muscles. At the terminal timepoint, TA, GS, and PL muscles all demonstrated near-complete recovery of motor function, regaining 96.4%, 91.9%, and 91.8% of native function, respectively.

In the presence of brief electrical stimulation, EMG responses in musculature distal to the site of nerve crush injury were significantly increased at 2-4 weeks post-operatively. EMG responses in TA and GS muscles were significantly greater at 2 and 3 weeks post-operatively in the presence of therapeutic electrical stimulation than in the absence of electrical stimulation (TA/Crush: 4.32 ± 0.66 mV, TA/Crush+Stim: 6.01 ± 0.59 mV, GS/Crush: 4.99 ± 0.67 mV, GS/Crush+Stim: 6.87 ± 0.58 mV). EMG responses in PL muscles were significantly greater at 2, 3, and 4 weeks post-operatively in the presence of therapeutic electrical stimulation (PL/Crush: 3.64 ± 0.34 mV, PL/Crush+Stim: 5.78 ± 0.35 mV). EMG recordings in TA, GS, and PL muscles 4 weeks post-operatively demonstrated recovery of 75.9%, 78.8%, and 78.1% of native function in the presence of therapeutic electrical stimulation, and recovery of 67.5%, 75.5%, and 49.2% of native function in the absence of therapeutic electrical stimulation. At the terminal timepoint, TA, GS, and PL muscles all demonstrated near-complete recovery of motor function in both the presence and absence of therapeutic electrical stimulation.

Serial EMG measurement facilitated by implanted wireless stimulators highlighted comparatively lower rates of functional recovery following nerve transection injury. EMG responses in musculature distal to the site of nerve transection injury

demonstrated progressive, gradual recovery of function over 13 week post-operatively in the absence of brief electrical stimulation. EMG recordings in TA and GS muscles demonstrated recovery of 25.1% and 25.8% of native function at 4 weeks post-operatively, while PL muscles demonstrated recovery of only 20.4% of native function at 4 weeks post-operatively. TA, GS, and PL muscles all demonstrated persistent motor deficits at the terminal time point, recovering only 65.4%, 64.2%, and 66.8% of native function, respectively. Serial EMG measurement facilitated by implanted wireless stimulators further elucidated variable rates of functional recovery in independent muscle groups, highlighting the delay in functional recovery experienced by distal PL muscles as compared to more proximal

			Week			
TA and GS muscles.			1	4	8	13
Comparatively, EMG responses in musculature distal to the site of nerve transection and repair were significantly increased between 4-13 weeks post-operatively in the presence of brief electrical stimulation. EMG responses in TA and PL muscles were significantly greater between	GM	Crush	98.2%	89.8%	82.5%	89.3%
		Crush + Stim	96.5%	94.9%	88.1%	93.3%
		Transection	94.0%	91.6%	87.4%	86.5%
		Transection + Stim	98.0%	91.1%	96.0%	95.7%
	GS	Crush	34.6%	75.5%	92.1%	91.9%
		Crush + Stim	42.8%	78.8%	92.9%	100.4%
		Transection	10.6%	25.8%	49.9%	64.2%
		Transection + Stim	9.9%	38.3%	65.8%	79.2%
	TA	Crush	19.3%	67.5%	89.8%	96.4%
		Crush + Stim	31.1%	75.9%	88.3%	100.3%
		Transection	11.1%	25.1%	47.6%	65.4%
		Transection + Stim	11.5%	35.4%	64.2%	79.0%
	PL	Crush	20.6%	49.2%	81.8%	91.8%
		Crush + Stim	35.3%	78.1%	101.9%	102.9%
		Transection	14.4%	20.4%	47.1%	66.8%
		Transection + Stim	15.0%	43.8%	66.9%	90.0%

Table 7-1. Overview of functional recovery observed in gluteal (GM), gastrocnemius (GS), tibealis anterior (TA), and plantaris (PL) over varying period of post-operative recovery following nerve crush and nerve transection injuries in the presence and absence of brief electrical stimulation. Values and represented as percent recovery compared to sham surgery, as measured via maximal EMG amplitude measured at corresponding time points.

3 - 13 weeks post-operatively in the presence of therapeutic electrical stimulation than in the absence of electrical stimulation (TA/Cut: 1.5 ± 0.49 mV, TA/Cut +Stim: 2.77 ± 0.48 mV, PL/Cut: 1.5 ± 0.44 mV, PL/Cut +Stim: 2.76 ± 0.39 mV). EMG responses in GS muscles were significantly greater between 4 - 13 weeks post-operatively in the presence of therapeutic electrical stimulation (GS/Cut: 2.0 ± 0.43 mV, GS/Cut +Stim: 2.59 ± 0.35 mV). EMG recordings in TA, GS, and PL muscles 4 weeks post-operatively demonstrated recovery of 35.4%, 38.3%, and 43.8% of native function in the presence of therapeutic electrical stimulation, and recovery of 25.1%, 25.8%, and 20.4% of native function in the absence of therapeutic electrical stimulation. At the terminal time-point 13 weeks post-operatively, TA, GS, and PL muscles demonstrated recovery of 79.0%, 79.2%, and 90.0% of native function in the presence of therapeutic electrical stimulation, as compared to 65.4%, 64.2%, and 66.8% in the absence of therapeutic electrical stimulation.

The present study demonstrates successful utilization of a minimally invasive wireless nerve stimulator to deliver therapeutic electrical stimulation to injured nerve tissue as a means of accelerating functional recovery. Thin-film implantable nerve stimulators were utilized to deliver brief electrical stimulation to peripheral nerve tissue following nerve crush and nerve transection injuries. Wireless nerve stimulators were then subsequently utilized to facilitate serial assessment of neuromuscular function post-operatively in individual animals. Therapeutic electrical stimulation following nerve crush and nerve transection injury was shown to accelerate functional recovery in multiple muscles below the level of injury, and improve terminal motor recovery following nerve transection / repair. These results further suggest that brief electrical

stimulation provided by macro-sieve electrodes may provide a unique non-biologic adjunct capable of accelerating axonal regeneration through implanted constructs. Given the similarities between nerve transection/repair and implantation of macro-sieve electrodes, this data suggests that brief electrical stimulation may be directly effective following sieve implantation. Furthermore, stimulus amplitudes required for brief electrical stimulation are readily reproducible via macro-sieve electrodes and therefore may be simply applied or deliver via existing interfacing strategies. Together, these results suggest that the therapeutic electrical stimulation offers a unique and effective method of accelerating functional nerve regeneration following nerve transection and may be uniquely applied via implanted macro-sieve electrodes to accelerating axonal regeneration and neural integration in vivo.

Chapter 8: Discussion

8-1: Conclusions

The present work illustrates a comprehensive investigation into the use of regenerative sieve electrodes as a means of electrically interfacing peripheral nerve tissue for the purpose of achieving muscle activation and motor control. Results of the present study demonstrate successful *in vivo* application and chronic implantation of custom regenerative electrodes possessing unique design features and via hole geometries distinct from prior devices. Observation of numerous myelinated axons within micro-sieve and macro-sieve sieve electrode assemblies confirm successful axonal regeneration through implanted electrodes and provide a histological basis for positive functional nerve regeneration and selective neural interfacing. Electrophysiological assessment of regenerative nerve tissue confirms functional nerve regeneration through both implanted micro- and macro-sieve electrodes. Sieve electrodes implanted in rat sciatic nerve further demonstrate the capability of selectively recruiting motor axons innervating multiple motor targets and evoking graded force output in distal musculature through modulation of stimulus amplitude, stimulus polarity, and the location of activated electrode sites. Together this work confirms that regenerative sieve electrodes are capable of both achieving a stable interface with peripheral nerve tissue and controlling force output in distal reinnervated musculature. This finding yields increasing credibility to the use of sieve electrodes as a means of achieving a chronic interface with peripheral nerve tissue in future neuroprosthetic systems.

The present work further elucidates the critical importance of sieve electrode design and geometry on neural integration and terminal nerve interfacing. Electrophysiological studies confirm that low-transparency sieve electrode geometries innately inhibit axonal regeneration and functional recovery when implanted into peripheral nerve tissue (Navarro et al; 1998). Data presented suggests that the primary cause of this inhibition is physical impedance of regenerating axons due to the use of small diameter via holes in fabricated micro-sieve electrodes (Wallman et al; 2001). Interestingly, contemporary studies have largely assumed that sacrificing total regenerative capacity to achieve ultra-high selectivity during neural interfacing is a reasonable trade-off. Yet, present electrophysiological studies demonstrate a direct correlation between successful axonal regeneration and successful electrical interfacing of distal musculature. Therefore, divergence from porous region geometries employed in early generations of regenerative electrodes may improve the capability of future devices to selectively stimulate or bi-directionally interface regenerative nerve tissue.

Along those lines, the present work provides an initial demonstration of the utility of high-transparency macro-sieve electrodes containing a novel porous region geometry. Macro-sieve electrodes were observed to support robust axonal regeneration and superior functional recovery compared to prior micro-sieve electrodes. The improved regenerative capacity of the device was largely attributed to the low-transparency, radial design of the porous region. Macro-sieve electrodes were further shown to facilitate a reliable, intimate electrical interface with regenerated nerve fibers, evidenced by initiation of muscle activation at lower stimulus amplitudes compared to epineurial electrodes. The present study additionally demonstrates that macro-sieve electrodes

facilitate selective, functional electrical stimulation of regenerated motor axons and distal musculature. Selective monopolar activation of electrode sites on implanted devices provided a successful method of controlling graded force output in antagonistic muscle groups, suggesting that macro-sieve electrode may provide an effective means of controlling motor function in neuroprosthetic applications.

The present study also confirms that the interfacial capabilities offered by novel macro-sieve electrodes greatly surpass that of prior micro-sieve electrodes. Prior studies theorize that the formation of regenerative micro-fascicles was critical to achieving a selective interface with peripheral nerve tissue. Results of the present study directly refute this hypothesis, suggesting instead that the presence of micro-scale via holes may be prohibitive to optimal function of regenerative electrodes as an effective neural interfacing. The present study instead validated the hypothesis that high-transparency macro-sieve electrodes facilitate both robust axonal integration and selective electrical interfacing of distal musculature. This report specifically provides the first demonstration of functional electrical stimulation of distal muscle tissue via a chronically-implanted regenerative electrode.

The present work also provides first evidence that application of field steering via regenerative electrodes facilitates increasingly selective, functional electrical stimulation of regenerated motor axons and distal musculature. Results of the present study validate that regenerative sieve electrodes are capable of applying multipolar stimulation paradigms and field steering techniques as a means of improving selective electrical stimulation of regenerative nerve tissue *in vivo*. Multipolar stimulation additionally demonstrates superior ability to activate independent musculature and evoke graded force

output in antagonistic muscle groups compared to monopolar stimulation. Multipolar stimulation of individual electrodes evidenced more consistent selectivity of motor recruitment and higher mean selectivity indices across a larger number of electrode sites. The present study also confirms that the interfacial capabilities offered by novel macro-sieve under multipolar stimulation paradigm surpass those of existing peripheral nerve interface presently in clinical use. Future studies may therefore focus on the use of multipolar stimulation paradigms in future *in vivo* testing of chronically implanted macro-sieve electrodes.

Integration of neurotrophic support into the design of implanted sieve electrode assemblies demonstrated another unique departure from prior investigations. Despite a limited number of studies investigating the use of seeded Schwann cells to enhance axonal regeneration through sieve electrodes *in vitro* (Schlosshauer et al; 2001, Stieglitz et al; 2002), no study has examined the use of neuroregenerative features in enhancing axonal regeneration through sieve electrodes *in vivo*. Similar assessments of regenerative nerve tissue present in sieve electrode assemblies containing delivery system demonstrate that controlled delivery of NGF and GDNF increases functional nerve regeneration across implanted substrates, the quantity, quality, and maturity of nerve fibers at the sieve electrode interface. Interestingly, the present study confirms that the use of neurotrophic factors is most critical in instances where the implanted electrode geometry challenges axonal regeneration. While the present study did not identify a significant difference in motor axon regeneration upon controlled delivery of GDNF vs NGF, results suggest that bulk neuroregenerative support enhances nerve regeneration through imposed artificial constructs. Results of the present study also greatly corroborate the results of prior

studies investigating the use of NGF-loaded delivery system to enhance peripheral nerve regeneration in silicone nerve guidance conduits (Lee et al; 2003). Success of fibrin-based delivery systems in promoting robust nerve regeneration through implanted sieve electrodes further advocates the investigation of such neuroregenerative systems in future implantable peripheral nerve interface technologies.

The present dissertation largely concludes that regenerative sieve electrodes present a unique and effective means of facilitating a stable and selective interface to peripheral motor axons for the purpose of restoring motor control. Based on this finding future studies should focus on the use of regenerative electrodes in a wider variety of clinical applications. The majority of investigations to date have focused on interfacing sensory fibers, and occasionally motor fibers within rat sciatic nerve. Despite one report of the use of sieve microelectrodes in interface rat vagus nerve (Kawada et al; 2004), use of peripheral nerve interfacing technology to selectively record and stimulate nerve fibers within autonomic and cranial nerves has been relatively unexplored. Diversification of *in vivo* models utilized in future studies will assist in enhancing the design and *in vivo* application of this unique neural interface. Furthermore, commonalities in neuronal structure between peripheral and central neurons may be eventually leveraged to achieve a high-specificity electrical interface to other neural targets (Heiduschka et al; 2001). Overall, increasing the anatomical and technological scope of future investigations will assist in elucidating the clinical utility of sieve microelectrode technologies.

8-2: Future Research

The present work suggests that porous region geometries facilitating selective stimulation of regenerated motor axons may be dramatically different than those designs facilitating high specificity recording of regenerated sensory axons. Specifically, prior studies suggest that smaller diameter via holes may selectively inhibit regeneration and support of motor axons, inducing the formation of microfascicles comprised largely of sensory nerve fibers (Negredo et al; 2004, Castro et al; 2008). While the mechanisms behind this phenomenon are not fully understood, there may be a relationship between observations of preferential motor regeneration in larger diameter intraneural tubes and observations of preferential motor regeneration in larger diameter via holes (Brushart et al; 1998). The ability to control the modality of regenerative nerve tissue contained in integrated via holes by adjusting via hole diameter may provide a unique method for selectively parsing and interfacing sensory and motor axons. Future studies may therefore specifically examine this concept through the use of sieve electrodes containing heterogeneous via holes and electrode sites. Application of computational models may further allow for quantitative optimization of sieve electrode geometries and design for independent clinical or anatomical applications.

Success of selective motor and sensory regeneration through heterogeneous via holes may further enable studies into simultaneous bidirectional interfacing of sensory and motor axons within regenerative nerve tissue. As the life expectancy of individuals affected by SCI continues to increase, neuroprosthetic technologies must continually adapt to maximally serve target patient populations. As a result, future studies may examine the ability of regenerative sieve electrodes to facilitate stable, long-lasting access

to both motor and sensory fiber population. Evaluation of the ability of sieve electrodes to simultaneously interface sensory and motor axons following chronic implantation serves a significant milestone in demonstrating superiority over existing neural interface technologies possessing limited longevity. Effective demonstration of the ability of regenerative sieve electrodes to selectively record and stimulate sensory nerve fibers may also open up novel clinical applications in the rehabilitation of individuals affected by limb loss or stroke.

Future studies may also investigate the implementation of regenerative sieve electrode as part of an advanced neuroprosthetic system employing brain computer interface technology. Neuroprosthetic technologies offer one of the most promising approaches to restoring native sensorimotor function following SCI (Ackery et al; 2004, Bradbury et al; 2006). Recent studies have demonstrated that microelectrode arrays placed on or in the primary motor cortex of quadriplegic subjects are capable of recording persistent, volitionally-modulated neural activity long after injury (Alexander et al; 2007). Additional studies have shown that through complex transformations, neural activity recorded from the primary motor cortex can be decoded to reliably predict motor intent, such as arm reaching trajectories, in paralyzed individuals (Moran et al; 1999, Wessberg et al; 2000, Wang et al; 2007, Heldman et al; 2006, Miller et al; 2007). Yet, despite significant advances in recording techniques, decoding algorithms, and kinematic models, few studies have focused on how best to utilize decoded cortical signals to restore motor function.

A superior rehabilitative strategy would utilize decoded cortical activity to directly re-establish motor control of a patient's own limb. Though generally unexplored,

one recent study utilized this strategy to restore motor function in transiently paralyzed macaque arms (Mortiz et al; 2008). Decoded cortical activity, acquired from single unit recordings in motor cortex, was utilized to control graded functional electrical stimulation of flexor and extensor muscles in the wrist, re-establishing volitional control of wrist movement following paralysis via nerve block. While demonstrating that cortical activity can directly control muscle activation, this study highlights the nascent stage of such neuroprostheses and the limitations associated with direct electrical stimulation of skeletal muscle. Future studies may examine the use of peripheral nerve interface technologies to control motor output origination from BCI systems. Specifically, regenerative sieve electrodes may offer an ideal platform to achieve stable, chronic interfacing of peripheral nerve tissue needed during functional electrical stimulation of distal musculature in the hand and forearm. Future studies may therefore provide a unique insight into the role of regenerative sieve electrodes in advanced neuroprosthetic systems designed to restore natural limb function.

References

Ackermann DA, et al., "Effect of Bipolar Cuff Electrode Design on Block Thresholds in High-Frequency Electrical Neural Conduction Block," IEEE Transactions on Neural Systems and Rehabilitation Engineering. 2009:17: 469-477.

Ackery A, et al. A global perspective on spinal cord injury epidemiology. J Neurotrauma 21:1355-1370, 2004.

Ahlborn P, et al. On hour electrical stimulation accelerates functional recovery after femoral nerve repair. Exp. Neurology. 2007; 137-144.

Akin T et al. A micromachined silicone sieve electrode for nerve regeneration applications. IEEE Trans. Biomed. Eng. 41: 305-13, 1994.

Alexander AL, et al. Diffusion tensor imaging of the brain. Neurotherapeutics 4:316-329, 2007.

Alkadhi H, et al. What disconnection tells about motor imagery: evidence from paraplegic patients. Cereb Cortex 15:131-140, 2005.

Al-Majed AA, et al. Brief electrical stimulation promotes the speed and accuracy of motor axonal regeneration. J. Neuroscience. 2000:20: 2602-2608.

Aydin MA et al. Force deficits in skeletal muscle after delayed reinnervation. Plast. Reconstr. Surg. 113: 1712-8, 2004.

Bain JR, et al. Functional evaluation of complete sciatic, peroneal, and posterior tibial nerve lesions in the rat. 1989:83:129-138.

Berthold CH, et al. "Axon diameter and myelin sheath thickness in nerve fibres of the ventral spinal root of the seventh lumbar nerve of the adult and developing cat.," Journal of Anatomy. 1981:136: 483-508.

Beuche W, et al., "A new approach toward analyzing peripheral nerve fiber populations. II. Foreshortening of regenerated internodes corresponds to reduced sheath thickness," Journal of Neuropathology and Experimental Neurology. 1985:41: 73-84.

Bhadra N, et al. "Simulation of high-frequency sinusoidal electrical block of mammalian myelinated axons," Journal of Computational Neuroscience. 2007:22: 313-326.

Boland RA, et al. Plasticity of lower limb motor axons after cervical cord injury. Clin. Neurophys. 120: 204-209, 2009.

Bradbury EJ, et al. Spinal cord repair strategies: Why do they work? Nat. Rev. Neuroscience. 7: 644-653, 2006.

- Bradley RM et al. Long term chronic recording from peripheral sensory fibers using a sieve electrode array. *J. Neurosci. Methods.* 73: 177-86, 1997.
- Branner A et al. Long-term stimulation and recording with a penetrating microelectrode array in cat sciatic nerve. *IEEE Trans. Biomed. Eng.* 51: 146-57, 2004.
- Branner A et al. Selective stimulation of cat sciatic nerve using an array of varying-length microelectrodes. *J. Neurophysiol.* 85: 1585-94, 2001.
- Brenner MJ, et al. Role of timing in assessment of nerve regeneration. *Microsurgery.* 2008;28: 265-272.
- Brindley GS, et al., "Sacral anterior root stimulators for bladder control in paraplegia: the first 50 cases,," *Journal of Neurology, Neurosurgery, and*
- Brown CJ, et al. Self-evaluation of walking track measurement using a Sciatic Function Index. *Microsurgery.* 1989;10:226-35.
- Brushart TM et al. Contributions of pathway and neuron to preferential motor reinnervation. *J. Neurosci.* 18: 8674-81, 1998.
- Brushart TM, et al. Electrical stimulation promotes motoneuron regeneration without increasing its speed or conditioning the neuron. *J. Neuroscience.* 2002;22: 6631-38.
- Brushart TM, et al. Electrical stimulation restores the specificity of sensory axon regeneration. *Exp. Neurology.* 2005: 194: 221-229.
- Campbell WW. Evaluation and management of peripheral nerve injury. *Clin. Neurophysiol.* 2008;119: 1951-65.
- Castro J et al. Fiber composition of the rat sciatic nerve and its modification during regeneration through a sieve electrode. *Brain Res.* 1190: 65-77, 2008.
- Chen MH et al. Gelatin-tricalcium phosphate membranes immobilized with NGF, BDNF, or IGF-1 for peripheral nerve repair: An in vitro and in vivo study. *J. Biomed. Mater. Res.* 79A: 846-57, 2006.
- Choi AQ, et al. "Selectivity of multiple-contact nerve cuff electrodes: a simulation analysis," *IEEE Transactions on Biomedical Engineering.* 2001;48: 165–172.
- Cole KS, et al. Electric impedance of the squid giant axon during activity. *J. Physiology.* 1939;22: 649-670.
- Coumans JV, et al. Axonal regeneration and functional recovery after complete spinal cord transection in rats by delayed treatment with transplants and neurotrophins. *J. Neuroscience.* 21: 9334-9344, 2001.

- Dagum AB. Peripheral nerve regeneration, repair, and grafting. *J. Hand Ther.* 1998;11: 111-7.
- Dahlin LB. Techniques of peripheral nerve repair. *Scand. J. Surgery.* 2008;97: 310-6.
- Dahlin LB. The role of timing in nerve reconstruction. *Int. Rev. Neurobiol.* 2013;109:151-64.
- De Medinaceli L, et al. An index of the functional condition of rat sciatic nerve based on measurement made from walking tracks. *Exp Neurol.* 1982;77:634-643.
- Della Santina CC et al. Multi-unit recording from regenerated bullfrog eighth nerve using implantable silicon-substrate microelectrodes. *J. Neurosci. Methods.* 72: 71-86, 1997.
- Dhillon GS, et al. Residual function in peripheral nerve stumps of amputees: Implications for neural control of artificial limbs. *J. Hand Surgery.* 29A: 605-615, 2004.
- Douglas Fields R, et al. "Axons regenerated through silicone tube splices: II. Functional morphology," *Experimental Neurology.* 1986;92: 61-74.
- Douglas R, et al. "Axons regenerated through silicone tube splices: I. Conduction properties," *Experimental Neurology.* 1986;52: 48-60.
- Enfors P et al. Expression of nerve growth factor receptor mRNA is developmentally regulated and increased after axotomy in rat spinal cord motoneurons. *Neuron.* 2: 1605-13, 1989.
- English AW, et al. Electrical stimulation promotes peripheral axon regeneration by enhanced neuronal neurotrophin signaling. *Dev. Neuroscience.* 2007;67:159-172.
- Evans GR. Peripheral nerve injury: a review and approach to tissue engineered constructs. *Anat. Rec.* 2001;263: 396-404.
- Evans PJ, et al. Regeneration across preserved peripheral nerve grafts. *Muscle Nerve.* 1995;18:1128-1138
- Evarts, et al. "Relation of Pyramidal Tract Activity to Force Exerted During Voluntary Movement", *Journal of Neurophysiology*, 1967: 31:14-27
- Fine EG et al. Nerve regeneration. In: *Principles of Tissue Engineering.* Langer R, Vacanti JP (Eds.) Academic Press, 2nd Ed., 2007.
- Fine EG et al. GDNF and NGF released by synthetic guidance channels support sciatic nerve regeneration across a long gap. *Eur. J. Neurosci.* 15: 589-601, 2002.
- Fox IK, et al. Experience with nerve allograft transplantation. *Semin. Plast. Surg.* 2007;21: 242-249.

- Friede RL, et al. "How are sheath dimensions affected by axon caliber and internode length?," *Brain Research*. 1982:235: 335-350.
- Friede RL. "Relation between myelin sheath thickness, internode geometry, and sheath resistance," *Experimental Neurology*. 1986:96: 234-247.
- Fu et al., "Neuronal Specification of Direction and Distance During Reaching Movements in the Superior Precentral Premotor Area and Primary Motor Cortex of Monkeys", *Journal of Neurophysiology*, 1993, 5:2097-2116.
- Gamble P, et al. Serial assessment of functional recovery following nerve injury utilizing implantable thin-film wireless nerve stimulators. (In Press)
- Gans C. Fiber architecture and muscle function. *Exer. Sport Sci. Rev.* 1982:10:160.
- Georgopoulos et al., "On the relations between the direction of two dimensional arm movements and cell discharge in primate motor cortex", *Journal of Neuroscience*, 1982,2:1527-1537.
- Geremia NM, et al. Electrical stimulation promotes sensory neuron regeneration and growth-associated gene expression. *Exp. Neurology*. 2007:205: 347-359.
- Gordon T, et al. Brief post-surgical electrical stimulation accelerates axon regeneration and muscle reinnervation with affecting the functional measures in carpal tunnel syndrome in patients. *Exp. Neurology*. 2010:223: 192-202.
- Gorman PH, et al. "The effect of stimulus parameters on the recruitment characteristics of direct nerve stimulation," *IEEE Transactions on Bio-Medical Engineering*. 1983:40: 407-414.
- Grill WM, et al. "Emerging clinical applications of electrical stimulation: Opportunities for restoration of function.," *Journal of Rehabilitation Research and Development* 38, 2001:6:641-653.
- Grill WM, et al. "Antidromic propagation of action potentials in branched axons: implications for the mechanisms of action of deep brain stimulation," *Journal of Computational Neuroscience*. 2008:24: 81-93.
- Grill WM, et al. "Inversion of the current-distance relationship by transient depolarization," *Biomedical Engineering, IEEE Transactions*. 1997:44: 1-9.
- Grill WM, et al. "The effect of stimulus pulse duration on selectivity of neural stimulation," *Biomedical Engineering, IEEE Transactions*. 1996:46: 161-166.
- Gunderson RW et al. The effects of conditioned media on spinal neuritis: Substrate-associated changes in neurite direction and adherence. *Dev. Biol.* 18: 104, 1984.

- Heiduschka P et al. Perforated microelectrode arrays implanted in the regenerating adult central nervous system. *Exp. Neurol.* 171: 1-10, 2001.
- Heldman DA et al. Local field potential spectral tuning in motor cortex during reaching. *IEEE Trans. Neu. Sys. Rehab. Eng.* 14: 180-3, 2006.
- Henderson CE et al. Neurotrophins promote motor neuron survival and are present in embryonic limb bud. *Nature.* 363: 266-70, 1993.
- Hildebrand C, et al., "Myelin sheath remodelling in regenerated rat sciatic nerve," *Brain Research* 1985:358: 163-170.
- Hille B. *Ion Channels of Excitable Membranes*, 3rd ed. (Sinauer Associates, 2001).
- Hochberg LR et al. Neuronal ensemble control of prosthetic devices by a human with tetraplegia. *Nature.* 442: 164-71, 2006.
- Hodgkin AL, et al. "A quantitative description of membrane current and its application to conduction and excitation in nerve," *The Journal of Physiology.* 1952:117: 500.
- Hodgkin AL, et al. Currents carried by sodium and potassium ions through the membrane of the giant axon of *Loligo*. *Journal of Physiology*, 116: 449-472.
- Houle JD et al. Regeneration of dorsal root axons is related to specific non-neuronal cells lining NGF-treated intraspinal nitrocellulose implants. *Exp. Neurol.* 118: 133-42, 1992.
- Hudson TW, et al. Engineering an improved acellular nerve graft via optimized chemical processing. *Tissue Eng.* 2004:10: 1346-1358.
- Hunter DA et al. Binary imaging analysis for comprehensive quantitative histomorphometry of peripheral nerve. *J. Neuro. Methods.* 166: 116-24, 2007.
- Jackson A, et al. Neural interfaces for the brain and spinal cord – restoring motor function. *Nat. Rev. Neurol.* 8: 690-699, 2012.
- Jesuraj NJ, et al. Schwann cells seeded in acellular nerve grafts improve functional recovery. *Muscle Nerve.* 2014: 49: 267-76.
- Jubran M et al. Repair of peripheral nerve transections with a fibrin sealant containing neurotrophic factors. *Exp. Neurol.* 181: 204-12, 2003.
- Kalliainen LK, et al. A specific force deficit exists in skeletal muscle after partial denervation. *Muscle Nerve.* 2002:25:31-8.
- Kawada T et al. A sieve electrode as a potential autonomic neural interface for bionic medicine. *IEEE-EMBS.* 6: 4318-21, 2004.
- Kilgore K, et al. "Nerve conduction block utilizing high-frequency alternating current," *Medical and Biological Engineering and Computing.* 2004:42: 394-406.

- Kilgore KL et al. A implanted upper-extremity neuroprosthesis using myoelectric control. *J. Hand Surg.* 33A: 539-50, 2008.
- Kim SP et al. Neural control of computer cursor velocity by decoding motor cortical spiking activity in humans with tetraplegia. *J. Neural Eng.* 5: 455-76, 2008.
- Kline DG. Physiological and clinical factors contributing to the timing of nerve repair. *Clin. Neurosurg.* 1977;24:425-55.
- Kline DG. Surgical repair of peripheral nerve injury. *Muscle Nerve.* 1990;13: 843-852.
- Klinge PM et al. Immunohistochemical characterization of axonal sprouting and reactive tissue changes after long-term implantation of a polyimide sieve electrode to the transected adult rat sciatic nerve. *Biomaterials.* 22: 2333-43, 2001.
- Kovacs GT et al. Silicon-substrate microelectrode array for parallel recording of neural activity in peripheral and cranial nerves. *IEEE Trans. Biomed. Eng.* 41: 567-77, 1994.
- Kovacs, GTA, et al. "Regeneration microelectrode array for peripheral nerve recording and stimulation," *Biomedical Engineering, IEEE Transactions.* 1992: 893-902.
- Lago N et al. Long term assessment of axonal regeneration through polyimide regenerative electrodes to interface the peripheral nerve. *Biomaterials.* 26: 2021-31, 2005.
- Lago N et al. Neurobiological assessment of regenerative electrodes for bidirectional interfacing injured peripheral nerves. *IEEE Trans. Biomed. Eng.* 54: 1129-37, 2007.
- Lawrence SM et al. Fabrication and characteristics of an implantable, polymer-based, intrafascicular electrode. *J. Neurosci. Methods.* 131: 9-26, 2003.
- Lee AC et al. Controlled release of nerve growth factor enhances sciatic nerve regeneration. *Exp. Neurol.* 184: 295-303, 2003.
- Lee JY, et al. Functional evaluation in the rat sciatic nerve defect model: A comparison of the sciatic functional index, ankle angles, and isometric tetanic force. *Plastic Reconstructive Surgery.* 2013;132; 1173-80.
- Leventhal DK et al. Chronic measurement of stimulation selectivity of the flat interface nerve electrode. *IEEE Trans. Biomed. Eng.* 51: 1649-58, 2004.
- Loeb GE et al. Cuff electrodes for chronic stimulation and recording of peripheral nerve. *J. Neurosci. Methods.* 64: 95-103, 1996.
- Loeb GE, et al. "Design and fabrication of hermetic microelectronic implants," in *Microtechnologies in Medicine and Biology, 1st Annual International, Conference On.* 2000, 2000, 455-459, 10.1109/MMB.2000.893825.

- MacDonnall D, et al. "Selective stimulation of cat sciatic nerve using an array of varying length microelectrodes". *J. Neurophysiol*, 85:1585-94, 2001
- MacEwan MR, et al. "Controlled delivery of nerve growth factor enhances sieve electrode interface with peripheral nerve tissue." *J Neural Eng*. [Manuscript submitted.]
- MacEwan MR, et al. "Selective stimulation of regenerated motor axons via macro-sieve electrodes." *J Neurosci*. [Manuscript submitted.]
- Mackinnon SE, et al. Clinical outcome following nerve allograft transplantation. *Plastic Recon. Surg.* 2001;107: 1419-1429.
- Malmivuo J, et al. *Bioelectromagnetism: principles and applications of bioelectric and biomagnetic fields* (Oxford University Press US, 1995).
- Martin JB. "The integration of neurology, psychiatry, and neuroscience in the 21st century". *The American journal of psychiatry* 159 (5): 695–704
- Maxwell DJ et al. Development of rationally designed affinity-based drug delivery systems. *Acta Biomaterialia*. 1: 101-13, 2005.
- McDonnall D et al. Interleaved, multisite electrical stimulation of cat sciatic nerve produces fatigue-resistant, ripple-free motor responses. *IEEE Trans. Neural. Sys. Rehabil. Eng.* 12: 208-15, 2004.
- McDonnall D et al. Selective motor unit recruitment via intrafascicular multielectrode stimulation. *Can. J. Physiol. Pharmacol.* 82: 599-609, 2004.
- McIntyre C, et al., "Selective Microstimulation of Central Nervous System Neurons," *Annals of Biomedical Engineering*. 2000;28: 219-233.
- McIntyre CC, et al., "Modeling the excitability of mammalian nerve fibers: influence of afterpotentials on the recovery cycle," *Journal of Neurophysiology*. 2002;87: 995.
- McIntyre CC, et al., "Sensitivity analysis of a model of mammalian neural membrane," *Biological Cybernetics*. 1998;79: 29-37.
- McNeal D, et al. "Selective activation of muscles using peripheral nerve electrodes," *Medical and Biological Engineering and Computing*. 1985;23: 249-253.
- Mendez J. Density and composition of mammalian muscle. *Metabolism*. 1960;9:184-8, 1960.
- Mensingher, et al., "Chronic recording of regenerating VIIIth nerve axons with a sieve electrode", *Journal of Neurophysiology*, 2000;83:611-615
- Metz S et al. Polyimide and SU-8 microfluidic devices manufactured by heat-polymerizable sacrificial material technique. *Lab Chip*. 4: 114-20, 2004.

- Miles JD, et al., "Effects of ramped amplitude waveforms on the onset response of high-frequency mammalian nerve block," *Journal of Neural Engineering*. 2007:4: 390-398.
- Miller KJ et al. Spectral changes in cortical surface potentials during motor movement. *J. Neurosci.* 27: 224-32, 2007.
- Miocinovic et al. "Sensitivity of temporal excitation properties to the neuronal element activated by extracellular stimulation," *Journal of Neuroscience Methods*. 2004:132: 91–99.
- Moore AM, et al. A transgenic rat expressing green fluorescent protein (GFP) in peripheral nerves provides a new hindlimb model for the study of nerve injury and regeneration. *J Neurosci Methods*. 2012:204: 19-27.
- Moore AM, et al. Acellular nerve allografts in peripheral nerve regeneration: a comparative study. *Muscle Nerve*. 2011:44: 221-34.
- Moran et al., "Motor Cortical Representation of Speed and Direction During Reaching", *Journal of Neurophysiology*, 1999, 82:2675-2692.
- Moritz CT et al. Direct control of paralyzed muscles by cortical neurons. *Nature*. 456: 639-42, 2008.
- Myckatyn TM, et al. A review of research endeavors to optimize peripheral nerve reconstruction. *Neurol Res*. 2004;26:124-138.
- Naples GG et al. Overview of peripheral nerve electrode design and implantation. In: *Neural Prostheses: Fundamental Studies, Biophysics, and Bioengineering Series*. Agnew WF, McCreery DB (Eds.) Prentice Hall, New Jersey, p107-44, 1990.
- Navarro X et al. A critical review of interfaces with the peripheral nervous system for the control of neuroprostheses and hybrid bionic systems. *J. Per. Nerv. Sys.* 10: 229-58, 2005.
- Navarro X et al. Stimulation and recording from regenerated peripheral nerves through polyimide sieve electrodes. *J. Peripheral Nerv. Sys.* 3: 91-101, 1998.
- Navarro X et al. Peripheral nerve regeneration through microelectrode arrays based on silicon technology. *Restor. Neurol. Neurosci.* 9: 151-60, 1996.
- Navarro X, et al. Neural plasticity after peripheral nerve injury and regeneration. *Progress in Neurobiology*. 2007:82:163-201.
- Navarro X, et al., "A critical review of interfaces with the peripheral nervous system for the control of neuroprostheses and hybrid bionic systems", *Journal of the Peripheral Nervous System*, 2005: 10:229-258

- Negredo P et al. Differential growth of axons from sensory and motor neurons through a regenerative electrode: A stereological, retrograde tracer, and functional study in the rat. *Neuroscience*. 128: 605-15, 2004.
- Nilsson I, et al. "Axon classes and internodal growth in the ventral spinal root L7 of adult and developing cats." *Journal of Anatomy*. 1988:156: 71-96.
- Noble J, et al. Analysis of upper and lower extremity peripheral nerve injuries in a population of patients with multiple injuries. *J Trauma*. 1998;45:116-122.
- Normann RA. Technology Insight: Future neuroprosthetic therapies for disorders of the nervous system. *Nat. Clin. Prac. Neurol*. 3: 444-52, 2007.
- Oppenheim RW et al. Glial cell line-derived neurotrophic factor and developing mammalian motoneurons: regulation of programmed cell death among motoneuron subtypes. *J. Neurosci*. 20: 5001-11, 2000.
- Otto D et al. Pharmacological effects of nerve growth factor and fibroblast growth factor applied to the transected sciatic nerve on neuron death in adult rat dorsal root ganglia. *Neurosci. Lett*. 83: 156-60, 1987.
- Panescu D. "Vagus nerve stimulation for the treatment of depression," *Engineering in Medicine and Biology Magazine, IEEE* 24, 2005:6: 68- 72
- Panetsos F et al. Neural Prostheses: Electrophysiological and histological evaluation of central nervous system alterations due to long-term implants of sieve electrodes in peripheral nerves in cats. *IEEE Trans. Neur. Sys. Rehab. Eng*. 16: 223-32, 2008.
- Peckham PH, et al. Challenges and opportunities in restoring function after paralysis. *IEEE Trans. Biomed. Engr*. 3:602-609, 2013.
- Ramachandran A, et al., "Design, in vitro and in vivo assessment of a multi-channel sieve electrode with integrated multiplexer," *Journal of Neural Engineering*. 2006:30: 114-124.
- Rattay, F et al. "Analysis of Models for External Stimulation of Axons," *Biomedical Engineering, IEEE Transactions on BME*. 1986:33: 974-977.
- Redondo-Castro E et al. Quantitative assessment of locomotion and interlimb coordination in rats after different spinal cord injuries. *J. Neurosci. Methods*. 213: 165-178, 2013.
- Richardson AG, et al.. "Modeling the effects of electric fields on nerve fibres: influence of the myelin sheath". *Med Biol Eng Comput*. 2000:38: 438-446.
- S. Y. Chiu et al., "A quantitative description of membrane currents in rabbit myelinated nerve." *The Journal of Physiology*. 1979:292: 149.

- Sakiyama-Elbert SE et al. Controlled release of nerve growth factor from a heparin-containing fibrin-based cell ingrowth matrix. *J. Control. Release.* 69: 149-58, 2000.
- Sakiyama-Elbert SE et al. Development of fibrin derivatives for controlled release of heparin-binding growth factors. *J. Control. Release.* 65: 389-402, 2000.
- Sakiyama-Elbert SE et al. Development of growth factor fusion proteins for cell-triggered drug delivery. *FASEB.* 15: 1300-2, 2001.
- Santos X et al. Regeneration of the motor component of the rat sciatic nerve with local administration of neurotrophic growth factor in silicone chambers. *J. Recon. Micro. Surg.* 15: 207-13, 1999.
- Schalk G, et al., "Brain-Computer Symbiosis", *Journal of Neural Engineering*, 2008:5:1-15
- Schalk G, et al., "Two-Dimensional Movement Control Using Electrographic Signals in Humans," *Journal of Neural Engineering* 5, 2008:1: 75-84.
- Schlosshauer B et al. Towards micro electrode implants: in vitro guidance of rat spinal cord neurites through polyimide sieves by Schwann cells. *Brain Res.* 903: 237-41, 2001.
- Schröder JM, et al. "Altered ratio between axon diameter and myelin sheath thickness in regenerated nerve fibers," *Brain Research.* 1972:45: 49-65.
- Schultz AE, et al. Neural interfaces for control of upper limb prostheses: the state of the art and future possibilities. *PM R.* 3: 55-67, 2011.
- Schwartz AB, et al., "Brain-Controlled Interfaces: Movement Restoration with Neural Prosthetics," *Neuron* 52, 2006: 205-220.
- Schwartz et al., "Primate Motor Cortex and Free Arm Movements to Visual Targets in Three-Dimensional Space. I. Relations Between Single Cell Discharge and Direction of Movement", *Journal of Neuroscience*, 1988,8:2913-2927.
- Schwarz JR, et al. "Action potentials and membrane currents in the human node of Ranvier," *Pflügers Archiv European Journal of Physiology.* 1995:195: 283-292.
- Slot PJ, et al. Effect of long term implanted nerve cuff electrodes on the electrophysiological properties of human sensory nerves. *Artif. Organs.* 21: 207-209, 1997.
- Stieglitz T et al. A biohybrid system to interface peripheral nerves after traumatic lesions: design of a high channel sieve electrodes. *Biosensors Bioelec.* 17: 685-96, 2002.
- Stieglitz T, et al. "A flexible, light-weight multichannel sieve electrode with integrated cables for interfacing regenerating peripheral nerves," *Sensors and Actuators A: Physical.* 1997:60: 240-243.

Sweeney JD, et al. "An asymmetric two electrode cuff for generation of unidirectionally propagated action potentials." *IEEE Trans Biomed Eng.* 1986;33: 541-9

Sweeney JD, et al., "Modeling of electric field effects on the excitability of myelinated motor nerve," in *Engineering in Medicine and Biology Society, 1989. Images of the Twenty-First Century., Proceedings of the Annual International Conference of the IEEE Engineering in, 1989, 1281-1282 vol.4, 10.1109/IEMBS.1989.96194.*

Swett JE, et al. Motoneurons of the rat sciatic nerve. *Exp. Neurology.* 1986;93: 227-252.

Taniuchi M et al. Induction of nerve growth factor receptor in Schwann cells after axotomy. *PNAS.* 83: 4094-8, 1986.

Taylor et al. "Functionally selective peripheral nerve stimulation with a flat interface nerve electrode", *IEEE Transactions on Neural systems and rehabilitation engineering,* 2002: 10:294-303.

Taylor SJ et al. Controlled release of neurotrophin-3 from fibrin gels for spinal cord injury. *J. Control. Release.* 98: 281-94, 2004.

Tyler DJ et al. A slowly penetrating interfascicular nerve electrode for selective activation of peripheral nerves. *IEEE Trans. Rehabil. Eng.* 5: 51-61, 1997.

Tyler DJ et al. Functionally selective peripheral nerve stimulation with a flat interface nerve electrode. *IEEE Trans. Neural Syst. Rehab. Eng.* 10: 294-303, 2002.

Tyler DJ et al. Interfascicular electrical stimulation for selectively activating axons. *IEEE-EMBS Mag.* 13: 575-83, 1994.

Tyler DJ, et al. "Chronic response of the rat sciatic nerve to the flat interface nerve electrode", *Annals of Biomedical Engineering,* 2003: 31:633-642

Ungar IJ, et al. "Generation of unidirectionally propagating action potentials using a monopolar electrode cuff", *Ann Biomed Eng.* 1986;14:437-50

Urbanek MG, et al. Specific force deficit in skeletal muscles of old rats is partially explained by the existence of denervated muscle fibers. *J. Gerontol. A Biol. Med. Sci.* 2001;56: B191-7.

Urbanek MS, et al. Rat walking tracks do not reflect maximal muscle force capacity. *J. Recon. Microsurg.* 1999;15:143-149.

Van den Honert C, et al. "A technique for collision block of peripheral nerve: single stimulus analysis" *IEEE Trans Biomed Eng.* 1981;28:373-8.

Van der Meulen JH et al. Denervated muscle fibers explain the deficit in specific force following reinnervation of the rat extensor digitorum longus muscle. *Plast. Reconstr. Surg.* 112: 1336-46, 2003.

- Varejo A, et al. Methods for the experimental functional assessment of rat sciatic nerve regeneration. *Neurol Res.* 2004;26: 186-194.
- Velliste M et al. Cortical control of a prosthetic arm for self-feeding. *Nature.* 453: 1098-101, 2008.
- Veraat C et al. Selective control of muscle activation with a multipolar nerve cuff electrode. *IEEE Trans. Biomed. Eng.* 40: 640-653, 2993.
- Wallman L, et al., "The geometric design of micromachined silicon sieve electrodes influences functional nerve regeneration," *Biomaterials.* 2001;22: 1187-1193.
- Wang CY et al. Regulation of neuromuscular synapse development by glial cell line-derived neurotrophic factor and neuturin. *J. Biol. Chem.* 277: 10614-25, 2002.
- Wang W et al. Motor cortical representation of position and velocity during reaching. *J. Neurophysiol.* 97: 4258-70, 2007.
- Warman EN, et al., "Modeling the effects of electric fields on nerve fibers: Determination of excitation thresholds," *Biomedical Engineering, IEEE Transactions.* 1992;39: 1244-1254.
- Warwick et al. The application of implant technology for cybernetic systems, *Archives of Neurology,* 2003: 60:1369:1373
- Wei XF, et al. Analysis of high-perimeter planar electrodes for efficient neural stimulation. *Front. Neuroengineering.* 2:15: 2009.
- Wessberg J et al. Real-time prediction of hand trajectory by ensembles of cortical neurons in primates. *Nature.* 408: 361-5, 2000.
- Willerth SM et al. Rationally designed peptides for controlled release of nerve growth factor from fibrin matrices. *J. Biomed. Mater. Res.* 80A: 12-23, 2007.
- Wolthers M et al. Comparative electrophysiological, functional, and histological studies of nerve lesions in rats. *Microsurg.* 25: 508-519, 2005.
- Wood MD et al. Affinity-based release of glial-derived neurotrophic factor from fibrin matrices enhances sciatic nerve regeneration. *Acta Biomaterialia.* Epublication ahead of print.
- Wood MD et al. Release rate controls biological activity of nerve growth factor released from fibrin matrices containing affinity-based delivery systems. *J. Biomed. Mater. Res.* 84: 300-12, 2008.
- Wood MD, et al. Fibrin matrices with affinity-based delivery systems and neurotrophic factors promote functional nerve regeneration. *Biotech. Biomat.* 2010: 106: 970-979.

Wood MD, et al. Outcome measures of peripheral nerve regeneration, *Annals of Anatomy*. 2011; 193: 321-333.

Xie J, et al. Nerve guidance conduits based on double-layered scaffolds of electrospun nanofibers for repairing the peripheral nervous system. *ACS Appl Mater Interfaces*. 2014;6: 9472-80.

Yan Y, et al. Evaluation of peripheral nerve regeneration via in vivo serial transcutaneous imaging using transgenic Thy1-YFP mice. *Experimental Neurology*. 2011;232:7-14.

Yoshida K, et al. "Selective stimulation of peripheral nerve fibers using dual intrafascicular electrodes," *Biomedical Engineering, IEEE Transactions*. 1993;40: 492-494.

Yoshimura K et al. The effect of reinnervation on force production and power output in skeletal muscle. *J. Surg. Res.* 81: 201-8, 1999.

Zellmer E, et al. Development of a high-power Class E oscillator for wireless power transmission in medical implants. (In Press)

Zhao Q, et al. Rat sciatic nerve regeneration through a micromachined silicon chip. *Biomaterials* 1997;18:75-80.

Curriculum Vitae

Program Director/Principal Investigator (Last, First, Middle): MacEwan, Matthew, Reagan

BIOGRAPHICAL SKETCH

Provide the following information for the Senior/key personnel and other significant contributors in the order listed on Form Page 2.
Follow this format for each person. **DO NOT EXCEED FOUR PAGES.**

NAME MacEwan, Matthew, Reagan eRA COMMONS USER NAME (credential, e.g., agency login) mmacewan	POSITION TITLE MD/PhD Candidate Department of Biomedical Engineering Washington University, St. Louis, MO		
EDUCATION/TRAINING <i>(Begin with baccalaureate or other initial professional education, such as nursing, include postdoctoral training and residency training if applicable.)</i>			
INSTITUTION AND LOCATION	DEGREE <i>(if applicable)</i>	MM/YY	FIELD OF STUDY
Case Western Reserve University (Cleveland, OH)	BS	5/04	Biomedical Engineering
Washington University in St. Louis (St. Louis, MO)	PhD*	5/15	Biomedical Engineering
Washington University School of Medicine, (St. Louis, MO)	MD*	5/17	Medicine

A. Positions and Honors

Positions and Employment

2013 – 2015 President / Founder, Acera Surgical, Inc.
 2010 – 2013 President / Founder, Retectix, LLC
 2006 – 2015 PhD Candidate, Department of Biomedical Engineering, Washington University, St. Louis, MO
 2004 – 2015 MD/PhD Candidate, Medical Scientist Training Program, Washington University School of Medicine, St. Louis, MO
 2003 – 2004 Research Associate, Department of Biomedical Engineering / Institute of Pathology, Case Western Reserve University, Cleveland, OH
 2001 – 2003 Research Associate, Department of Biomedical Engineering / Department of Macromolecular Science & Engineering, Case Western Reserve University, Cleveland, OH

Professional Memberships

2012 – Present American Association of Neurological Surgeons
 2004 – Present American Medical Student Association
 2010 – Present American Physician Scientist Association
 2012 – Present American Society of Peripheral Nerve
 2009 – Present Biomedical Engineering Society
 2013 – Present Congress of Neurological Surgeons
 2004 – Present Society for Biomaterials
 2009 – Present Society for Neuroscience
 2003 – Present Tau Beta Pi

Honors

2014 Hope Center Award
 2014 Emerging Growth Company - ADVAMED
 2012 PIPELINE Innovator, Kauffman Foundation
 2011 "40 Under 40", St. Louis Business Journal
 2011 Finalist - Purdue Lifescience Business Plan Competition
 2011 Finalist - St. Louis Regional Business Plan Competition
 2011 Grand Prize - Global LES Business Plan Competition
 2011 1st Place - Missouri/Illinois Regional I2P Competition
 2011 Winner – Washington University Olin Cup Competition
 2010 Best Presentation - Washington University Biomedical Engineering Research Symposium

Program Director/Principal Investigator (Last, First, Middle): MacEwan, Matthew, Reagan

2005 Student Research Award, Society for Biomaterials
2004 USA TODAY All-American College Academic Team
2004 Jose Ricardo Alcala Memorial Award
2003 Whitaker Foundation Research Fellowship
2003 Ronald Thrope and Michael Hollander Student Award
2003 Case Western Reserve University Alumni Scholarship
2003 Best Presentation, *BioOhio* Conference
2002 Ruhlin Scholarship
2000 Case Western Reserve University President's Scholarship

B. Peer-reviewed Publications

1. MacEwan MR, Zellmer E, Siewe DY, Wheeler JJ, Moran DW. "Selective stimulation of regenerated motor axons via macro-sieve electrodes." *J Neural Eng.* [Manuscript submitted.]
2. MacEwan MR, Wheeler JJ, Kim J, Williams JC, Sakiyama-Elbert SE, Moran DW. "Controlled delivery of nerve growth factor enhances sieve electrode interface with peripheral nerve tissue." *J Neural Eng.* [Manuscript submitted.]
3. MacEwan MR, Gamble P, Stephen M, Ray WZ. "Therapeutic Electrical Stimulation of Injured Peripheral Nerve Tissue Utilizing Implantable Thin-Film Wireless Nerve Stimulators." *J. Neurosurgery.* [Manuscript submitted.]
4. Gamble P, Stephen M, MacEwan MR, Ray WZ. "Serial Assessment of Functional Recovery Following Nerve Injury Utilizing Implantable Thin-Film Wireless Nerve Stimulators." *Muscle & Nerve.* [Manuscript submitted.]
5. MacEwan MR, Talcott MR, Moran DW, Leuthardt EC. "Novel osteogenic spinal instrumentation induces early posterior lumbar interbody fusion in goat model." *Spine.* [Manuscript submitted.]
6. MacEwan MR, Li W, Xie J, Ray WZ, Talcott MR, Xia Y. "Patterned nanofiber matrices as effective dural substitutes." *J. Neurosurg.* [Manuscript in preparation.]
7. MacEwan MR, Zellmer E, Wheeler JJ, Moran DW. "Dual layer macro sieve electrodes facilitate unidirectional action potential initiation in regenerated peripheral nerve." *J Neurophys.* [Manuscript in preparation.]
8. MacEwan MR, Zellmer E, Leuthardt E, Moran DW. "Osteogenic pedicle screws enable direct current electrical stimulation of the intervertebral disc space during lumbar spinal fusion." [Manuscript in preparation.]
9. Zellmer E, MacEwan MR, Moran DW. "Optimization of functional electrical stimulation of regenerated peripheral nerve tissue." *J Neural Eng.* [Manuscript in preparation.]
10. Xie J, MacEwan MR, Liu W, Jesuraj N, Li X, Hunter D, Xia Y. "Nerve guidance conduits based on double-layered scaffolds of electrospun nanofibers for repairing the peripheral nervous system." *ACS Applied Mat Interfaces.* 2014; 6(12): 9472-80.
11. Xie J, Liu W, MacEwan MR, Bridgman PC, Xia Y. "Neurite outgrowth on electrospun nanofibers with uniaxial alignment: the effects of fiber density, surface coating, and supporting substrate." *ACS Nano.* 2014; 8(2): 1878-85.
12. Laughner JI, Marrus SB, Zellmer ER, Weinheimer CJ, MacEwan MR, Cui SX, Nerbonne JM, Efimov IR. "A fully implantable pacemaker for the mouse: from battery to wireless power." *PLOS One.* 2013; 8(10): Epub ahead of print.
13. Jesuraj N, Santosa KB, MacEwan MR, Moore AM, Kasukurthi R, Ray WZ, Flagg ER, Hunter DA, Borschel GH, Johnson PJ, Mackinnon SE, Sakiyama-Elbert SE. "Schwann cells seeded in acellular nerve grafts improve functional recovery." *Muscle Nerve.* 2014; 49(2): 267-76.
14. Yan Y, MacEwan MR, Hunter DA, Faber S, Newton P, Tung TH, Mackinnon SE, Johnson PJ. "Nerve regeneration in rat limb allografts: evaluation of acute rejection rescue." *Plastic Reconstr Surgery.* 2013; 131(4): 499e-511e.
15. Choi SW, Zhang Yu, MacEwan MR, Xia Y. "Neovascularization in biodegradable inverse opal scaffolds with uniform and precisely controlled pore sized." *Adv Healthcare Mater.* 2012; 2(1): 145-54.

16. Santosa KB, Jesuraj NJ, Viader A, **MacEwan MR**, Newton P, Hunter DA, Mackinnon SE, Johnson PJ. "Nerve allografts supplemented with Schwann cells overexpressing GDNF." *Muscle Nerve*. 2013; 47(2): 213-23.
17. Cai X, Zhang Y, Li L, Choi SW, **MacEwan MR**, Yao J, Kim C, Xia Y, Wang LV. "Investigation of neovascularization in three-dimensional porous scaffolds in vivo by a combination of multiscale photoacoustic microscopy and optical coherence tomography." *Tissue Engr. Part C Methods*. 2013; 19(3): 196-204.
18. Ebersole GC, Buettman EG, **MacEwan MR**, Tang ME, Frisella MM, Matthews BD, Deeken CR. "Development of novel electrospun absorbable polycaprolactone scaffolds for hernia repair applications." *Surgical Endoscopy*. 2012; 26(10): 2717-2728.
19. Lin KF, Sun HH, **MacEwan MR**, Mackinnon SE, Johnson PJ. "GDNF overexpression fails to provoke muscle recovery from botulinum toxin poisoning: a preliminary study." *Microsurgery*. 2012; 32(5): 370-6.
20. Xie J, Michael PL, Zhong S, **MacEwan MR**, Tim CT. "Mussel inspired protein-mediated surface modification of electrospun nanofibers and their potential biomedical applications." *J. Biomaterial Research*. 2012 Apr;100(4):929-38
21. Smith AH, Segar CE, Nguyen PK, **MacEwan MR**, Efimov IR, Elbert DL. "Long term culture of HL-1 cardiomyocytes in modular poly(ethylene glycol) microsphere-based scaffolds crosslinked in the phase separated state." *Acta Biomaterialia*. 2012 Jan;8(1):31-40.
22. Xie J, Liu W, **MacEwan MR**, Yeh YC, Xia Y. "Nanofiber membranes with controllable microwells and structural cues and their use in forming cell microarrays and neuronal networks." *Small*. 2011 Feb 7;7(3):293-7
23. Moore AM, **MacEwan MR**, Santosa KB, Chenard K, Ray WZ, Hunter DA, Mackinnon SE, Johnson PJ. "Acellular nerve allografts in peripheral nerve regeneration: A comparative study." *Muscle & Nerve*. 2011 Aug;44(2):221-34.
24. **MacEwan MR**, Xie J, Li X, Liu W, Siewe DY, Ray WZ, Xia Y. "Radially aligned, electrospun nanofibers as dural substitutes for wound closure and tissue regeneration applications." *ACS Nano*. 2010 Sep 28;4(9):5027-36. [Cover article.]
25. Li X, **MacEwan MR**, Xie J, Siewe D, Yuan X, Xia Y. "Fabrication of Density Gradients of Biodegradable Polymer Microparticles and Their Use in Guiding Neurite Outgrowth." *Advanced Functional Materials*. 2010 May 25;20(10):1632-1637.
26. Kasukurthi R, **MacEwan MR**, Yan Y, Moore AM, Ray WZ, Santosa K, Mackinnon SE, Myckatyn TM. "Effects of neurturin on recovery from Botulinum toxin type A poisoning in mice." *J. Plastic Reconstructive Surgery*. [Manuscript submitted.]
27. **MacEwan MR**, Xie J, Jesuraj N, Siewe DY, Li X, Sakiyama-Elbert SE, Xia Y. "Schwann cell-seeded nanofiber scaffolds enhance the growth and guidance of regenerating neurites in vitro and in vivo." *Tissue Engineering*. [Manuscript accepted.]
28. Wood MD, **MacEwan MR**, French AR, Mackinnon SE, Moran DW, Borschel GH, Sakiyama-Elbert SE. "Fibrin matrices with affinity-based delivery systems and neurotrophic factors promote functional nerve regeneration." *Biotechnology and Bioengineering*. 2010 Aug 15;106(6):970-9.
29. Ray WZ, Magill CK, Moore AM, Yan Y, **MacEwan MR**, Yee A, Hayashi A, Hunter DA, Tong A, Johnson PJ, Parsadanian A, Mackinnon SE, Myckatyn TM. "The differential effect of centrally versus peripherally derived glial cell line-derived neurotrophic factor (GDNF) on peripheral nerve regeneration." *J. Neurosurgery*. 2010 Jul;113(1):102-9.
30. Xie J, **MacEwan MR**, Schwartz AG, Xia Y. "Electrospun nanofibers for neural tissue engineering." *Nanoscale*. 2009 Oct 27. 2010,2, 35-44.
31. Xie J, **MacEwan MR**, Li X, Sakiyama-Elbert SE, Xia Y. "Neurite Outgrowth on Nanofiber Scaffolds with Different Orders, Structures, and Surface Properties." *ACS Nano*. 2009 May 26;3(5):1151-9. [Cover article.]
32. Xie J, **MacEwan MR**, Willerth SM, Li X, Moran DW, Sakiyama-Elbert SE, Xia Y. "Conductive Core-Sheath Nanofibers and Their Potential Application in Neural Tissue Engineering." *Adv. Functional Materials*. 2009 July;19(14):2312-2318.

Program Director/Principal Investigator (Last, First, Middle): MacEwan, Matthew, Reagan

33. Xie J, Willerth SM, Li X, **MacEwan MR**, Rader A, Sakiyama-Elbert SE, Xia Y. "The differentiation of embryonic stem cells seeded on electrospun nanofibers into neural lineages." *Biomaterials*. 2009 Jan;30(3):354-62. Epub 2008 Oct 17.
34. **MacEwan MR**, Brodbeck WG, Matsuda T, Anderson JM. "Monocyte / lymphocyte interactions and the foreign body response: in vitro effects of biomaterial surface chemistry." *J Biomed Mater Res A*. 2005 Sep 1;74(3):285-93.
35. Brodbeck WG, **MacEwan M**, Colton E, Meyerson H, Anderson JM. "Lymphocytes and the foreign body response: lymphocyte enhancement of macrophage adhesion and fusion." *J Biomed Mater Res A*. 2005 Aug 1;74(2):222-9.
36. Shawgo RS, Voskerician G, Duc HL, Li Y, Lynn A, **MacEwan M**, Langer R, Anderson JM, Cima MJ. "Repeated in vivo electrochemical activation and the biological effects of microelectromechanical systems drug delivery device." *J Biomed Mater Res A*. 2004 Dec 15;71(4):559-68.
37. Wiggins MJ, **MacEwan M**, Anderson JM, Hiltner A. "Effect of Soft-Segment Chemistry on Polyurethane Biostability During In Vitro Fatigue." *J Biomed Mater Res A*. 2004 Mar 15;68(4):668-83.
38. Wiggins MJ, **MacEwan M**, Anderson JM, Hiltner A. "Effect of strain and strain rate on fatigue-accelerated biodegradation of polyurethane." *J Biomed Mater Res A*. 2003 Sep 1;66(3):463-75.

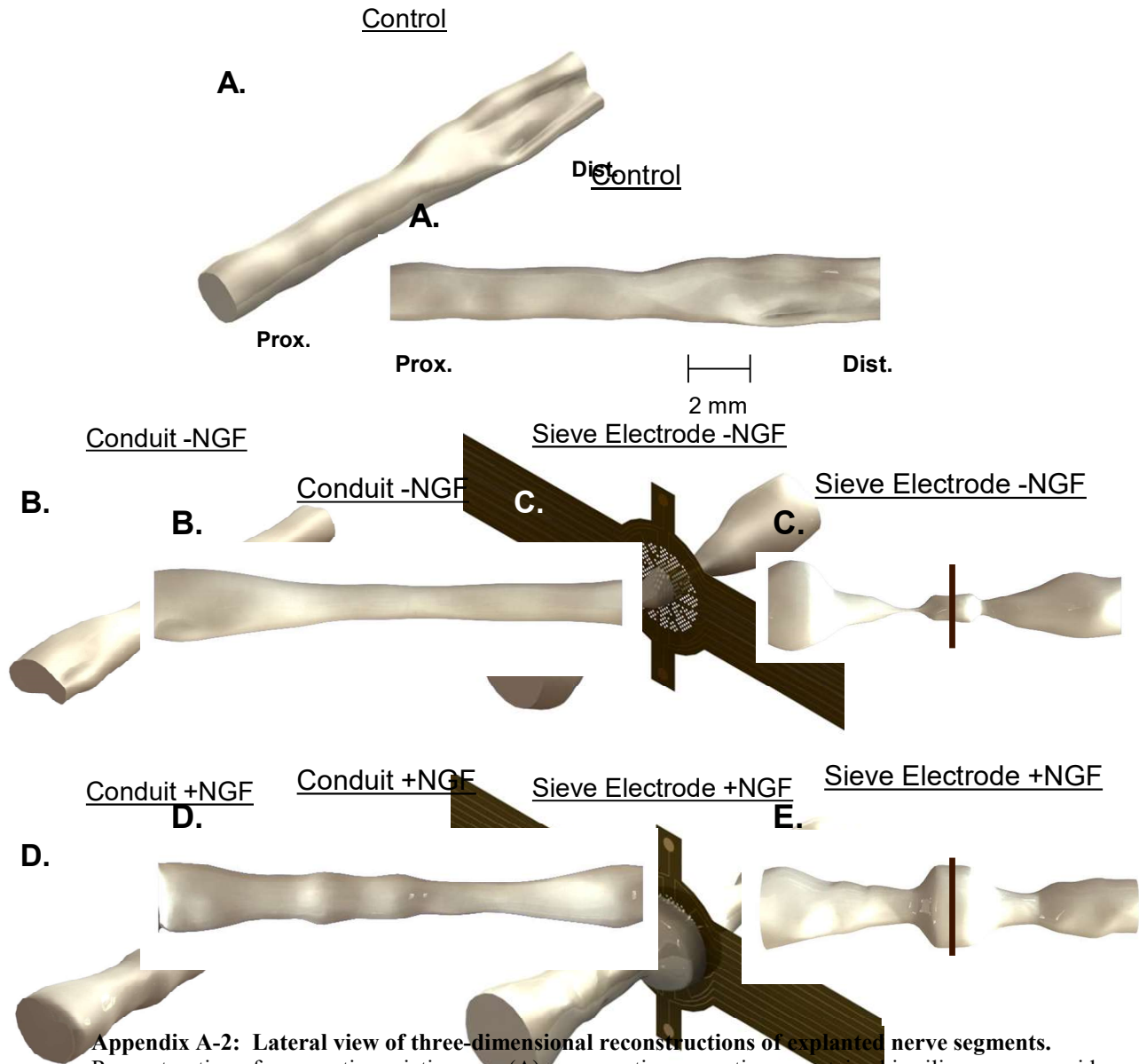
C. Completed Research Support

Washington University Fund for Translation Research 11/2008 – 11/2009
Bipolar Sieve Electrode Design and Implementation
The major goal of this project was to develop a novel, bipolar regenerative sieve electrode capable of providing stable, selective interfacing of peripheral nerve tissue for neuroprosthetic applications.
Role: Co-Investigator

Washington University Fund for Translation Research 1/2008 – 6/2009
Osteogenic Spinal Instrumentation
The major goal of this project was to develop a novel class of bone screw / orthopedic instrumentation capable of routing micro-electric stimulation to proximal bony tissue to improve local osteogenesis and improve hardware integration.
Role: Co-Investigator

McDonnell Center for Higher Brain Function 07/2005 – 07/2007
Selective Stimulation and Recording of Mammalian Peripheral Nerve Fibers Using Sieve Microelectrode Arrays
The major goal of this project was to develop regenerative sieve microelectrodes for use in chronic stimulation and recording of peripheral nerve tissue.

Appendix A: Regenerative Nerve Morphometry and Histology

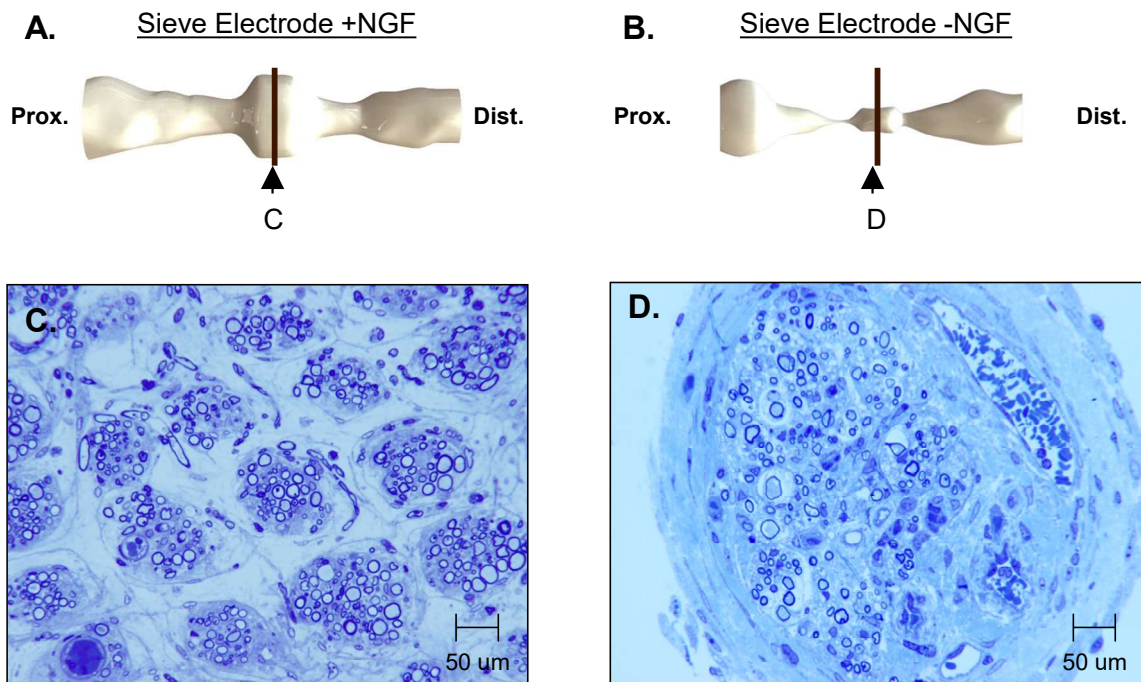


Appendix A-2: Lateral view of three-dimensional reconstructions of explanted nerve segments.

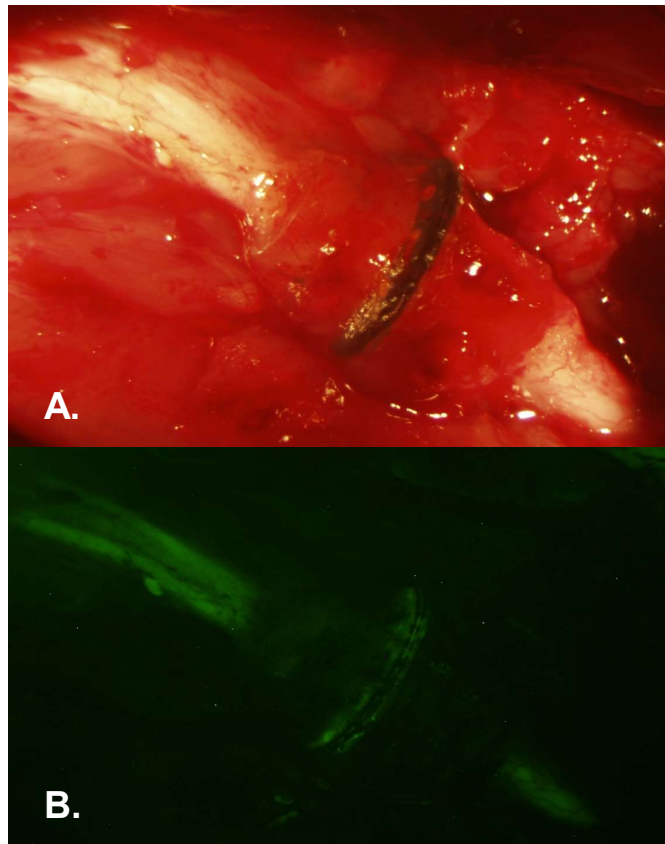
Reconstruction of unoperative sciatic nerve (A), regenerative nerve tissue contained in silicone nerve guidance conduits with (D) and without (B) the fibrin-based delivery system, and regenerative nerve tissue contained in sieve electrode assemblies with (E) and without (C) the fibrin-based delivery system. Representative reconstructions from each experimental group are shown in similar scale.

Appendix A-1: Trimetric view of three-dimensional reconstructions of explanted nerve segments.

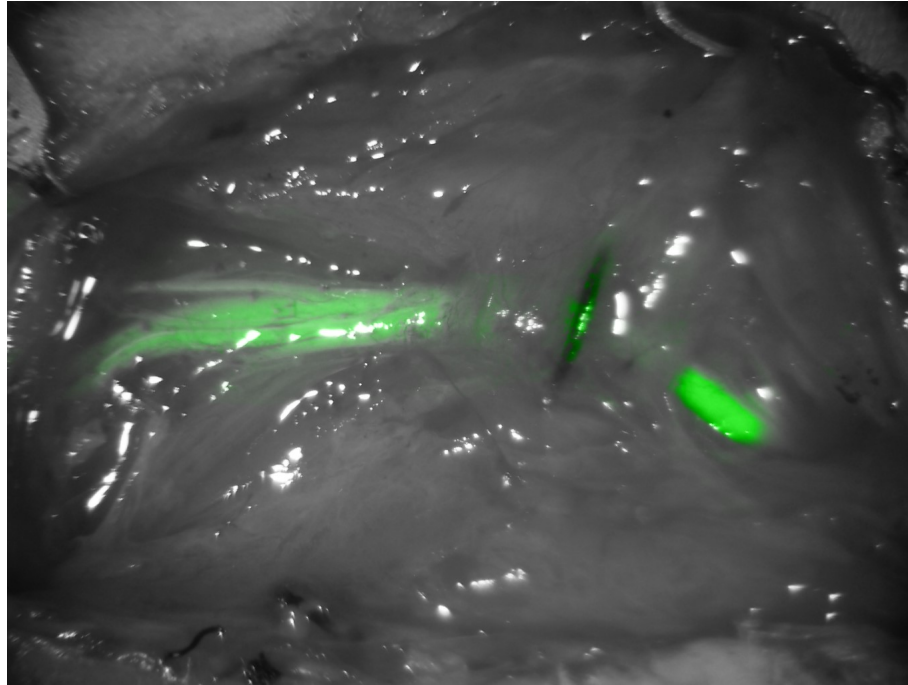
Reconstruction of unoperative sciatic nerve (A), regenerative nerve tissue contained in silicone nerve guidance conduits with (D) and without (B) the fibrin-based delivery system, and regenerative nerve tissue contained in sieve electrode assemblies with (E) and without (C) the fibrin-based delivery system. Representative reconstructions from each experimental group are shown in similar scale.



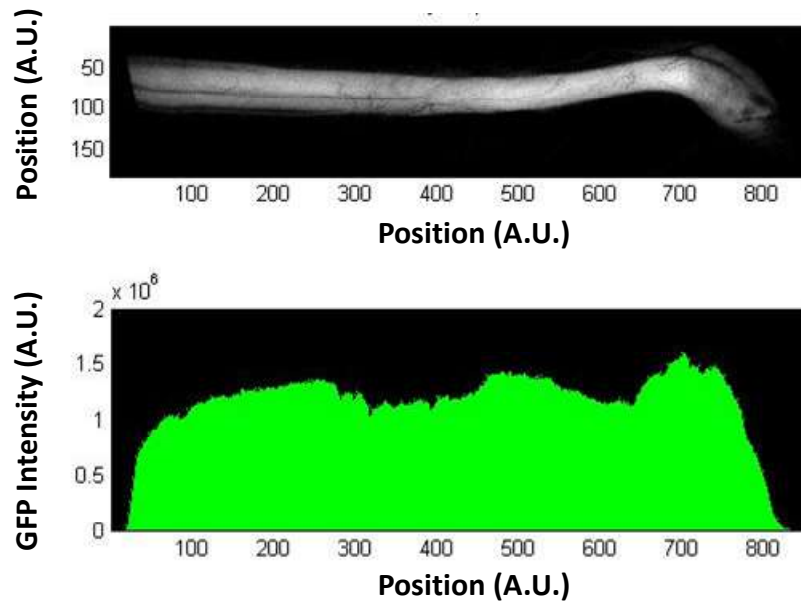
Appendix A-3: Histological epoxy sections of regenerative nerve tissue explanted from sieve electrode assemblies with and without fibrin-based delivery system loaded with NGF. Three-dimensional reconstruction of explanted nerve segments from sieve electrode assemblies with (A) and without (B) fibrin-based delivery system demonstrate the location of displayed sections. Sections taken at the sieve electrode interface demonstrate greater numbers of microfascicles and myelinated axons in the presence of the fibrin-based delivery system (C) than in the absence of the delivery system (D). Representative sections from each experimental group are shown in similar scale.



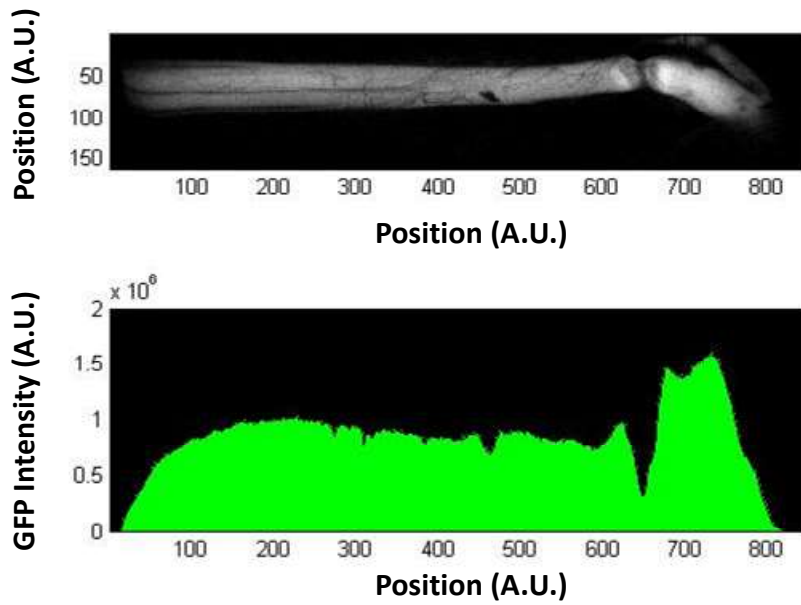
Appendix A-4: Implantation of macro-sieve electrode in transgenic Sprague Dawley rat expressing GFP in neural tissue. Terminal observation of macro-sieve electrode implanted in the sciatic nerve of a transgenic Sprague Dawley rat expressing green fluorescent protein (GFP) in neural tissue under the thyl promoter at 3 months post-operatively (A). Fluorescent micrograph demonstrating fluorescent neural tissue in the host sciatic nerve proximal (right) and distal (left) to the implanted macro-sieve electrode (B). Evidence of GFP-expressing axons in the sciatic nerve distal to the site of implantation confirm successful axonal regeneration through the implanted macro-sieve electrodes.



Appendix A-5: Implanted macro-sieve electrode in transgenic Sprague Dawley rat: Merged image. Terminal observation of macro-sieve electrode implanted in the sciatic nerve of a transgenic Sprague Dawley rat expressing green fluorescent protein (GFP) in neural tissue under the thyl1 promotor at 3 months post-operatively. Merged images of GFP-expression (green) and light micrograph (gray). Evidence of GFP-expressing axons in the sciatic nerve distal to the site of implantation confirm successful axonal regeneration through the implanted macro-sieve electrodes.



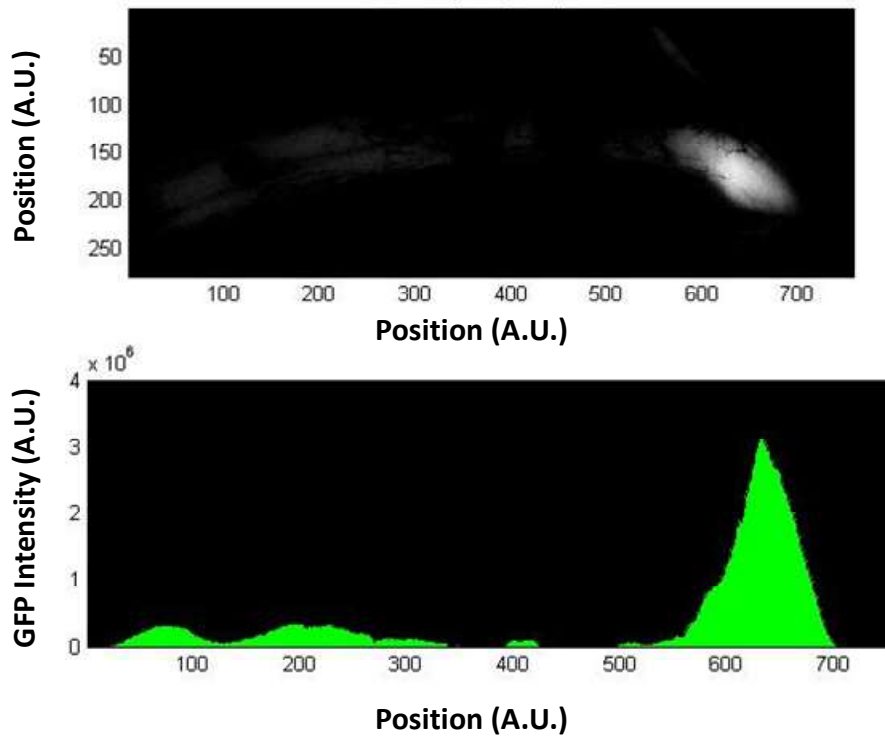
Appendix A-6: Quantification of GFP expression in pre-operative transgenic rodent nerve (Day 0): Fluorescent micrograph of unoperative (healthy) sciatic nerve in a transgenic Sprague Dawley rat expressing green fluorescent protein (GFP) in neural tissue under the *thyl* promoter (Top). Quantification of GFP expression in identical rat sciatic nerve as a function of position along the length of the nerve (Bottom). Consistent GFP expression throughout demonstrates the presence of numerous peripheral nerve fibers.



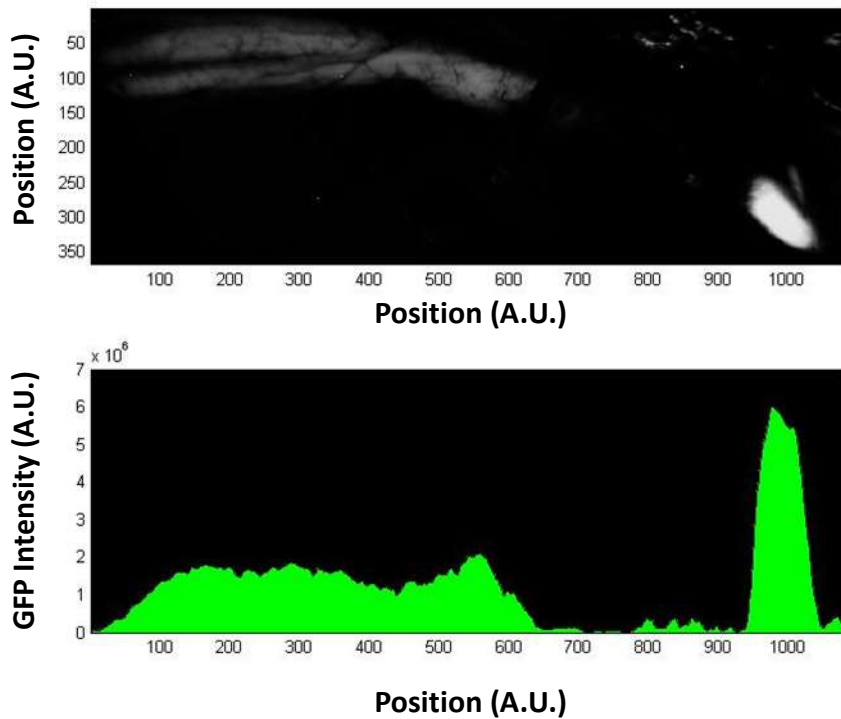
Appendix A-7: Quantification of GFP expression in crushed transgenic rodent nerve (Day 0):

Fluorescent micrograph of sciatic nerve immediately after nerve crush in a transgenic Sprague Dawley rat expressing green fluorescent protein (GFP) in neural tissue under the thy1 promoter (Top).

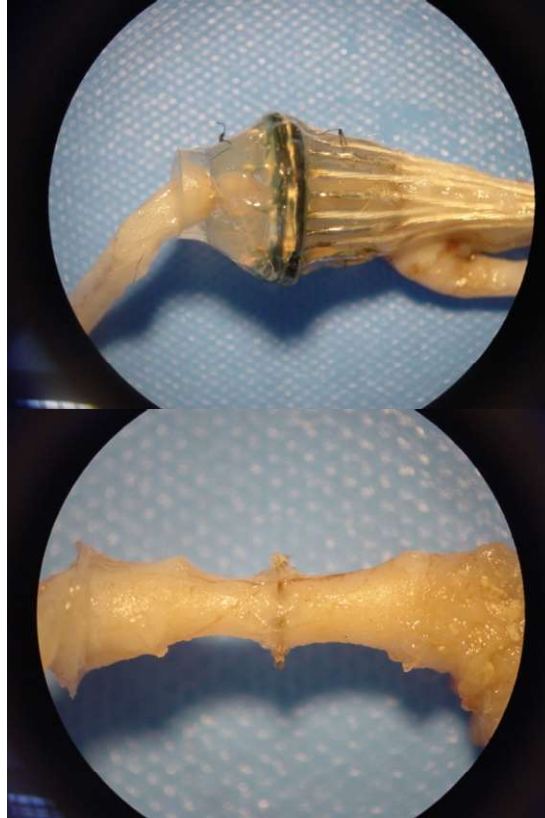
Quantification of GFP expression in identical rat sciatic nerve as a function of position along the length of the nerve (Bottom). Focal reduction in GFP express confirms the severity of axonal injury upon nerve crush.



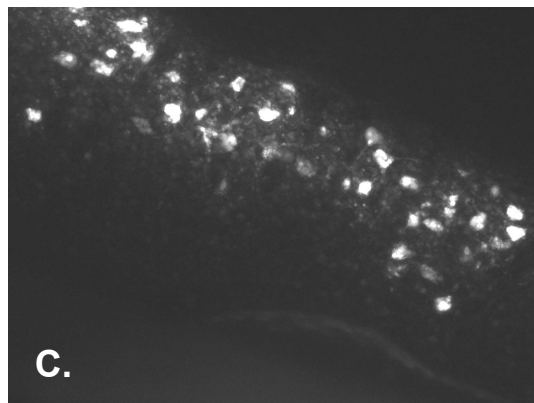
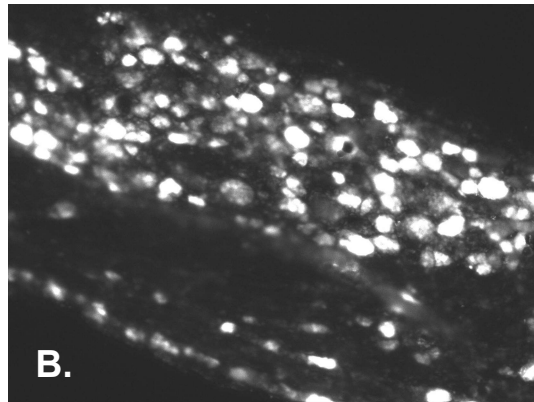
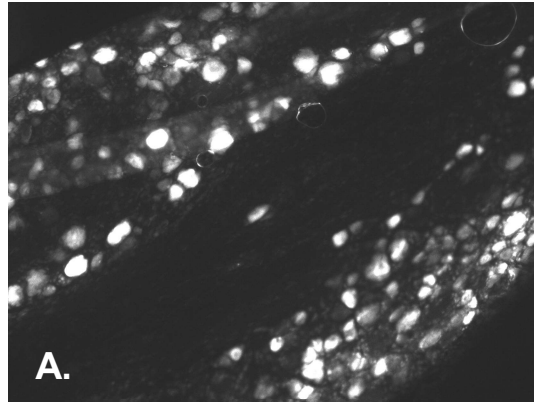
Appendix A-8: Quantification of GFP expression in transgenic rodent nerve (Day 14): Fluorescent micrograph of sciatic nerve 14 days after nerve crush in a transgenic Sprague Dawley rat expressing green fluorescent protein (GFP) in neural tissue under the thy1 promoter (Top). Quantification of GFP expression in identical rat sciatic nerve as a function of position along the length of the nerve (Bottom). Global reduction in GFP expression distal to the site of nerve crush injury confirms degradation of axons in the distal nerve.



Appendix A-9: Quantification of GFP expression in transgenic rodent nerve after sieve electrode implantation (6 wks): Fluorescent micrograph of sciatic nerve 6 weeks after nerve crush injury and macro-sieve implantation in a transgenic Sprague Dawley rat expressing green fluorescent protein (GFP) in neural tissue under the thy1 promoter (Top). Quantification of GFP expression in identical rat sciatic nerve as a function of position along the length of the nerve (Bottom). Notable GFP expression distal to the site of nerve crush injury and macro-sieve electrode implantation confirms regeneration of axons through implanted sieve electrode.

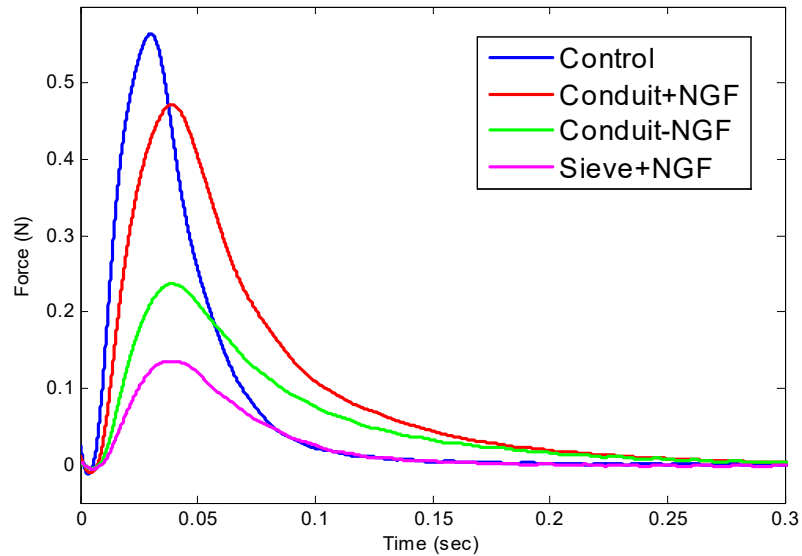


Appendix A-10: Dual-layer macro-sieve electrodes chronically implanted in rat sciatic nerve. Explanted dual-layer macro-sieve electrodes (top). Devices were implanted in the rodent nerve for 3 months post-operatively. Successful regeneration across the porous region of the device (bottom) confirm that dual-layer macro-sieve electrodes do not inhibit axonal regeneration compared to single-layer macro-sieve electrodes.

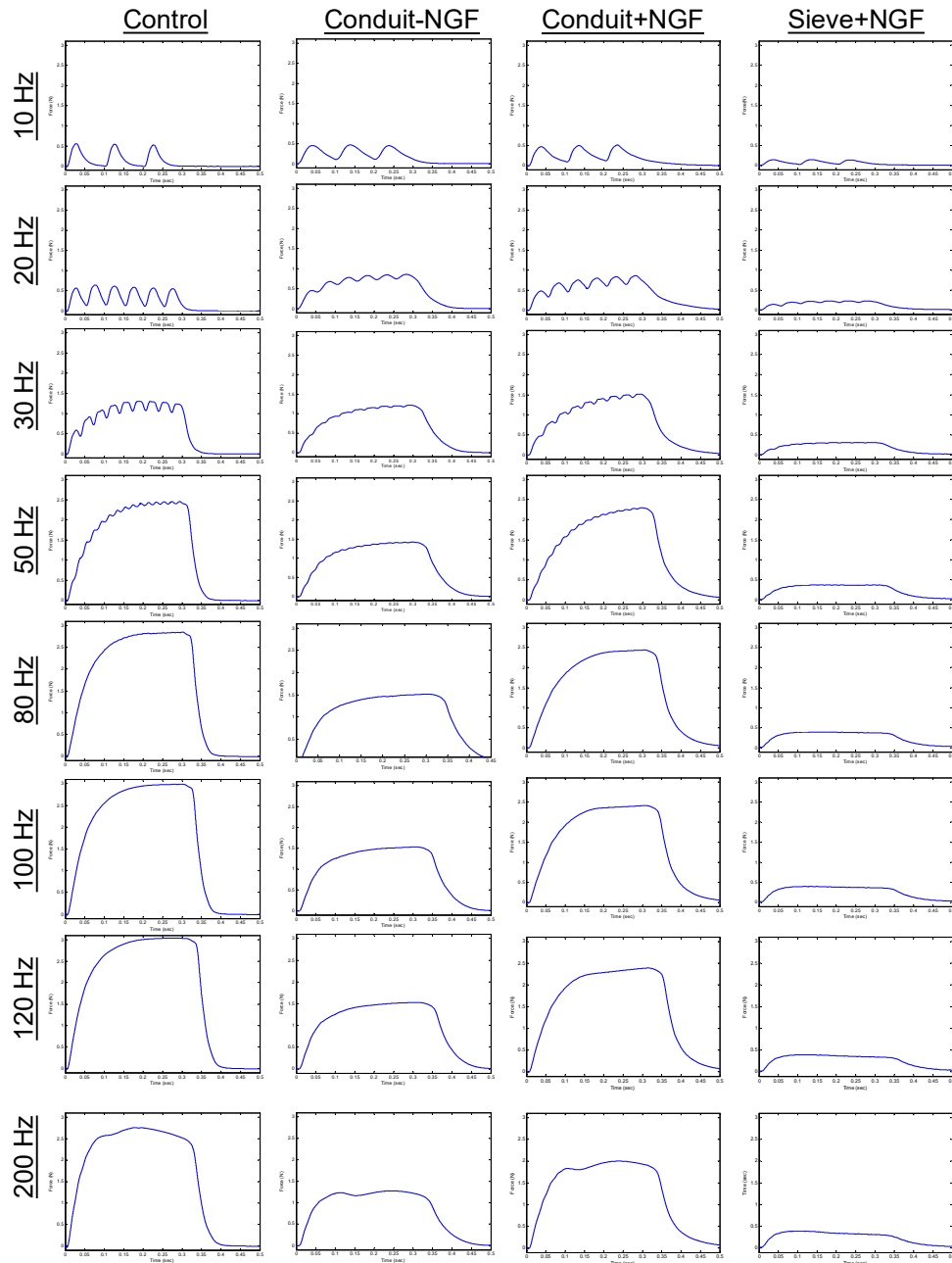


Appendix A-11: Retrograde labelled neurons in the dorsal root ganglia and ventral horn of the spinal cord following Fluorogold treatment of peripheral nerve tissue distal to implanted macro-sieve electrodes. Male Lewis rats underwent surgical implantation of macro-sieve electrodes into the sciatic nerve. At the terminal time point (3 mo), all animals underwent secondary nerve transection 10mm distal to the integrated macro-sieve electrode. The end of the proximal nerve stump was treated with 20ul of fluorogold solution for 1 hr. Animals were then recovered for seven days prior to perfusion and explantation of L4 DRG, L5 DRG, and the lumbar spinal cord. Sectioned tissues revealed positively labelled neuronal cell bodies both in the L4 DRG (A), L5 DRG (B), and ventral horn of the SC (C) confirming successful regeneration of both sensory and motor axons through implanted macro-sieve electrodes.

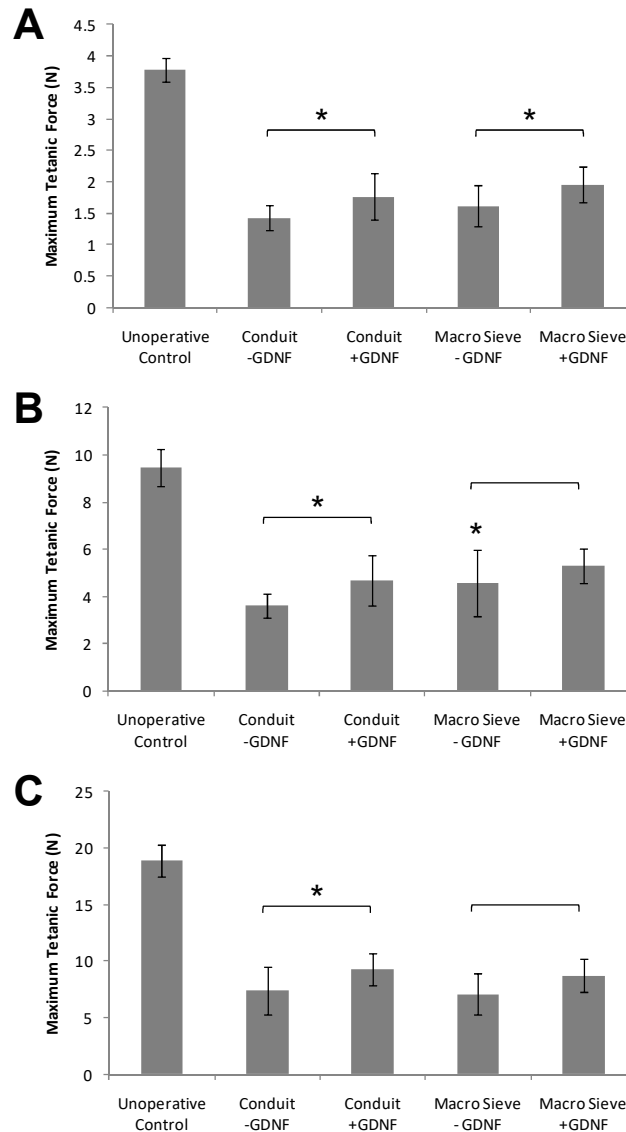
Appendix B: Evoked Muscle Force Measurement



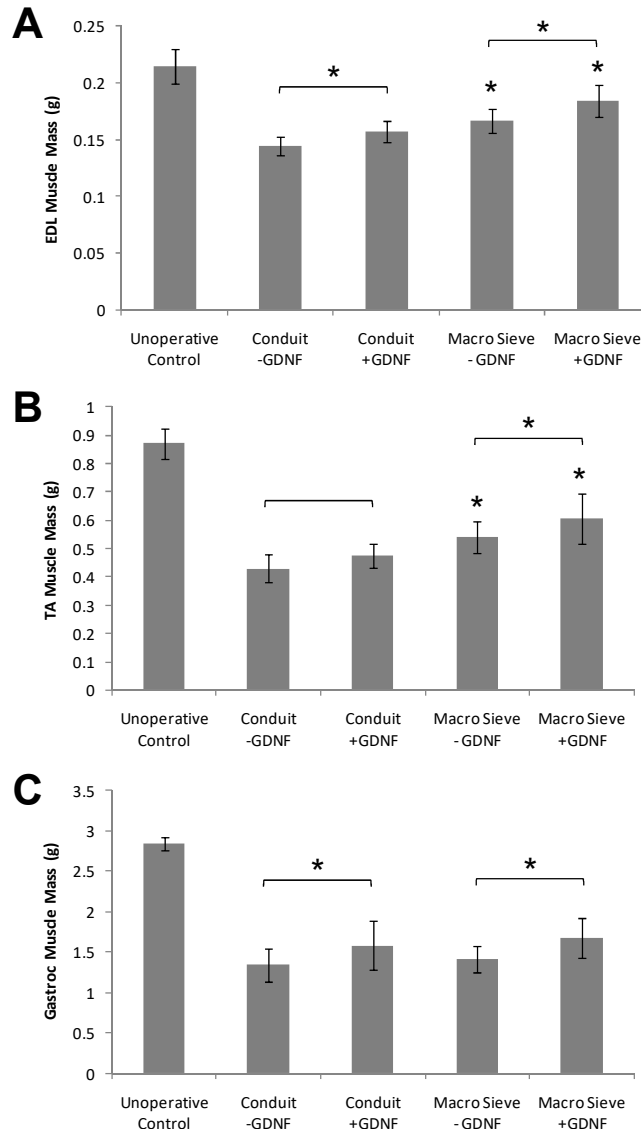
Appendix B-1: Maximum twitch response of reinnervated extensor digitorum longus (EDL) muscles upon stimulation of the sciatic nerve proximal to implanted devices using silver wire electrodes. Representative force recordings acquired from each experimental group are shown. No force recording is displayed for the experimental group employing sieve electrode assemblies without the fibrin-based delivery system as EDL muscles distal to the implanted device did not exhibit any functional recovery at the terminal time point.



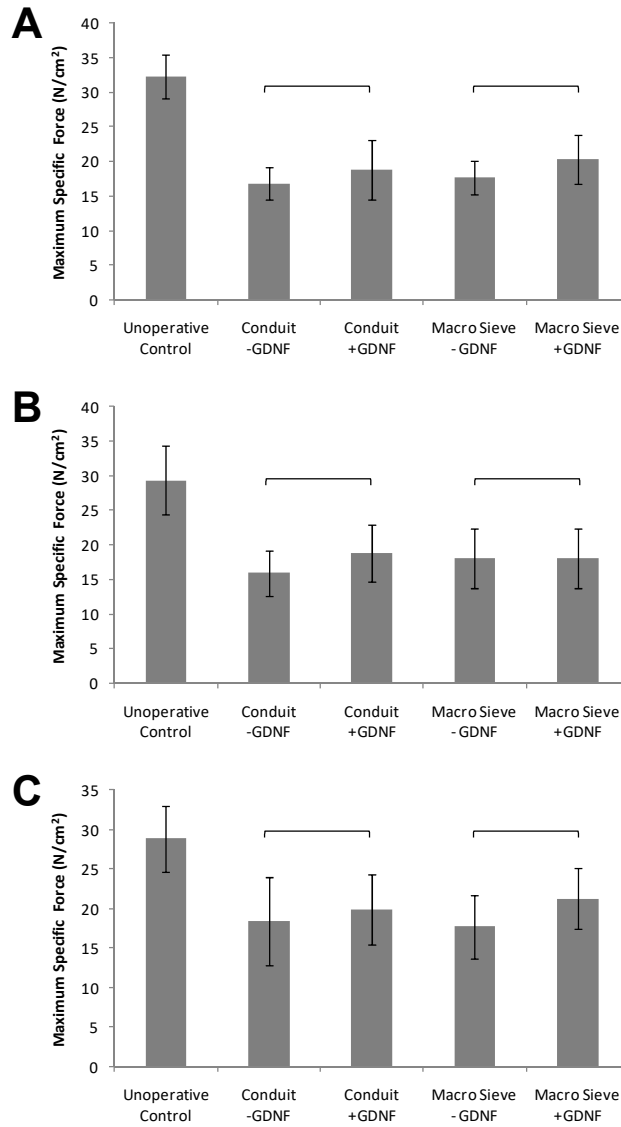
Appendix B-2. Maximum tetanic responses of reinnervated extensor digitorum longus (EDL) muscles upon variable frequency stimulation of the sciatic nerve proximal to implanted devices using silver wire electrodes. Representative force recordings acquired from each experimental group are shown. No force recordings are displayed for the experimental group employing sieve electrode assemblies without the fibrin-based delivery system as EDL muscles distal to the implanted device did not exhibit any functional recovery at the terminal time point.



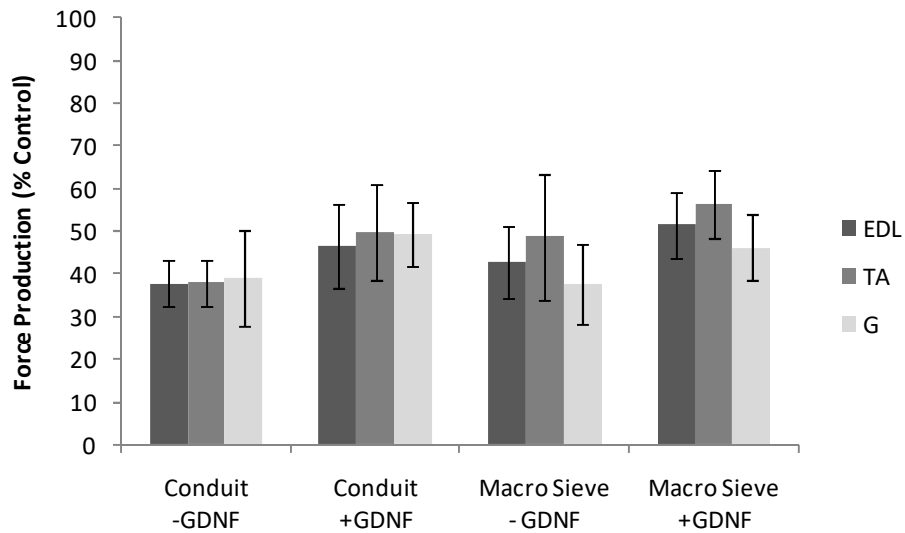
Appendix B-3. Maximum isometric force production in reinnervated muscle following implantation of macro-sieve electrodes. Maximum tetanic force evoked in EDL muscle (A), TA muscle (B), and G muscle (C) measured 3 month after implantation of macro-sieve electrodes and silicone guidance conduits with and without delivery system. Mean values and standard deviations are shown. * denotes $p < 0.05$ versus similar device with dissimilar presence/absence of fibrin-based delivery system loaded with GDNF. ** denotes $p < 0.05$ versus sieve electrode assembly with similar presence/absence of fibrin-based delivery system loaded with GDNF.



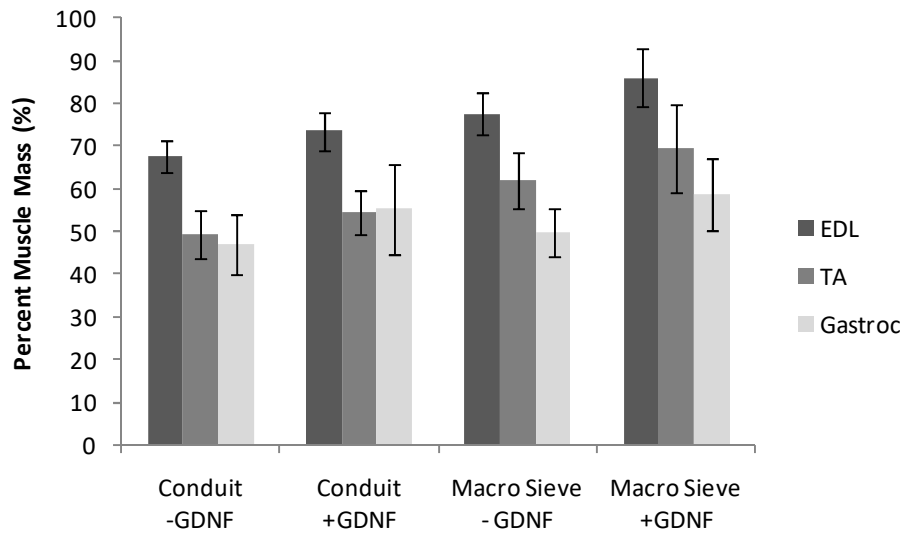
Appendix B-4. Muscle mass measurements in reinnervated muscle following implantation of macro-sieve electrodes. Wet muscle mass of EDL muscle (A), TA muscle (B), and G muscle (C) measured 3 month after implantation of macro-sieve electrodes and silicone guidance conduits with and without delivery system. Mean values and standard deviations are shown. * denotes $p < 0.05$ versus similar device with dissimilar presence/absence of fibrin-based delivery system loaded with GDNF. ** denotes $p < 0.05$ versus sieve electrode assembly with similar presence/absence of fibrin-based delivery system loaded with GDNF.



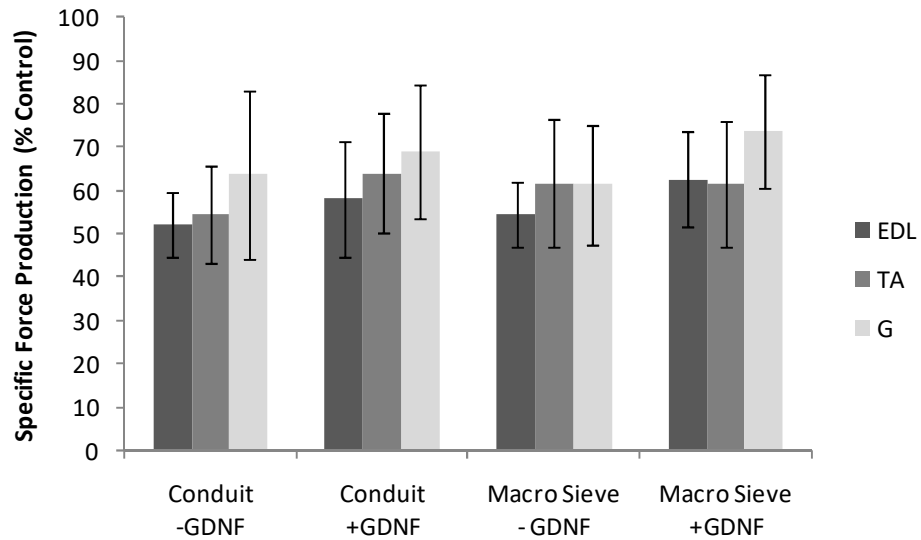
Appendix B-5. Maximum specific force production in reinnervated muscle following implantation of macro-sieve electrodes. Maximum specific force produced in EDL muscle (A), TA muscle (B), and G muscle (C) measured 3 month after implantation of macro-sieve electrodes and silicone guidance conduits with and without delivery system. Mean values and standard deviations are shown. * denotes $p < 0.05$ versus similar device with dissimilar presence/absence of fibrin-based delivery system loaded with GDNF. ** denotes $p < 0.05$ versus sieve electrode assembly with similar presence/absence of fibrin-based delivery system loaded with GDNF.



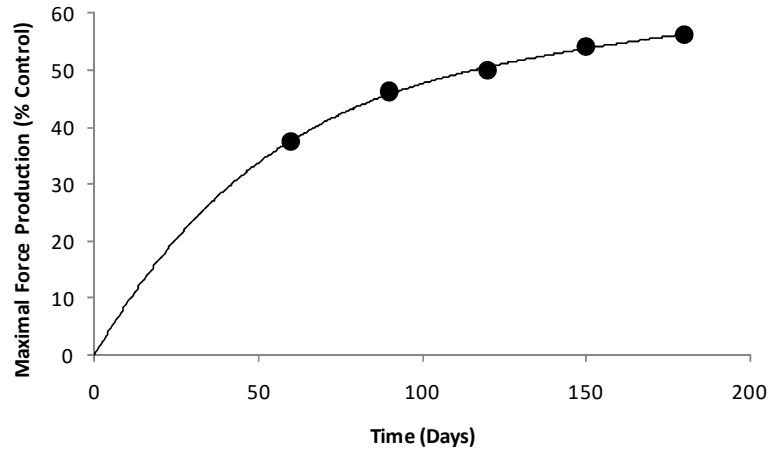
Appendix B-6. Recovery of force production in reinnervated muscle following implantation of macro-sieve electrodes. Recovery of isometric tetanic force production in EDL muscle, TA muscle, and G muscle following implantation of macro-sieve electrodes and silicone guidance conduits with and without delivery system. Measurements were made 3 month post-operatively. All measurements were calculated as percent unoperative (healthy) control. Mean values and standard deviations are shown. * denotes $p < 0.05$ versus similar device with dissimilar presence/absence of fibrin-based delivery system loaded with GDNF. ** denotes $p < 0.05$ versus sieve electrode assembly with similar presence/absence of fibrin-based delivery system loaded with GDNF.



Appendix B-7. Preservation of muscle mass in reinnervated muscle following implantation of macro-sieve electrodes. Preservation of muscle mass in EDL muscle, TA muscle, and G muscle following implantation of macro-sieve electrodes and silicone guidance conduits with and without delivery system. Measurements were made 3 month post-operatively. All measurements were calculated as percent unoperative (healthy) control. Mean values and standard deviations are shown. * denotes $p < 0.05$ versus similar device with dissimilar presence/absence of fibrin-based delivery system loaded with GDNF. ** denotes $p < 0.05$ versus sieve electrode assembly with similar presence/absence of fibrin-based delivery system loaded with GDNF.

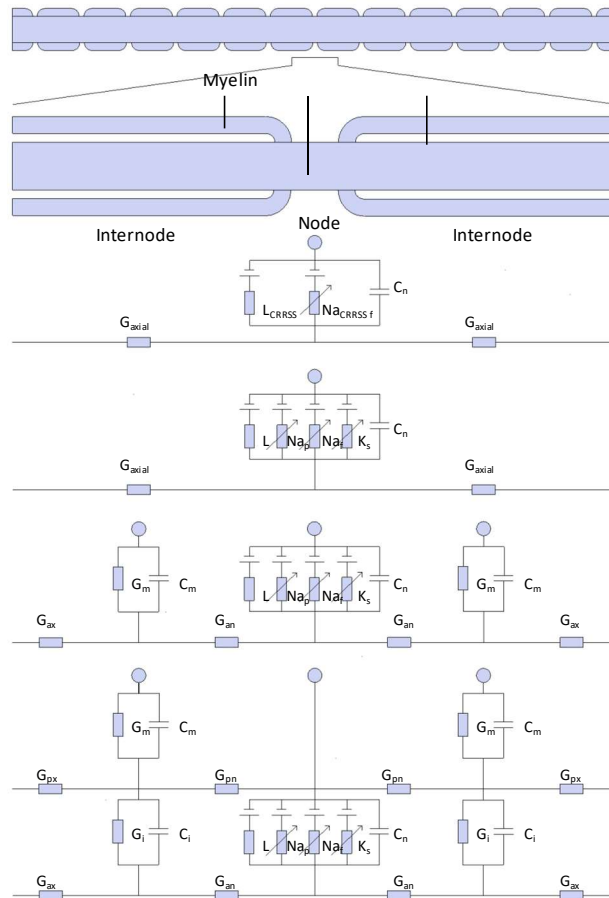


Appendix B-8. Recovery of specific force production in reinnervated muscle following implantation of macro-sieve electrodes. Recovery of specific force production in EDL muscle, TA muscle, and G muscle following implantation of macro-sieve electrodes and silicone guidance conduits with and without delivery system. Measurements were made 3 month post-operatively. All measurements were calculated as percent unoperative (healthy) control. Mean values and standard deviations are shown. * denotes $p < 0.05$ versus similar device with dissimilar presence/absence of fibrin-based delivery system loaded with GDNF. ** denotes $p < 0.05$ versus sieve electrode assembly with similar presence/absence of fibrin-based delivery system loaded with GDNF.

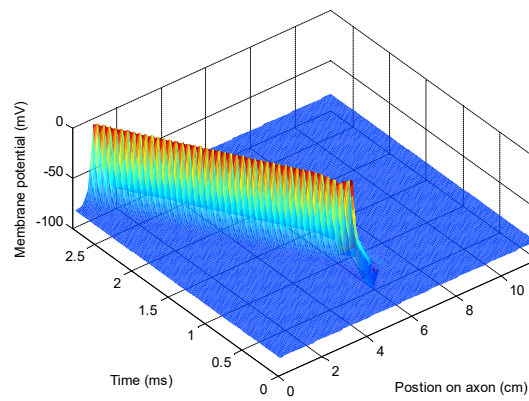
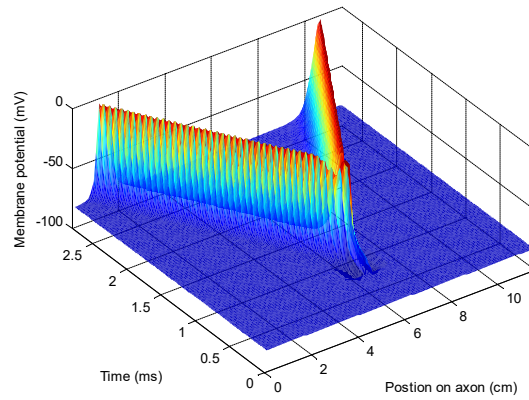


Appendix B-9. Time course of functional motor recovery following macro-sieve electrode implantation. Recovery of isometric tetanic force production in EDL muscle following implantation of macro-sieve electrodes without delivery system. Measurements were made 2, 3, 4, 5, 6 months post-operatively. All measurements were calculated as percent unoperative (healthy) control.

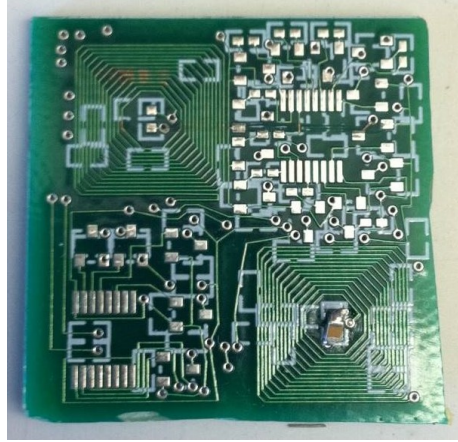
Appendix C: Computational Modeling of Macro-Sieve Electrodes



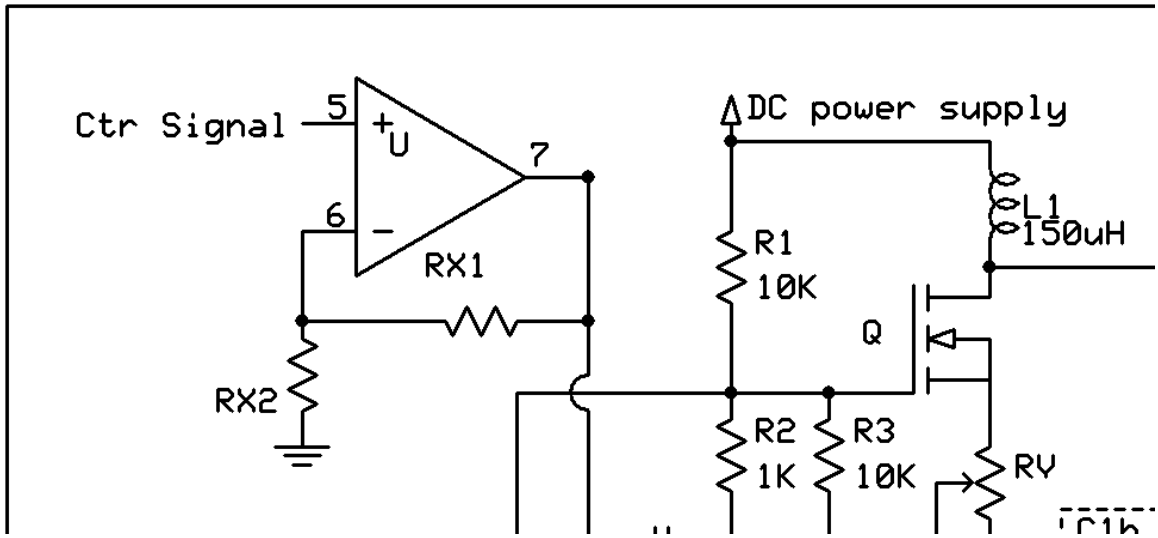
Appendix C-1. Circuit diagrams illustrating electrical behavior of mammalian axons. Circuit diagrams outlining the mathematical models of mammalian axon behavior tested in present computational models of macro-sieve electrode performance. CRRSS (top), Model A, Model B, and Model C (bottom) circuit diagrams are shown.



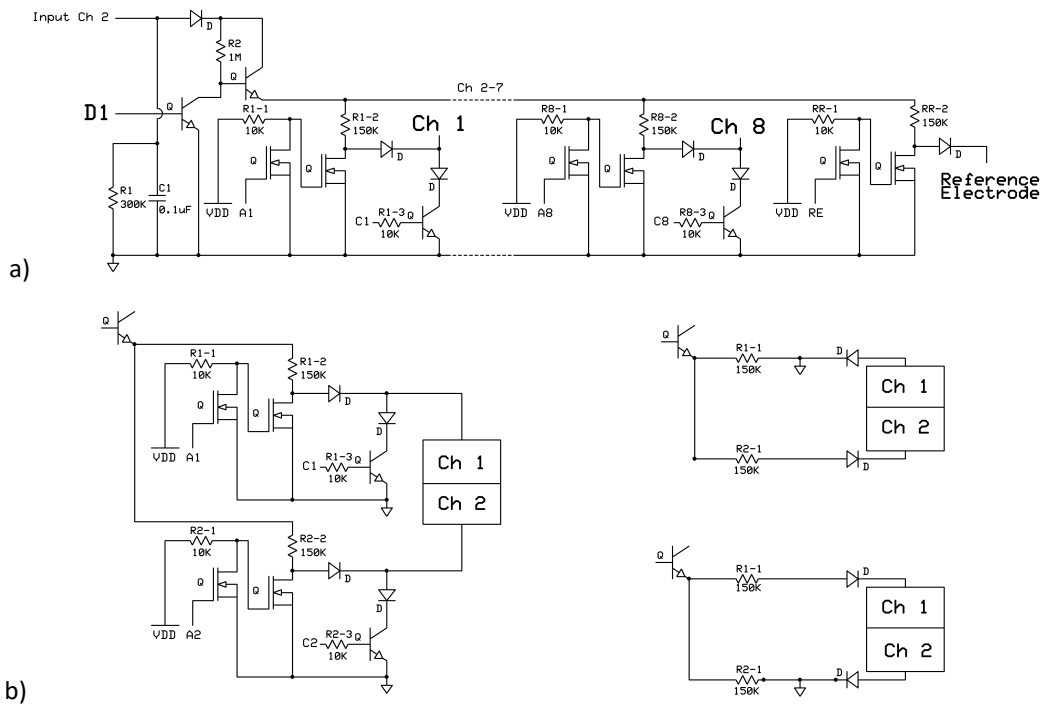
Appendix C-2. Initiation of uni-directional action potentials in peripheral nerve fiber. Results of computational modeling studies demonstrating non-specific initiation of bi-directional action potentials (top) and selective initiation of uni-direction action potentials (bottom) in virtual axon arrays placed inside of model macro-sieve electrodes. Plots demonstrate propagation of initiated action potentials in both time and space.



Appendix C-3. Two-channel implantable receiver for wireless electrical stimulation via implanted macro-sieve electrode. Micrograph of implantable wireless receiver capable of facilitating wireless power delivery and channel selection in implantable macro-sieve electrodes.



Appendix C-4. Schematic for implantable wireless transmitter and receiver for use with implanted macro-sieve electrode.



Appendix C-5. Schematic outlining capacity for channel selection and bipolar stimulation via implantable wireless transmitter and receiver.